AD-A189 538   INVESTIGATION OF HEAT TRANSFER TO A FLAT PLATE IN A   1/3
              SHOCK TUBE(U) AIR FORCE INST OF TECH WRIGHT-PATTERSON
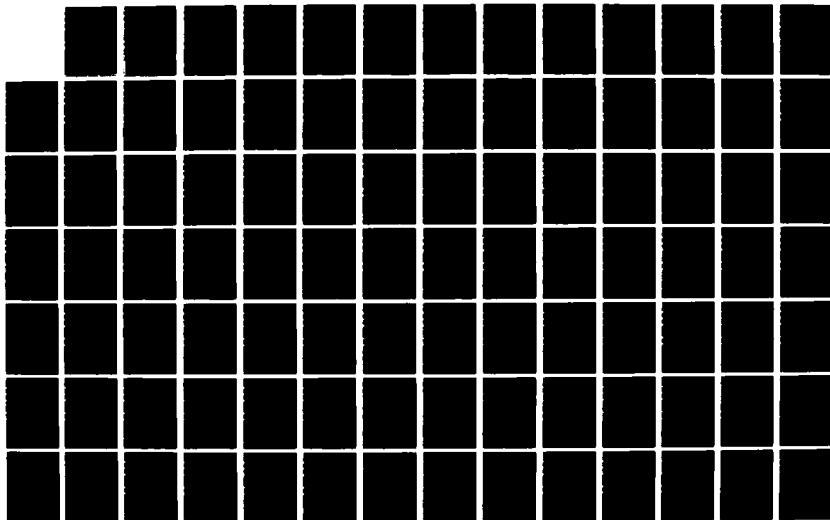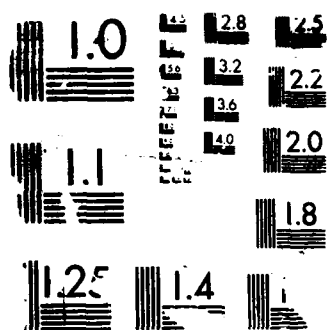   AFB OH SCHOOL OF ENGINEERING   J T NOVAK DEC 87
UNCLASSIFIED AFIT/GA/AA/87D-5   F/G 20/13   NL

MICROCOPY RESOLUTION TEST CHART

AD-A189 538

INVESTIGATION OF HEAT TRANSFER

TO A FLAT PLATE IN A SHOCK TUBE

THESIS

Joseph T. Novak
Captain, USAF

AFIT/GA/AA/87D-5

DEPARTMENT OF THE AIR FORCE
AIR UNIVERSITY
AIR FORCE INSTITUTE OF TECHNOLOGY

Wright-Patterson Air Force Base, Ohio

88 3 01 132

INVESTIGATION OF HEAT TRANSFER

TO A FLAT PLATE IN A SHOCK TUBE

THESIS

Joseph T. Novak
Captain, USAF

AFIT/GA/AA/87D-5

DTIC
ELECTE
MAR 0 3 1988

H

INVESTIGATION OF HEAT TRANSFER

TO A FLAT PLATE IN A SHOCK TUBE

THESIS

Presented to the Faculty of the School of Engineering

of the Air Force Institute of Technology

Air University

In Partial Fulfillment of the

Requirements for the Degre of

Master of Science in Astronautical Engineering

Joseph T. Novak, M.S.

Captain, USAF

December 1987

Acknowledgements

It would be very difficult to perform a study such as this without the help of many others. I could not have hoped for more capable guidance and steadfast encouragement than that which I received from my advisor, Dr. William C. Elrod. His patience, understanding, and humor made this project an enjoyable experience. Special thanks go to Dr. James Hitchcock for stimulating my interest in the field of heat transfer and for providing invaluable advice and assistance whenever I asked. I must also say thanks to the AFIT laboratory staff for providing quick and capable assistance whenever needed. In particular, I am deeply indebted to Mr. Jay Anderson for his untiring and selfless efforts in assisting me throughout this study. Without his expertise in instrumentation and computer systems, I could not have performed this investigation. I am also greatly appreciative to Bret J. Smith for giving much of his time to aid me in understanding the computer software used in this study. But no thanks would be complete without those that I would like to give to my wife, Sharon; without her unwavering support and understanding, none of this would have been possible. And, last of all, thanks go to my kids, Kristi and Nicholas, for just being there.

Joseph T. Novak

ii

Table of Contents

List of Figures

List of Tables

List of Symbols

Symbol	Description	Units
C_f	Coefficient of friction	
C_p	Constant pressure specific heat	Btu/lbm-F
h	Heat transfer coefficient	Btu/ft-s-F
k	Ratio of specific heats, Thermal conductivity	Btu/h-ft-F
M	Mach number	
Nu	Nusselt number	
P	Pressure	in Hg
Pr	Prandtl number	
q	Heat flux	Btu/ft-s
r	Recovery factor	
Re	Reynolds number	
t	time	s
T	Temperature	F or R
U	Velocity	ft/s
x	Axial position	
$\propto$	Laminar transition factor	

Symbol	Description	Units

Subscripts

aw	Adiabatic wall	
n	Number of finite element divisions	
s	Incident shock	
1	Driven fluid conditions	
2	Conditions behind incident shock	
4	Driver fluid conditions	
w	Wall	
∞	Freestream	

Superscripts

*	Reference state	

Greek letters

τ	Time integration variable	
ρ	Density	lbm/ft
ν	Kinematic viscosity	ft/s

Abstract

The heat transfer mechanisms taking place in the flow induced behind a shock wave travelling across a flat plate were investigated for flat plates with sharp and rounded leading edges. The boundary layer behind the shock is described by a transient boundary layer followed by a steady-state boundary layer as the effects of the leading edge are transmitted downstream. The use of a multichannel high speed transient data recorder allowed thin film heat transfer gages at up to eight axial locations along the length of the flat plate to be simultaneously sampled. Heat transfer rate histories for each axial location were time correlated to the same flow conditions. The results indicate the existence of a threshold free stream velocity (relative to the plate) above which yields transition times, for all locations along the plate, which are confined to some narrow interval. The leading edge disturbance appears to have no influence on transition. For Mach numbers below 1.22, the sharp edge flat plate experienced heat transfer rates in excess of theory, but the rounded edge flat plate exhibited data which matched or was less than what theory predicted for each Mach number tested. The sharp edge flat plate data showed a consistent correlation between heat transfer magnitude and axial location on the plate; with limited data, the rounded plate showed no such correlation.

INVESTIGATION OF HEAT TRANSFER
TO A FLAT PLATE IN A SHOCK TUBE

I. Introduction

Turbine blade heat transfer is a topic of prime interest in the aerospace community today. Studies in this field often utilize shock tube facilities since the shock tube provides a means to simulate turbine flow conditions. Dunn (1981) performed such a study utilizing turbine blades instrumented with thin film heat flux gages. Fillingim (1985) also conducted turbine blade heat transfer research but did not produce conclusive results; it was believed that complexities in the flow geometry (associated with the turbine blade cascade) and in the instrumentation system hindered his efforts to provide useful heat transfer information. In an effort to simplify the flow geometry and perform initial studies which are requisite to better understanding turbine blade heat transfer, Smith (1986) performed limited research on the heat transfer to a sharp leading edge flat plate in a shock tube. Clearly, in order to relate the results from such a study to the turbine blade geometry, the transient boundary layer generated by the passing shock wave must be well understood; much of Smith's work was concerned with this. The purpose of the present investigation is to further study flat

1

plate heat transfer by using a shock tube under varying flow conditions for two leading edge geometries in an effort to ultimately provide a better understanding of the heat transfer mechanism associated with turbine blade research.

Background

Consider a flat plate suspended in a shock tube and surrounded by undisturbed (still) air. A normal shock wave moving down the shock tube passes over the flat plate, impulsively starting to move the fluid with a velocity, U_∞, in the direction of the moving shock. As explained by Abbott, Walker and Liu (1973), the viscous flow in the boundary layer on the plate is characterized by two distinct regions (see Figure 1). At any position x on the plate (and any position y above the plate) the disturbance propagates with the local velocity $u(x,y,t)$, with the maximum downstream disturbance travelling at velocity U_∞ at the outer edge of the boundary layer. For $x > U_\infty t$, the flow is unaware of the presence of the leading edge and in this region (denoted by T, for transient) the solution is given by Mirels (1956) for the boundary behind a normal shock advancing along an infinite flat plate. For $x < U_\infty t$ there is a region of interaction between the downstream influence of the leading edge and the boundary layer created by the passage of the shock wave. It has been found that both upstream and downstream boundary conditions must be utilized to solve the problem in this region (Abbott, Walker and Liu, 1973:463).
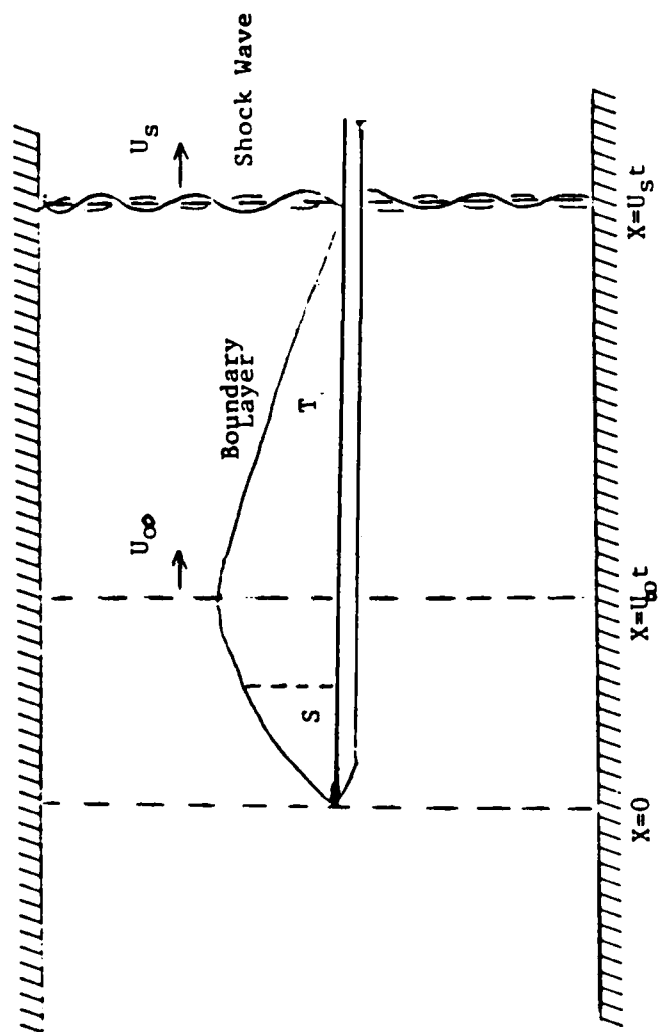
Figure 1. Flow over a Flat Plate after the Shock
Wave has passed the Leading Edge

For very weak shock waves, this problem is identical to the impulsively started semi-infinite flat plate problem studied by Stewartson (1951). To summarize his discussion, Stewartson found that at $\alpha = x/U_\infty t = 1$, there is an essential singularity of the boundary layer equations such that the solution for $\alpha < 1$ is not an analytical continuation of the solution for $\alpha > 1$, although all derivatives with respect to α are continuous at $\alpha = 1$. At any specific location, the value $\alpha = 1$ corresponds to the first time that the flow is aware of the effect of the leading edge.

Lam and Crocco (1958) first studied the present problem but were unable to obtain convergence of their numerical procedure. Felderman (1968), using the same procedure as Lam and Crocco, utilized weighting factors to obtain a convergent solution to the iteration scheme. He also observed that the flow region behind the shock wave becomes steady at some time based on α. Davies and Bernstein (1969) studied the problem of heat transfer and transition to turbulent flow in the shock induced boundary layer and found that for $\alpha < 0.3$, the flow is substantially steady. Abbott, Walker and Liu devised a finite differencing scheme that successfully converged to a solution and closely matched Felderman's data and that of Davies and Bernstein regarding the elapsed time for the plate heat transfer to reach 95% of the steady state value for any location x on the plate surface.

Dillon and Nagamatsu (1984) measured the heat transfer to a shock tube wall behind a passing shock wave. They

4

obtained excellent agreement between their experimental data

and Mirels' theory for the laminar transitional boundary

layer, as well as between their turbulent data and

von Karman's theory for incompressible turbulent boundary

layers. In approximately 20% of their tests, "turbulence

bursting" of the laminar flow was evident. Brostmeyer and

Nagamatsu (1984) used a reflected shock wave to create a

high enthalpy, low velocity flow across a blunt (rounded)

leading edged flat plate. Their data matched Mirels' theory

very well for laminar flows and their turbulent data was a

close match to theoretical turbulent values. Fillingim (1985)

investigated the heat transfer to a flat plate behind a

shock wave and obtained results which were a good match with

Mirels' transient theory. But his turbulent

experimental data did not consistently match turbulent

theoretical values. Smith (1986) did a similar study and

obtained close agreement with Mirels' laminar theory, but

his turbulent data produced heat transfer values which were

much higher than predicted by theory. He concluded that for

each location along the flat plate, the flow transitioned to

turbulent conditions at a common time relative to shock

passage as long as the axial locations were at a "sufficient"

distance from the leading edge to preclude any leading edge

influence on transition.

Objectives and Scope

The purpose of this study was to investigate the heat

transfer to a flat plate due to the flow induced by the

passage of a shock wave. The specific objectives were as follows:

1. For a sharp leading edge flat plate, obtain and examine time correlated heat transfer data for insight into boundary layer heat transfer and transition.

2. For varying flow conditions, investigate experimental heat transfer magnitudes in an effort to better understand the heat transfer mechanism associated with flat plates with sharp and rounded leading edges.

This study was performed utilizing a high speed multichannel transient data recorder. Many previous heat transfer studies of this kind have been limited by the relatively few data points available through digitizing oscilloscope traces. The instrumentation system used here allows for simultaneous collection of eight channels of data sampled at two microsecond intervals, providing a capability to almost continuously record data in an effort to understand the mechanism of transient heat transfer.

Atmospheric air was the medium of study. Although the range of shock Mach numbers used in this study was quite limited (approximately 1.1 to 1.6), the pressure ratios used varied considerably (1.6 to 9.4), allowing for a fairly wide range of flow conditions. Free stream velocities, relative to the plate, varied from 198 ft/sec to 936 ft/sec. Steady Reynolds numbers, defined ahead by Eq (10), ranged from 1.9×10^5 to 1.3×10^7 and transient Reynolds numbers, defined ahead by Eq (18), ranged from 1.9×10^4 to 9.2×10^5.

6

II. THEORY

Shock Tube Principles

The high temperature, high pressure flows required for this investigation were produced using a shock tube consisting of a high pressure driver section and a lower pressure driven section separated by a diaphragm (see Figure 2). The gas located in the higher pressure section is defined as the driver gas and all properties of that gas are identified by region 4. The lower pressure gas on the other side of the diaphragm is defined as the driven gas whose properties are identified by region 1. The gases of both regions initially have no velocity.

When the diaphragm is ruptured, pressure waves emanate from the diaphragm's original position and a number of distinct regions appear within the shock tube. Figure 2(b) illustrates four of these regions. In the direction of the driven gas the pressure waves, continually propagating into a gas of increasing sonic speed, quickly coalesce to form a shock wave that moves down the tube. As the shock wave moves through the driven gas, the gas properties are changed from those identified by region 1 to those identified by region 2. The new properties can be determined with normal shock relations. The gas rises to temperature T_2, is compressed to pressure P_2 and given a velocity U_2 as a result of the passage of the shock wave (the property changes take place instantaneously and non-isentropically).

7
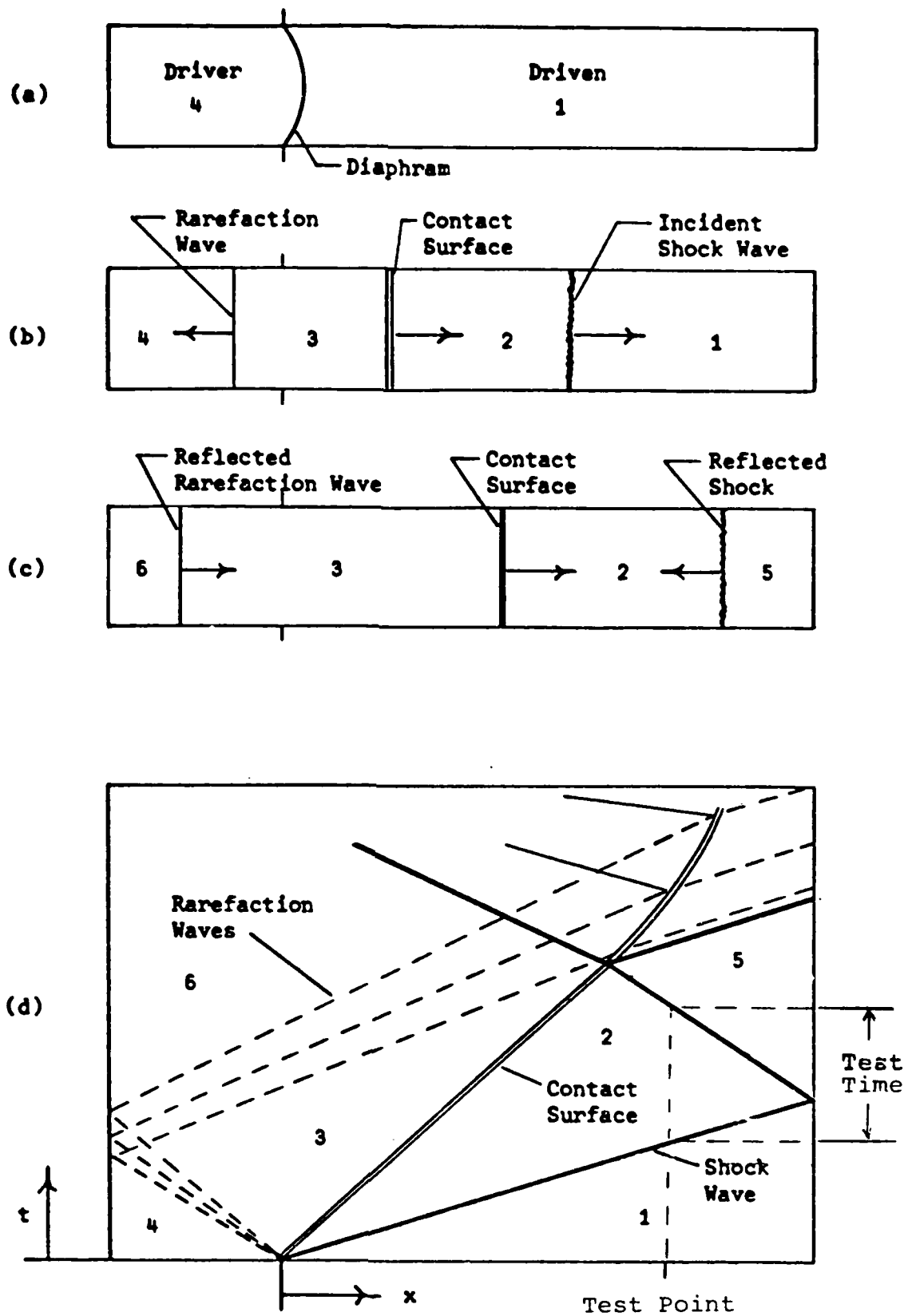
Figure 2.   Shock Tube Wave Phenomena

8

In the direction of the driver gas the pressure waves,
travelling into a cooling gas of continually decreasing
sonic speed, expand and spread with time forming a rarefaction
wave. Similar to shock waves, a rarefaction wave changes the
properties of the gas through which it is moving; region 4
properties are changed continuously and isentropically to new
properties identified by region 3. The pressures and
velocities in regions 2 and 3 are identical, but the
temperatures in the two regions differ due to the non-
isentropic compression forming region 2 versus the isentropic
expansion forming region 3. The temperature discontinuity
location is defined as the contact surface and propagates
at a determinable rate down the shock tube.

Figure 2(c) shows region 5 which is formed after the
shock wave reflects from the closed end of the shock tube,
and region 6 which is formed after the rarefaction wave
reflects from the other end of the tube. The properties
associated with regions 5 and 6 can be determined from
normal shock relations and rarefaction wave relations,
respectively. Gaydon and Hurle (1963) and Glass (1958) may
be referenced for additional information on the subject of
shock tube physics.

After the diaphragm is ruptured, the shock wave moves
through region 1 at a speed which is determined by the
pressure ratio across the diaphragm and the temperature in
region 1. The shock wave's Mach number (M_s) can be found
by the relation (Chapman and Walker, 1971):

9

$$\frac{P_4}{P_1} = \left(\frac{K-1}{K+1}\right)\left(\frac{2K}{K-1}M_s^2 - 1\right)\left(1 - \frac{\left(\frac{K-1}{K+1}\right)(M_s^2-1)}{M_s}\right)^{-2K/K-1} \tag{1}$$

where P_4 is the driver gas pressure, P_1 is the driven gas pressure and k is the ratio of specific heats.

The conditions of region 2 are of primary interest for this study. The properties of region 2 can be determined from the known properties of region 1 and the value of M by the relations (Shapiro, 1985:1001-1002):

$$\frac{P_2}{P_1} = 1 + \frac{2K}{K+1}\left(M_s^2 - 1\right) \tag{2}$$

$$\frac{T_2}{T_1} = 1 + \frac{2(K-1)}{(K+1)^2}\left[KM_s^2 - \frac{1}{M_s^2} - (K-1)\right] \tag{3}$$

$$U_2 = c_1\left(\frac{2}{K+1}\right)\left(1 - \frac{1}{M_s^2}\right)M_s \tag{4}$$

where T_1 and T_2 are static temperatures, P_1 and P_2 are static pressures, c_1 is the speed of sound in region 1 and U_2 is the velocity behind the shock wave.

Shock tube studies are limited in available test time, as can be seen by Figure 2(d). For any test point x, the gas properties at that point will remain unchanged for only a few milliseconds after the diaphragm is ruptured. Once the shock wave passes the test point, gas properties will remain constant until either the reflected shock wave or the contact

10

surface arrives at the test point. The passage of the incident shock wave and the arrival of either the reflected shock wave or the contact surface determines the available test time.

Boundary Layer Theory

The boundary layer formed behind a normal shock moving along a flat plate is illustrated in Figure 1. Since the shock wave imparts a velocity, U_∞, to the gas through which it is moving and since the velocity at the surface of the flat plate is zero, steep velocity gradients exist over a very thin region of space above the flat plate. As the shock wave moves to the right, it creates a transient disturbance or boundary layer that extends away from the plate. This transient boundary layer is similar to, but slightly thicker than one which is formed by an impulsively started flat plate (Schlichting, 1979:441). The equations for this boundary layer were developed by Mirels and will be discussed later.

The boundary layer is formed by disturbances originating from all postitons on the plate from the leading edge to the moving shock. As time progresses, the boundary layer thickness at any plate location is increasingly influenced by the disturbance coming from the leading edge of the plate and less from the transient disturbance created behind the moving shock wave. Blasius (1908) determined the governing equations for the region where the leading edge disturbance is dominant. It should be noted that the transition from

11

laminar to turbulent flow can occur in the transient

disturbance region or in the region dominated by the leading

edge disturbance.

Heat Transfer

One of the important goals of this study is to better

understand the boundary layer / heat transfer mechanism

behind an incident shock wave. In order to be able to

predict what kind of heat transfer rates to expect behind

such shock waves, it is necessary to compare experimental

data with theoretical predictions associated with each of the

boundary layers previously mentioned. This, hopefully will

give interested parties some indication of how to predict

heat transfer to vital components subject to high speed

flows.

The equations presented in this section, when used with

Eqs (2), (3), and (4), provide theoretical heat transfer

results to be compared with experimental data. The steady

boundary layer equations will be summarized first, followed

by the transient boundary layer equations.

The equation which determines the rate of heat transfer

to the flat plate for a high speed flow is given by (Kays and

Crawford, 1980:299):

$$q = h_x \left(T_{aw} - T_w \right) \tag{5}$$

where h_x is the local heat transfer coefficient, T_{aw} is the

adiabatic wall temperature and T_w is the temperature of the

flat plate. The adiabatic wall temperature can be found by (Kays and Crawford, 1980:297):

$$T_{aw} = T_{\infty} + r \frac{U_{\infty}^2}{2c_p}$$

(6)

where T_{∞} is the free stream static temperature, c_p is the constant pressure specific heat, U_{∞} is the free stream flow velocity and r is the recovery factor.

The heat transfer coefficient in Eq (5) can be obtained from the local Nusselt number (Nu_x), position from the leading edge (x), and thermal conductivity (k) by:

$$h = \frac{Nu_x k}{x}$$

(7)

where for laminar boundary layers

$$Nu_x = 0.332 \, Re^{*(.5)} Pr^{*(.333)}$$

(8)

and for turbulent boundary layers

$$Nu_x = 0.0287 \, Re^{*(.8)} Pr^{*(.6)}$$

(9)

The Reynolds number for Eqs (8) and (9) is given by:

$$Re = \frac{U_{\infty} x}{v}$$

(10)

where v is the momentum diffusivity (kinematic viscosity) and x is the distance from the leading edge. All properties used in Eqs (8), (9), and (10) are evaluated at a reference

13

temperature defined by (Kays and Crawford, 1980:304):

$$T^* = \frac{T_\infty + T_w}{2} + \phi.22\left(T_{aw} - T_\infty\right)$$

(11)

This reference temperature is to account for temperature variations through the boundary layer. The recovery factor r used in Eq (6) has the value of the square root of the Prandtl number for laminar flow and the cube root of the Prandtl number for turbulent flow. Properties denoted by the ∞ subscript can be obtained from Eqs (2), (3), and (4) where the subscript 2 corresponds to the ∞ subscript. Equations (5) through (11) were used to develop the theoretical steady heat transfer solution to be used in comparison with the experimental results.

The unsteady laminar heat transfer solution is obtained from theory developed by H. Mirels (1955). According to Mirels, when the Prandtl number of the gas differs little from unity, his transient boundary solution can be approximated using the equations that follow.

The heat transfer equation for the unsteady boundary layer is given by Eq (5) with the adiabatic wall temperature defined by Eq (6) or by (Schlichting, 1979:442-443):

$$T_{aw} = T_\infty \left(1 + \frac{K-1}{2} M_\infty^2 r\right)$$

(12)

where M_∞ is the free stream Mach number behind the shock wave and r is the recovery factor given by:

14

$$r = Pr^\alpha \tag{13}$$

with

$$\alpha = 0.39 - \frac{0.62}{1-(U_\infty/U_s)} \tag{14}$$

where U_∞ is the free stream velocity and U_s is the velocity of the incident shock wave.

For the unsteady boundary layer, the heat transfer coefficient magnitude used in Eq (5) is given by:

$$h = \frac{Nu_x k}{U_\infty t} \tag{15}$$

where Nu_x is the unsteady local Nusselt number, k is the thermal conductivity, U_∞ is the free stream velocity and t is the time after shock passage. The unsteady local Nusselt number can be written as:

$$Nu_x = 0.5 \, C_f' \, Re \, Pr^\lambda \tag{16}$$

where C_f' is the local skin friction factor defined by:

$$C_f' = \frac{1.128}{Re^{1/2}} \left(1 - \beta \frac{U_\infty}{U_s}\right)^{1/2} \tag{17}$$

$$\beta = 0.375$$

and where Re is the local Reynolds number defined by:

$$Re = \frac{U_\infty^2 t}{\nu_\omega} \qquad (18)$$

where t is the time after shock passage, U_∞ is the free stream velocity and ν_ω is the momentum diffusivity evaluated at the wall temperature. It should be noted that the characteristic length for the steady Reynolds number is defined as $U_\infty t$ in the unsteady definition.

The exponent of the Prandtl number in Eq (16) is given by:

$$\lambda = 0.48 + \frac{0.62}{1-(U_\infty/U_s)} \qquad (19)$$

Equations (12) through (19) were used to calculate the theoretical heat flux values for the unsteady laminar region immediately following the shock wave, with all properties evaluated at the temperature of the flat plate.

The theoretical unsteady turbulent solution was found by first using the unsteady Reynolds number, from Eq (18), in Eq (9) to calculate the local turbulent Nusselt number, evaluating the properties at the wall temperature. The local heat transfer coefficient was obtained from Eq (7) and the heat flux was obtained from Eq (5).

Heat Transfer Measurement

By using fast response thin film heat transfer gages and a semiconductor thermocouple, the time history of the flat plate's surface temperature was recorded. The heat transfer

16

rate, q, to the flat plate was calculated utilizing this time history of temperature in the manner described below.

The gages mentioned above utilize a thin film of platinum vapor deposited on an insulating substrate with known thermal properties. For the purpose of calculating heat transfer, this substrate was modelled as a semi-infinite slab as shown in Figure 3.

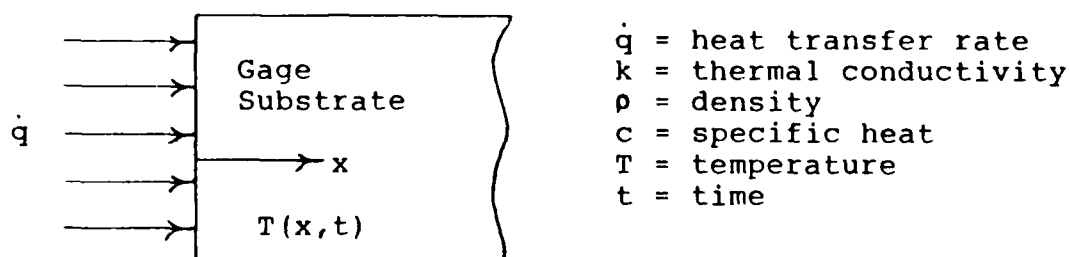|	
$\dot{q}$	= heat transfer rate
k	= thermal conductivity
ρ	= density
c	= specific heat
T	= temperature
t	= time

Figure 3. Heat Transfer Model for Gage Substrate

Assuming constant substrate properties, the energy equation can be written:

$$\frac{\partial T(x,t)}{\partial t} = \frac{k}{\rho c_p} \frac{\partial^2 T(x,t)}{\partial x^2} \tag{20}$$

with the boundary conditions

$$T(x,\phi) = \phi \quad , x > \phi$$
$$\dot{q}(\phi,t) = -k \ \partial T(x,t)/\partial x \quad , t > \phi$$
$$T(x,t) = \phi \quad , x \to \infty , t > \phi$$

(Bogdan and Garberoglio, 1967; Kendall and Schulte, 1968).

17

The solution results in the relation:

$$q(\phi,t) = \frac{1}{2}\left(\frac{\rho c_p k}{\pi}\right)^{1/2}\left[T(t) + \frac{1}{\pi}\int_0^t \frac{\tau^{1/2}T(t) - t^{1/2}T(\tau)}{(t-\tau)^{3/2}}\, d\tau\right]$$ (21)

where T is the substrate surface temperature and τ is an integration variable. Therefore, the heat transfer for the flat plate can be calculated by knowing $T(t)$. The thermocouple used in this study produces a voltage which could be read directly. The thin film heat transfer gages change resistance with change in temperature. By utilizing a Wheatstone Bridge circuit, a voltage output was produced which was proportional to the resistance change and hence the surface temperature of the gage.

Cook and Felderman (1966) developed a numerical relation using a finite differencing scheme to approximate the integral in Eq (21). It can be written as:

$$q(\tau_n) = 2\left(\frac{\rho c_p k}{\pi}\right)^{1/2}\left[\frac{T_s(t_0)}{2\, t_n^{1/2}} + \sum_{i=1}^{n}\left[\frac{T(t_i) - T(t_{i-1})}{(t_n-t_i)^{1/2} + (t_n-t_{i-1})^{1/2}}\right]\right]$$ (22)

This relation makes no assumptions about the form of the temperature function and its accuracy is limited only by the size of the discrete intervals into which the known temperature history is divided. This method treats the data as a piecewise continuous linear function.

Bogdan (1963) found that the first term of Eq (22),

$$\left(\frac{\rho c_p k}{\pi}\right)^{1/2}$$

18

can be treated as a constant for quartz-based heat flux gages (such as were used in this investigation) for the range of temperatures used in this study.

III. Experimental Apparatus

Hardware

Shock Tube. The primary investigative tool of this
study was the AFIT rectangular shock tube. It was 19.5 feet
long with the driver section spanning the first four feet
and the driven section encompassing the remaining 15.5 feet.
The test section was located in the last 3.5 feet of the
driven section. The internal cross section of the tube was 8
inches by 4 inches. The driver section and the driven
section were separated by a Mylar diaphragm with thicknesses
varying from .001 inches to .012 inches, depending on the
pressure ratios being used. Ordinary laboratory compressed
air was used to pressurize the driver section and, for some
tests, a vacuum pump system was used to evacuate air from the
driven section in order to produce changes in Reynolds
numbers without necessarily changing the pressure ratios. A
pressure gage, calibrated from 0 to 200 inches of mercury
mounted to the shock tube control panel, was used to monitor
the driver pressure and a differential manometer indicated
vacuum pressures in the driven section. A pneumatic plunger
mounted in the driver section was used to rupture the Mylar.

Instrumented Flat Plate. An instrumented flat plate
26 inches long, 4 inches wide and .5 inches thick was
installed on the test section centerline. One end of the flat
plate had a sharp leading edge, defined by a 20 degree
diagonal from the top surface to the bottom surface. The

other end was rounded, semicylindrical in shape. The majority

of the testing was done with the sharp edge acting as the

leading edge, but some testing was performed using the

rounded edge forward. The leading edge of the plate was 12

feet and 4 inches from the Mylar diaphragm. Figure 4 shows

the layout of the testing apparatus.

Instrumentation

Waveform Recorder. The Datalab DL1200 Multichannel

Waveform Recorder was the heart of the instrumentation

system. It was an eight channel, digital transient recorder

with which voltage inputs were recorded in the same manner

as is done with an oscilloscope, except that the input

voltage was given a digital value referenced against a user

selected voltage scale. Each channel was connected to a heat

gage through an amplifier / Wheatstone Bridge circuit or a

thermocouple / amplifier input. The voltage on each channel

was sampled simultaneously at 2 microsecond intervals. These

digital values, 4096 samples per channel, were stored in a

memory buffer until they were dumped to a floppy disc via a

Hewlett Packard 9836 computer. The test time, on the order of

4-6 msec, was established by the shock tube steady flow

conditions behind the incident shock as indicated in Figure 2.

Heat Flux Gages. Thermal Systems Incorporated Model

1471 Miniature Heat Flux Gages were used to measure the

surface heat flux. Each gage consisted of a 4-6 ohm thin film

platinum resistor mounted on a .06 inch diameter by .03 inch
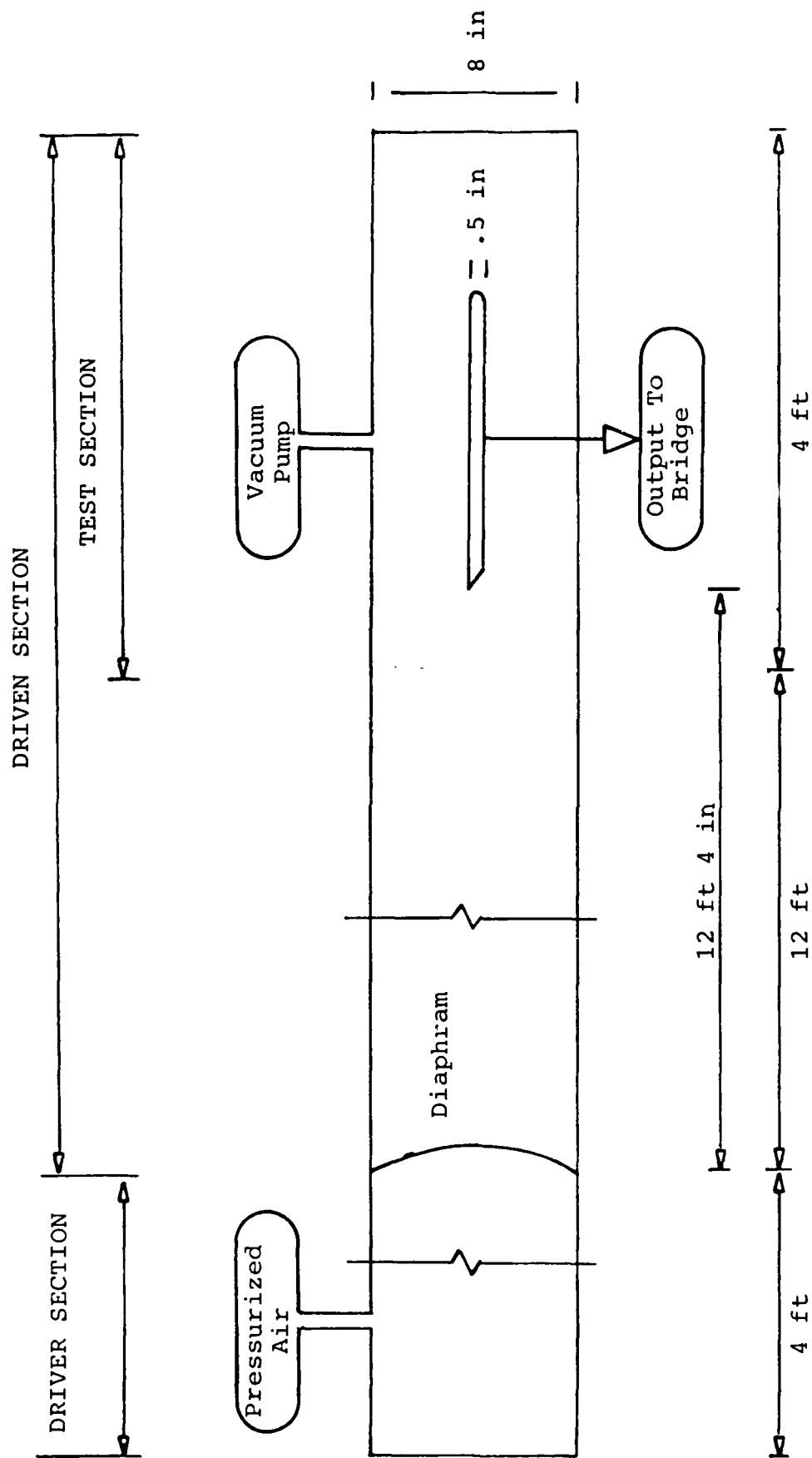
Figure 4. Shock Tube and Flat Plate

thick pyrex cylinder, with very fine gold leads extending
from the platinum surface. A schematic of a single gage is
shown in Figure 5.

Platinum
Thin Film

Gold
Leads

Quartz
Base

.060 in

.030 in
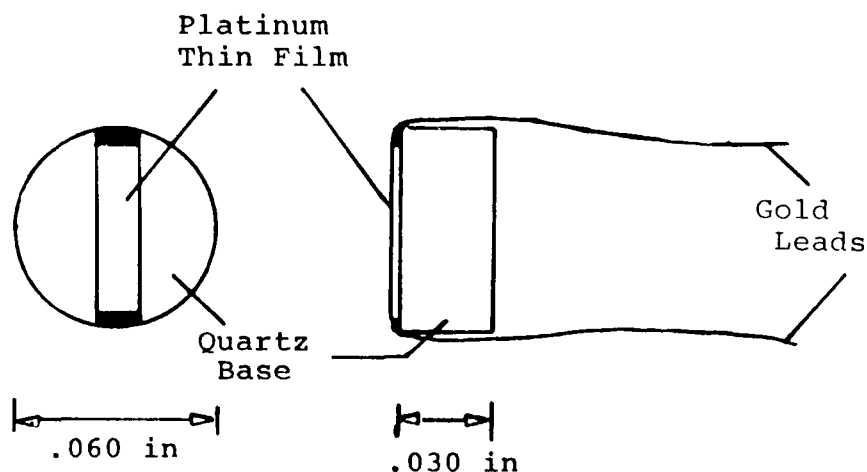
Figure 5.   Heat Flux Gage

Sixteen of the gages, each with a sensitivity on the order
of 0.005 ohms/F, were flush-mounted down the centerline of the
flat plate, 2 inches from the shock tube wall on each side.
This precluded any influence on the boundary layer at the
center of the plate from the tube walls. The first and last
gages were located 2 inches from their respective ends of the
flat plate. All gages were 1.4 inches apart with the
exception of gages 8 and 9, which were 1.9 inches apart.
Since only eight channels existed on the waveform recorder
and since not every gage was functional during the entire
testing period of this study, it was not possible to utilize
all 16 gages for each data run. The specific gages used for
each test are listed in the first paragraph of Chapter V. The
output signal from these gages was processed through a

Wheatstone Bridge / amplifier circuit before being stored in the waveform recorder.

Wheatstone Bridge / Amplifier. Processing of each heat gage signal was accomplished using a Wheatstone Bridge / amplifier module built by Transamerica Instruments. The high thermal resistivity of the thin film platinum resistor was utilized by making each gage one leg of a Wheatstone Bridge (PSC 8115 Bridge Supply Module). The resistances of the fixed legs of the bridge were nearly equal to that of the gage, maximizing the sensitivity of the bridge. Since the surface temperature changes of the gages were small, the resistance changes were small, preserving the linearity of the bridge. Amplification of the bridge output by a factor of 1000 was accomplished by using a PSC 8015-1 High Gain Differential Amplifier. Figure 6 illustrates one gage / bridge / amplifier circuit. One such circuit was required for each heat gage.

Thermocouple. A single thin film Germanium Surface Thermocouple was flush-mounted on the flat plate. Located parallel to gage #1, it was used during almost all tests when the sharp end of the plate was forward. The excellent response characteristics and high sensitivity (1.02 mV/F) made this gage very useful as a check of the heat flux gage responses and as an independent data source to aid in verifying the bridge / amplifier circuitry. Details of the thermocouple design were given by Gochenaur (1984). Output amplification of 1000 was produced utilizing an Analog
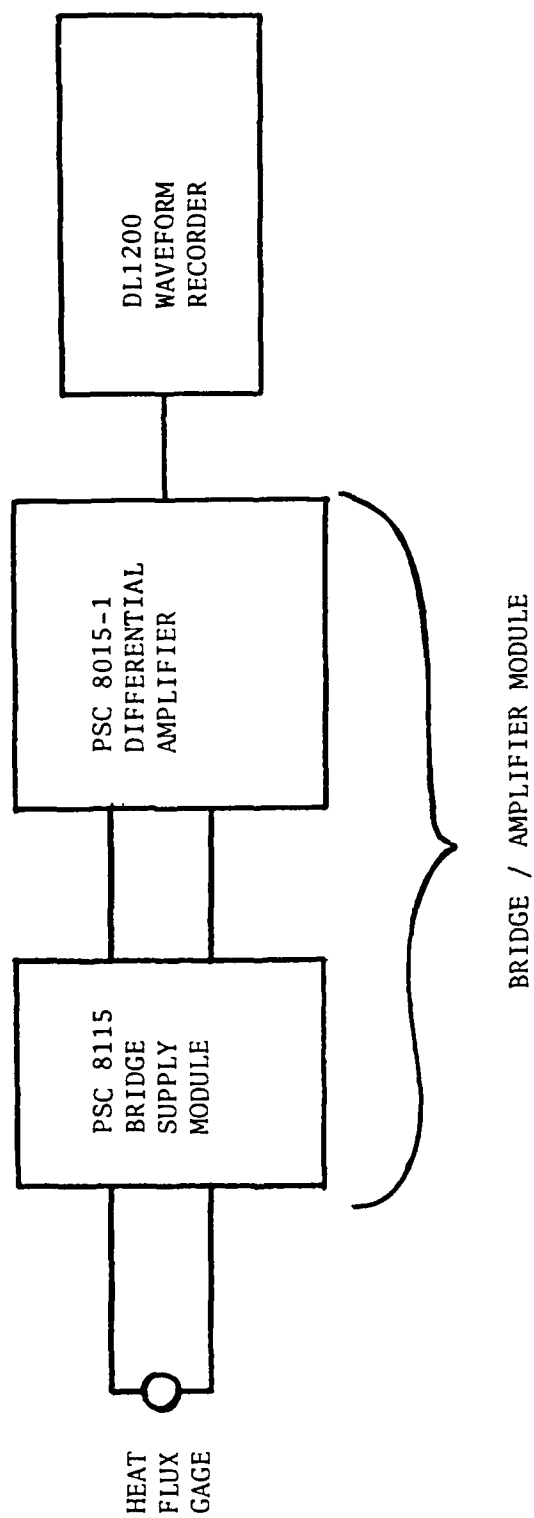
Figure 6. Wheatstone Bridge / Amplifier Circuit

Device Model AD524B instrumentation amplifier and the
resulting signal was sent to the waveform recorder.

IV. Data Collection and Data Reduction

Data Collection

The integrated data collection / reduction system is shown in Figure 7. A Hewlett Packard 9836 computer was used to interface with the waveform recorder and a Hewlett Packard 9874A Digitizer. The interface to the waveform recorder was accomplished using Datalab Products MALPAK3 software, enabling the output traces of the heat gages to be stored on disc for future data reduction.

All equipment was operated for a sufficient time prior to data collection in order to stabilize system temperatures. The Wheatstone Bridges were mechanically balanced using the modules' internal variable potentiometers and using the modules' electronic balancing feature. Also prior to each run, pertinent data such as temperatures and pressures were recorded using the MALPAK3 software.

The bridge / amplifier modules included a feature which allowed filtering of the signal coming from the gage. After much experimenting, it was found that placing a 10 KH low pass filter in the circuit removed noise from the signal while preserving the signal's important characteristics. Figure 8 shows a typical output trace utilizing no filter and Figure 9 shows a similar output signal using the 10 KH filter. Almost all data taken during this study used the 10 KH filter.
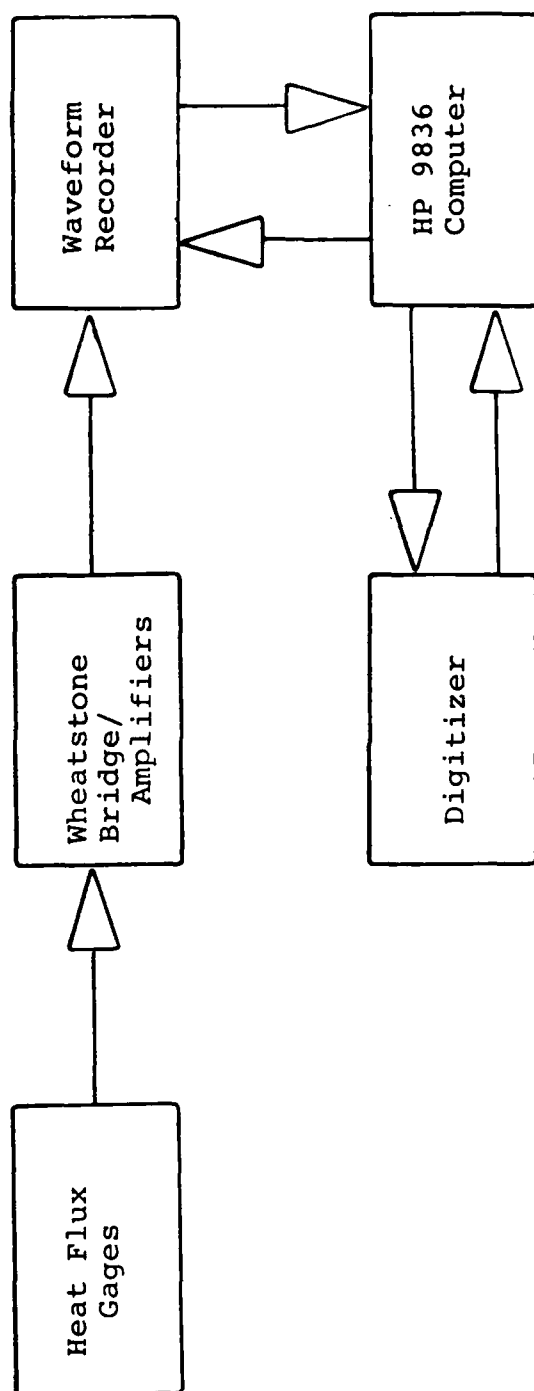
Figure 7. Data Collection System

AVG DATA FILE   AVGS11_999 FOR   DRIVER PRESSURE=29.3
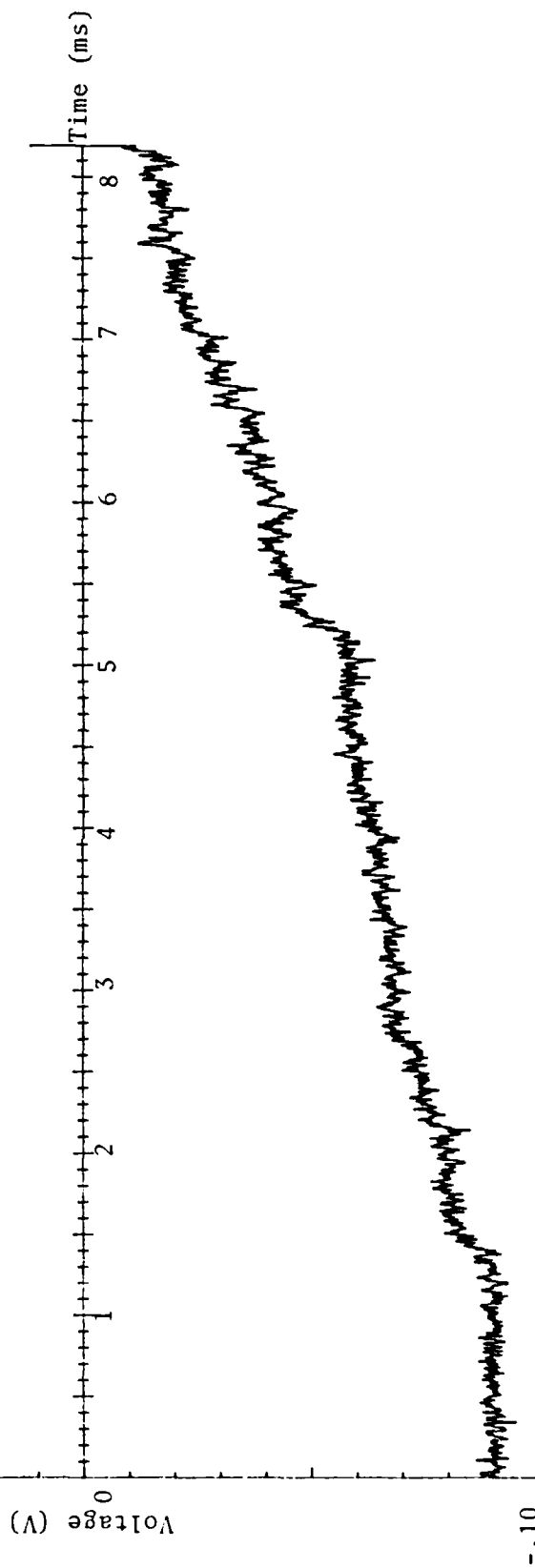
Figure 8. Heat Flux Gage Output without Filter

AVG DATA FILE   AVGS11_999 FOR   DRIVER PRESSURE=29.4
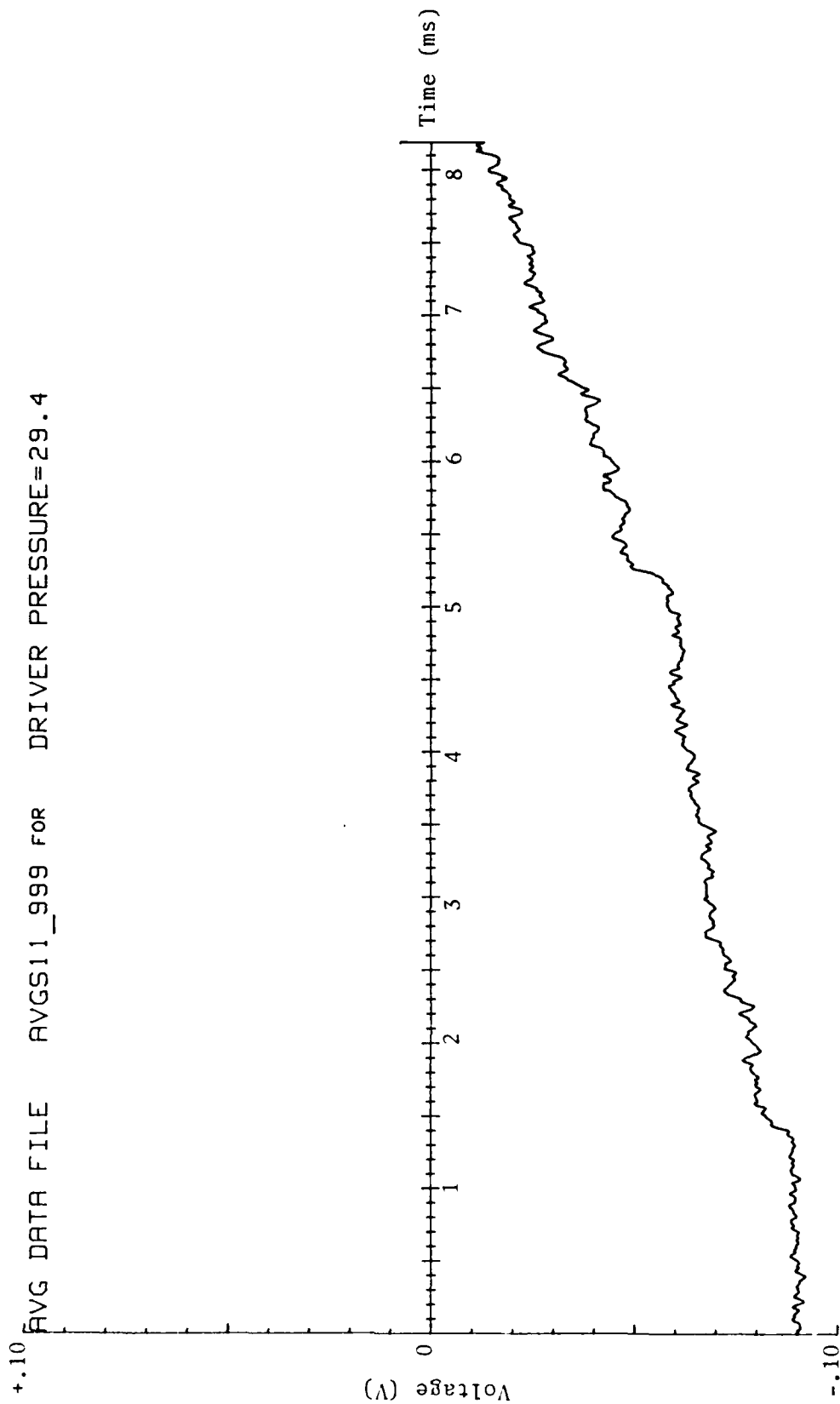
Figure 9.   Heat Flux Gage Output with 10 KH Filter

Outputs of the heat gages and the thermocouple were
recorded on the eight individual channels of the waveform
recorder for varying pressure ratios and Reynolds numbers
with simultaneous sampling of all channels occurring every 2
microseconds. Lower Reynolds number flows were created by
drawing a vacuum in the driven section of the tube. After
each data run, the output of each channel was reviewed on the
computer's monitor via the MALPAK3 software and stored on
disc to await data reduction.

Experimental data was collected in three plate
configurations. The first runs were taken with the sharp
edge forward while monitoring only the back half of the
plate (Smith, in 1986, investigated the front half). The
majority of the runs involved monitoring the entire length
of the plate with the sharp edge forward, while the
remainder of the runs used the entire length of the plate
with the rounded edge forward.

Data Reduction

It was necessary to determine the Mach number of the
shock wave for each run in order to calculate the theoretical
heat transfer for comparison with experimental results. The
recorded output traces of the thermocouple and selected heat
flux gages provide a means to calculate the shock speed and,
with the known air temperature, the Mach number. Shock passage
produced a very distinguishable feature on each output
trace: an abrupt rise in the signal from the previously

31

quiescent baseline level. Because each channel of the waveform recorder was sampled simultaneously at a known rate with all channels being triggered at the same time and since the distance between each gage was well known, calculation of the shock's Mach number was a simple matter.

Correct interpretation of the experimental results compared to the theoretical values derived using the observed Mach number is dependent on the accuracy in determining the observed Mach number. As stated above, the Mach numbers were calculated using the points of shock passage on the individual output traces. Although use of the 10 KH filter greatly improved the ability to distinguish the point of shock passage, it was often quite difficult to choose the exact passage point because of relatively high noise levels (mainly for runs involving low strength shock waves). This matter is of concern since the Mach number was very sensitive to the shock passage point found by using the MALPAK3 software. Depending on the pressure ratio used for the run, a unit change in shock position on the output trace using the MALPAK3 software can amount to a Mach number change of 0.1 or greater. This can be significant in its effect on theoretical heat transfer values. This could be responsible for some of the discrepancies found between experimental results and theoretical heat transfer values; this will be discussed later. In any event, the shock passage points were located in a manner which was as consistent as possible.

For the first group of runs, using the sharp leading edge configuration while monitoring only the back half of the plate, gages 11, 13 and 16 were used in the Mach number calculation. For the second group of runs which monitored the entire length of the plate with the sharp leading edge, the thermocouple and gages 7 and 16 were originally used for the calculation of Mach numbers. But due to consistently high Mach number values in the mid-plate region, the calculations finally involved using the thermocouple and gages 7, 11 and 16 and an average of the observed Mach numbers from the front and back ends of the plate. This will be discussed further in the Results and Discussion section. For the final group of runs, using the rounded leading edge, the Mach numbers were calculated in a similar fashion using gages 1, 6, 9 and 14.

A trace of the heat flux gage output (after filtering) plotted with MALPAK3 software and shown in Figure 9 is characteristic of the weak shocks generated in this study. The noise has been reduced considerably by use of the 10 KH filter. Further reduction in noise level was achieved by averaging three runs taken under identical conditions. Figure 10 is the average of three such runs; Figure 9 is one of the filtered runs which was used in generating the averaged plot in Figure 10. This not only reduces the noise in the trace, increasing one's ability to distinguish important trace characteristics, but it also demonstrates the system's excellent repeatability characteristics.

AVG DATA FILE   AVGS11_999 FOR   DRIVER PRESSURE=29.4

Time (ms)

Voltage (V)

+.10

0

-.10
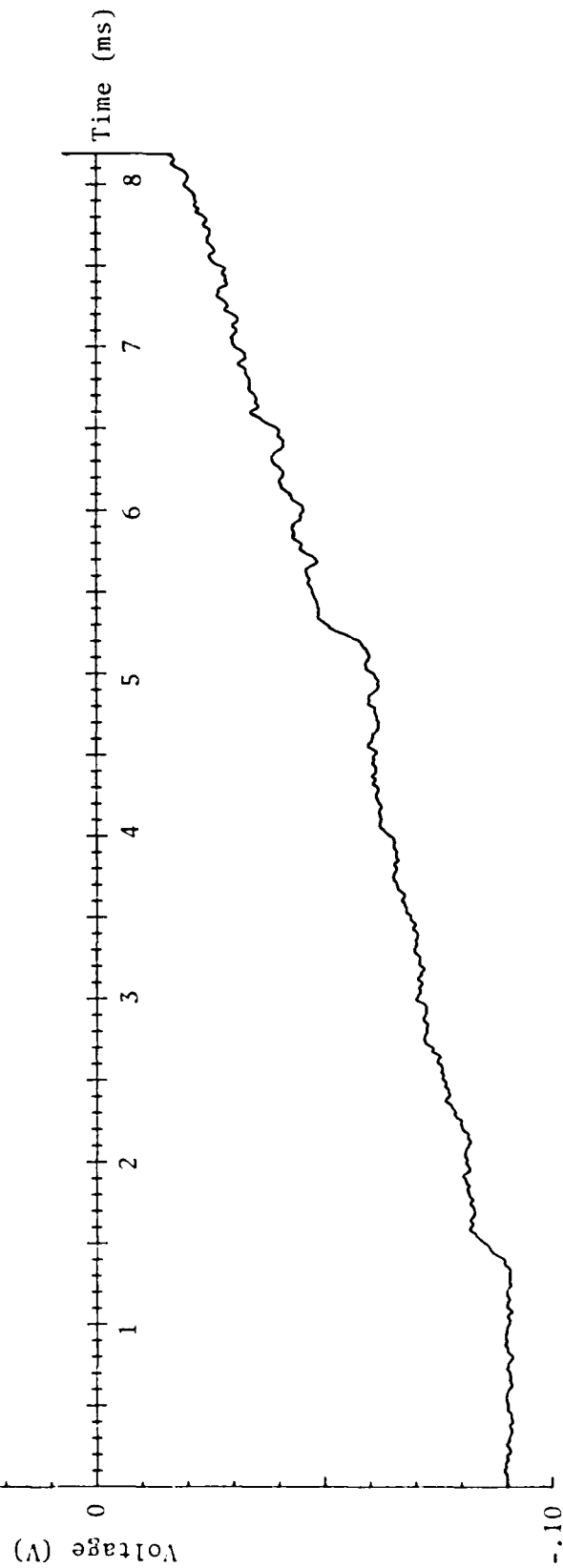
Figure 10.   Averaged Heat Flux Gage Output

At the weak shock conditions used in this study, the noise level on the output signal was still great enough to make the calculation of the heat transfer to the plate by Eq (22) unrealistic. The assumption of a piecewise smooth function was violated by the erratic noise. Therefore, a curve representing the median of the signal was traced through the averaged plot. Then by using a Hewlett Packard 9874A Digitizer, the averaged plot was digitized in an effort to manually smooth the data without disturbing any of the trace's characteristic features. Figure 11 is the digitized plot of Figure 10.

The points of incident shock passage and reflected shock passage are identified by the arrows in Figure 10. Between these points, only the flow conditions induced by the passage of the incident shock exist; these are the conditions that are the focus of this study. Therefore, only the region of the averaged plot located between those two points was digitized. Typically, the test time was approximately 4-6 milliseconds, generating about 2000-3000 data points. The speed at which the digitizer's cursor was moved along the averaged trace determined the number of points in the digitized sample; this number was normally on the order of 1200. Then, since 1200 points required more than an hour to process, the number of sample points was reduced to a value between 100 and 200 equally distributed over the test time, depending on which gage's trace was digitized. Using more data points would significantly increase the processing time.
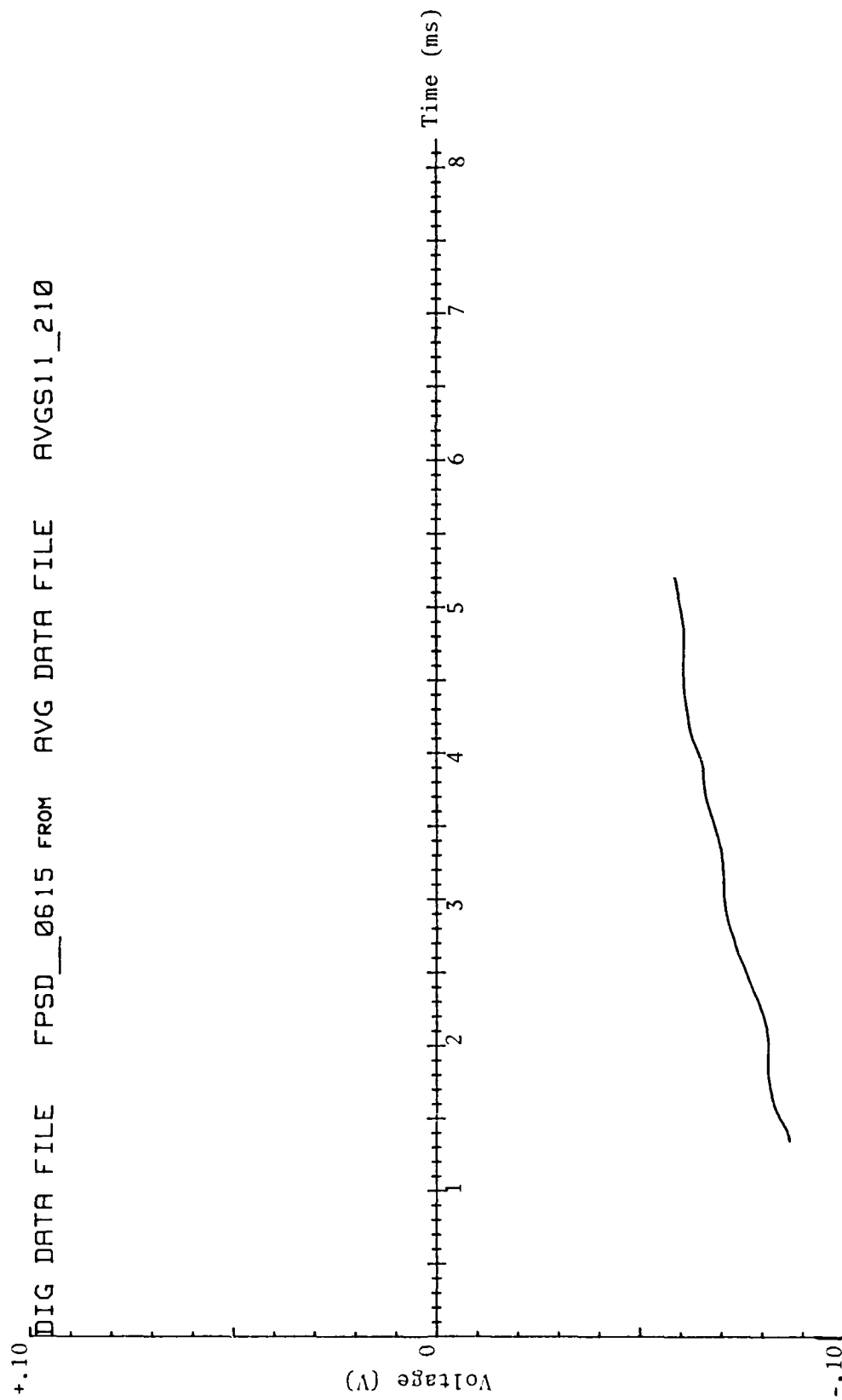
Figure 11. Digitized Heat Flux Gage Output

The filtered output traces obtained by the instrumentation system can be related to actual physical events during flow over the flat plate. Figure 12 is a typical trace of the output from the thermocouple. The passage of the shock causes an abrupt increase in surface temperature followed by a period of constant temperature indicative of the unsteady laminar boundary layer. The increase in temperature seen immediately after that is the start of the transition to turbulent flow. The heat transfer rates associated with these flow phenomena will be discussed in detail in the next section.

AVG DATA FILE   AVGTC__206 FOR   DRIVER PRESSURE=30.1
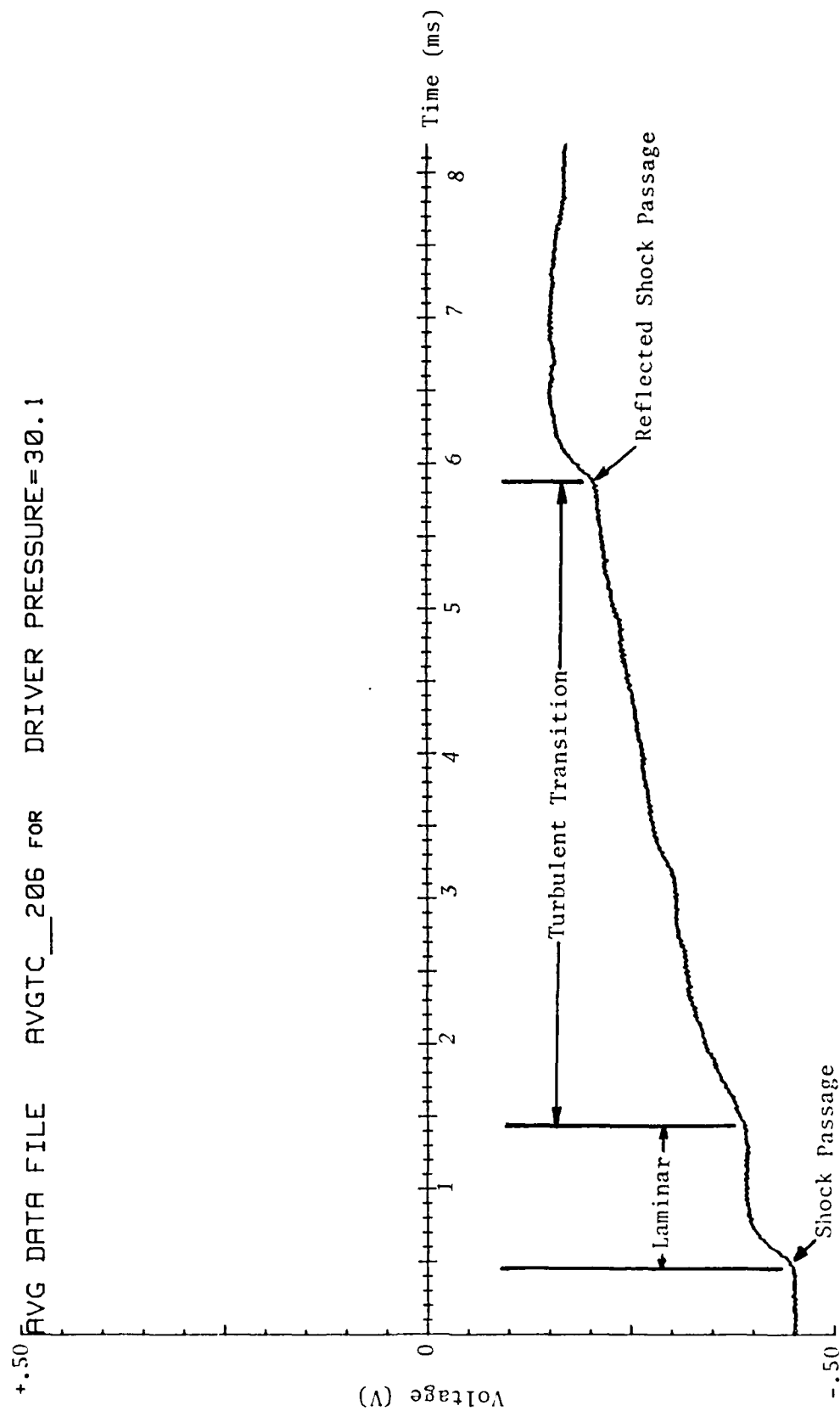
Figure 12. Thermocouple Output

V. Results and Discussion

Data was obtained for three plate configurations. First, with the sharp end of the flat plate as the leading edge, the thermocouple and heat gages 11 through 16 were used to record the heat transfer to the plate. Data Sets A through F were done in this manner. Since Smith (1986) performed studies on the front half of the same flat plate, this was done in order to compare data with Smith's front half results. Second, to obtain heat transfer data spanning the entire plate (sharp edge forward), the thermocouple and gages 1,2,4,7,11,13, and 16 were used. This configuration yielded Data Sets H through U. Finally, the plate was turned around so that the rounded edge was used as the leading edge. Using gages 14,12,9,6,4, and 1 (leading edge to trailing edge), three data sets were taken: V,W, and X. Table I lists the test conditions for those three plate configurations. The reader should note that several runs were taken while drawing a vacuum in the driven section of the tube, indicated by P_1 values less than the nominal atmospheric value of 29.2 inches of mercury. These runs were taken in order to reduce the Reynolds numbers for some flows and, in some cases, to permit runs to be taken using higher pressure ratios.

The digitized trace for each heat gage within each data set was reduced to a heat transfer rate by Eq (22) and plotted against time, which is referenced from the moment

39

TABLE I

Test Conditions

Data Set	P_o (in Hg)	P_1 (in Hg)	P_o/P_1	T_1 (°F)	M_s(thr)	M_s(obs)
A	88.5	28.5	3.1	79.8	1.27	1.16*
B	73.8	21.4	3.4	84.2	1.30	1.30*
C	59.4	29.4	2.0	85.2	1.16	1.14*
D	69.4	25.0	2.8	86.9	1.24	1.19*
E	44.2	21.9	2.0	80.6	1.16	1.14*
F	37.2	18.4	2.0	81.3	1.16	1.30*
H	44.5	22.0	2.0	78.6	1.16*	1.24
I	37.5	18.6	2.0	78.3	1.16*	1.32
J	47.0	29.4	1.6	78.6	1.11*	1.15
K	58.8	29.4	2.0	78.6	1.16	1.13*
L	88.2	29.4	3.0	78.4	1.27	1.20*
M	117.6	29.4	4.0	78.6	1.34*	1.28
N	52.9	29.4	1.8	78.6	1.13*	1.07
O	73.5	29.4	2.5	78.6	1.22*	1.17
P	102.9	29.4	3.5	78.6	1.31	1.27*
Q	39.0	24.4	1.6	78.8	1.11*	1.18
R	53.5	21.4	2.5	78.6	1.22*	1.32
S	149.8	21.4	7.0	76.3	1.50	1.48*
T	159.4	19.4	8.2	76.6	1.55	1.54*
U	172.4	18.4	9.4	76.6	1.59	1.61*
V	58.4	29.2	2.0	80.3	1.16*	1.18
W	87.6	29.2	3.0	80.5	1.27*	1.30
X	116.8	29.2	4.0	80.5	1.34*	1.41

Note: * indicates the value of M_s used for theoretical plots

40

that the shock wave crosses the heat gage. Therefore, the
zero time point on each plot is the time when the shock
passed that gage. In addition to the experimental heat
transfer data, the theoretical heat transfer results for
unsteady laminar, unsteady turbulent, and steady turbulent
flows were displayed on each plot for comparison. These
theoretical results, found by utilizing the equations shown
in Chapter II, required values for T_t , P_t , and M_s to be
specified for each test condition (data set). The composite
heat transfer plot for each gage of each data set can be
found in the appendix: data sets are presented alphabetically
and gages within each set are presented from leading edge to
trailing edge.

The characteristic shape of the theoretical unsteady
laminar curves are shown in Figure 13. The shock passage
across a gage causes a theoretically instantaneous but
finite jump (increase) in the surface temperature. In
theory, an infinite heat transfer rate is produced
corresponding to the temperature jump; however, due to the
shock thickness and gage response, the heat transfer rate
immediately following the shock is high, but not infinite.
The heat transfer rate decreases rapidly from that point
since the surface temperature remains constant in the
unsteady laminar region.

As can be seen in Figure 13, the theoretical unsteady
laminar results are quite sensitive to M_s for the lower
strength shocks. The curves shown are for a 2% variation of

41
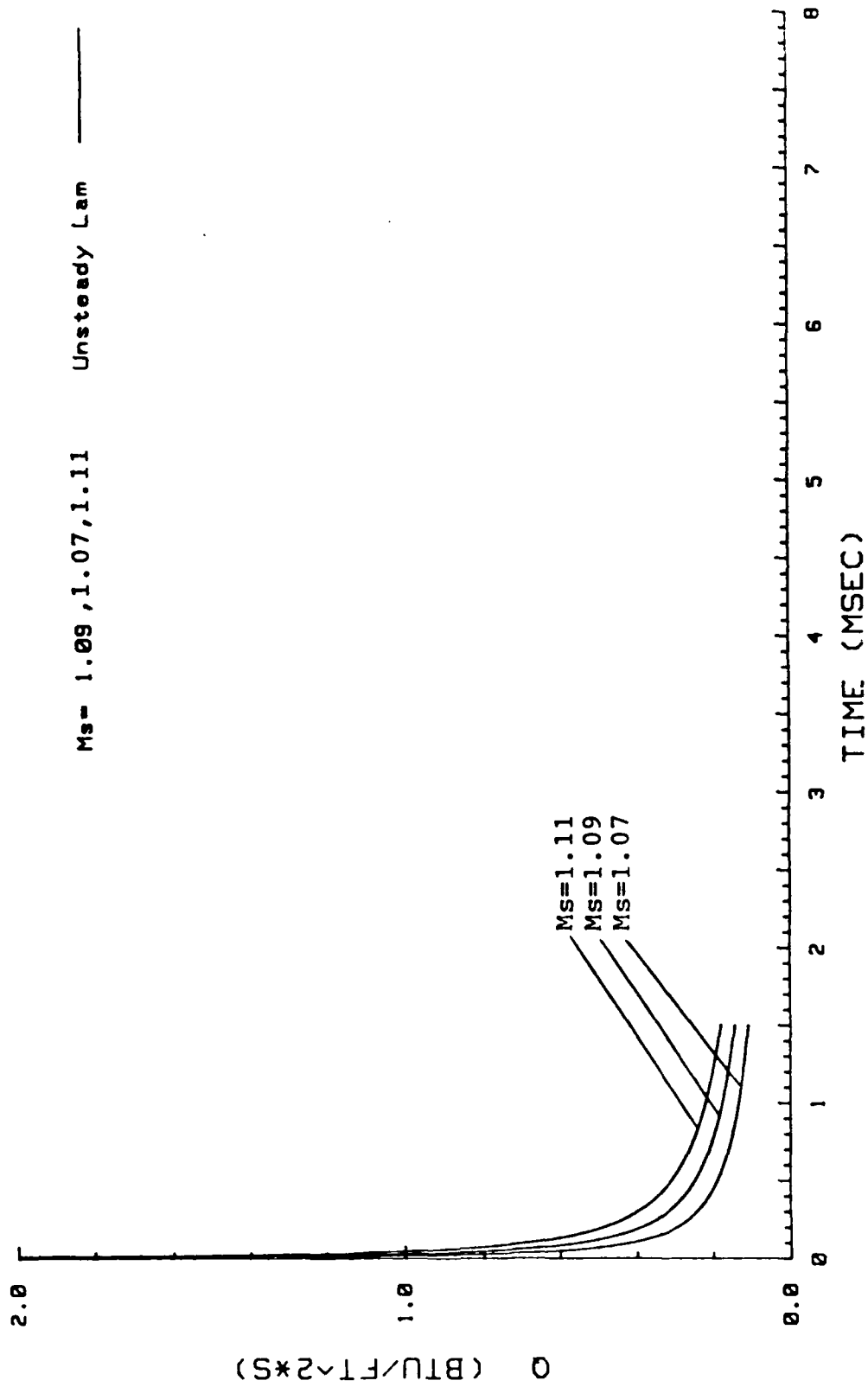
Figure 13. Effect of M_s on Heat Transfer

42

M_s about $M_s = 1.09$. Therefore, even a slight uncertainty in the value of M_s would have a significant effect on the comparison between experimental results and theoretical values for unsteady laminar flows. The theoretical turbulent equations are also sensitive to changes in M_s. Figures 183 and 184 (in the appendix) display theoretical heat transfer curves for Mach numbers of 1.17 and 1.27, respectively, versus identical experimental data. This explicitly illustrates that any comparison between experimental results and theoretical values is very dependent on the Mach number used for calculating the theoretical results. The next section explains how Mach numbers were obtained for the theoretical curves of each data set.

Mach Number Calculation

As stated earlier, each data set consisted of an average of three runs performed under identical conditions. Therefore, the Mach number for each data set was an average of the three runs, calculated in the following manner.

Data Sets A-F (Sharp Edge Forward). For the first group of runs involving the sharp leading edge while monitoring only the back half of the plate, gages 11,13, and 16 were used in the Mach number calculation. Using the MALPAK3 software, the time correlated shock passage point was located for each of the three gages and a Mach number was calculated between gages 11 and 13, 13 and 16, and

43

11 and 16 for each individual run. Then these three Mach

numbers were averaged to obtain an average Mach number for

the run. The three such Mach numbers for each data set were

then averaged to obtain the overall observed Mach number for

the data set. This averaging technique was used primarily

in an effort to minimize the impact of the sensitivity of the

M_S value with respect to the shock passage point determined

with the use of the MALPAK3 software. This observed Mach

number, M_S(obs), is listed for each of Data Sets A through F

in the last column of Table I and was used to plot the

theoretical heat transfer curves seen in the appendix,

Figures 14-55. In the sixth column is listed the theoretical

Mach number, M_S(thr), determined from the pressure ratio by

means of Eq (1). Data Sets B,C,D, and E show observed Mach

numbers quite close to the theoretical values. Data Set A

shows a relatively low observed value, but still quite close

to the theoretical Mach number considering the accuracy

tolerance we can expect from the calculation technique using

the MALPAK3 software (see Chapter IV). Only Data Set F

showed an observed Mach number in excess of the theoretical

value. It should be noted that the experimental data for Data

Set F (Figures 49-55) is indicative of a Mach number

somewhat below the observed value used to plot the theoretical

unsteady laminar curve since decreasing M_S(thr) would move

the unsteady theoretical laminar curve in line with the

experimental data. And since the theoretical Mach number is

somewhat lower than the observed Mach number, the heat

44

transfer seems to confirm the accuracy of the theoretical value and perhaps indicate an anomaly in the Mach number calculation utilizing the MALPAK3 software.

Data Sets H-U (Sharp Edge Forward). The observed Mach number calculation for the second group of sets which monitored gages spaced along the entire length of the plate was initially done in the same manner as for Data Sets A through F but using gages 1,7, and 16. But, in every case, the observed Mach number was found to be far in excess (on the order of 0.2 or more) of the theoretical value. After closer examination of the Mach number values calculated along the entire plate and for all of the sets in this group, it was found that the values would be reasonably accurate (i.e., closer to theory) if they were calculated between gages 1 and 7, and between 11 and 16, and then averaged. The values calculated between gages 7 and 11 gave unreasonably high results. For example, the initial observed Mach number calculation for Data Set K gave a value of 1.30, much higher than the theoretical value of 1.16. Therefore, Mach numbers were calculated between gages 1 and 7 and then 11 and 16 for each of the three runs in the data set. Then those two observed Mach numbers for each run were averaged to give an average Mach number for each of the three runs. These three numbers were then averaged to obtain a value of 1.13. This is the observed Mach number for Data Set K, a value which is quite close to the theoretical value of 1.16. The reader should note that the averaged observed Mach number between

gages 7 and 11 was 2.18, very much higher than theory predicts.

All of the observed Mach numbers listed in Table I for Data Sets H through U were calculated in the manner described above for Data Set K. In each of the data sets, a high value for the Mach number was obtained between gages 7 and 11 and more reasonable values were found for the front and back portions of the plate. At first it was thought that this Mach number anomaly could be due to a sampling rate error, growing with time, in the DL1200 Waveform Recorder. But a change in the sampling rate yielded similar results, indicating that the "problem" was not isolated to a specific sampling rate. The DL1200 was then replaced with a spare and a number of runs were taken, only to find very similar results. Finally, a storage oscilloscope was placed in the circuit parallel to the DL1200 and confirmed the previous results. No reasonable explanation has been found for this anomaly. Gaydon and Hurle (1963:79-80) state that the shock speed can exceed that which is expected for a particular pressure ratio, but that applies to shocks which are still in the process of forming. Since the flat plate is relatively far downstream from the diaphragm in this experiment, the shock is probably fully formed. Gaydon and Hurle go on to show that Mach number does indeed vary with distance from the diaphragm, but their data shows Mach numbers in excess of 5. Since the Mach numbers used in this study were much less than 5, one can only speculate whether there is a similar

46

variation in Mach number with distance from the diaphragm in this experimental setup without further investigation.

The theoretical heat transfer curves for Data Sets H through U (Figs. 56-164) were plotted using the value of M_s which gave results that more closely resembled the laminar region of the experimental data. By matching the unsteady laminar regions in this way, a valid comparison of the heat transfer magnitudes between the experimental and theoretical results is assured. (The results of this comparison will be detailed in the pages ahead.) The particular Mach number value used for each set is indicated by an asterisk (*) in Table I. It can be seen from Table I that the observed Mach numbers calculated for Data Sets H through U in the manner described above are reasonable considering the degree of accuracy which can be expected with the software. Data Sets H,I,J,Q,R, and U show observed Mach numbers which are in excess of the theoretical values. Of those sets, only Data Set R has some gages which have data that could possibly support the argument for a Mach number in excess of the theoretical value. Therefore, since the observed Mach number calculations do not seem to be consistently representative of the observed heat transfer results, it would be desirable in future investigations to find a means to more accurately calculate the observed Mach number. This is quite important since the observed Mach number is used to aid in comparing the experimental heat transfer results with theory and to analyze other significant correlations. A greater confidence

in the observed Mach number would be a definite asset in an attempt to accurately depict what can be expected under experimental conditions such as those used for this study. But even with values which are only "reasonably close" to theoretical values, certain trends in the data can be noted, analyzed, and become candidates for further study.

Data Sets V-X (Rounded Edge Forward). The Mach numbers for the sets done with gages spanning the flat plate with the curved leading edge, were calculated using gages 14,9,6, and 1 using the same technique as for the second group of sets. This group also showed unusually high Mach numbers in the center of the plate. The theoretical Mach numbers were used to plot the theoretical heat transfer results shown in the appendix (Figs. 165-182) since they more closely matched the Mach numbers required to produce the experimental laminar heat transfer results.

Transition

As can be seen from each heat transfer trace shown for each gage in the appendix, the heat transfer during the time immediately following the shock passage is indicative of unsteady laminar flow. By comparing traces, it can also be seen that the data seems to depart from the theoretical unsteady laminar curve at some later time, normally within a half millisecond. The precise time of departure is not always clear for a couple of reasons. First, as explained above, the experimental data does not always fall directly on

48

the theoretical unsteady laminar curve because the Mach

number used to calculate the curve, whether it was M_s(obs)

or M_s(thr), does not precisely match the one experienced

during the run. This makes it difficult to specify the time

when the data departs from the laminar regime, i.e.,

transitions to data indicative of turbulent flow. The other

reason for a less than precise determination for transition

time is that some data appears to depart from the theoretical

laminar curve, but later return to the laminar curve for a

brief time before definite transition to turbulent flow

occurs. In an effort to be consistent in determining

transition times from the traces, transition is defined here

as being the time when the experimental data first appears to

leave the laminar regime, i.e., when the heat transfer data

indicates that the gage is first experiencing something

other than purely laminar flow. An argument can be made for

defining the transition time as the time at which the flow

definitely goes fully turbulent and that may be useful. But

for analysis in this study, transition time will be defined

as stated above.

With this in mind, transition times were determined for

each heat transfer plot and a range of transition times (Δt_t)

was determined for each data set. For example, Data Set A

showed transition times ranging from 0.05 msec (for gages 14

and 16) to 0.15 msec (for gage 11 and the thermocouple),

yielding Δt_t =0.10 msec. These values are listed in Table II.

Also listed in that table are values for U_∞ for each data

49

TABLE II

Gage Transition Time / Heat Transfer Ranges

Data Set	U_∞(ft/sec)	Δt_t (msec)	ΔRe_t ($\times 10^{-4}$)	ΔRe_s ($\times 10^{-5}$)	P_4/P_1
J	198	.58	2.6-19.4	2.3-26.8	1.6
Q	198	.42	1.9-12.0	1.9-22.2	1.6
K	232	.20	2.1-10.4	2.8-32.3	2.0
N	232	.16	2.1-8.7	2.8-32.3	1.8
E	250	.33	3.2-15.2	2.2-26.0	2.0
C	251	.35	2.4-10.6	2.9-34.5	2.0
I	282	.01	3.3-3.7	2.2-26.9	2.0
H	282	.07	3.9-7.3	2.6-30.6	2.0
A	283	.10	3.1-9.4	3.4-39.5	3.1
V	283	.11	5.8-12.9	8.3-40.4	2.0
D	334	.07	4.0-9.5	3.5-41.6	2.8
O	380	.13	6.6-23.6	5.1-59.3	2.5
R	380	.02	7.6-9.5	3.7-43.2	2.5
P	458	.09	4.2-22.9	6.5-75.9	3.5
W	458	.02	41.2-72.2	15.3-75.0	3.0
L	488	.13	19.6-51.5	7.1-82.8	3.0
F	504	.12	14.9-34.7	4.6-53.6	2.0
B	506	.11	9.6-42.1	5.3-62.0	3.4
M	563	.04	21.3-35.4	8.6-100.7	4.0
X	564	.08	28.1-87.7	20.3-99.6	4.0
S	761	.05	17.7-47.1	9.7-113.9	7.0
T	843	.08	14.2-71.2	10.2-120.0	8.2
U	936	.06	36.6-91.5	11.4-133.3	9.4

set. It should be clearly understood that these U_∞ values are based on the Mach number which was used to plot the theoretical unsteady laminar curve for each individual data set (but, recall that this Mach number is the one that best seemed to fit the experimental data). In addition, columns four and five of Table II consist of the range of transient Reynolds numbers (ΔRe_t) and the range of steady Reynolds numbers (ΔRe_s), respectively. The transient Reynolds numbers listed are defined by Eq (18) and utilize the transition time in order to show the ranges of transient Reynolds numbers for a data set, evaluated at the time of transition. The steady Reynolds number is defined by Eq (10).

Data sets are listed in order of increasing values of U_∞. When done in this manner, it is possible to observe a value of U_∞ where Δt_t appears to significantly decrease from the magnitude observed for preceeding values. At values of U_∞ of 251 ft/sec and below, the average value for Δt_t is 0.34 msec, and at values for U_∞ above 251 ft/sec, $\Delta t_t = 0.08$ msec. This seems to indicate that above a threshold value of about 250 ft/sec for U_∞, each location on the plate may be experiencing transition to turbulent flow at approximately the same time (referenced to shock passage at that particular location) as all other locations on the plate. A constant transition time (or even a narrow interval of transition times like those experienced here) would yield an orderly transitioning of gages from front to back, as the flow follows the shock down the plate. This implies that

51

transitioning is occurring due to some mechanism associated with the unsteady boundary layer behind the shock since any leading edge influence would cause an increasing difference in transition times between the gages.

Using a threshold value of 251 ft/sec, Table II shows that some data sets which have free stream velocities above that threshold value possess steady Reynolds numbers below what is normally expected for transition to turbulent flow over a flat plate. This supports the argument that transition is associated with the unsteady boundary layer.

At U_∞=251 ft/sec and below, the range of transition times within each data set are significantly larger than the ones with U_∞ greater than 251 ft/sec, although one gage in a data set may be mainly responsible for the large range in times. This yields transitions which are not very orderly down the length of the plate. Each of the data sets with values of U_∞ equal to or below 251 ft/sec were checked for the possibility of leading edge influence on transition; the location of the leading edge disturbance was found by multiplying the transition time by the value for U_∞. Only one instance occurred where the leading edge disturbance was in the vicinity of the gage in question at the time of transition. This occurred in Data Set E at the location of the thermocouple, where this location experienced a transition time of 0.42 msec, a time far in excess of the transition times exhibited by other gages in the set. Since no other gages in this group of sets below the threshold U_∞

52

exhibited the possibility of being influenced by the leading edge disturbance, any purported influence correlation would be very speculative without further study.

It must be understood that the apparent threshold value of about 250 ft/sec is based upon the Mach number which was used to plot the theoretical unsteady laminar curve. And as was stated previously, this Mach number has a degree of uncertainty associated with it. Any attempt to assign a specific value to the threshold under these conditions would be quite presumptuous and misleading. The value of 250 ft/sec is used here only from the context of the data presented, with uncertainties inherent throughout. But a threshold, whatever the value, seems to exist nevertheless.

The results stated above agree quite nicely with Smith, although he did not mention the possibility of a threshold value for U_∞. He stated that transition seemed to occur "at the same time after shock passage at axial positions a sufficient distance from the leading edge." He also concluded that "the leading edge appeared to delay the onset of transition" at gages close to the leading edge; no such claim is made here, with the possible exception noted above.

Heat Transfer

One very important point must be made at this time. Since the averaged voltage data plots were digitized by hand, the resulting curves are not exact. Slight variances may exist from the actual data which, experience shows, can create significant alterations to the final heat transfer

53

plots. Although the digitizing was done as meticulously as possible, the resulting data sets can only realistically be treated as close approximations to the actual event. Heat transfer magnitudes and trends can be observed with much confidence, but minor fluctuations in the trace should not be viewed as indicating a trend. For this reason, computerized digitizing is recommended for future studies of this kind.

It should be noted that the thermocouple almost always showed higher heat transfer rates than the heat flux gages. And with only one exception, in all data sets for which the thermocouple was used (A-R), the magnitude of the heat transfer rates recorded by the thermocouple after transition had clearly occurred were in excess of the theoretical turbulent (steady and unsteady) values. For those same data sets, the heat flux gages, for the most part, also showed rates in excess of theory. However, there were some heat flux gages in those same data sets which did show heat transfer rates which matched theoretical steady or unsteady turbulent values; e.g., Data Set O (Figs. 112-119) shows gages 1,11, and 16 experiencing heat transfer rates close to theoretical unsteady turbulent values and gages 2 and 13 exhibiting rates matching theoretical steady turbulent flow.

Smith found similar results to the ones described above. In fact, he listed three possible explanations for the heat transfer rates, obtained from Dillon. These involved large transitional eddy influences and the possibility of a

significant influence due to the flat plate wall conditions. The mixing action of transition may make wall temperature a larger influence than previously expected. Macmullin (1986) showed that by inducing free stream turbulence in the flow over a flat plate, turbulent values for heat transfer were evident at Reynolds numbers normally associated with laminar flow. These values were higher than those associated with turbulent flow over a flat plate with no induced free stream turbulence. It is, therefore, quite possible that free stream turbulence may be contributing to the heat transfer rates and transition times observed in experimental setups such as the one in this study. Further investigation involving the measurement of free stream turbulence and its possible correlation with transition and increased heat transfer rates is recommended.

Expanding on this idea further, an interesting observation can be made concerning the data sets which utilized the sharp leading edge flat plate (Data Sets A through U). Recall that the Mach number used to plot the theoretical heat transfer curves was the one that seemed to best match the experimental results in the unsteady laminar region (the only exception was Data Set F). Examination of the heat transfer plots for Data Sets A-U (Figs. 14-164) show that experimental results match quite closely with theoretical turbulent values for most gages (after transition has clearly occurred) when this Mach number was approximately 1.22 or greater. For Mach numbers less than 1.22, the

experimental heat transfer values were greater than theoretical predictions for most gages, although some matching did occur.

All three data sets which utilized the rounded leading edge flat plate (V,X, and W), with Mach numbers ranging from approximately 1.16 to 1.34, indicated experimental heat transfer rates equal to or less than theoretical values. It is interesting to note that for this plate configuration, the Mach number value of 1.16 produced experimental results which matched theory when the same Mach number value for the sharp edge flat plate produced heat transfer values in excess of theory. Since data in this configuration was quite limited in this study, additional investigation is required in order to observe if a threshold Mach number similar to the one indicated for the sharp edge configuration is to be found. This data indicates that a change in leading edge geometry influences the magnitude of heat transfer along the plate. Exactly how this occurs is unclear at this time and further study is highly recommended.

Another interesting observation can be made concerning heat transfer magnitudes, but this time with respect to gage location. For each of the data sets taken over the entire sharp edge plate (A-U), the heat transfer magnitudes are seen to be increasing from gage 1 through gage 4. Then, the heat transfer rates decrease in magnitude starting with gage 7 and continuing to gage 16 (gage 16 in some cases indicated an increase from the value exhibited by gage 13). This trend was

observed in each of the Data Sets, H-U, indicating a correlation between heat transfer rate and axial location on the flat plate for the sharp edge configuration (see Figure 185 in the appendix). For Data Sets A-F (sharp edge, back half gages), a very similar trend can be observed with a slight deviation. Recall that these sets utilized gages 11 through 16. Generally, gages 13 and 14 indicated slight increases in heat transfer magnitudes, but gages 12,15, and 16 showed decreasing values. The increasing magnitudes for gages 13 and 14 were slight and therefore may be obscured in Data Sets H through U because of the fact that gages 12 and 14 were not monitored in those sets. Since Data Sets A through F indicate a more complex variation of heat transfer magnitude with respect to axial plate location, further study is required in order to precisely determine the nature of that variation. But from this study, one can conclude that such a variation does exist for the sharp leading edge plate; it is consistent between data sets and does not seem to be influenced by Mach number. Data Sets V,W, and X (for the rounded edge flat plate) do not seem to show the same trend, but it must remain clear that the data for this configuration is quite limited. Data Sets W and X revealed constant heat transfer magnitudes for the sensors closest to the leading edge and an increasing magnitude for gage 4 (located on the back half of the plate in this configuration), followed by a decrease in magnitude at the trailing end. Data Set V indicated increasing heat transfer rates on the front half of

the rounded plate and decreasing magnitudes thereafter, except for the increase exhibited again by gage 4. Further study is necessary for better understanding of any existing correlation between heat transfer rates and axial location on the rounded leading edge flat plate.

One final observation can be made regarding heat transfer magnitudes. Most heat transfer traces exhibited wavering values of heat transfer after transition had already taken place. These wavering values seemed to adhere to similar time periods when comparing traces within a data set. This possible periodicity cannot be studied in detail within this investigation primarily because digitizing by hand could obscure or alter any existing trends. But further studies on this possibility can be accomplished using computerized digitizing, and are recommended.

Since the heat transfer plots are very sensitive to the digitized trace and since the digitizing was done by hand, some slight fluctuation in the heat transfer data may be evident even though exact digitizing may have produced an unwavering curve. For that reason, a positive confirmation of Davies' assertion, that for $\alpha < 0.3$ steady heat transfer is observed, is not entirely possible. But for those plate locations which allowed test times for which values of $\alpha < 0.3$ could be obtained, as long as the free stream velocities were low, Davies' prediction seems to hold. Computerized digitizing would aid greatly in testing Davies' claim.

VI. Conclusions

Consideration of the results of this investigation lead
to the following conclusions:

1. There appears to exist a threshold free stream velocity
above which yields transition times, for all locations along
the plate, which are confined to some narrow interval. This
would provide an orderly transition to turbulent flow along
the plate, front to back.

2. There appears to be no influence on transition due to the
leading edge disturbance. Transition almost always occurred
when the leading edge disturbance was still far upstream.

3. For the sharp leading edge flat plate, shock Mach numbers
below approximately 1.22 generally produce heat transfer
magnitudes after transition in excess of theoretical
turbulent values. For Mach numbers of 1.22 and above, the
experimental data appears to match theoretical results quite
well.

4. The limited data presented indicates that the rounded
leading edge flat plate produces turbulent heat transfer
magnitudes equal to or less than theoretical turbulent
values for Mach numbers of 1.16 and above. This indicates
that leading edge geometry influences the magnitude of heat
transfer to the plate.

5. Results indicate that there exists a variation in heat
transfer magnitudes with respect to axial location along the
sharp leading edge flat plate, consistent between data sets

and not correlated with Mach number. No consistent variation
is evident for the rounded leading edge flat plate, based on
the limited data of this study.

6. Davies' assertion, that for $\alpha < 0.3$ steady heat transfer
will be observed, could not be verified or refuted.

VII. Recommendations

1. High speed, high quality motion pictures of the shock wave transversing the entire length of the flat plate would aid greatly in the effort to understand what is occurring at the surface of the plate. This would help in understanding the Mach number questions generated by this investigation.

2. To aid in understanding the mechanism behind transition and the variation of heat transfer rates encountered in this study, it would be beneficial to devise a means to measure free stream turbulence at all times during the flow.

3. For studies where digitizing of data is necessary, obtain or create the software necessary to enable the work to be done by computer.

4. Continue the rounded leading edge flat plate studies and relate the results to the findings of this study of both plate configurations. Specifically, check for correlations between such parameters as free stream velocity, shock Mach number, transition, free stream turbulence, and heat transfer magnitude.

5. Perform detailed investigations into the correlation between heat transfer magnitudes and axial plate locations by monitoring heat transfer at closely spaced positions cn the sharp and rounded edge flat plates.

Appendix: Heat Transfer Results

Figures 14 through 182 display the reduced heat transfer data and, for the experimental flow conditions, the predicted heat transfer values for unsteady laminar, unsteady turbulent, and steady turbulent flows versus time since shock passage. Each figure represents the results for one gage of a particular data set; this information is clearly specified in each figure's caption. Data Sets A through F, Figs. 14-55, display the results for the sharp leading edge configuration of the flat plate and utilized the thermocouple and heat flux gages 11,12,13,14,15, and 16. Data Sets H through U, Figs. 56-164, used the same plate configuration and gages 1,2,4,7,11,13, and 16; in addition, the thermocouple was used for Data Sets H through R, but was inoperative for Data Sets S,T, and U. Finally, Data Sets V,W, and X, Figs. 165-182, utilized the rounded leading edge flat plate configuration and gages 14,12,9,6,4, and 1 (with gage 14 closest to the leading edge).

Figures 183 and 184 display how the theoretical heat transfer curves are affected by a change in Mach number. (The experimental data for each figure is identical.) Figure 185 displays the heat transfer variation versus axial gage location (with Mach number as a parameter) for the sharp leading edge flat plate.
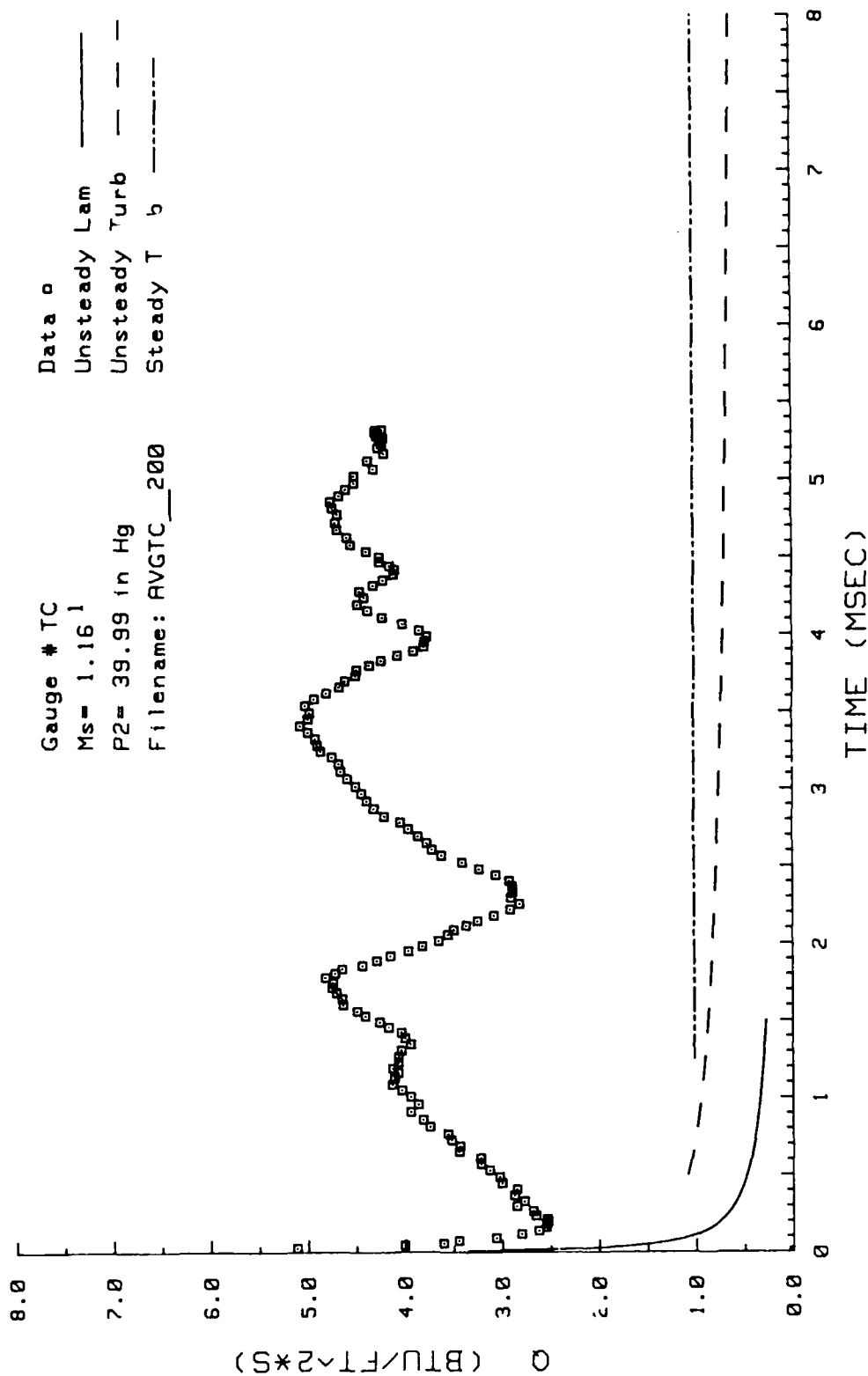
Figure 14. Heat Transfer: Data Set A Thermocouple
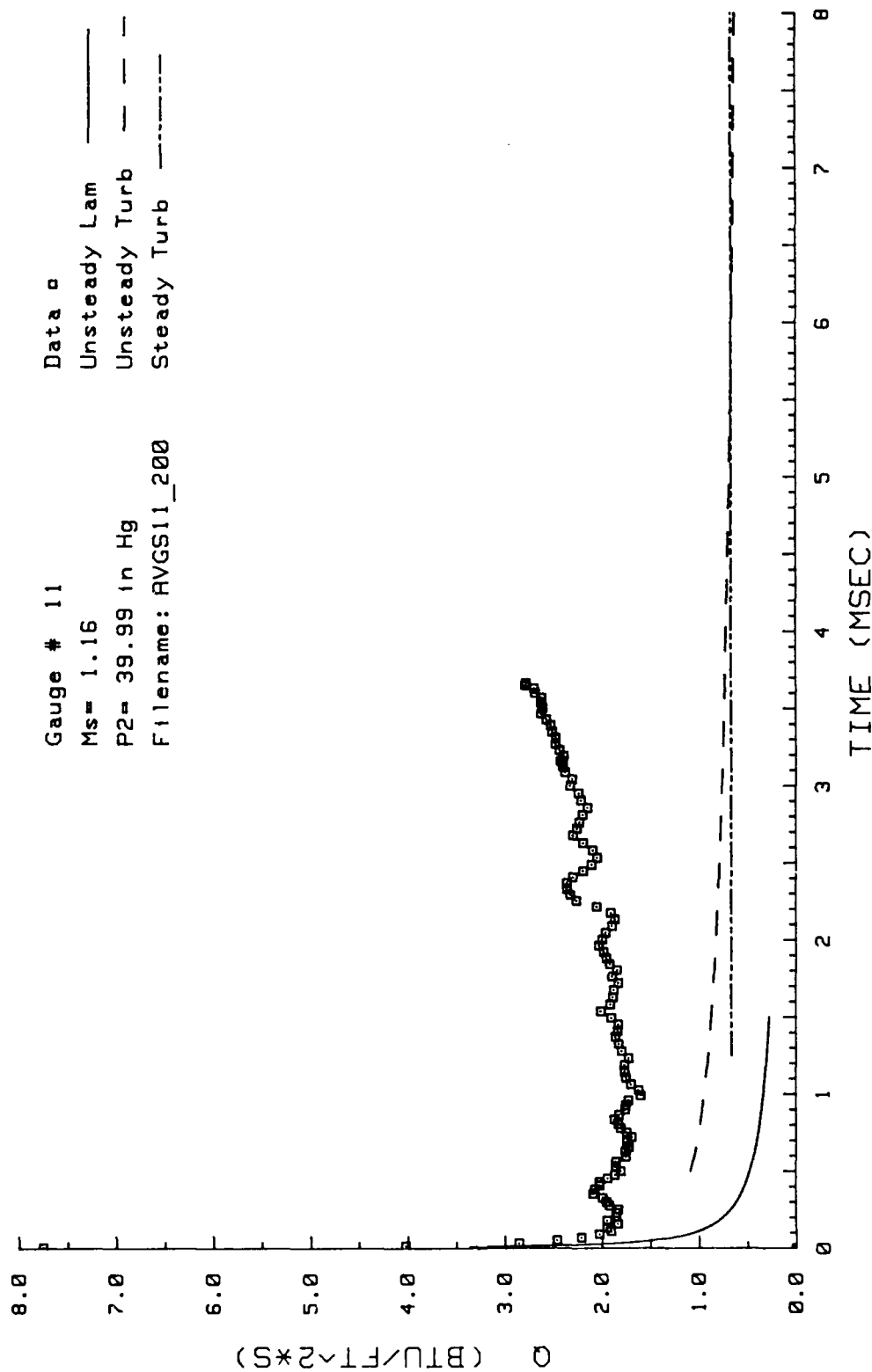
Figure 15. Heat Transfer: Data Set A Gage #11
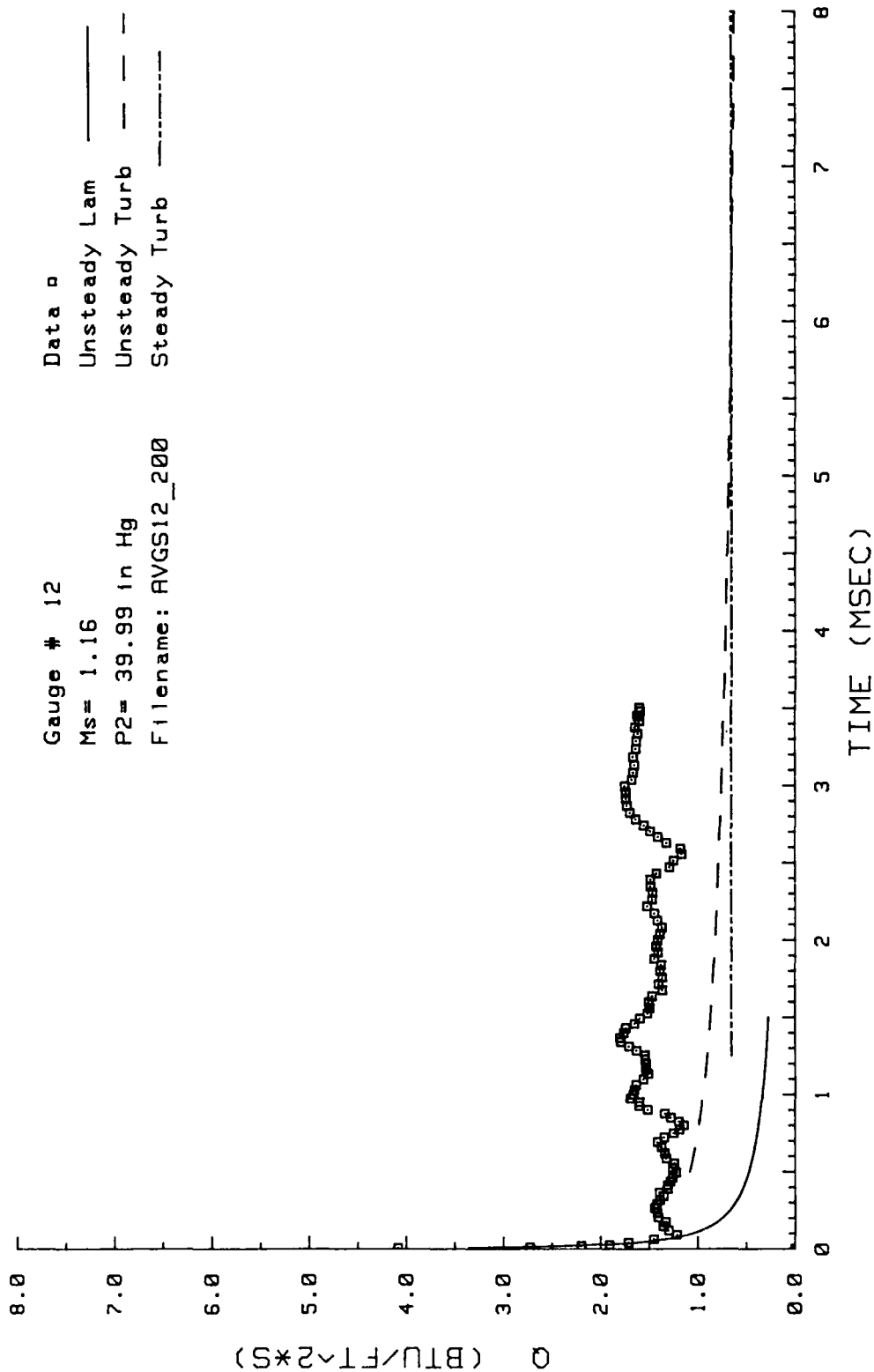
Figure 16. Heat Transfer: Data Set A Gage #12
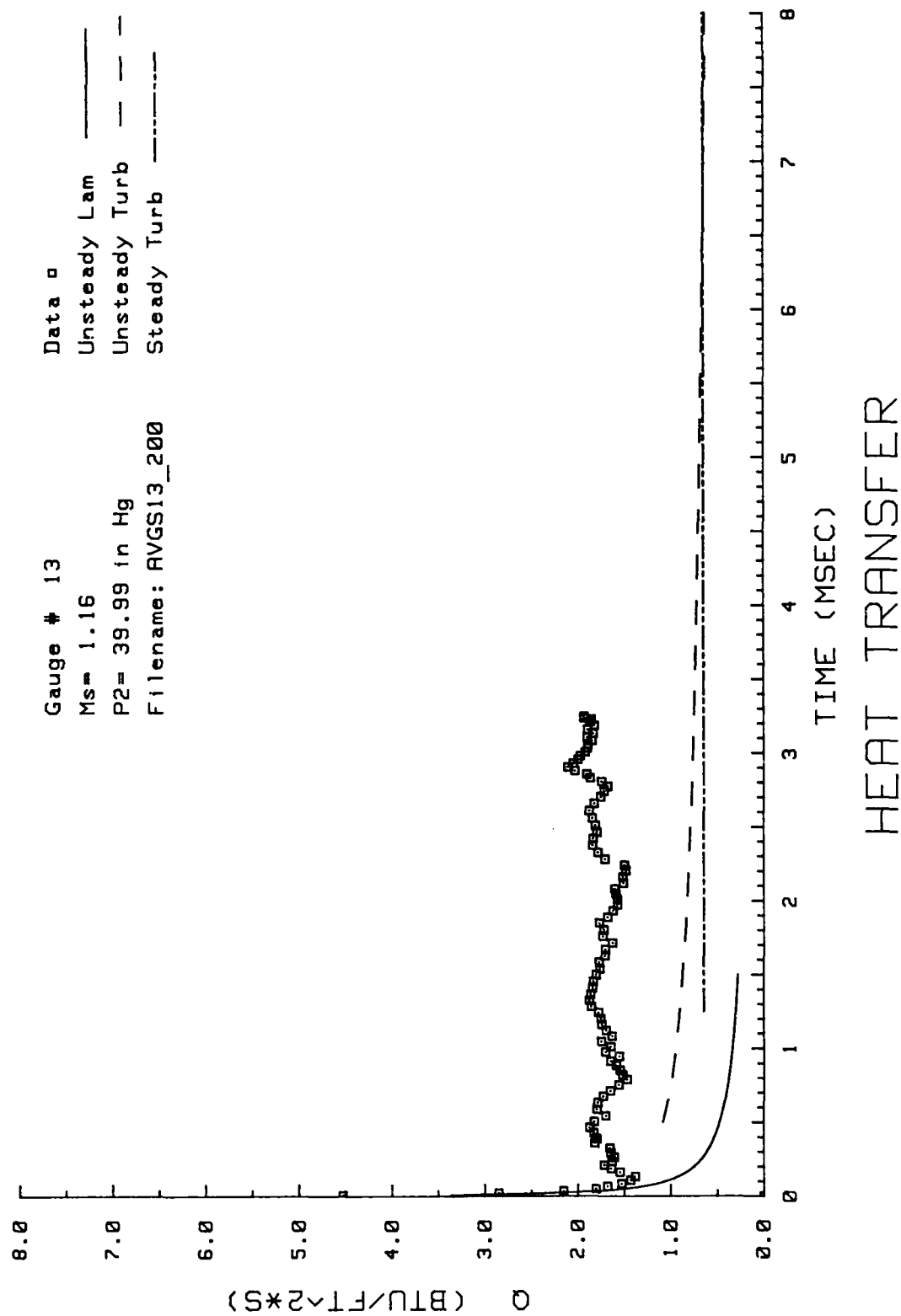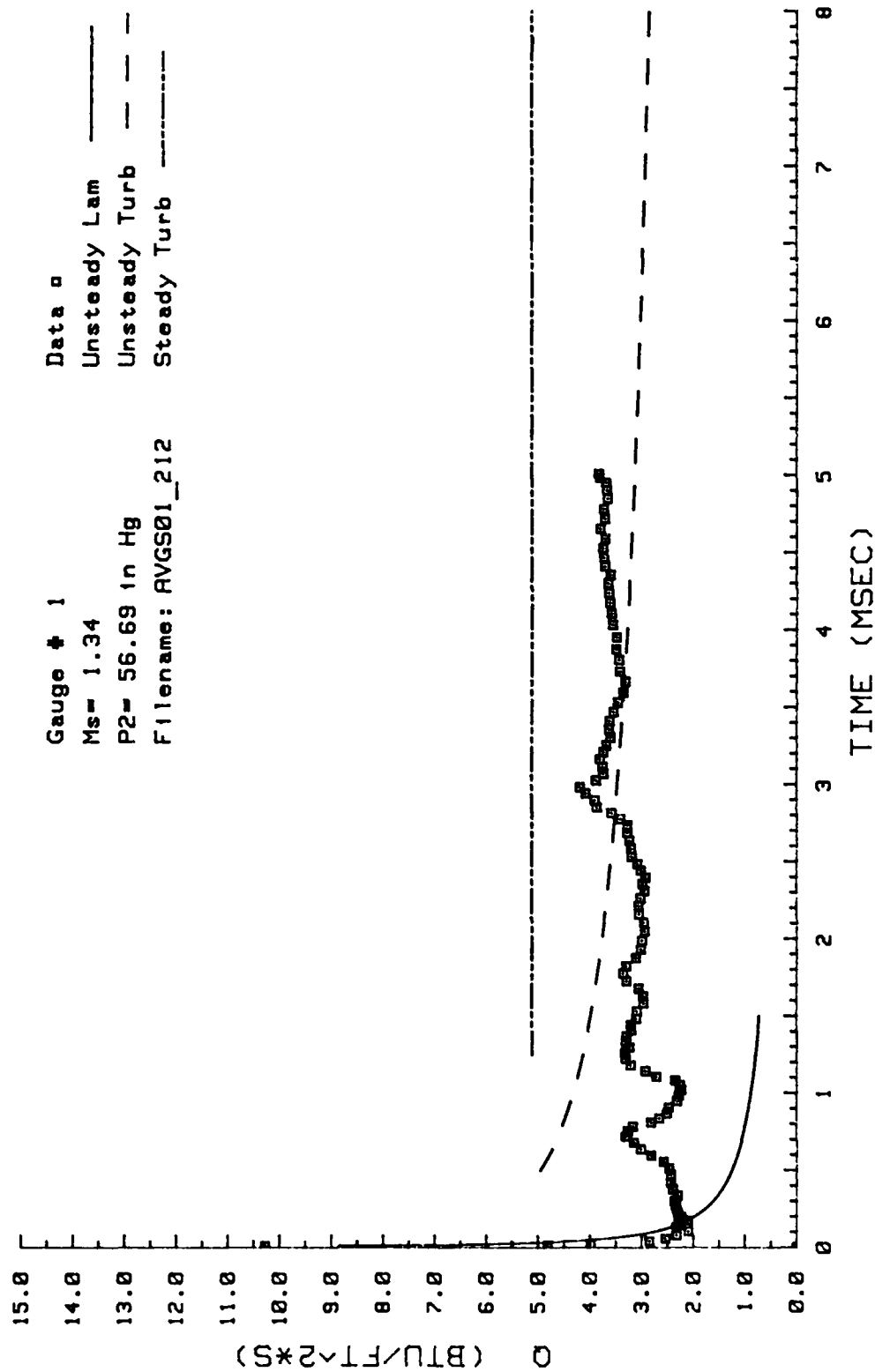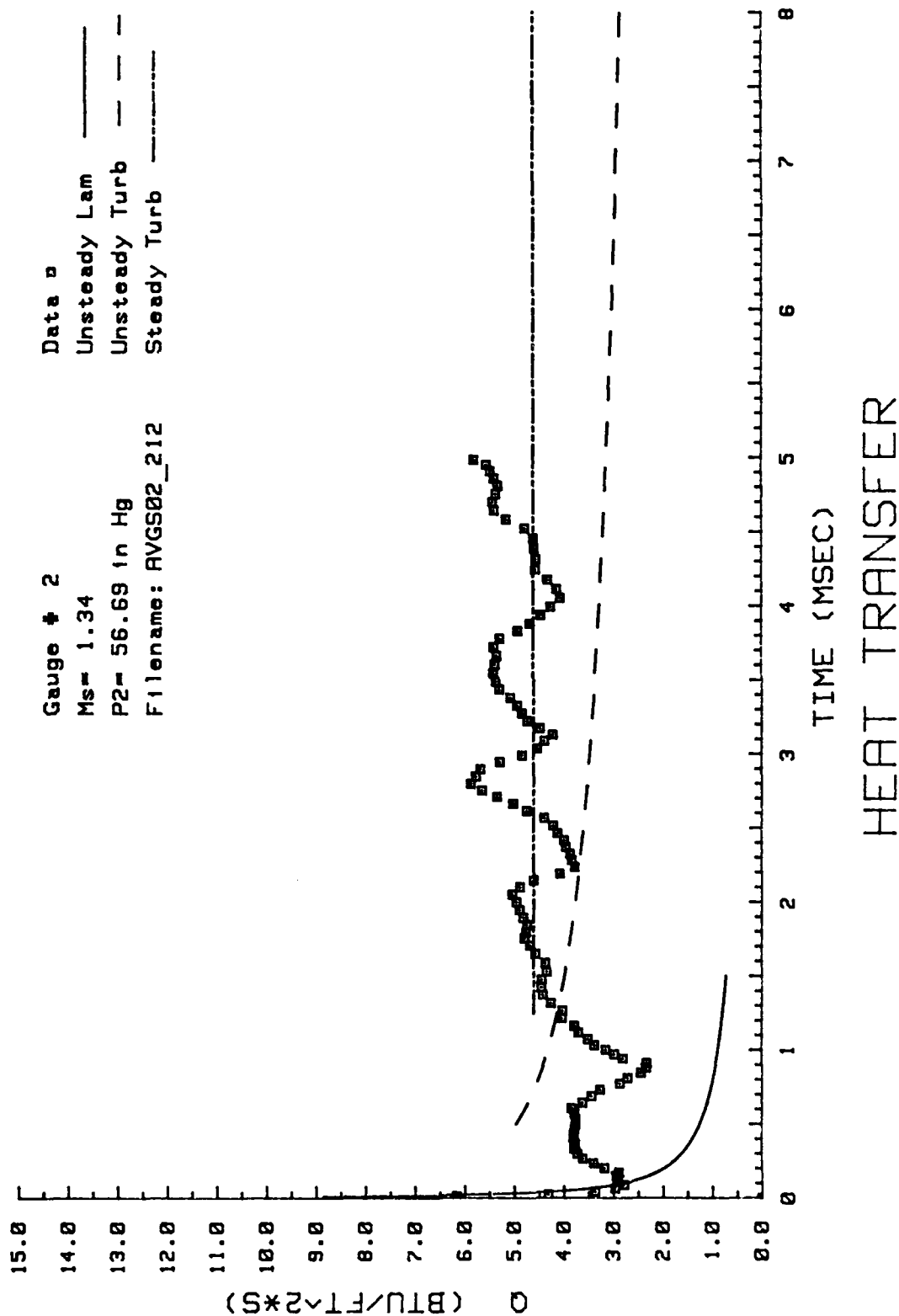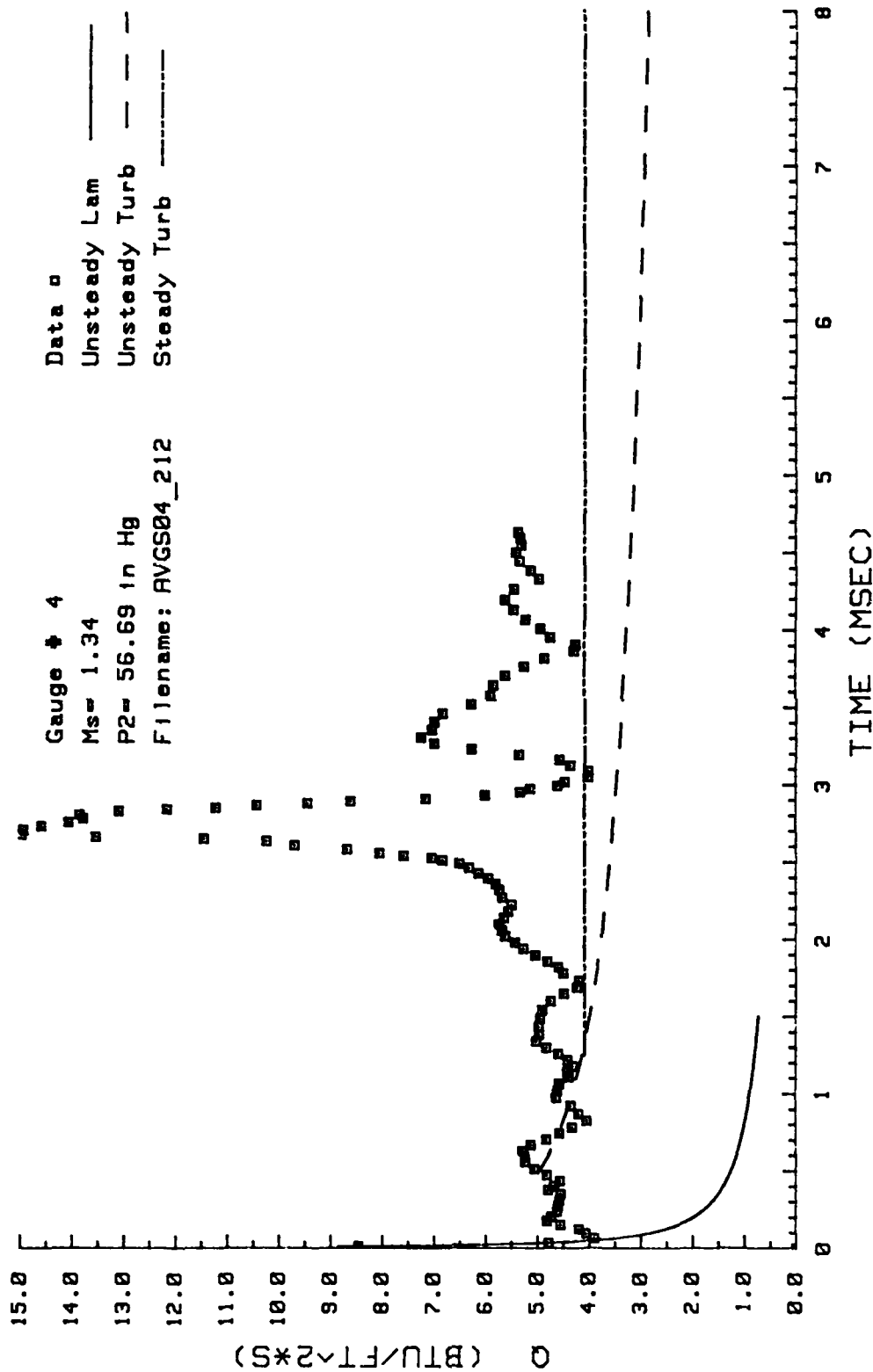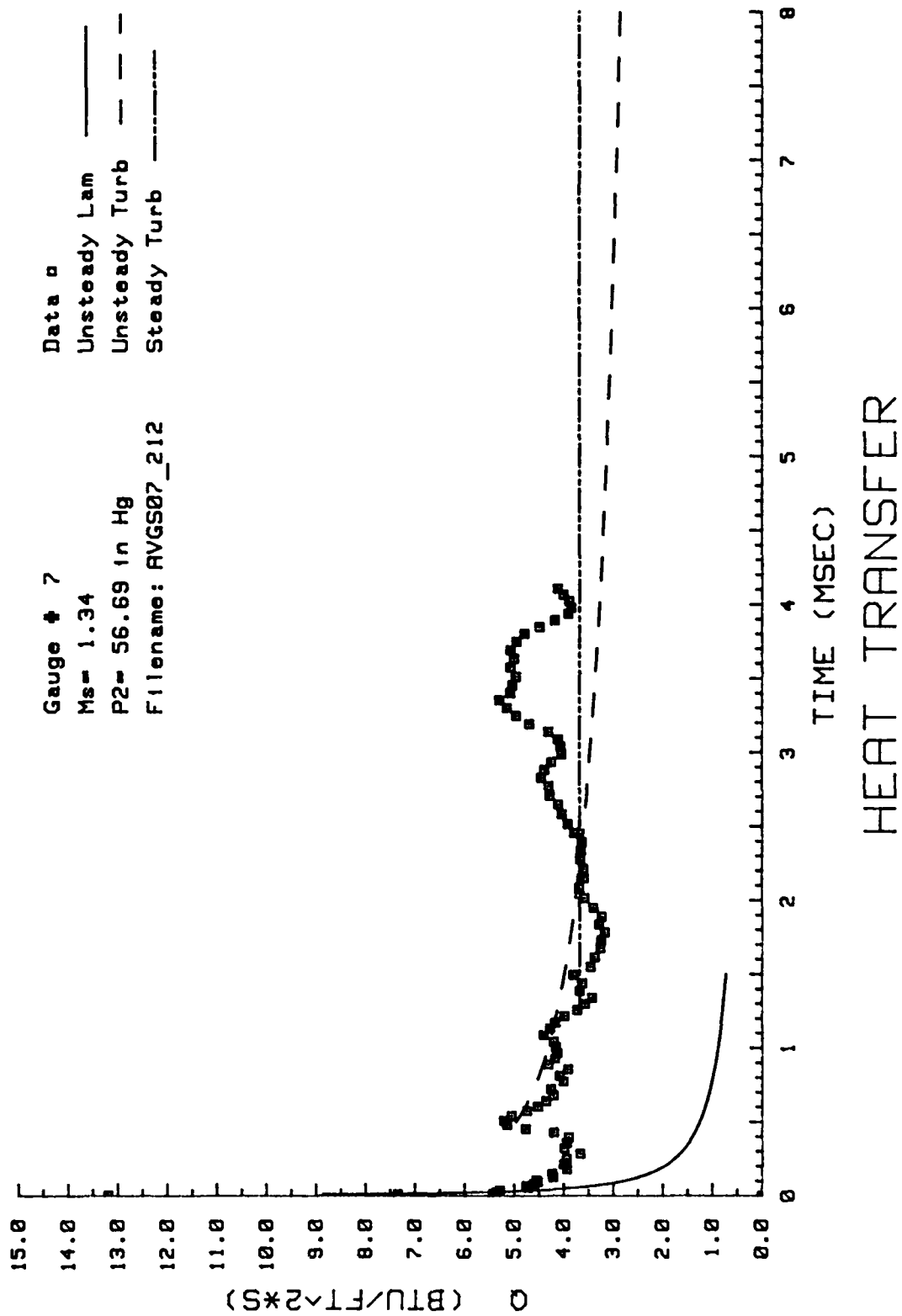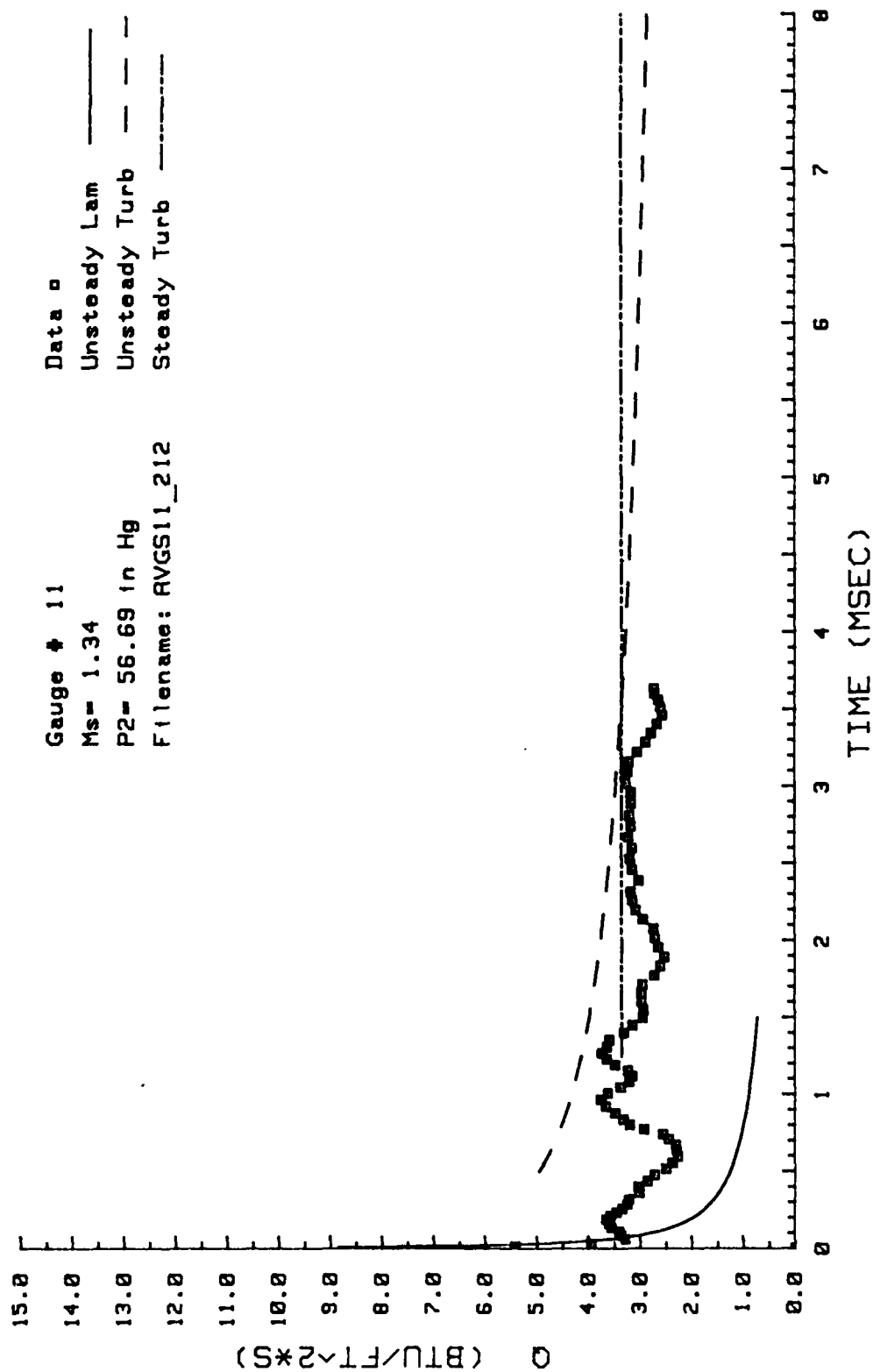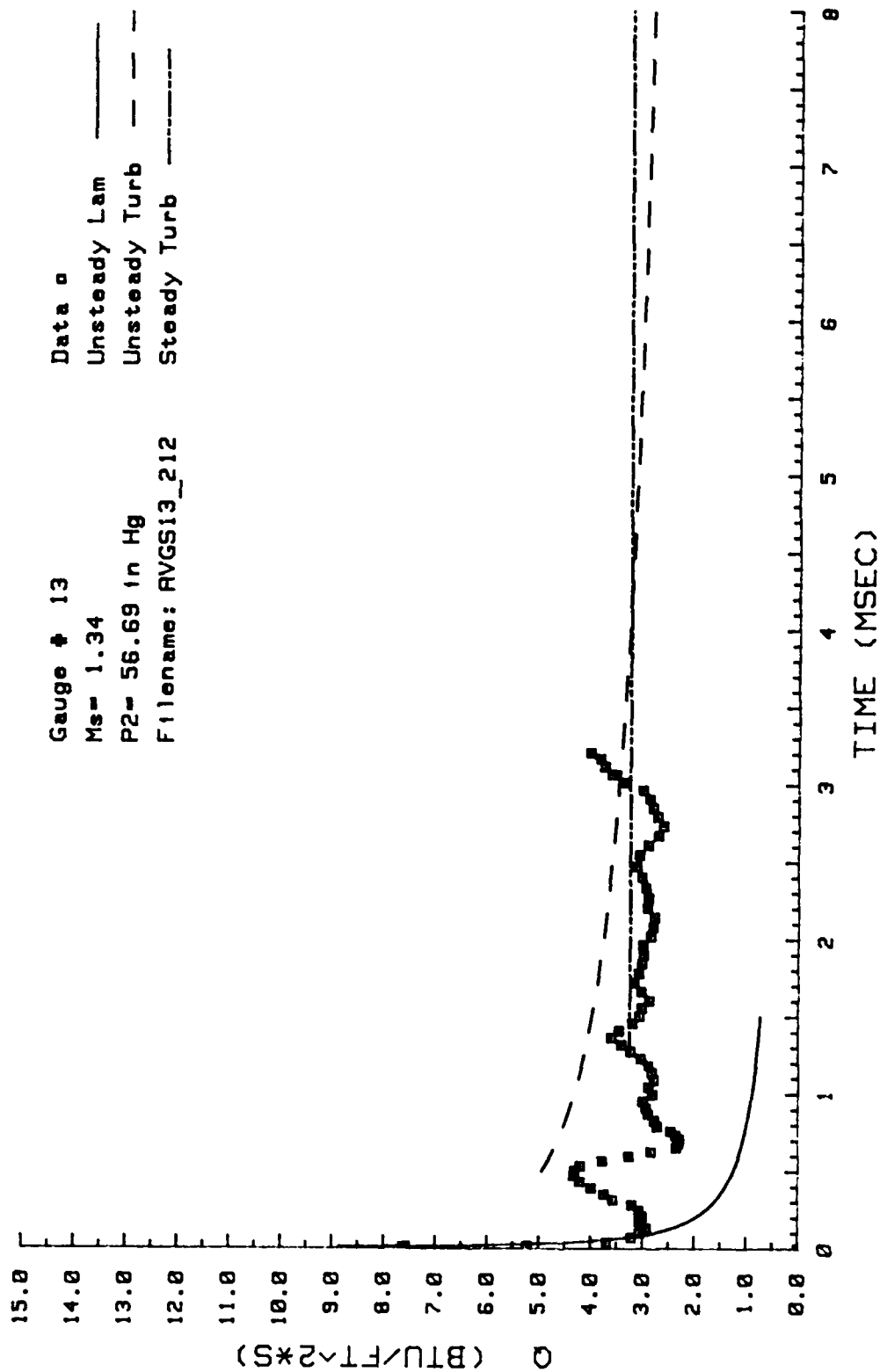
Figure 17. Heat Transfer: Data Set A Gage #13
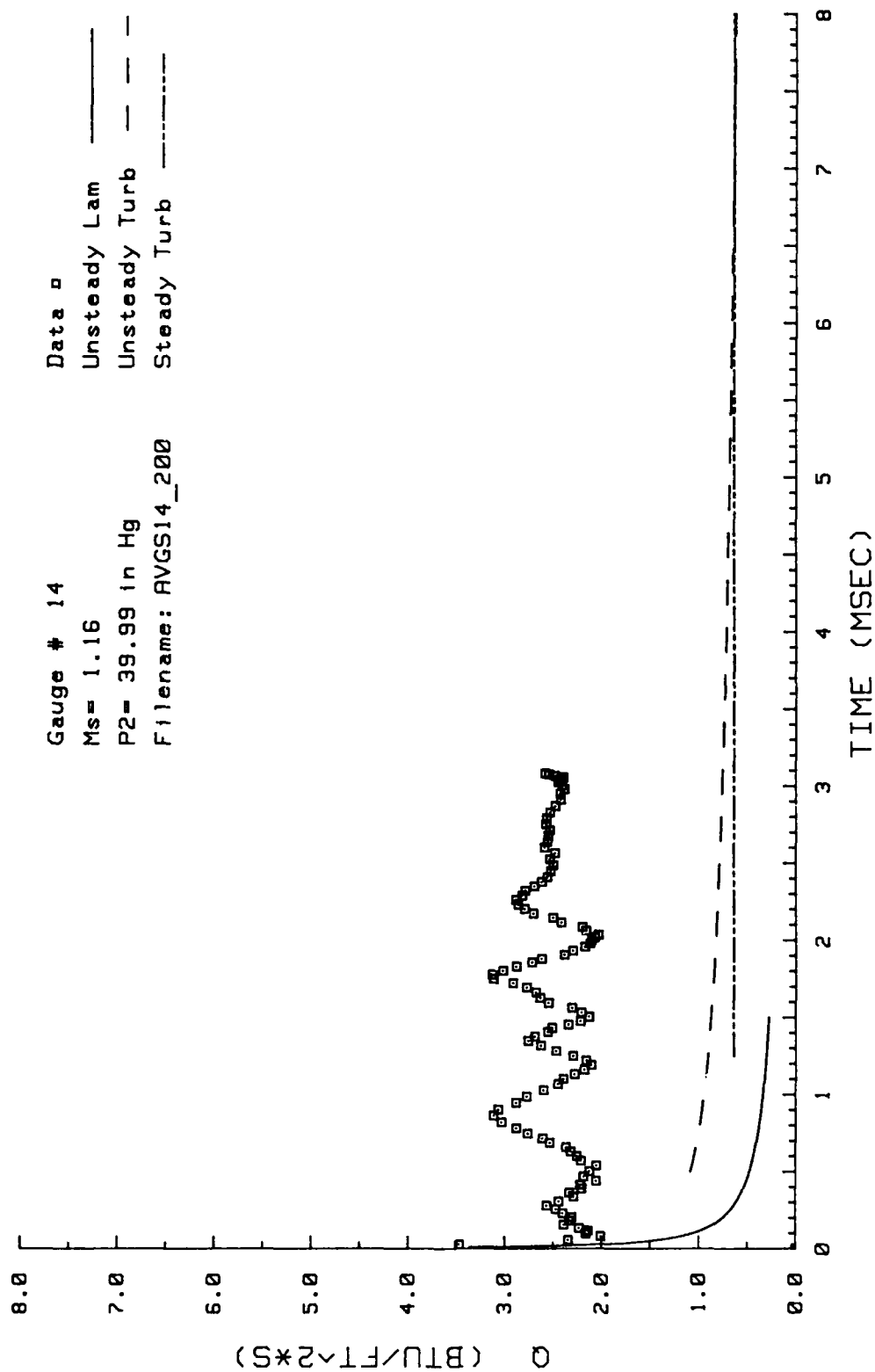
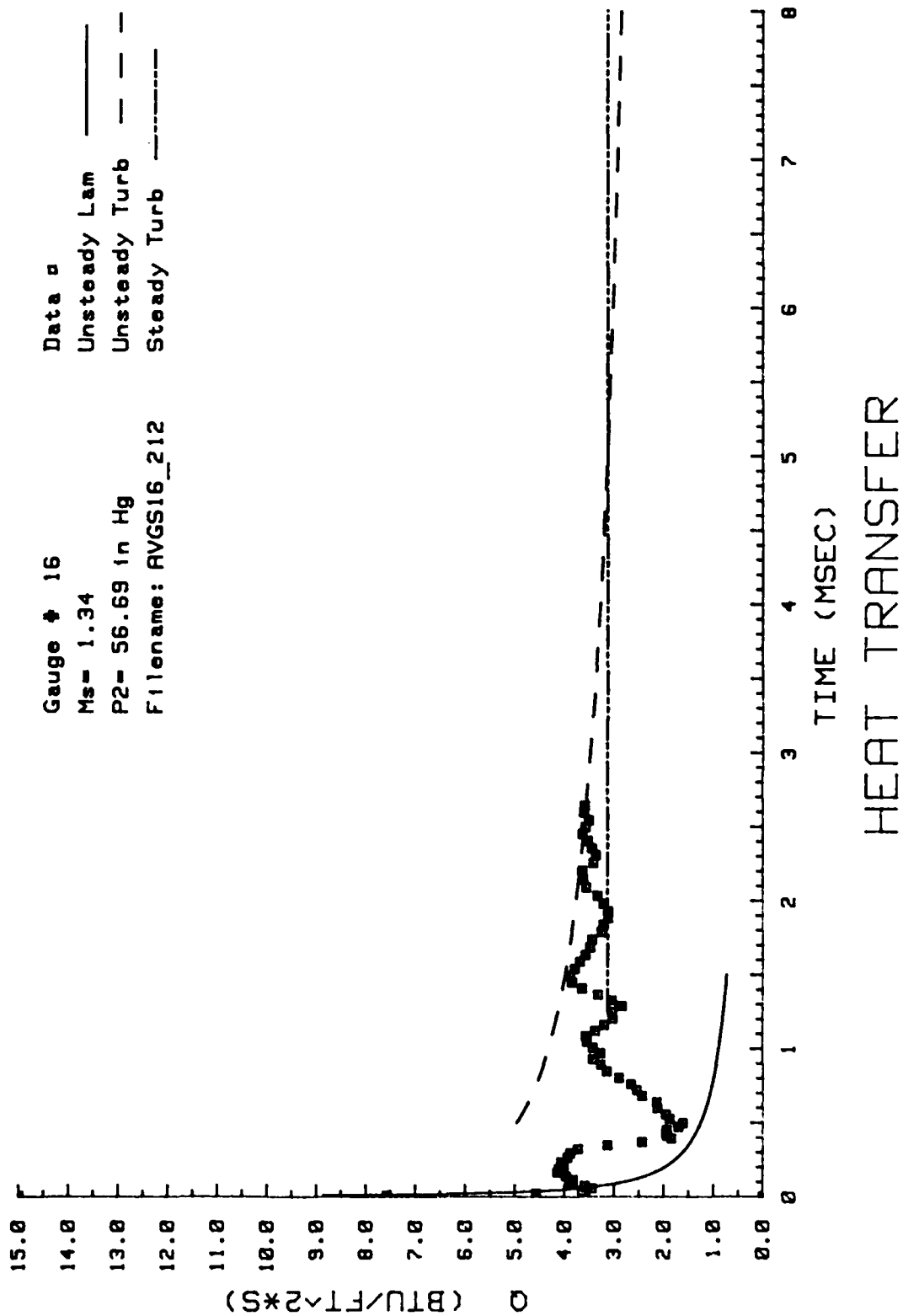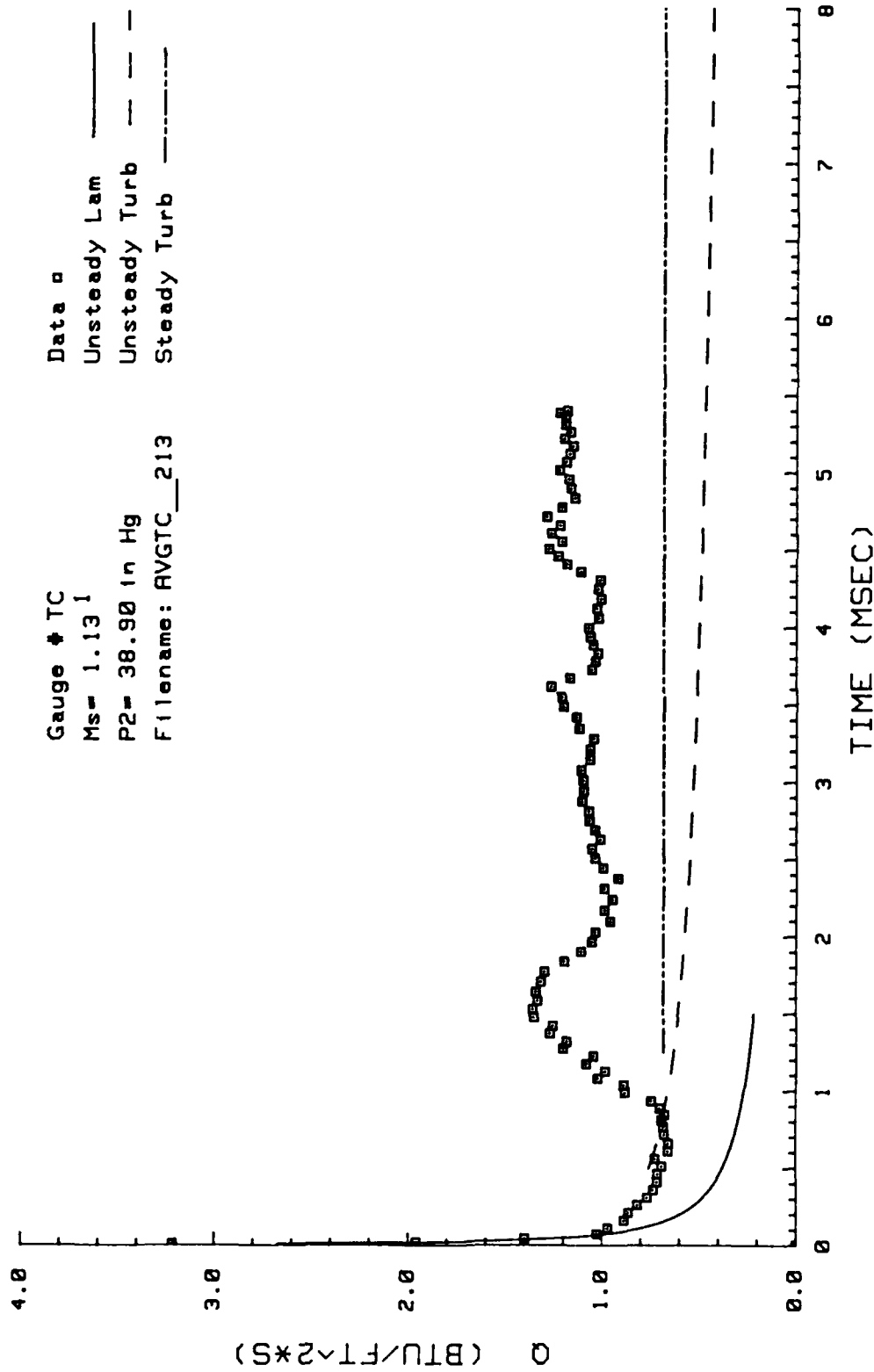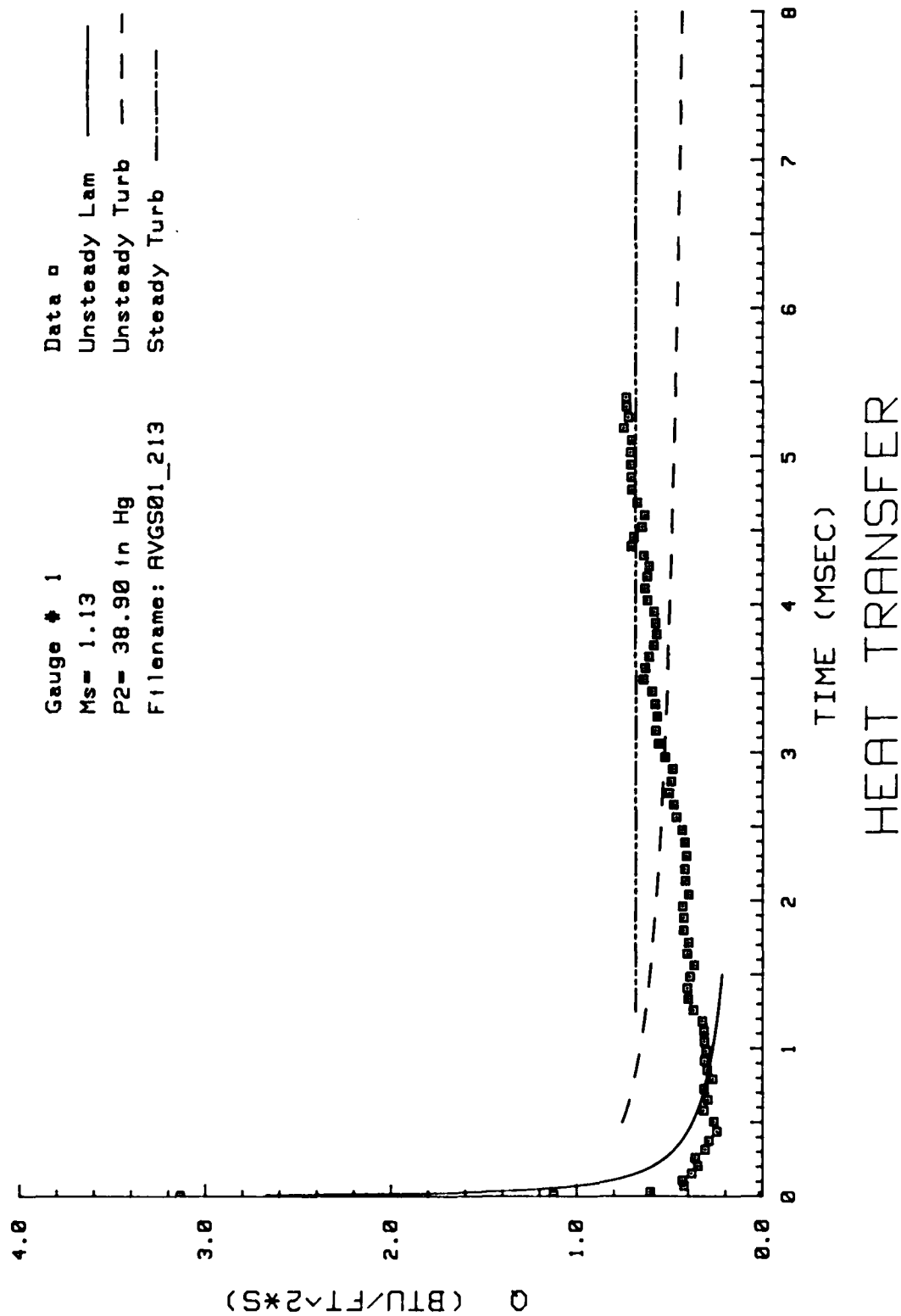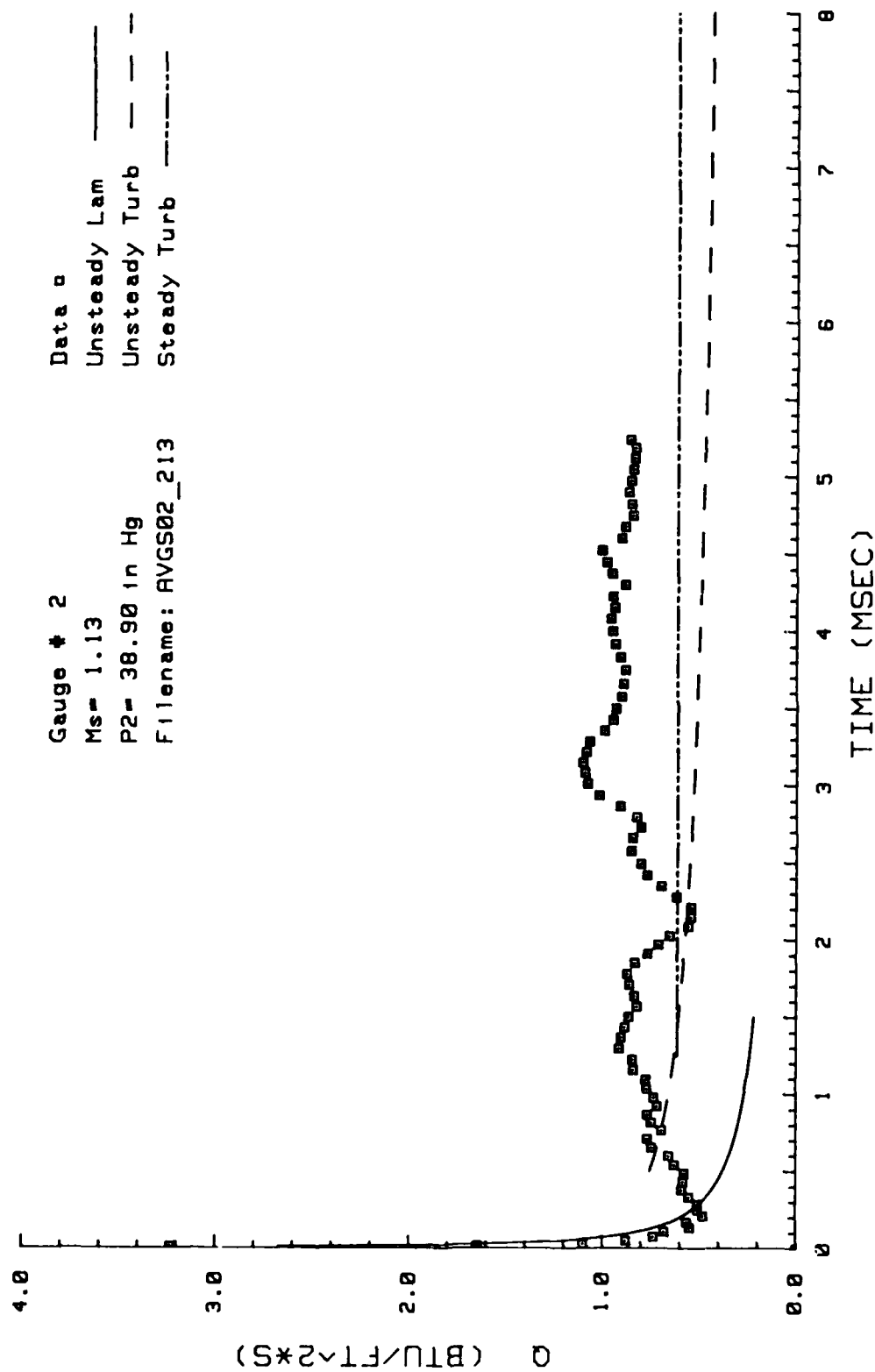Figure 18. Heat Transfer; Data Set A Gage #14

67
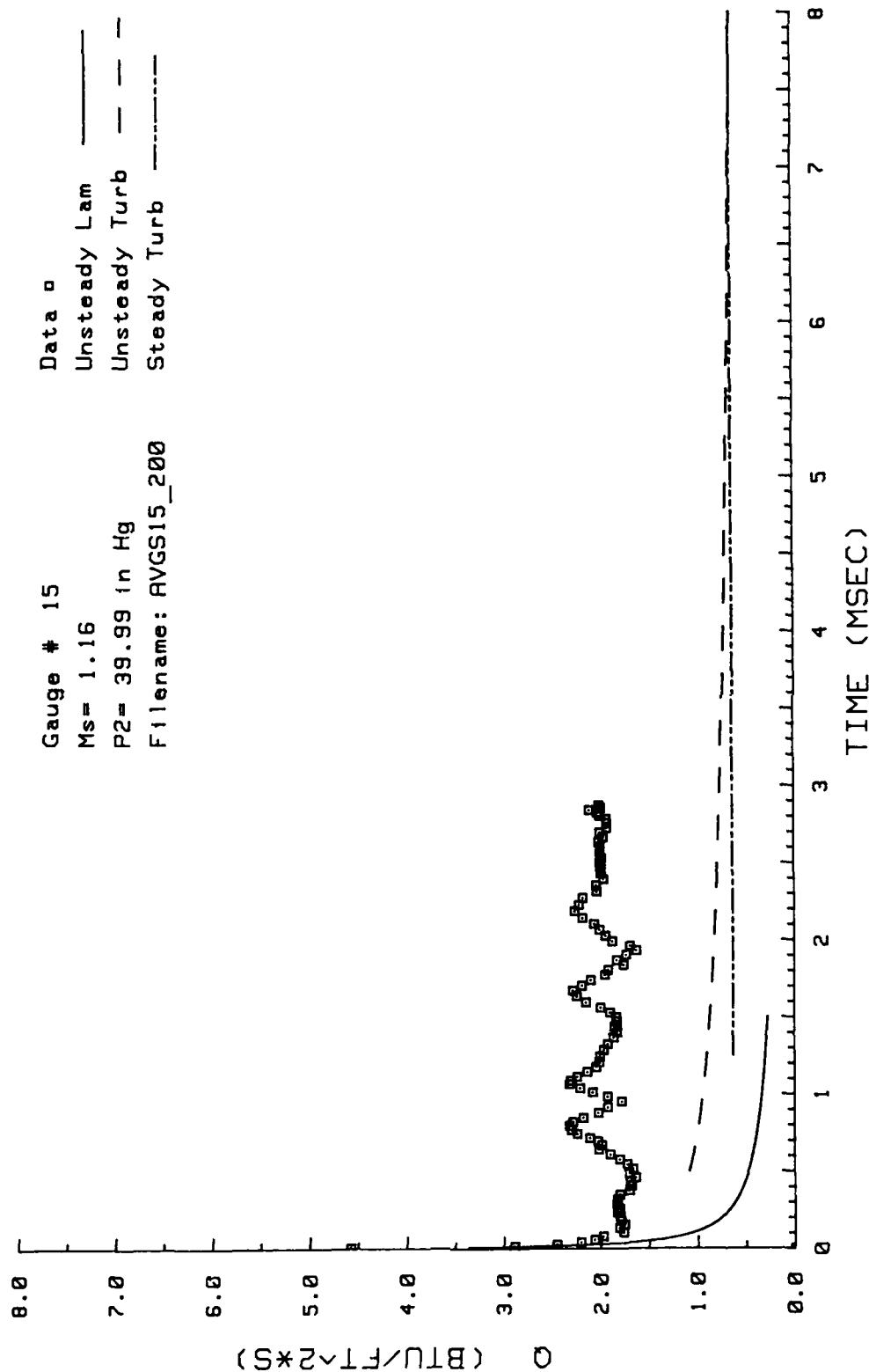
Figure 19. Heat Transfer: Data Set A Gage #15
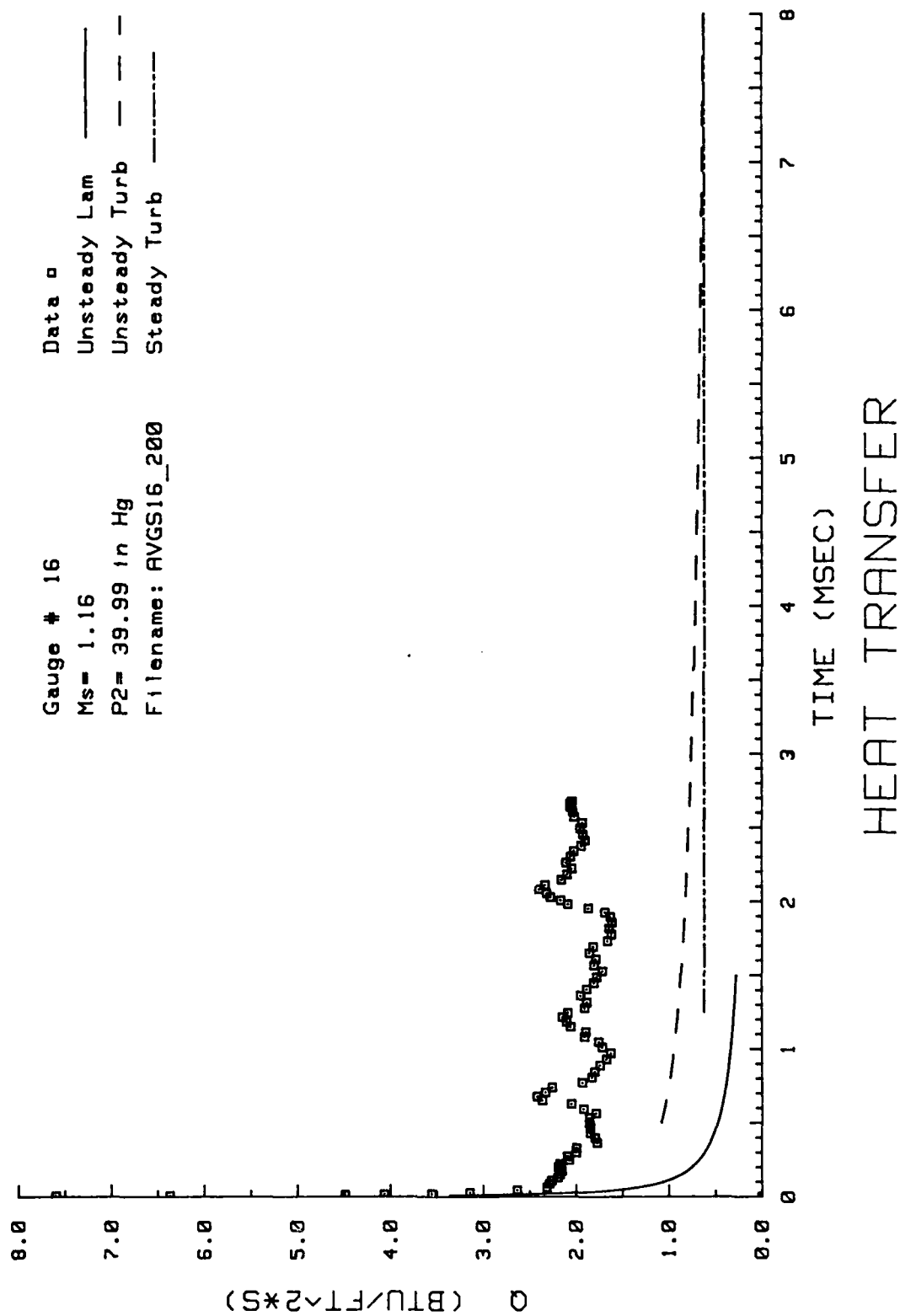
Figure 20. Heat Transfer; Data Set A Gage #16

69

HEAT TRANSFER

Gauge # TC
Ms= 1.3 1
P2= 38.63 in Hg
Filename: AVGTC_201

Data □
Unsteady Lam ———
Unsteady Turb — — —
Steady Turb ———·———

TIME (MSEC)

Q (BTU/FT^2*S)
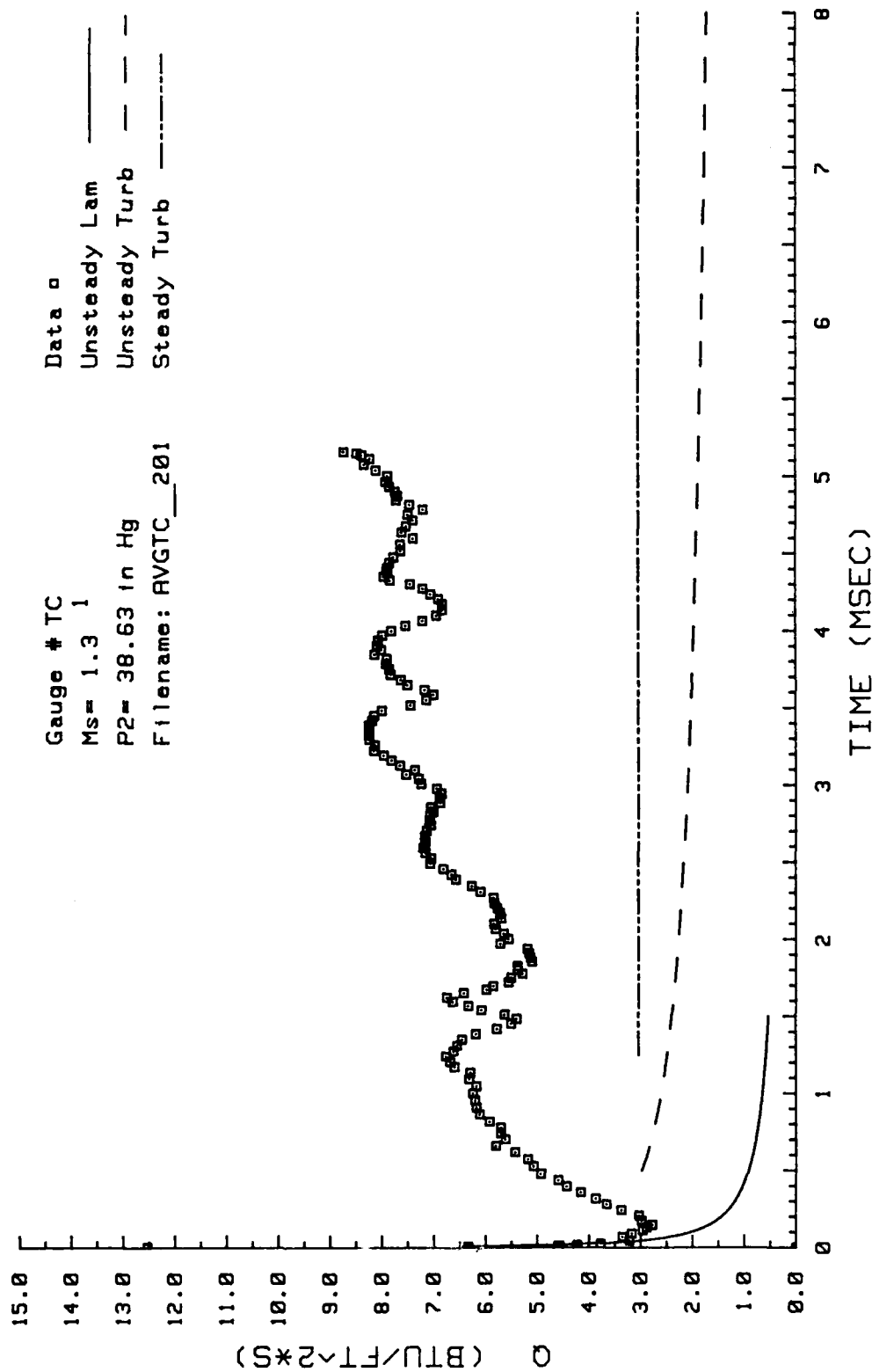
Figure 21. Heat Transfer: Data Set B Thermocouple
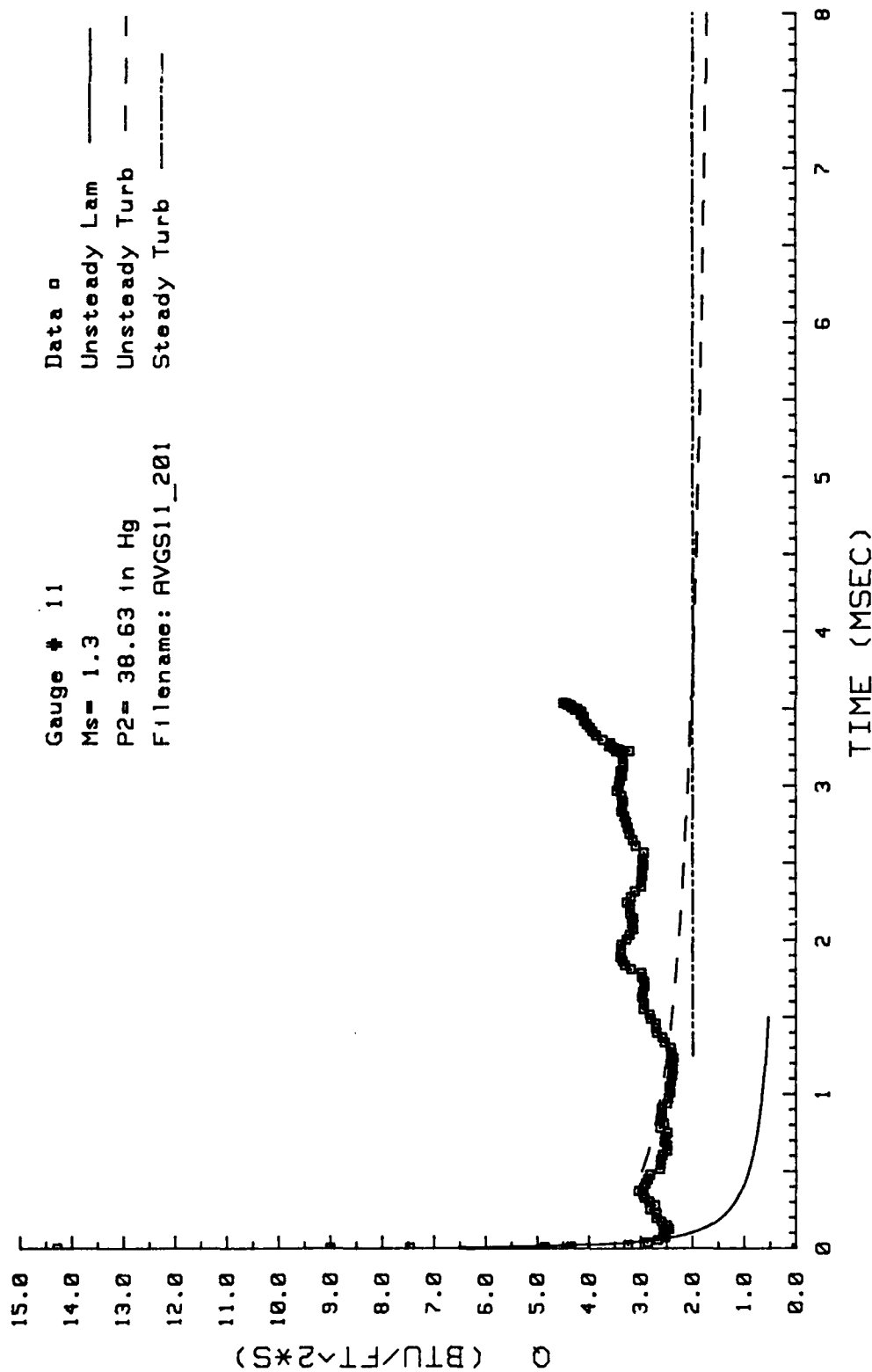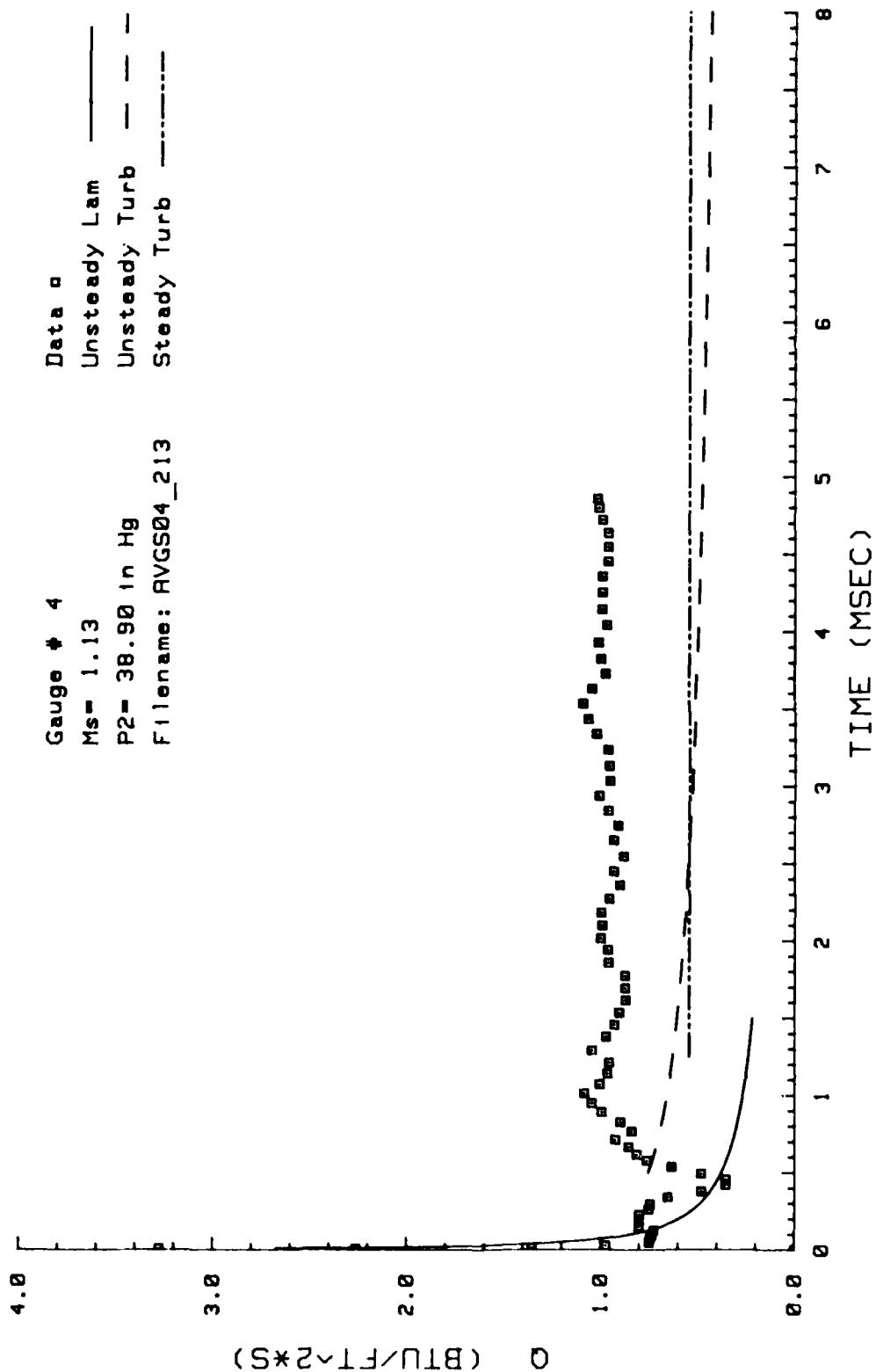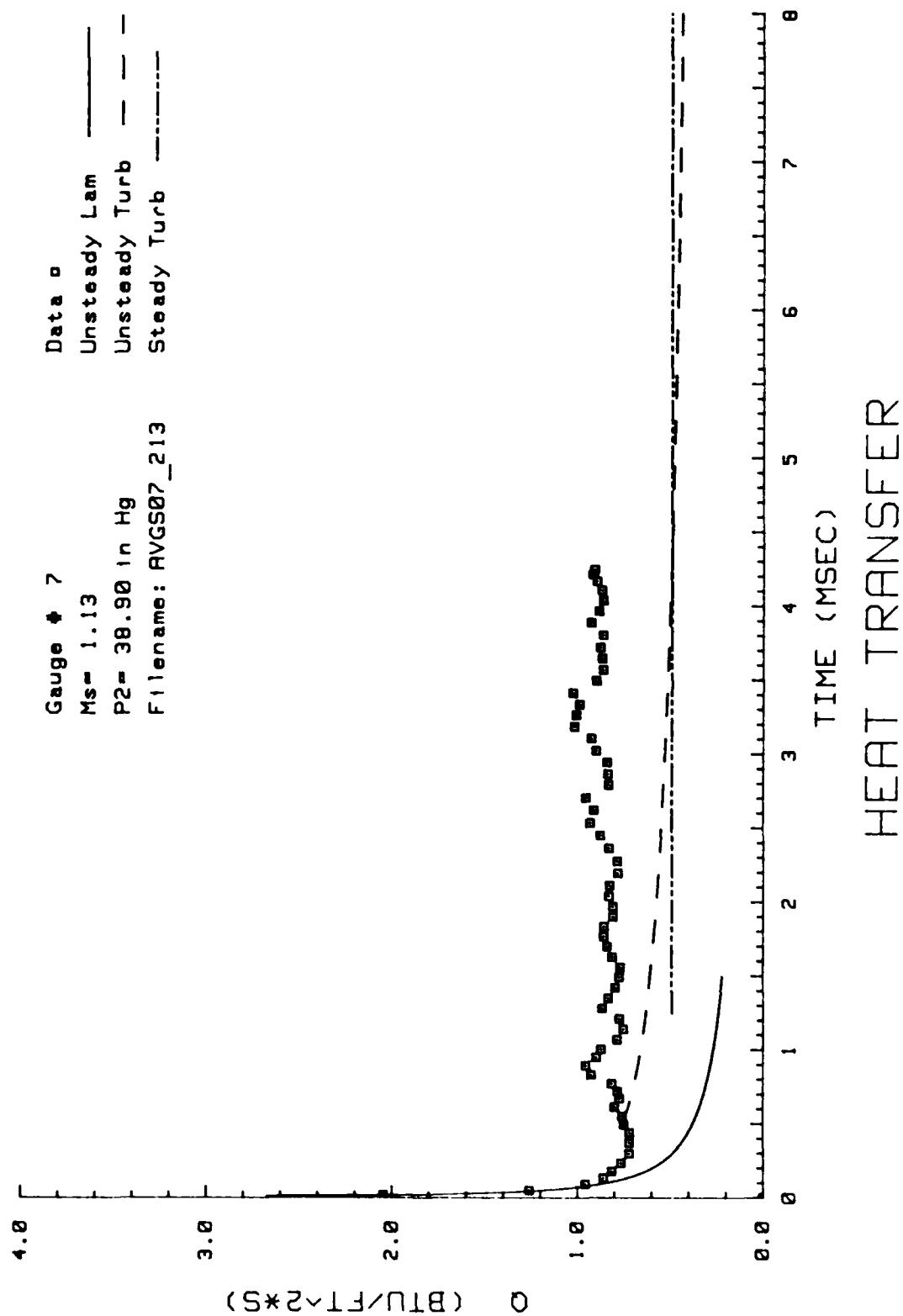
Figure 22. Heat Transfer: Data Set B Gage #11

71
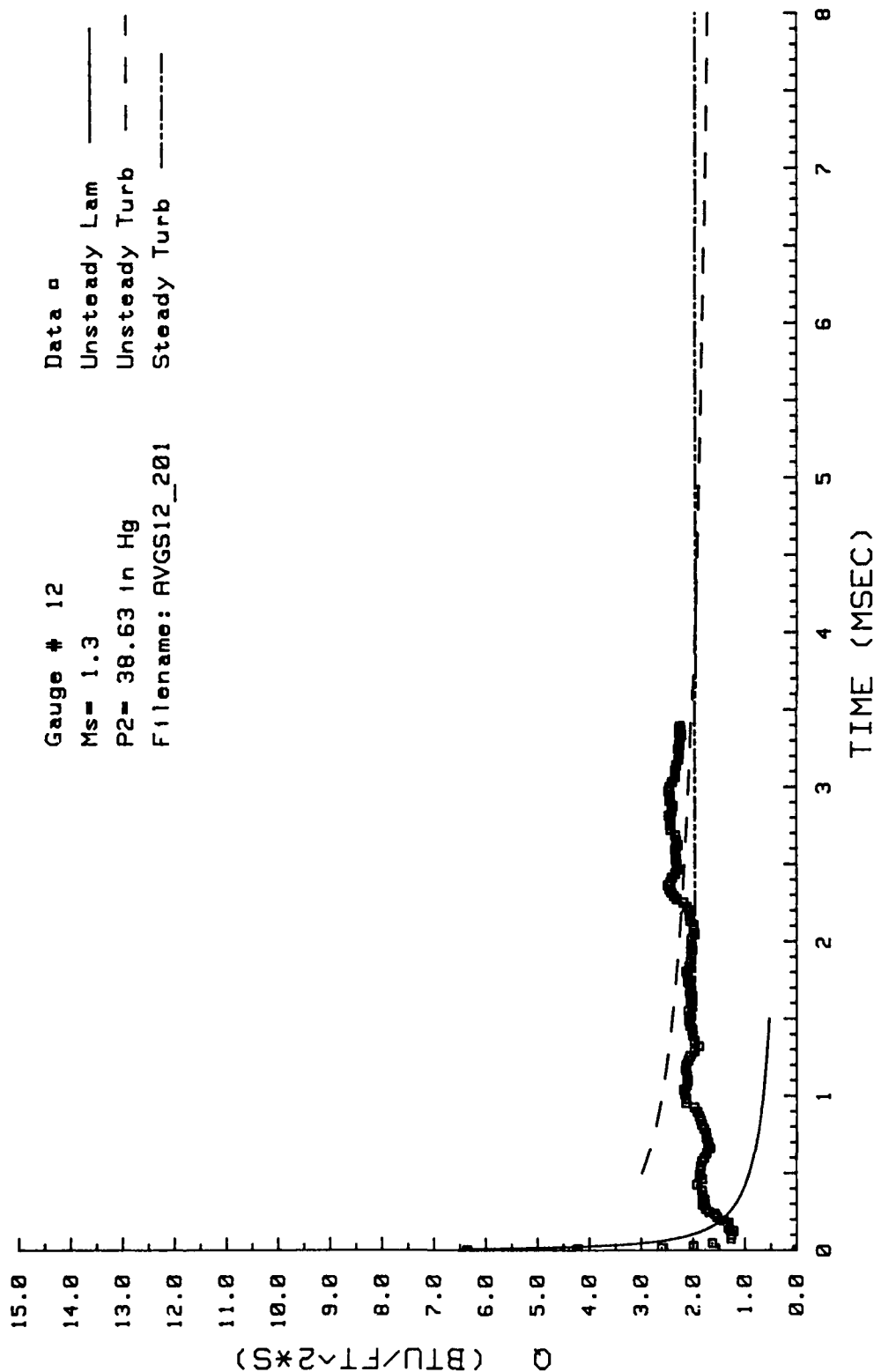
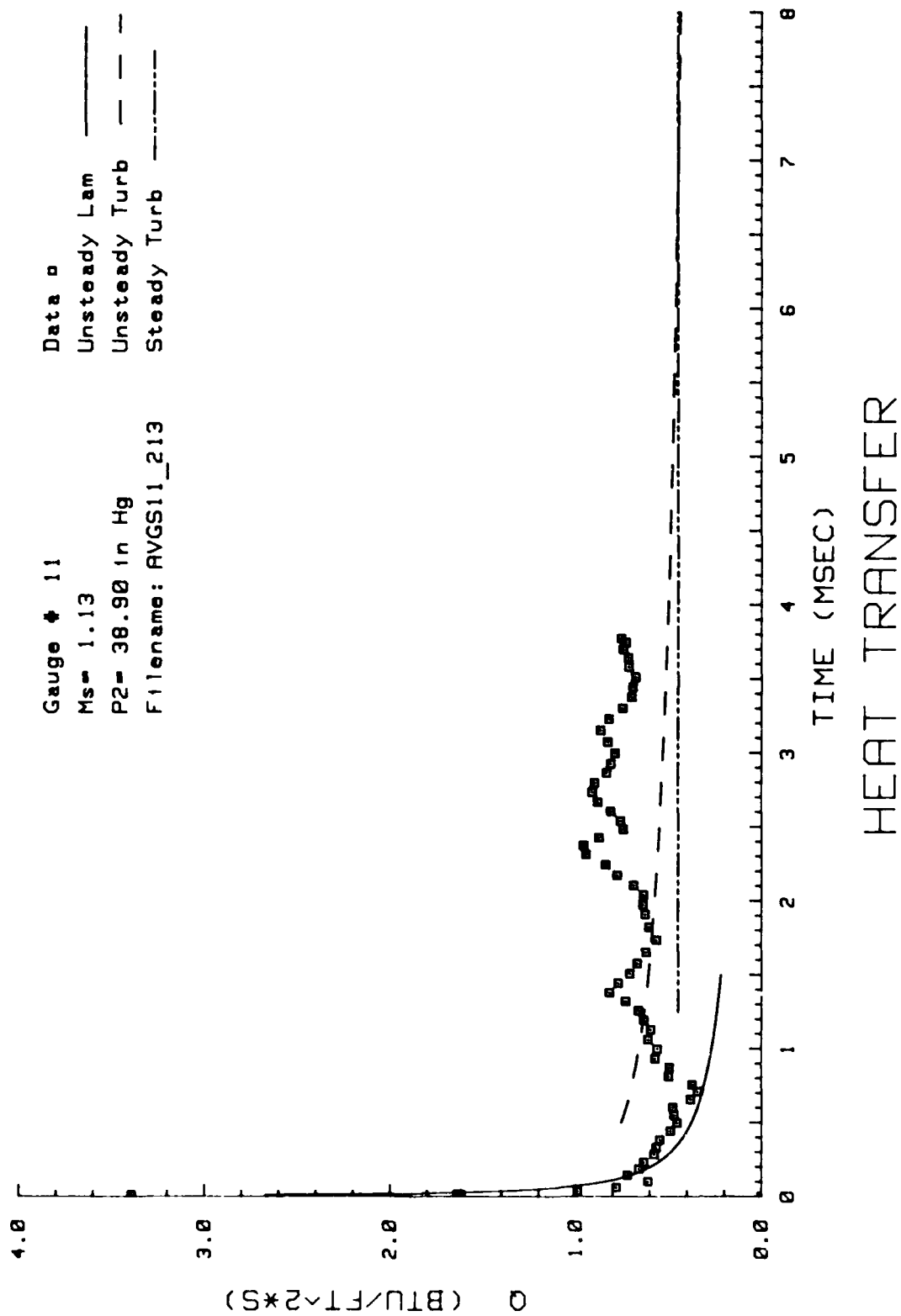Figure 23.   Heat Transfer: Data Set B Gage #12
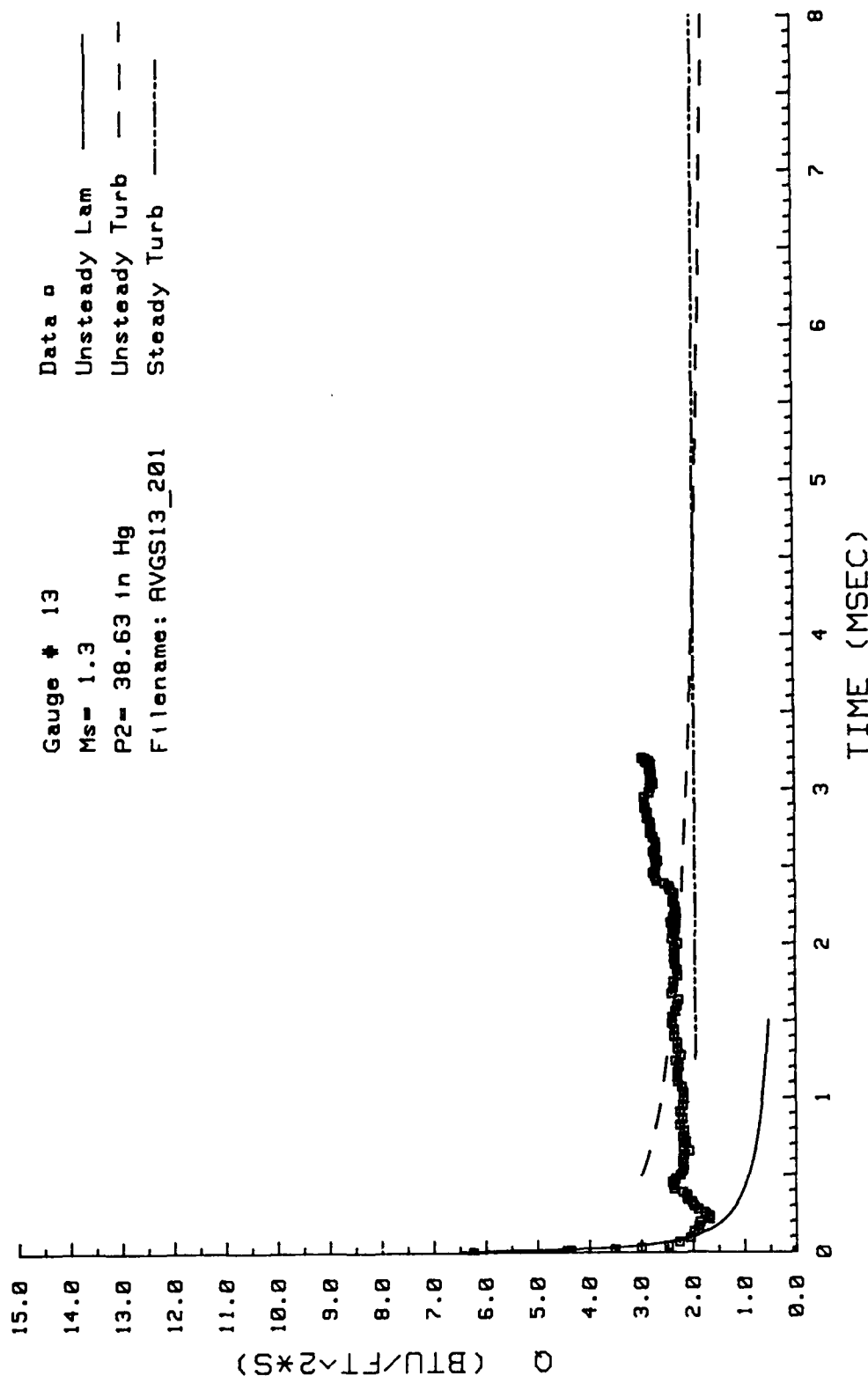
Figure 24. Heat Transfer: Data Set B Gage #13

73
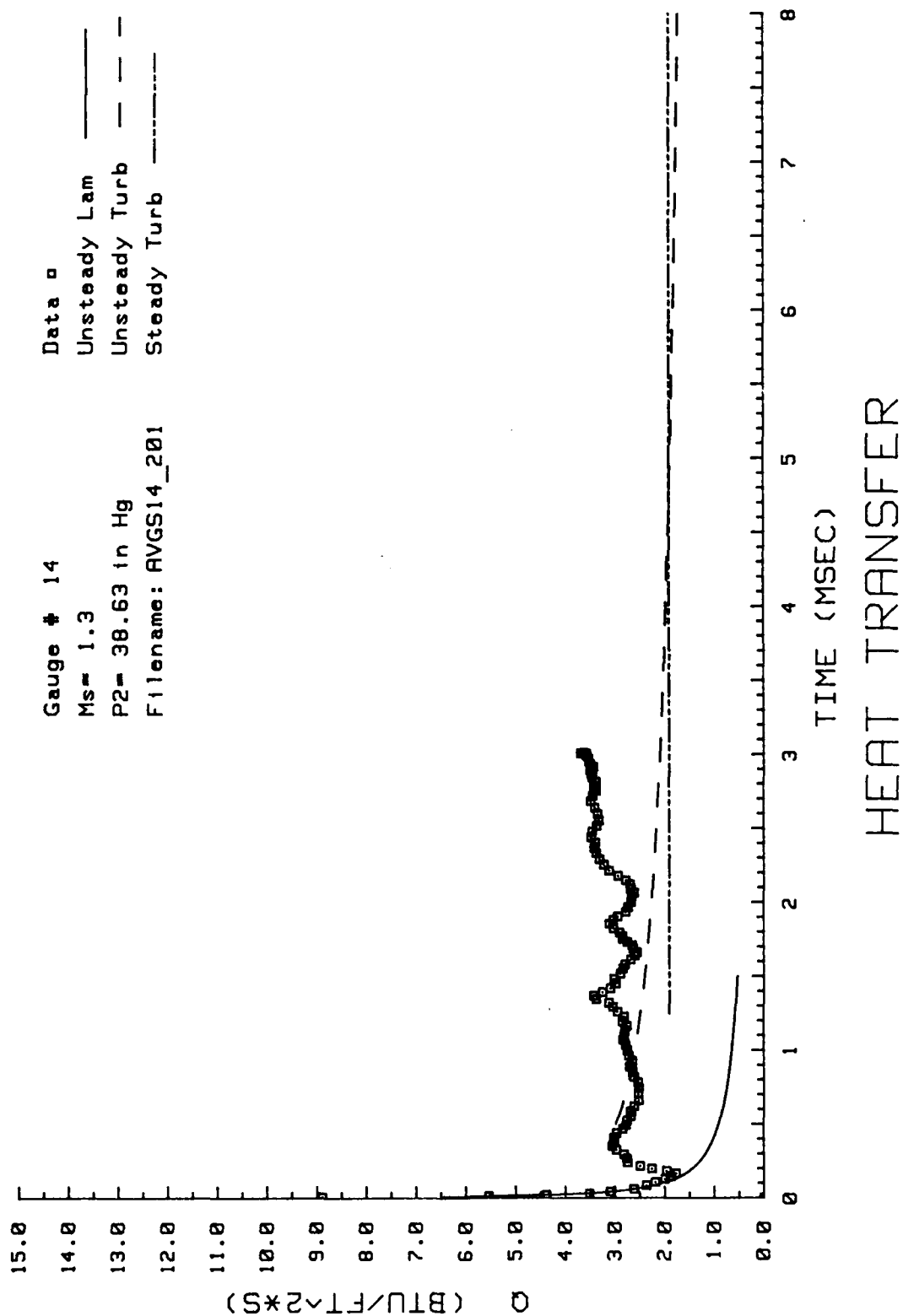
Figure 25. Heat Transfer: Data Set B Gage #14
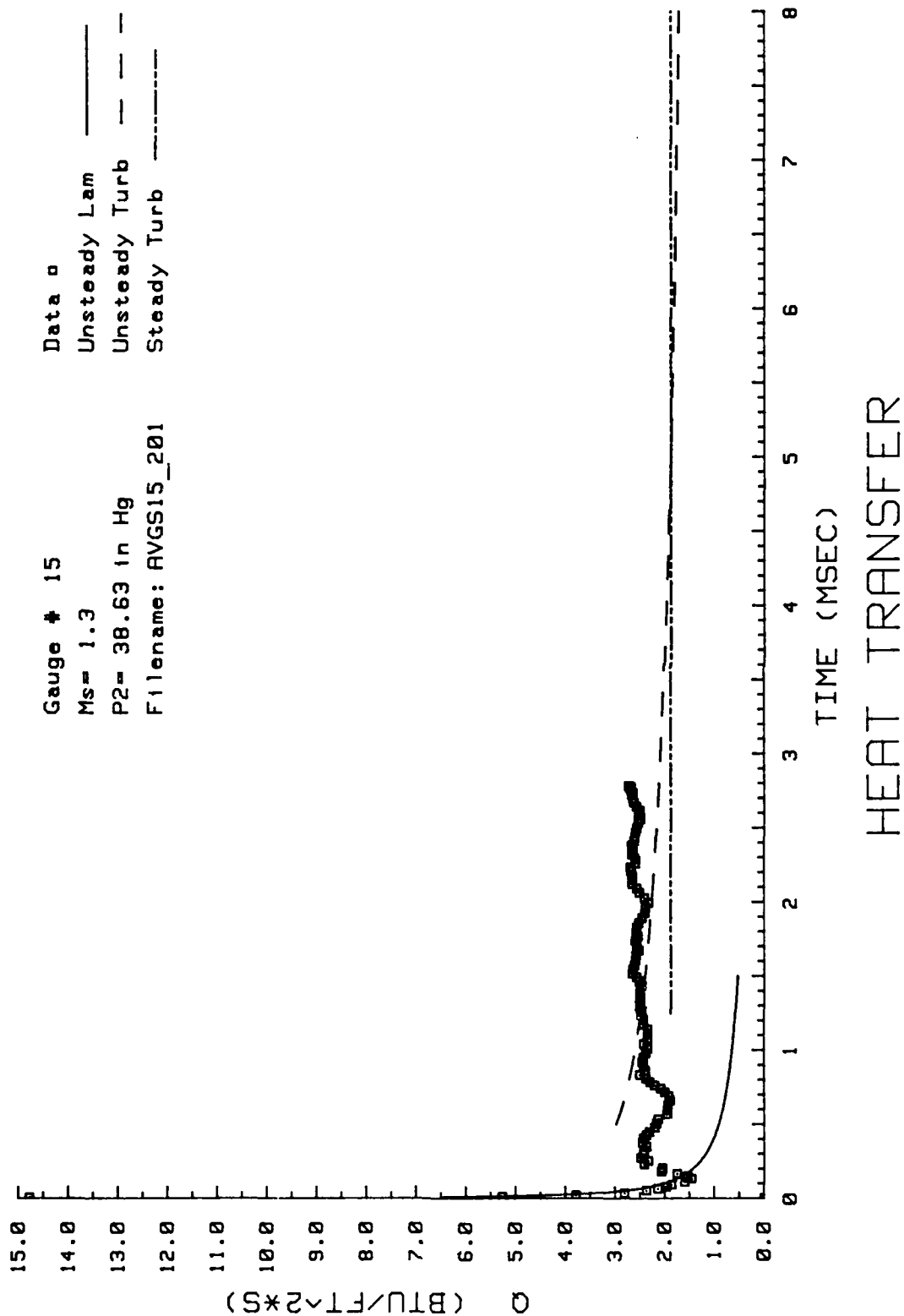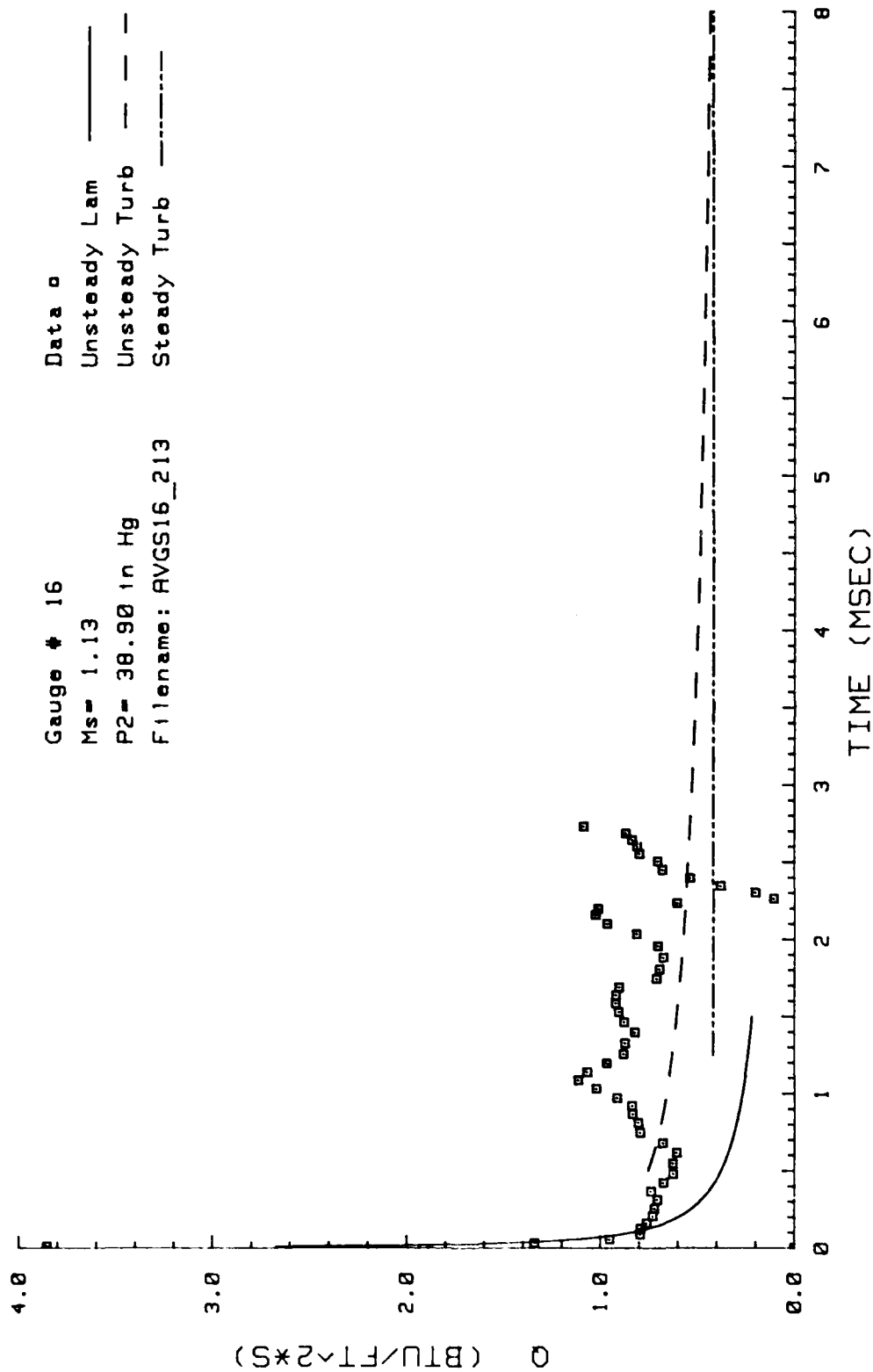
Figure 26. Heat Transfer: Data Set B Gage #15
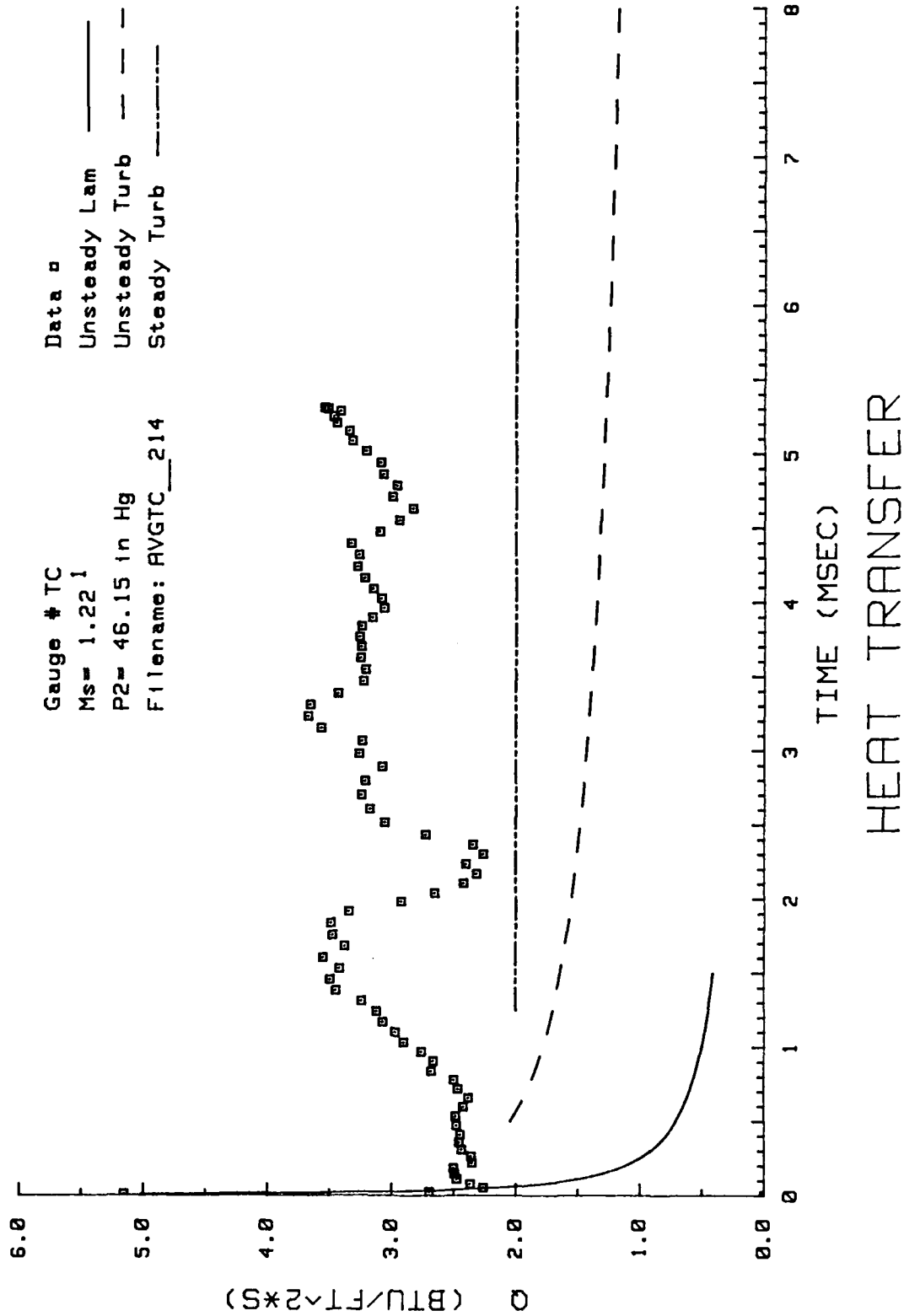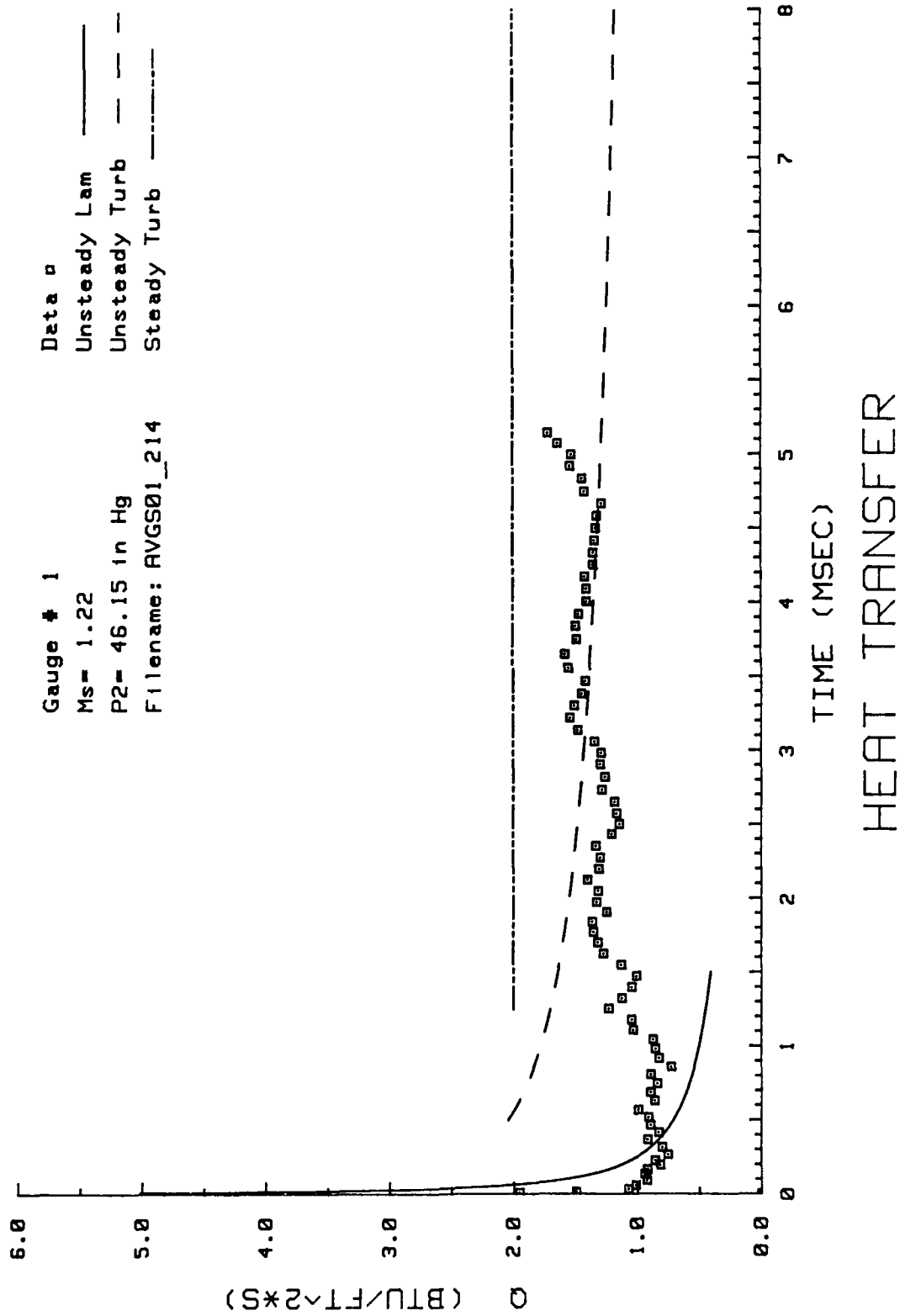
Figure 27. Heat Transfer: Data Set B Gage #16

Figure 28. Heat Transfer: Data Set C Thermocouple
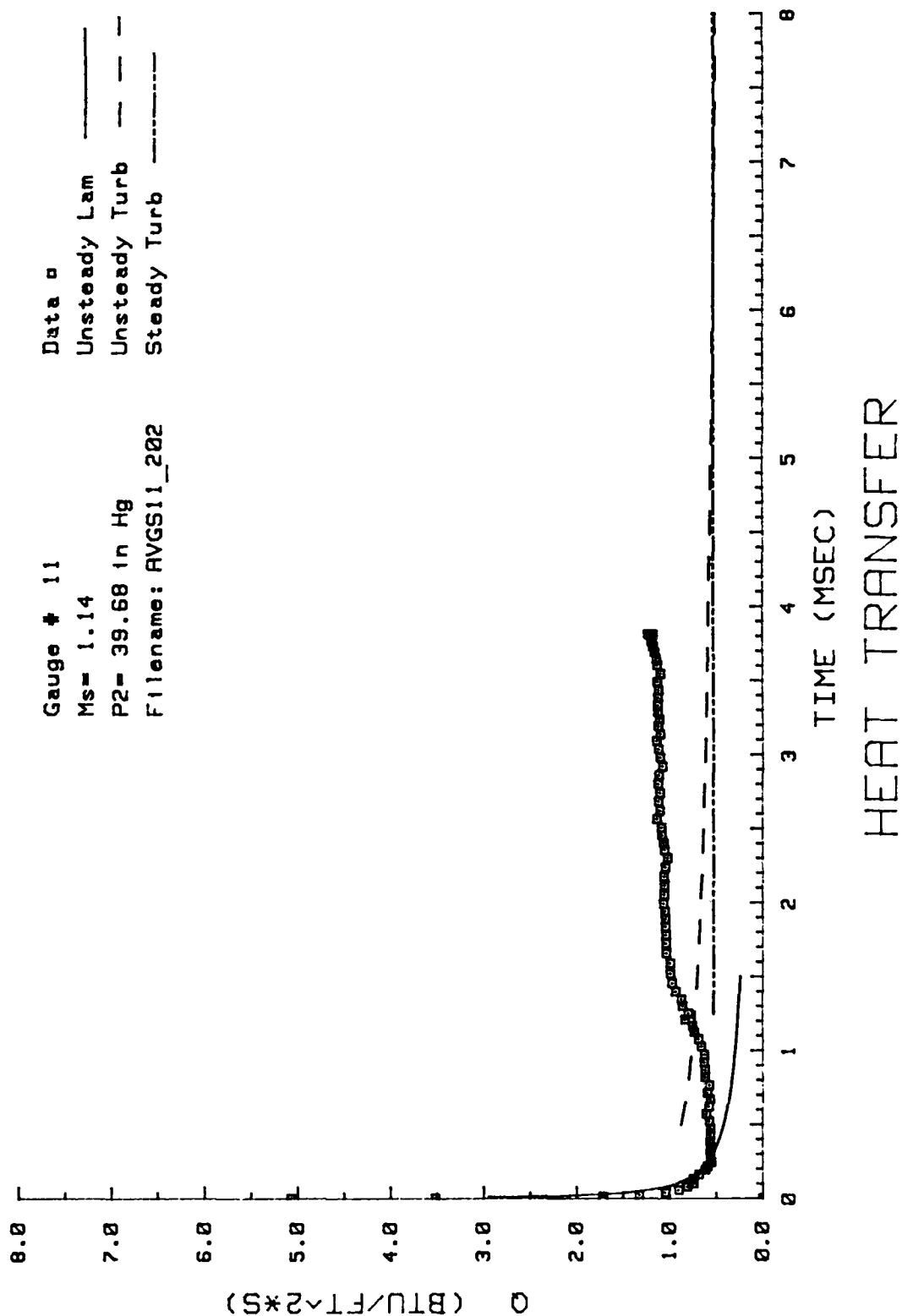
Figure 29. Heat Transfer: Data Set C Gage #11
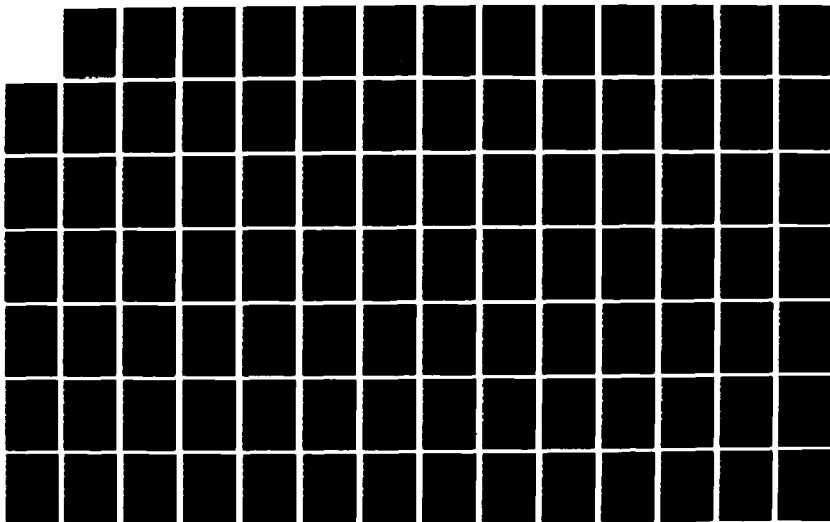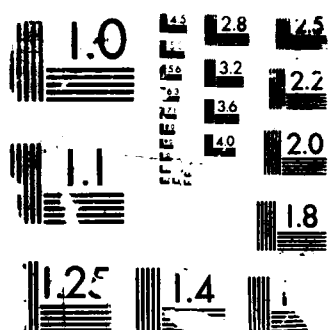
MICROCOPY RESOLUTION TEST CHART
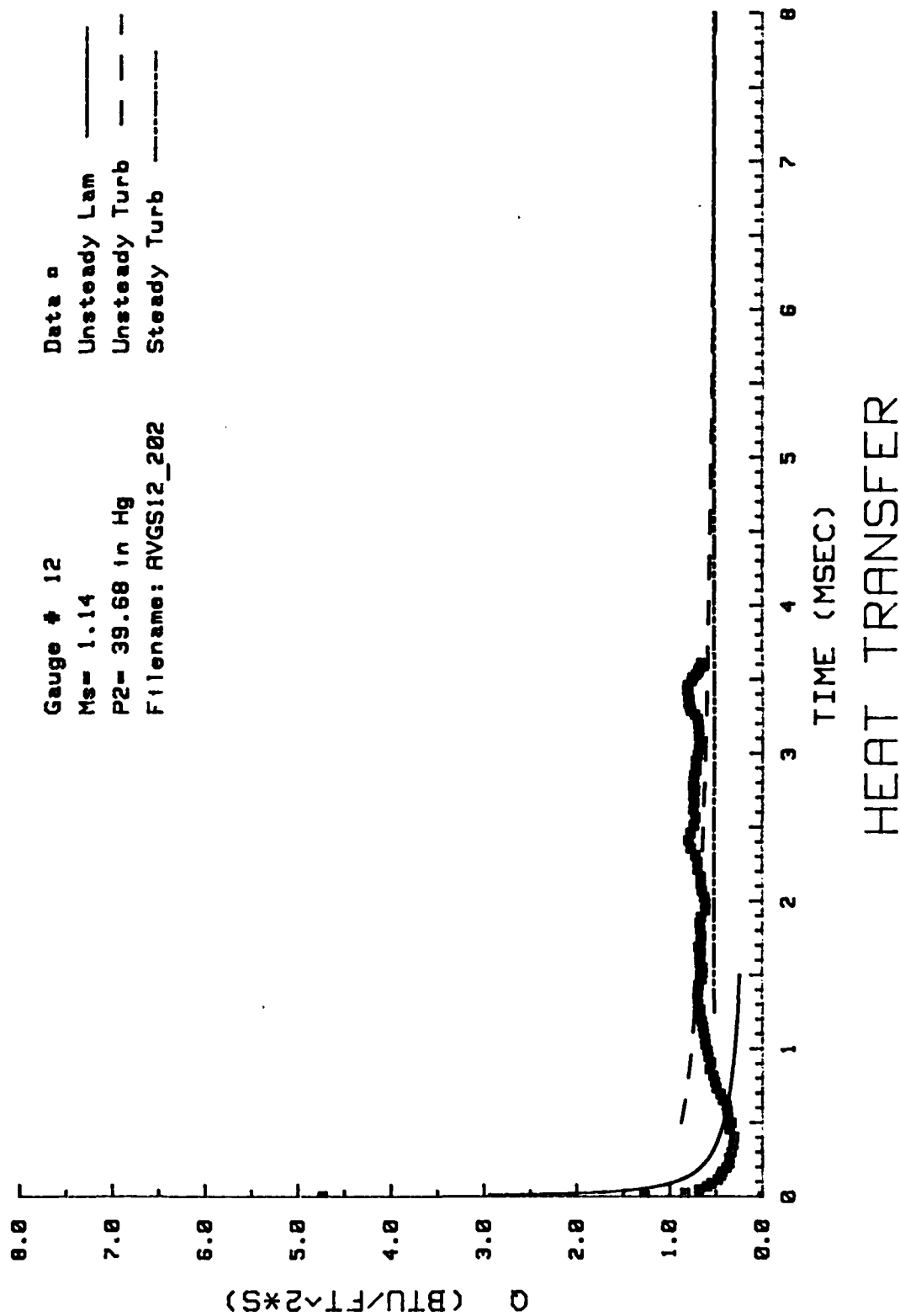
Figure 30. Heat Transfer: Data Set C Gage #12
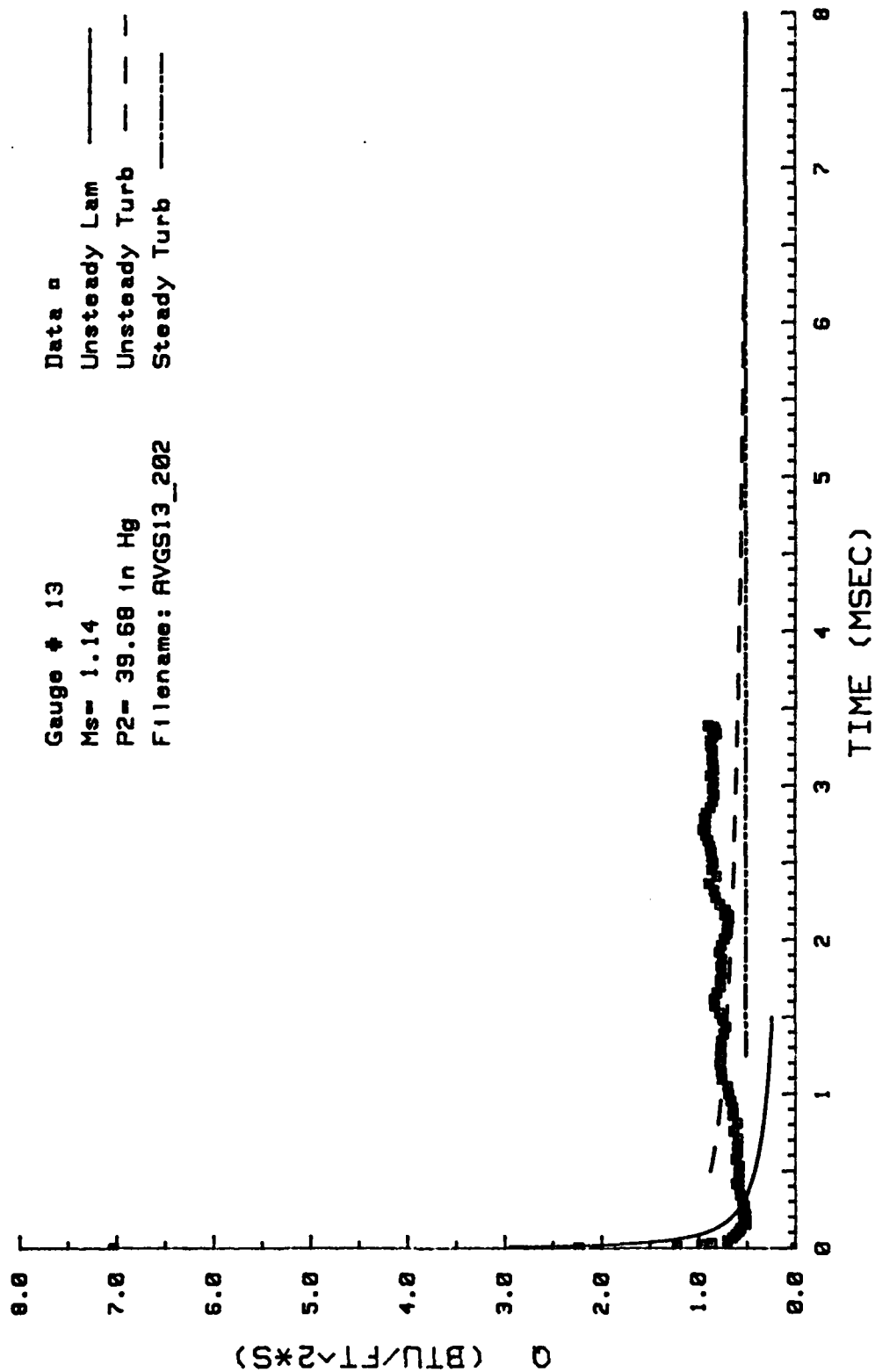
Figure 31.   Heat Transfer: Data Set C Gage #13

80

HEAT TRANSFER

Gauge # 14
Ms= 1.14
P2= 39.68 in Hg
Filename: AVGS14_202

Data □
Unsteady Lam ——
Unsteady Turb — —
Steady Turb ········

Q (BTU/FT^2*S)

8.0
7.0
6.0
5.0
4.0
3.0
2.0
1.0
0.0

0   1   2   3   4   5   6   7   8

TIME (MSEC)
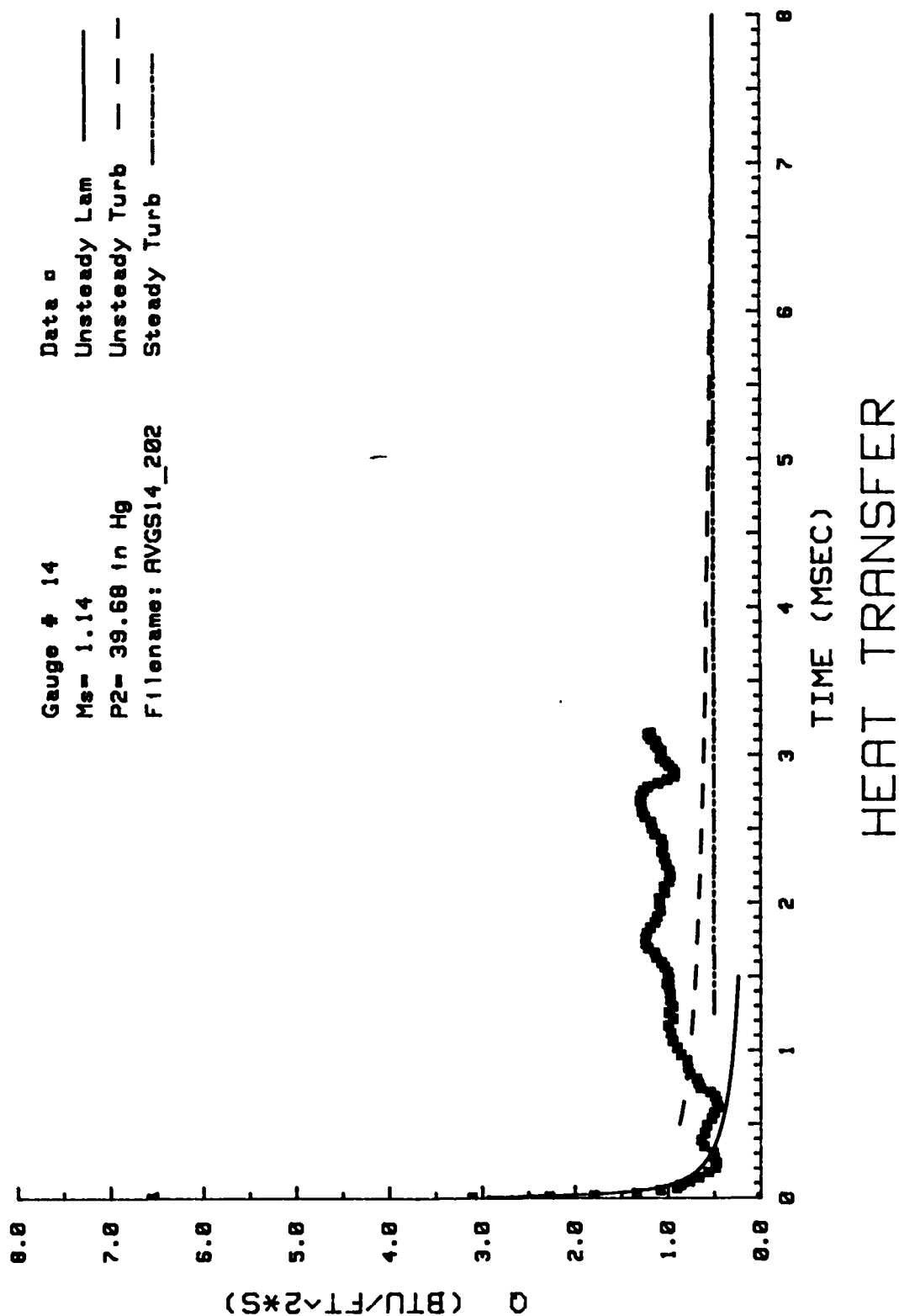
Figure 32. Heat Transfer: Data Set C Gage #14

81
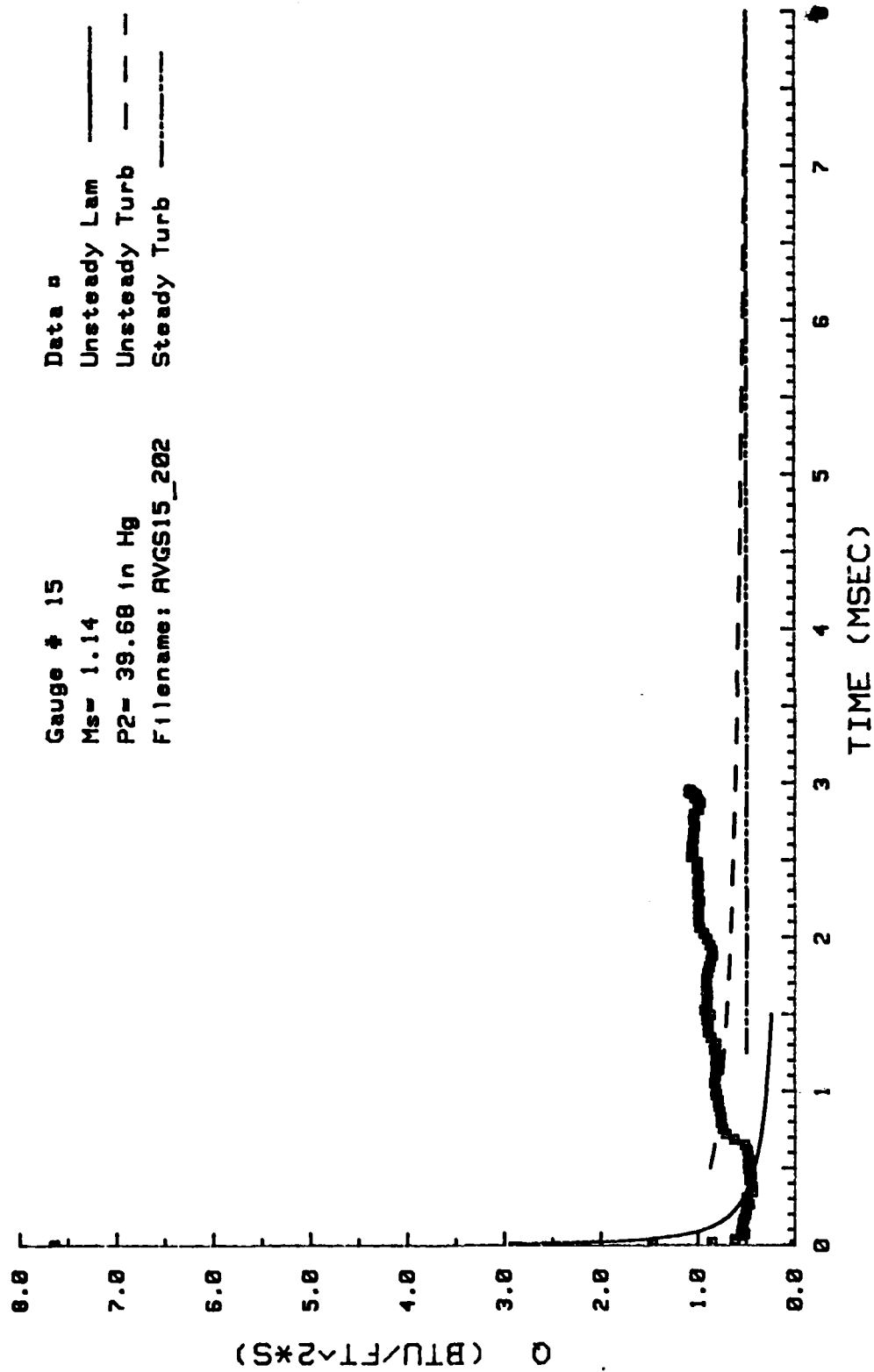
Figure 33. Heat Transfer: Data Set C Gage #15

HEAT TRANSFER

Gauge # 16   Data =

Ms= 1.14   Unsteady Lam ———

P2= 39.68 in Hg   Unsteady Turb — — —

Filename: AVGS16_202   Steady Turb   ———————

TIME (MSEC)

Q (BTU/FT^2*S)
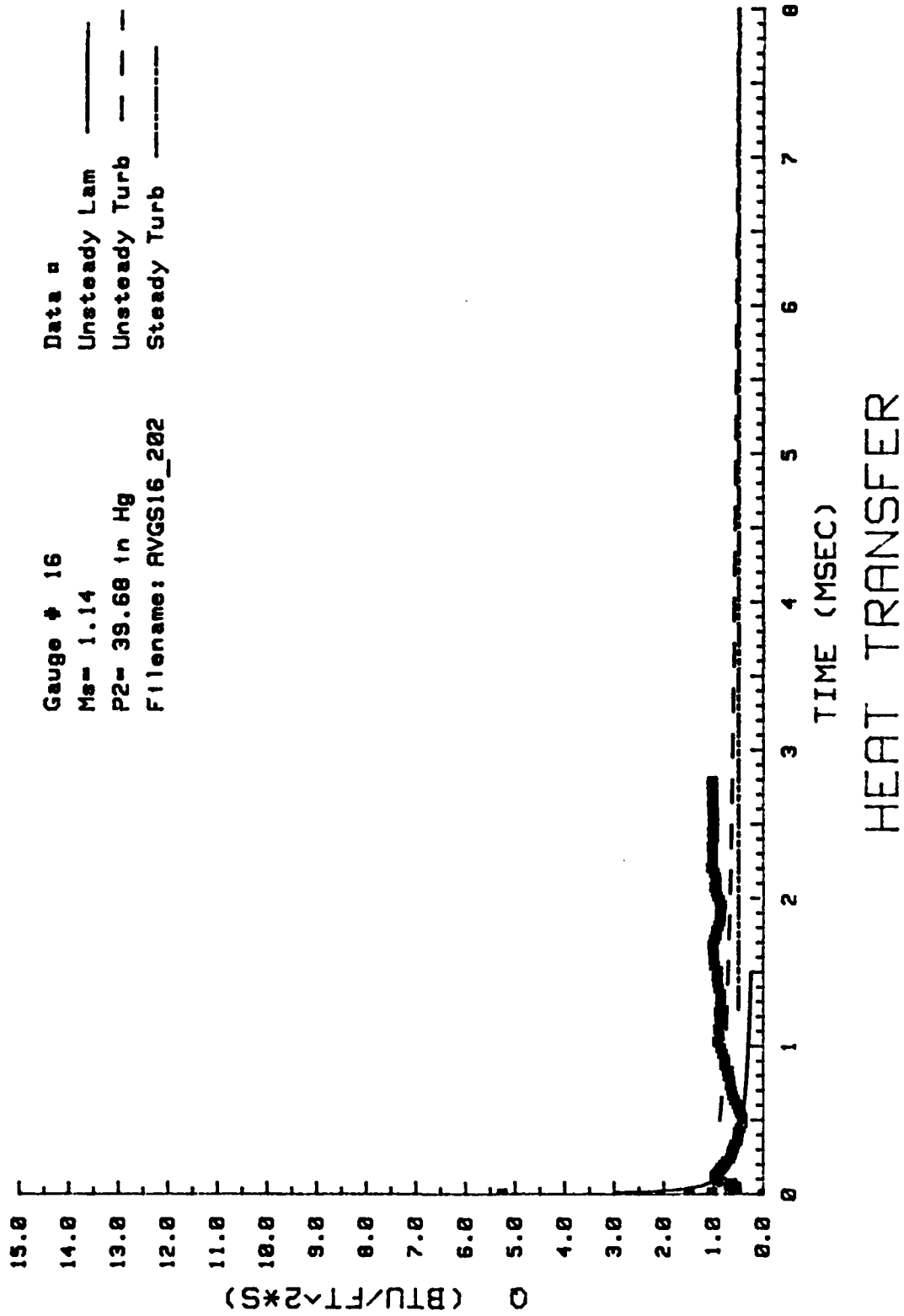
Figure 34. Heat Transfer: Data Set C Gage #16
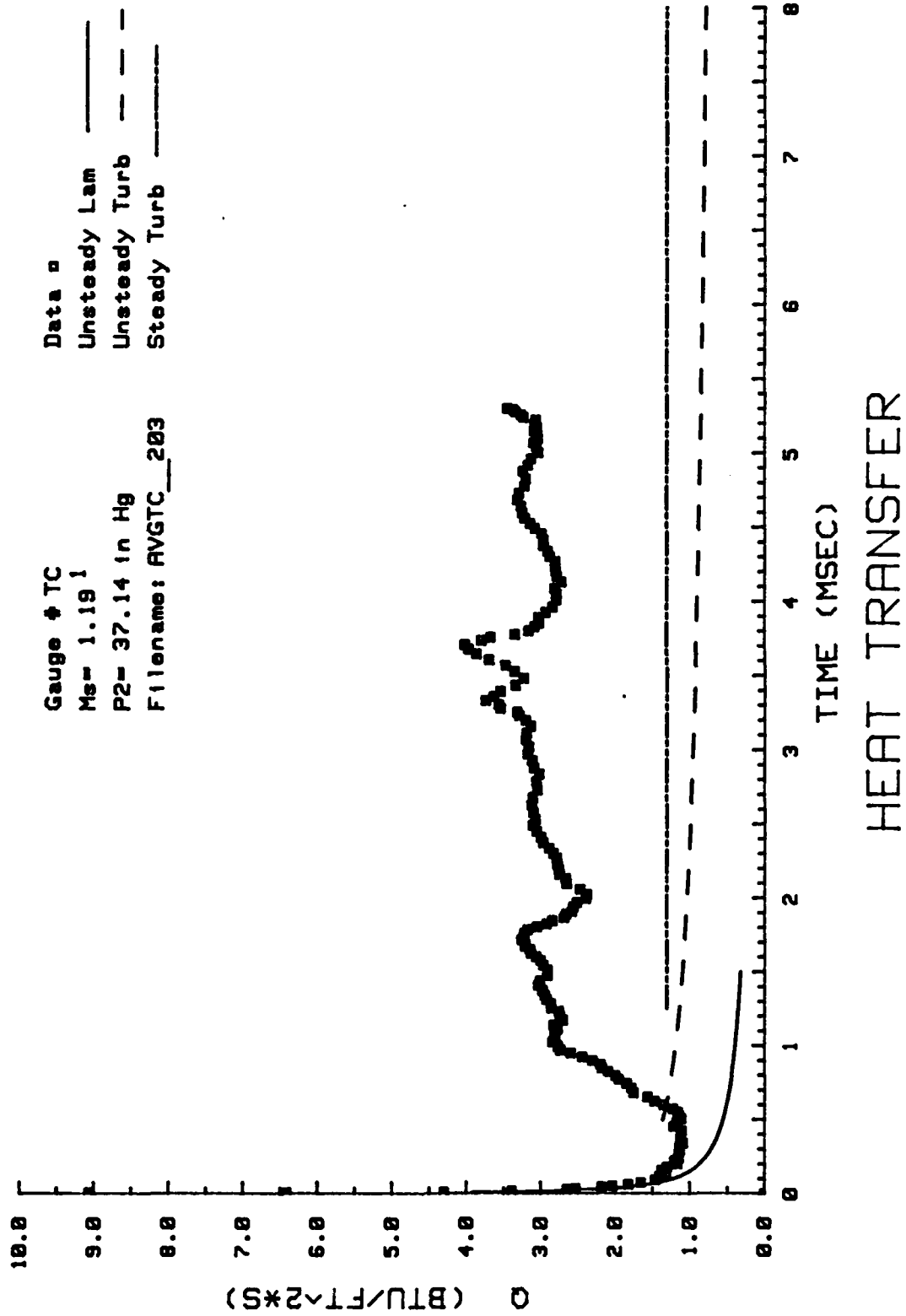
Figure 35. Heat Transfer: Data Set D Thermocouple

84

Figure 36. Heat Transfer: Data Set D Gage #11
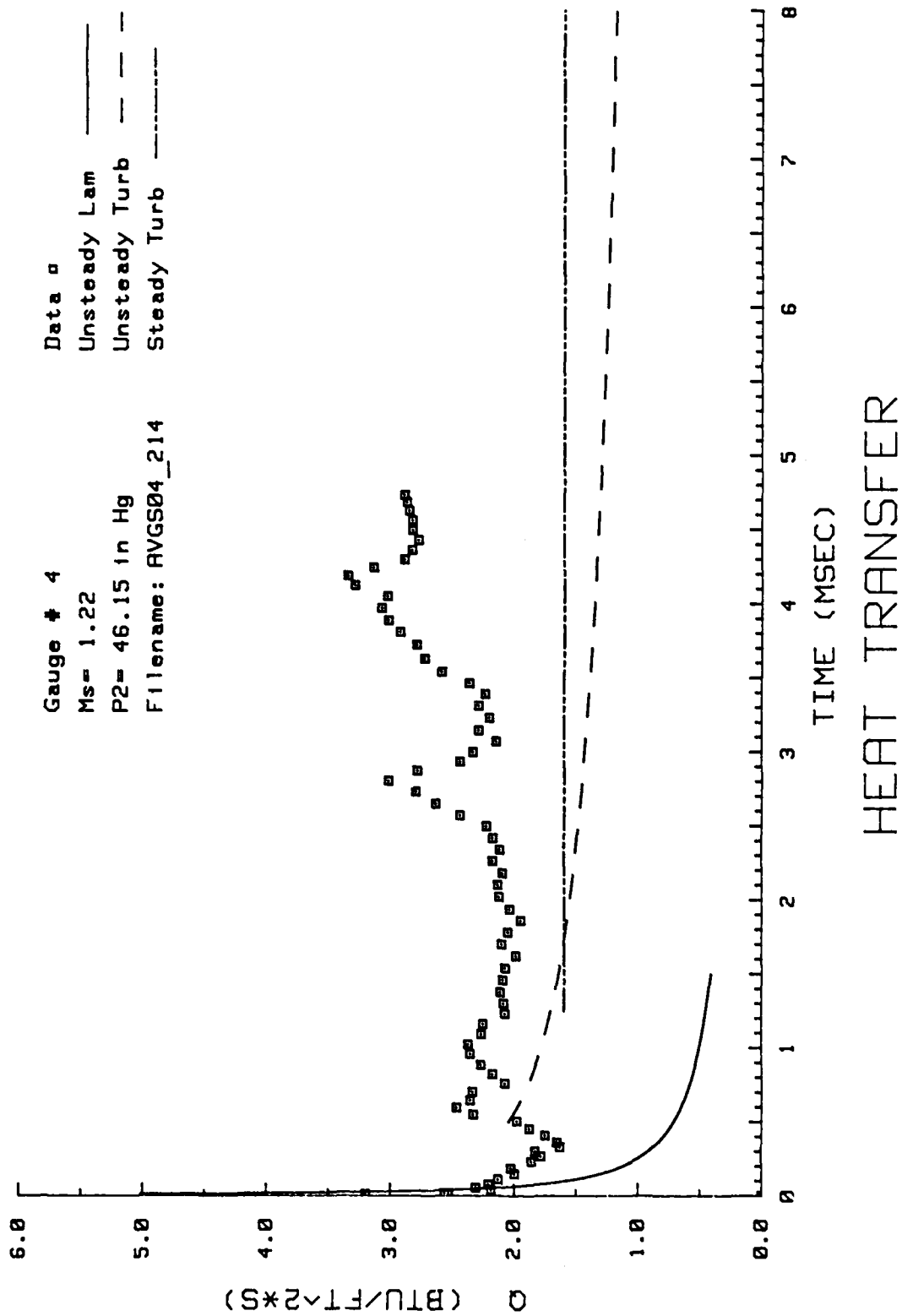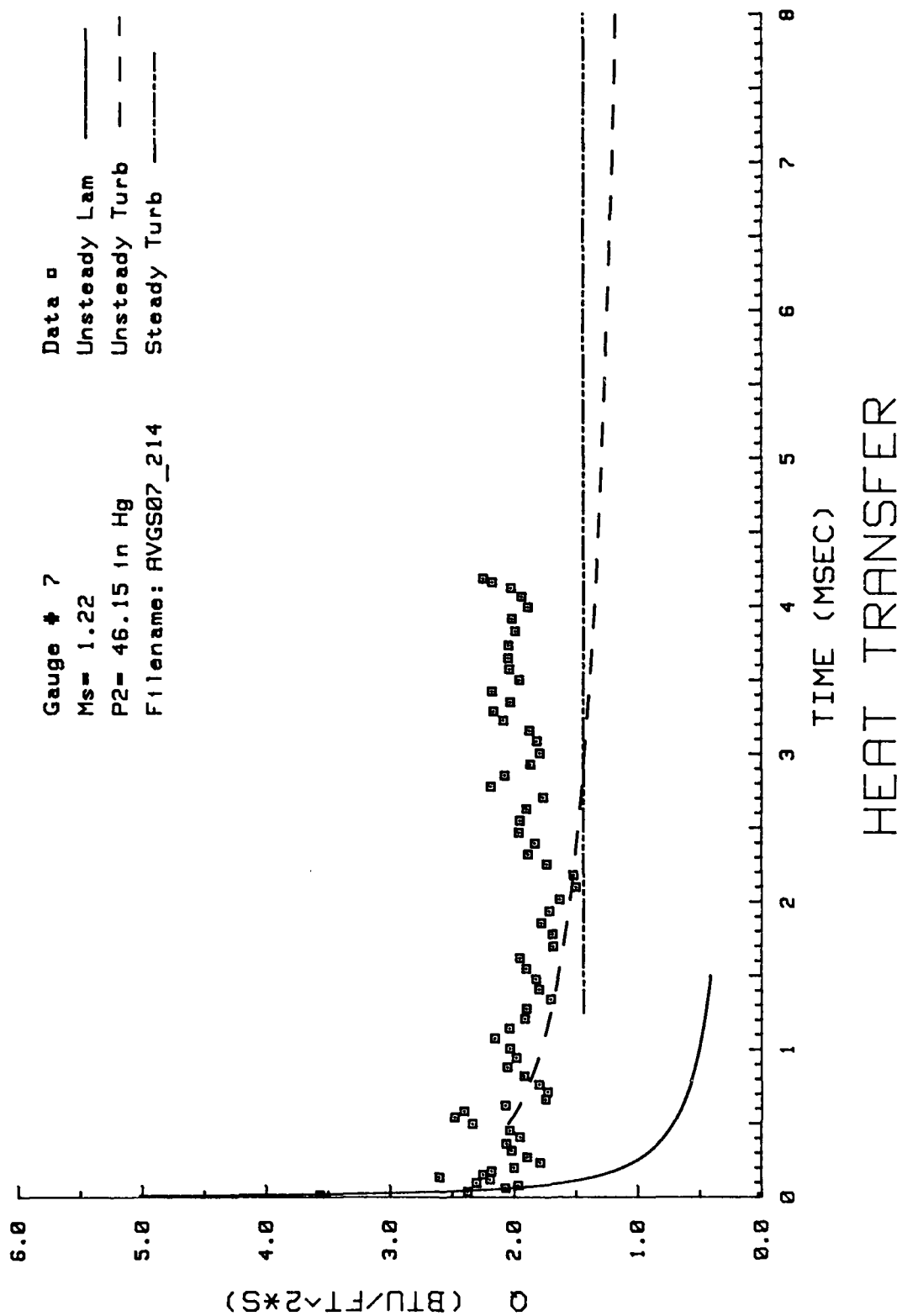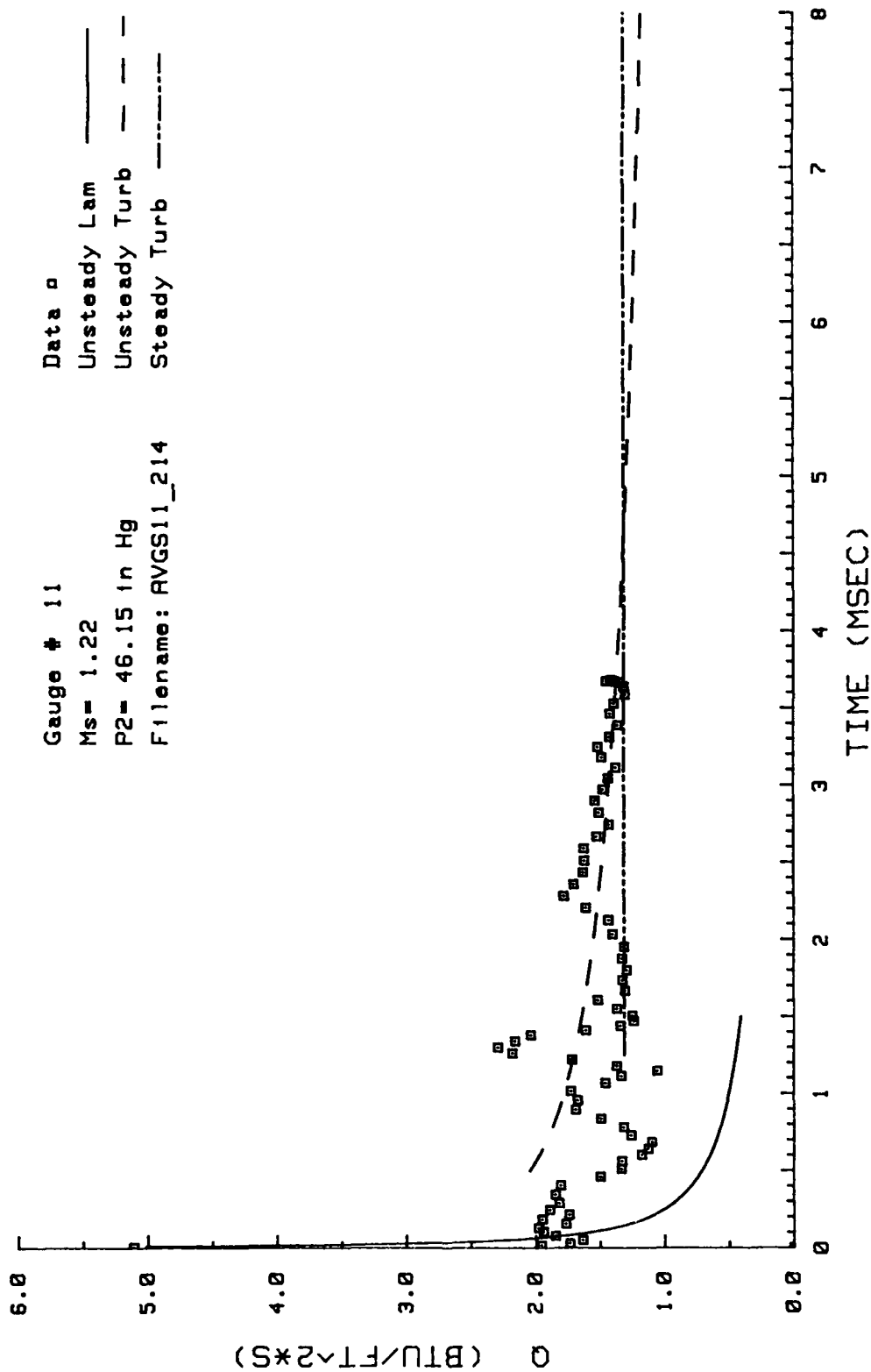
Figure 37.   Heat Transfer: Data Set D Gage #12
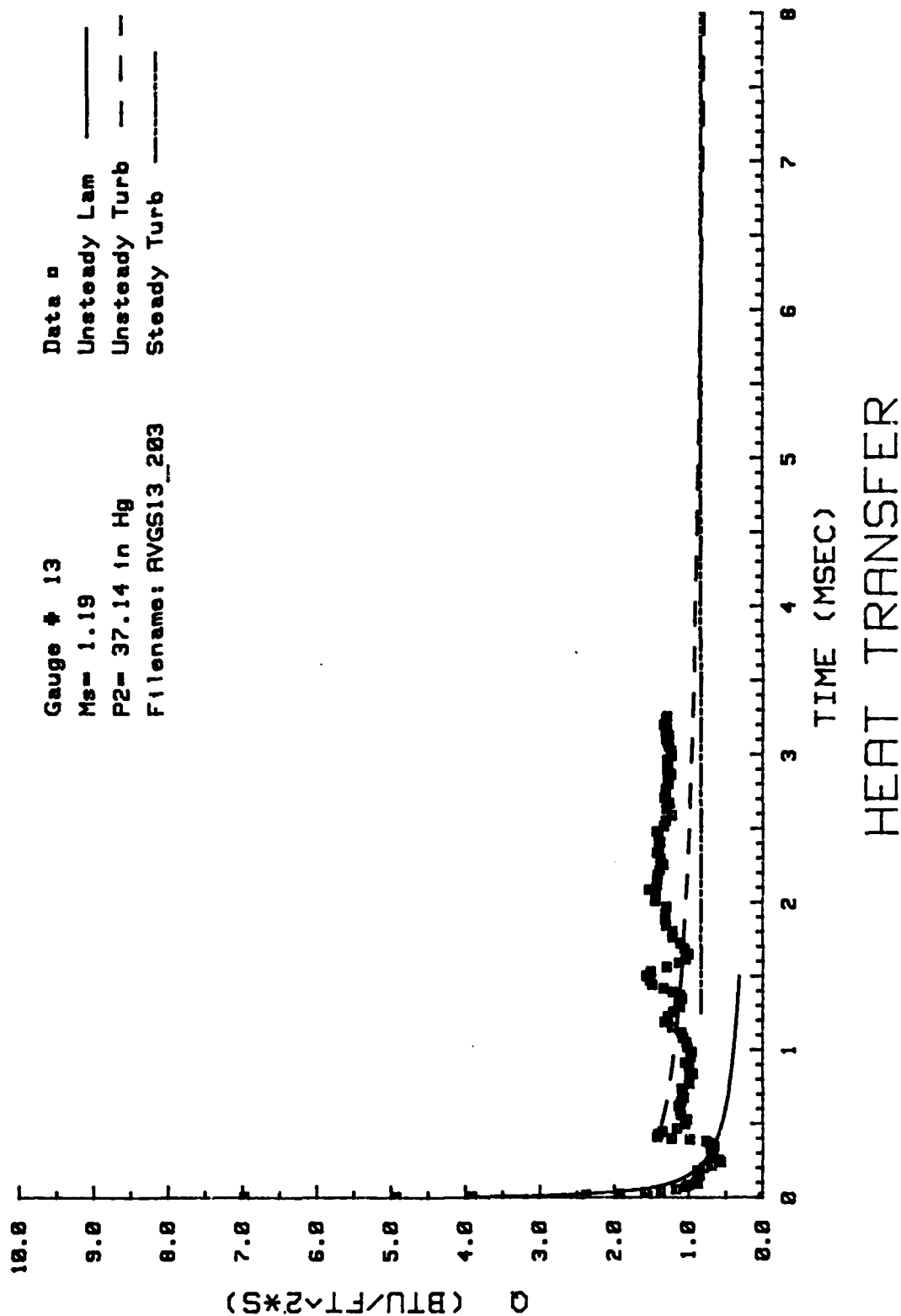
Figure 38. Heat Transfer: Data Set D Gage #13

HEAT TRANSFER

Gauge # 14
Ms= 1.19
P2= 37.14 in Hg
Filename: AVGS14_203

Data □
Unsteady Lam ——
Unsteady Turb — —
Steady Turb ————

TIME (MSEC)

Q (BTU/FT^2*S)

10.0
9.0
8.0
7.0
6.0
5.0
4.0
3.0
2.0
1.0
0.0

0   1   2   3   4   5   6   7   8
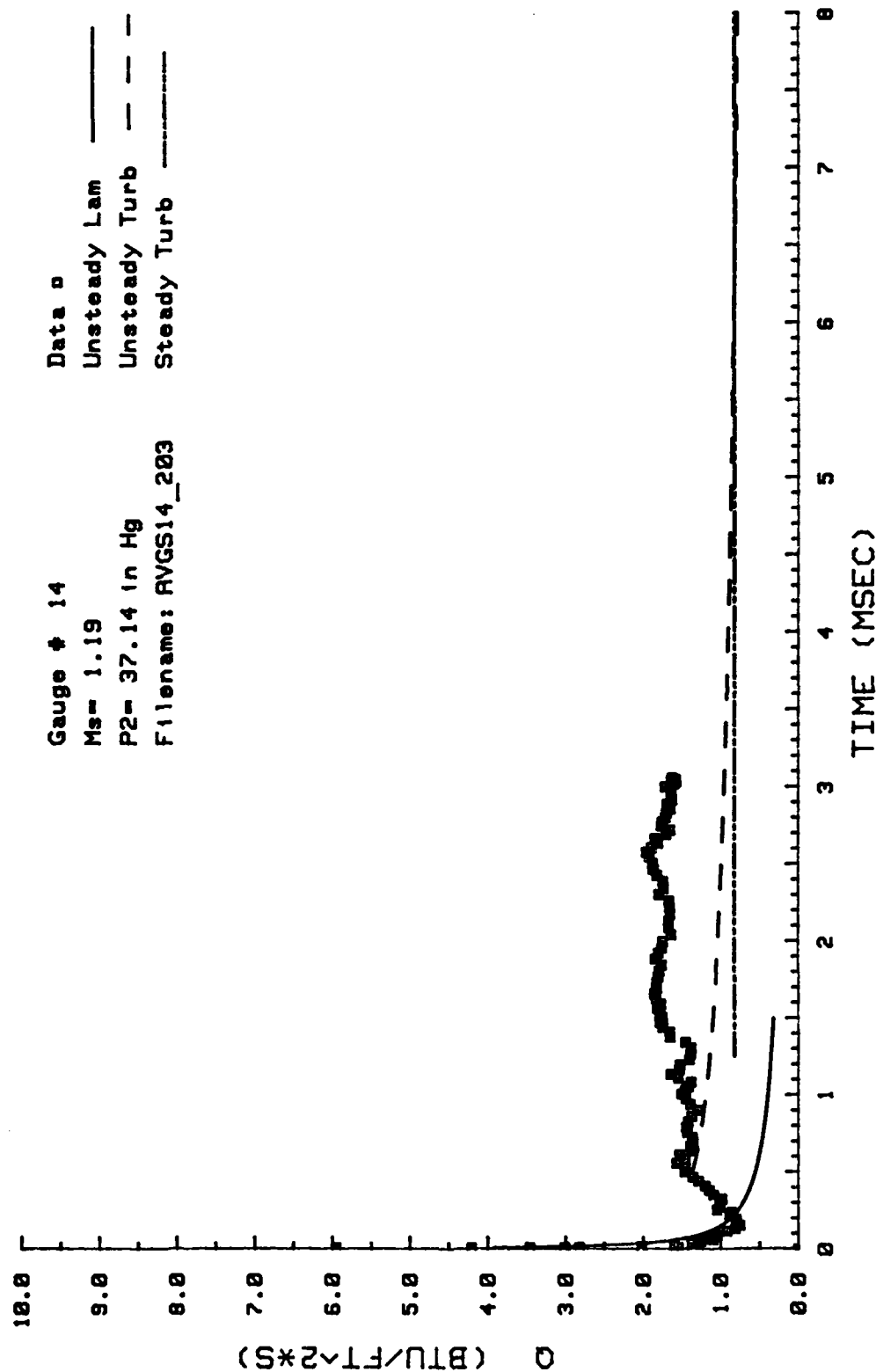
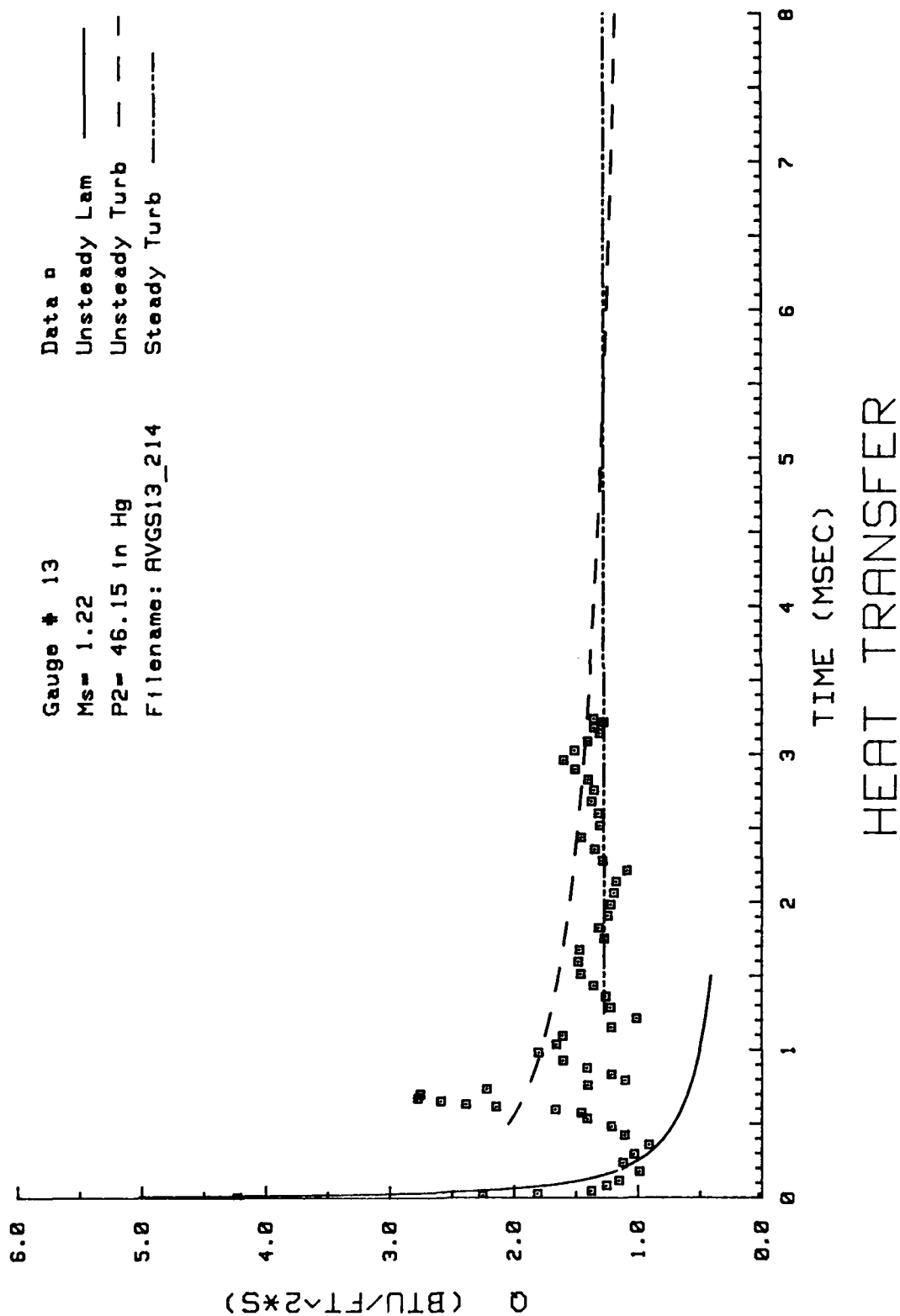Figure 39. Heat Transfer: Data Set D Gage #14

88
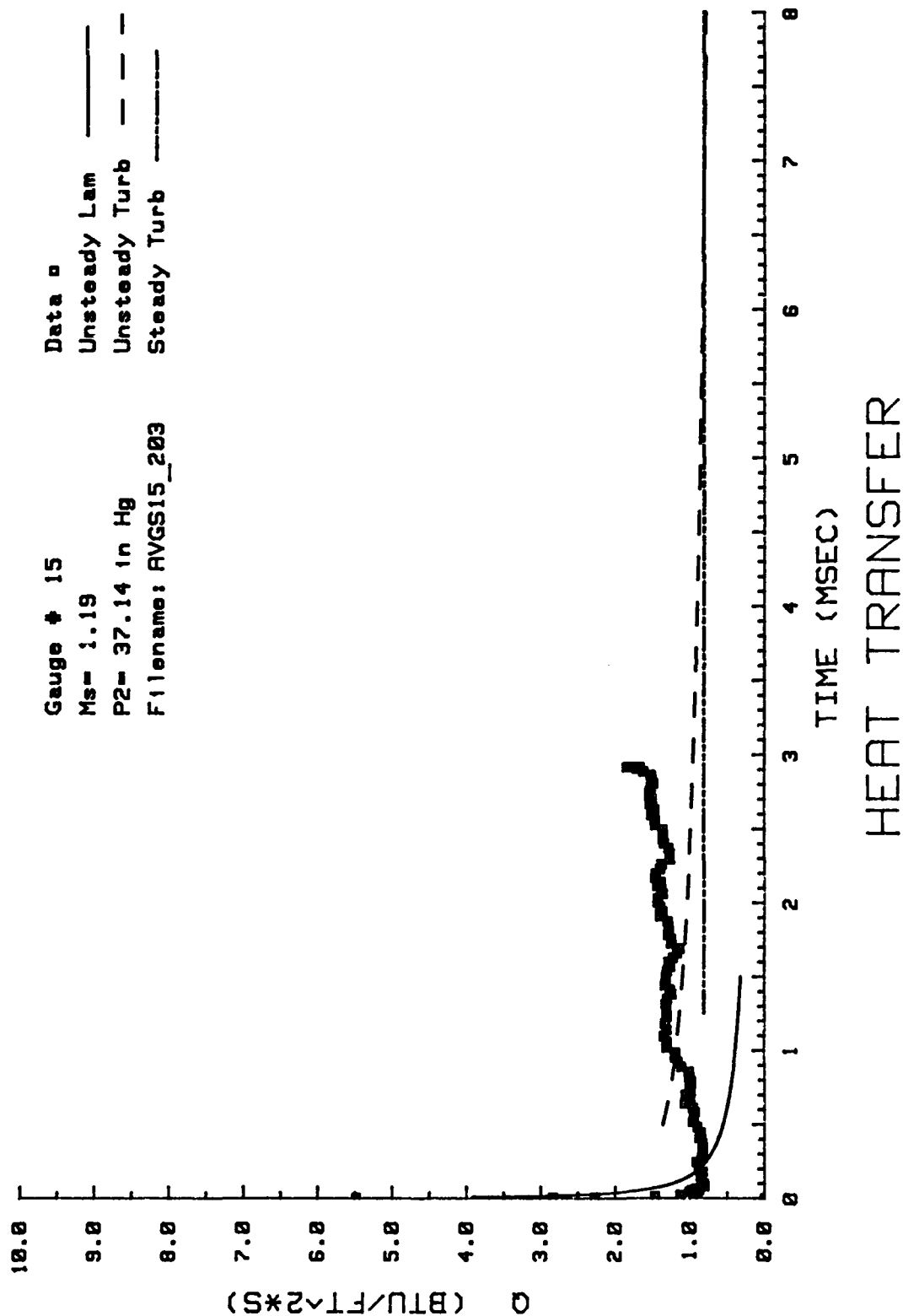
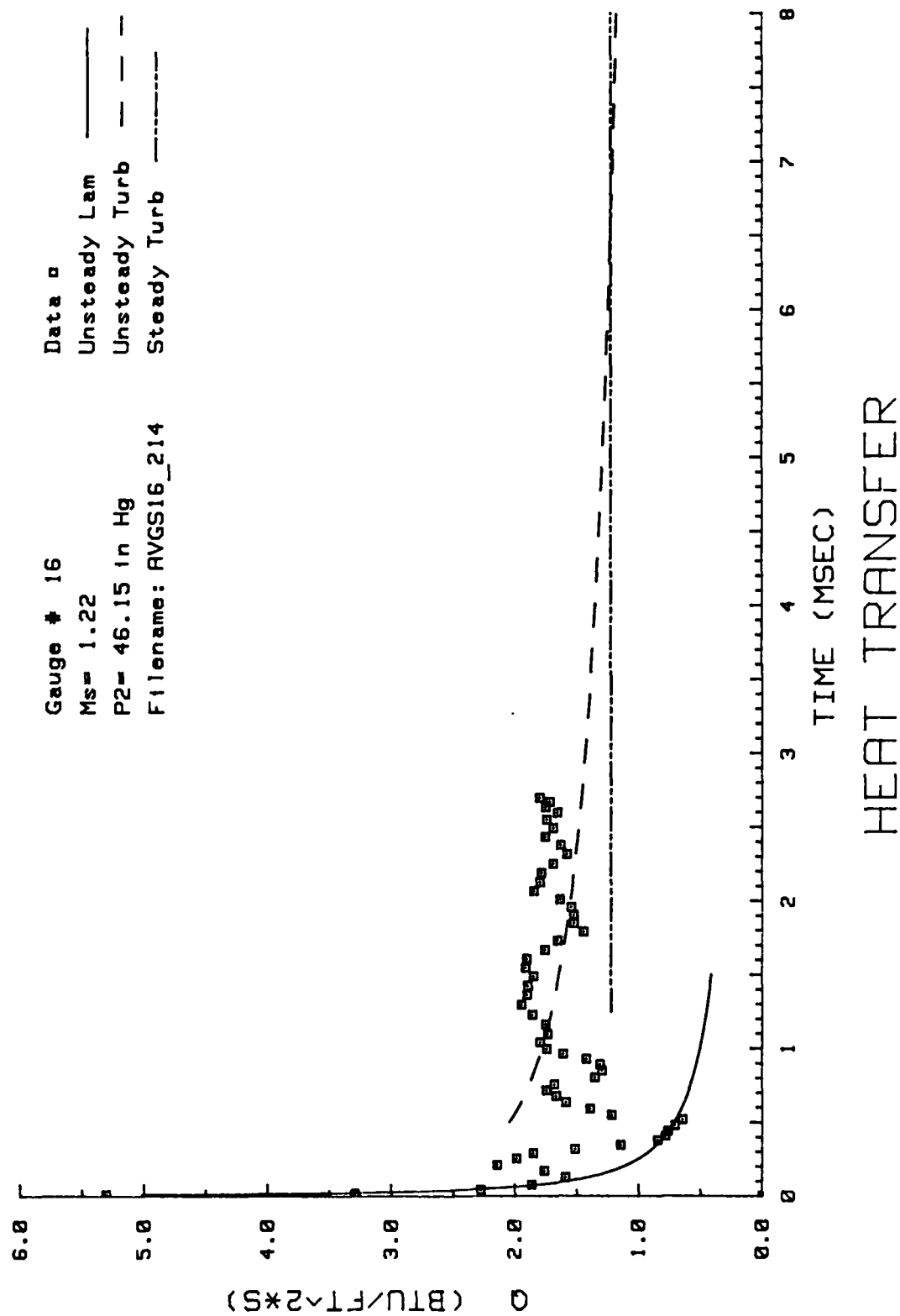HEAT TRANSFER

Figure 40. Heat Transfer: Data Set D Gage #15
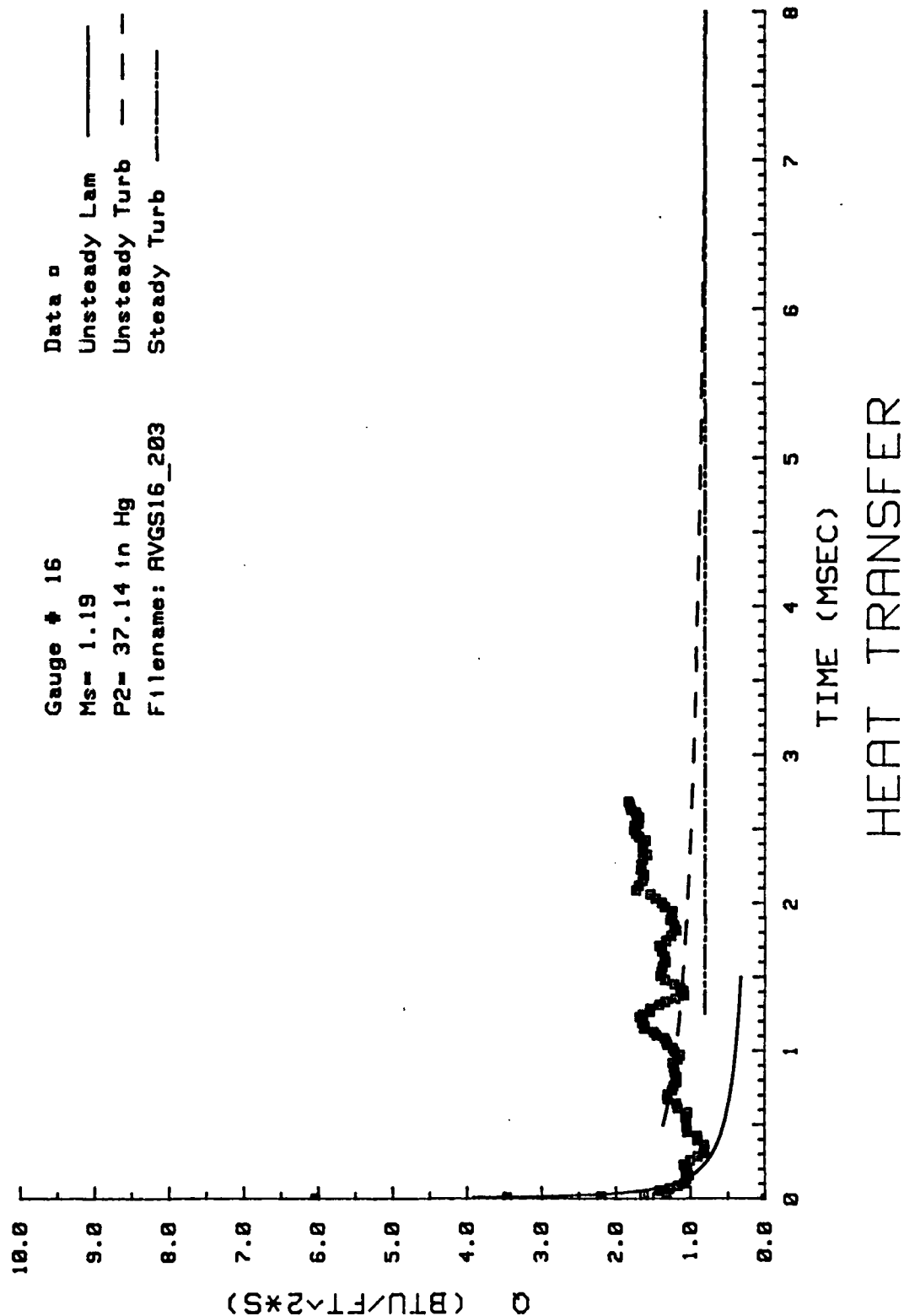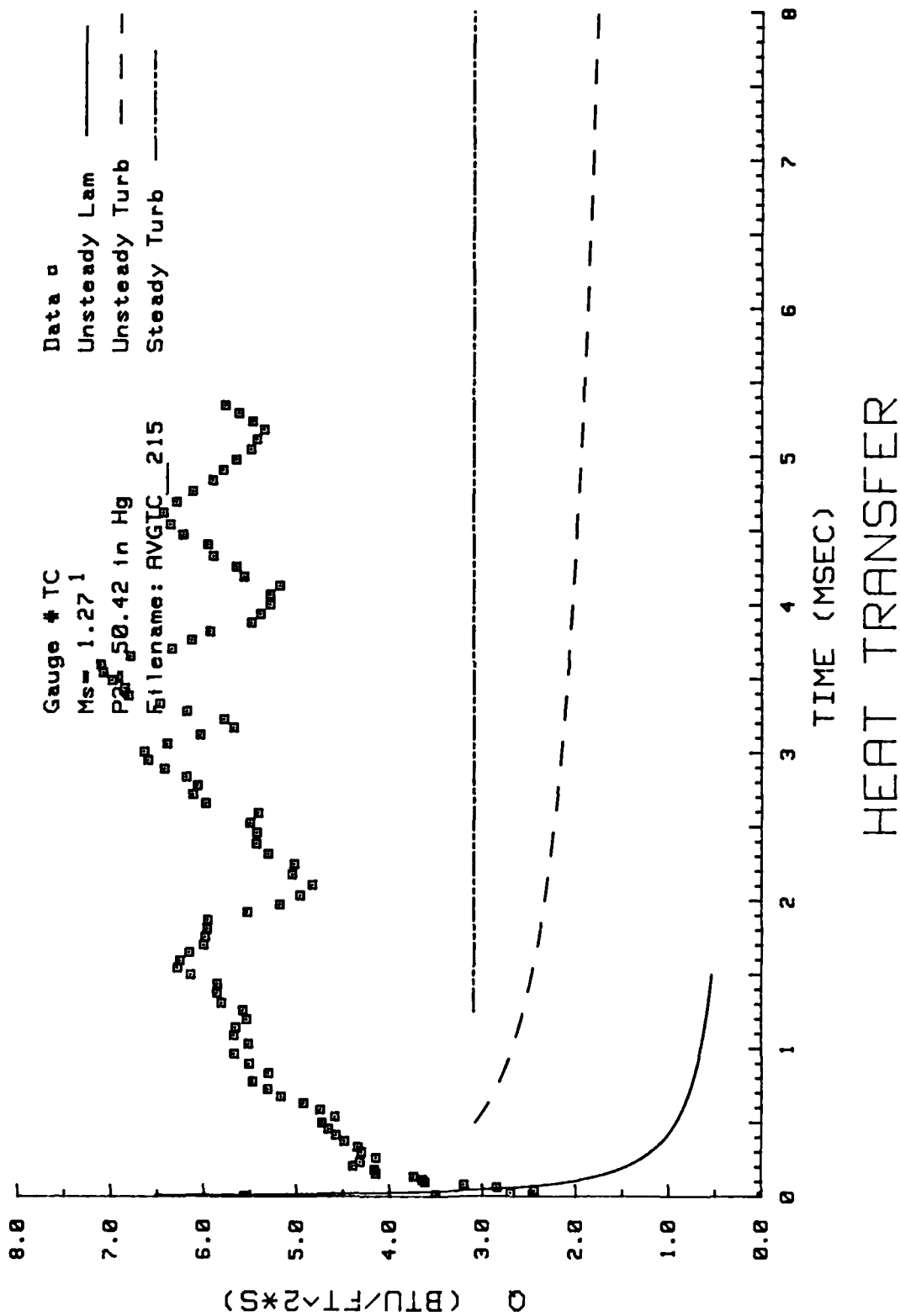
Figure 41. Heat Transfer: Data Set D Gage #16
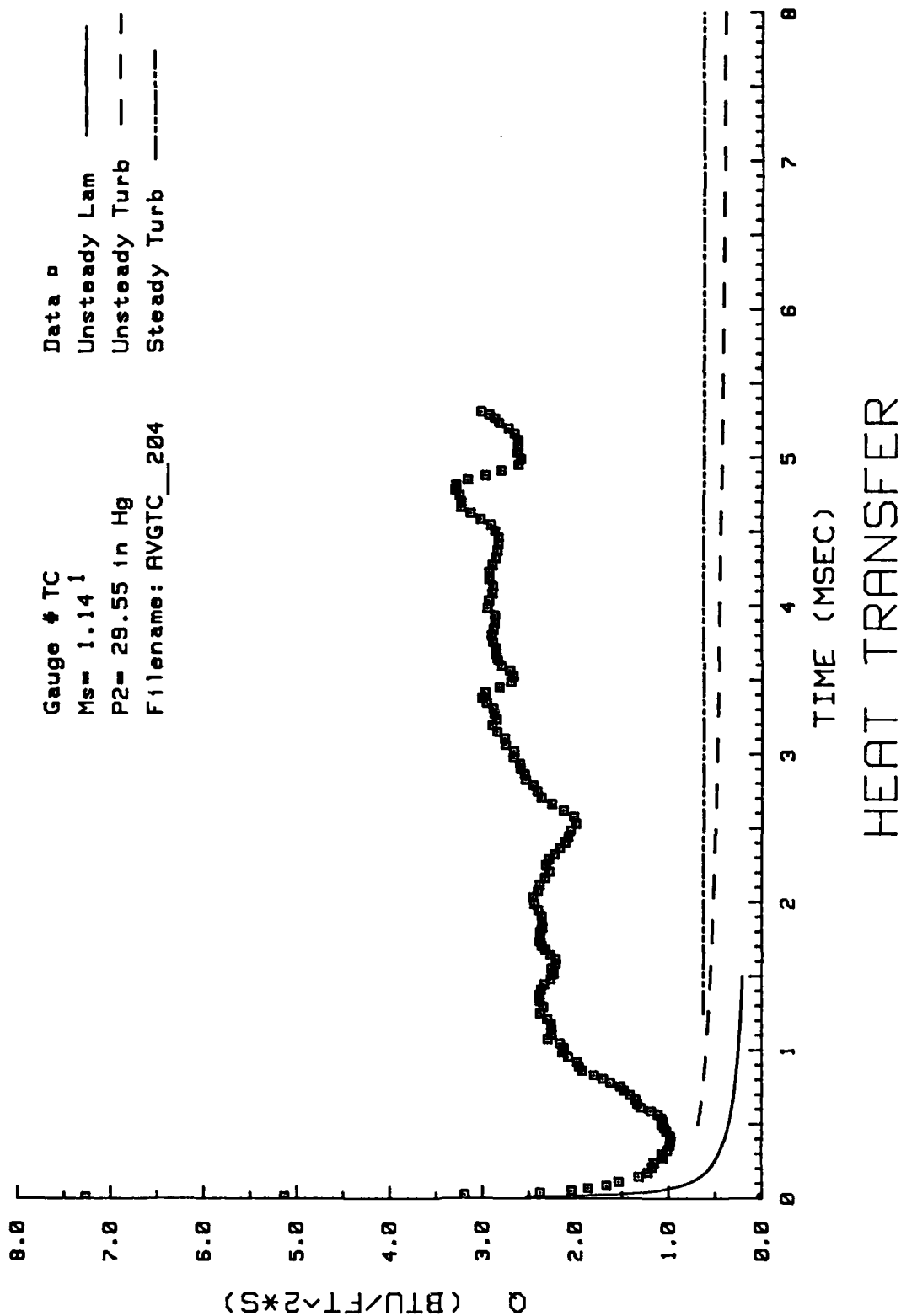
Figure 42. Heat Transfer: Data Set E Thermocouple
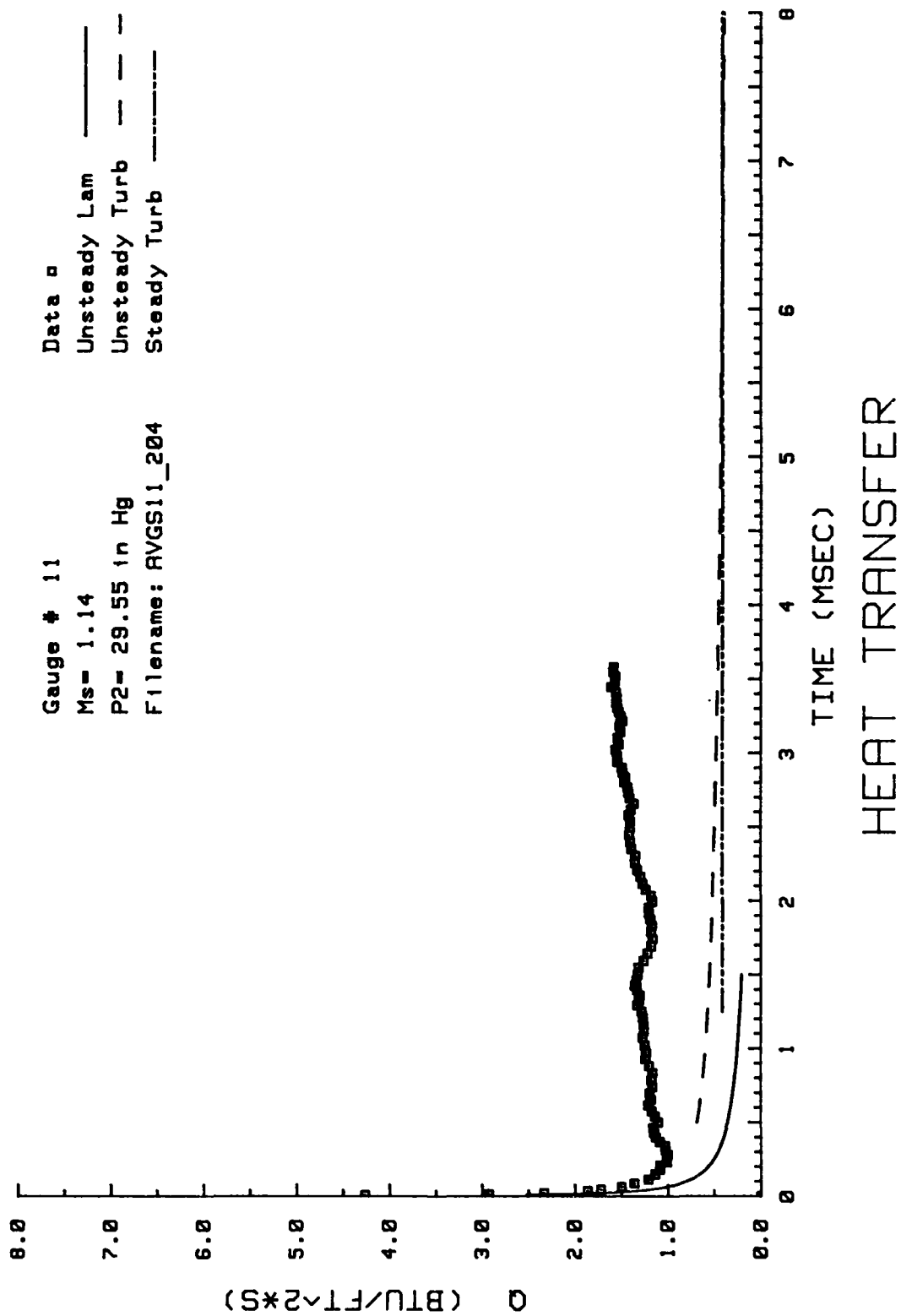
Figure 43. Heat Transfer: Data Set E Gage #11
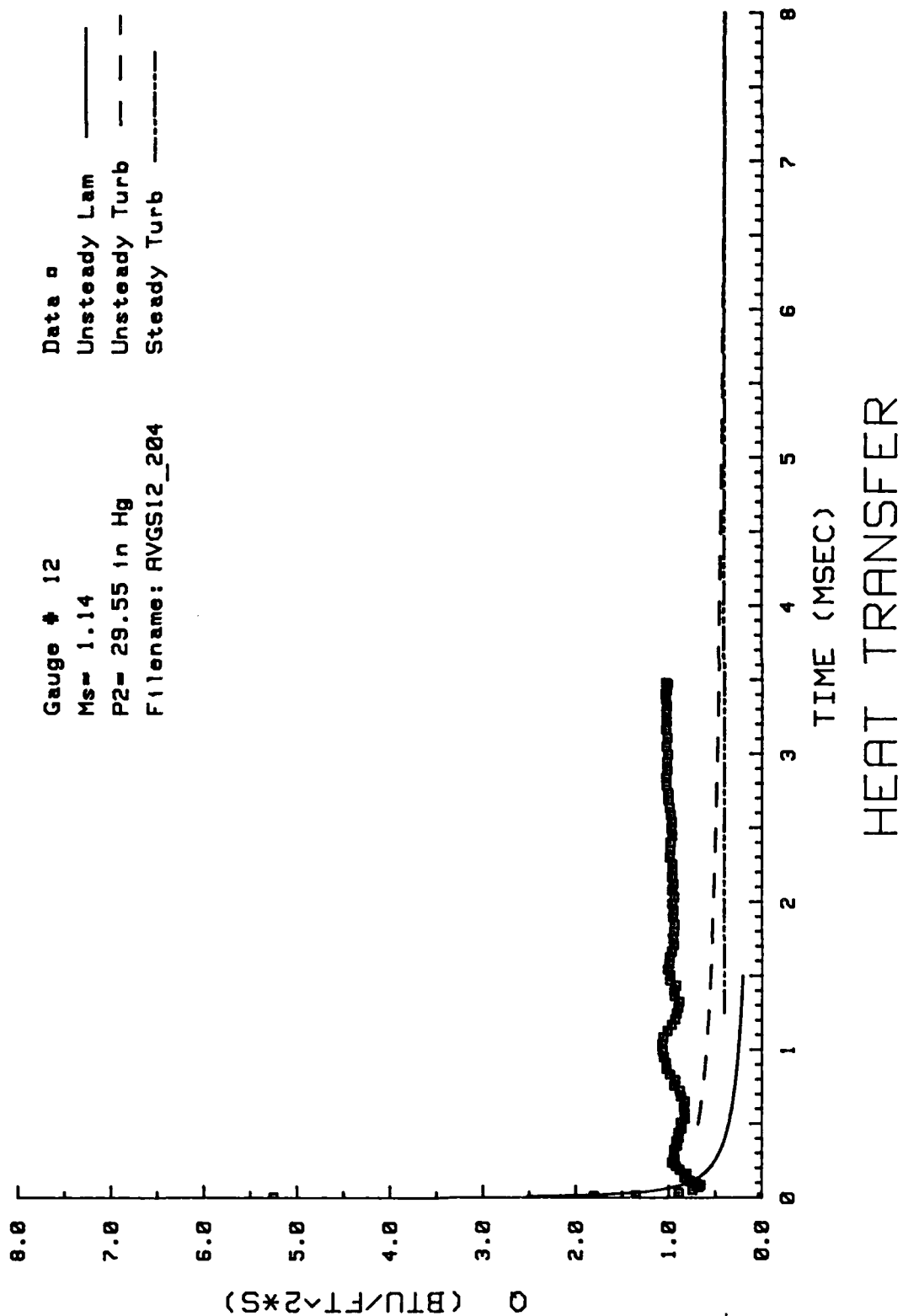
Figure 44. Heat Transfer: Data Set E Gage #12

93
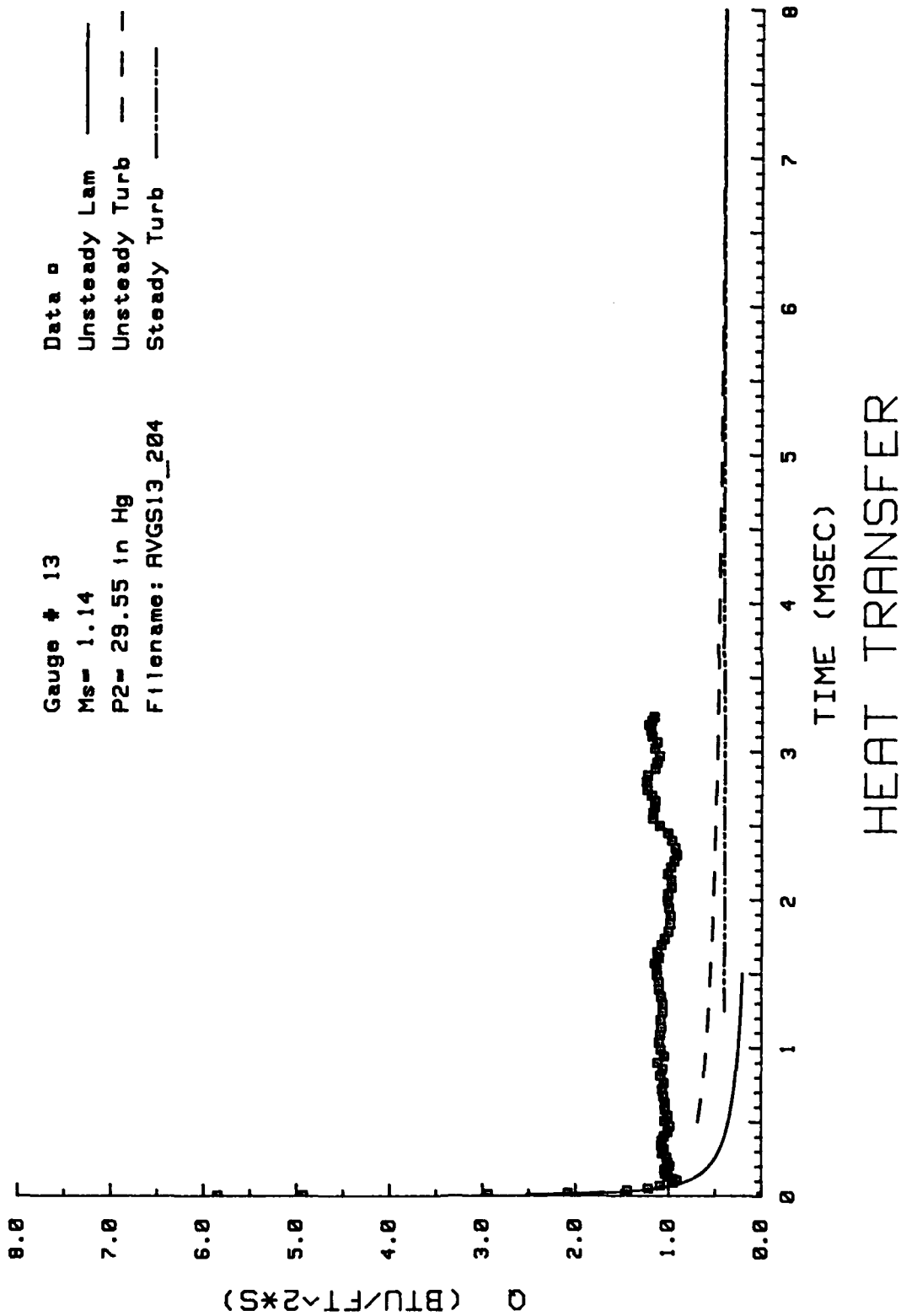
Figure 45. Heat Transfer: Data Set E Gage #13

94
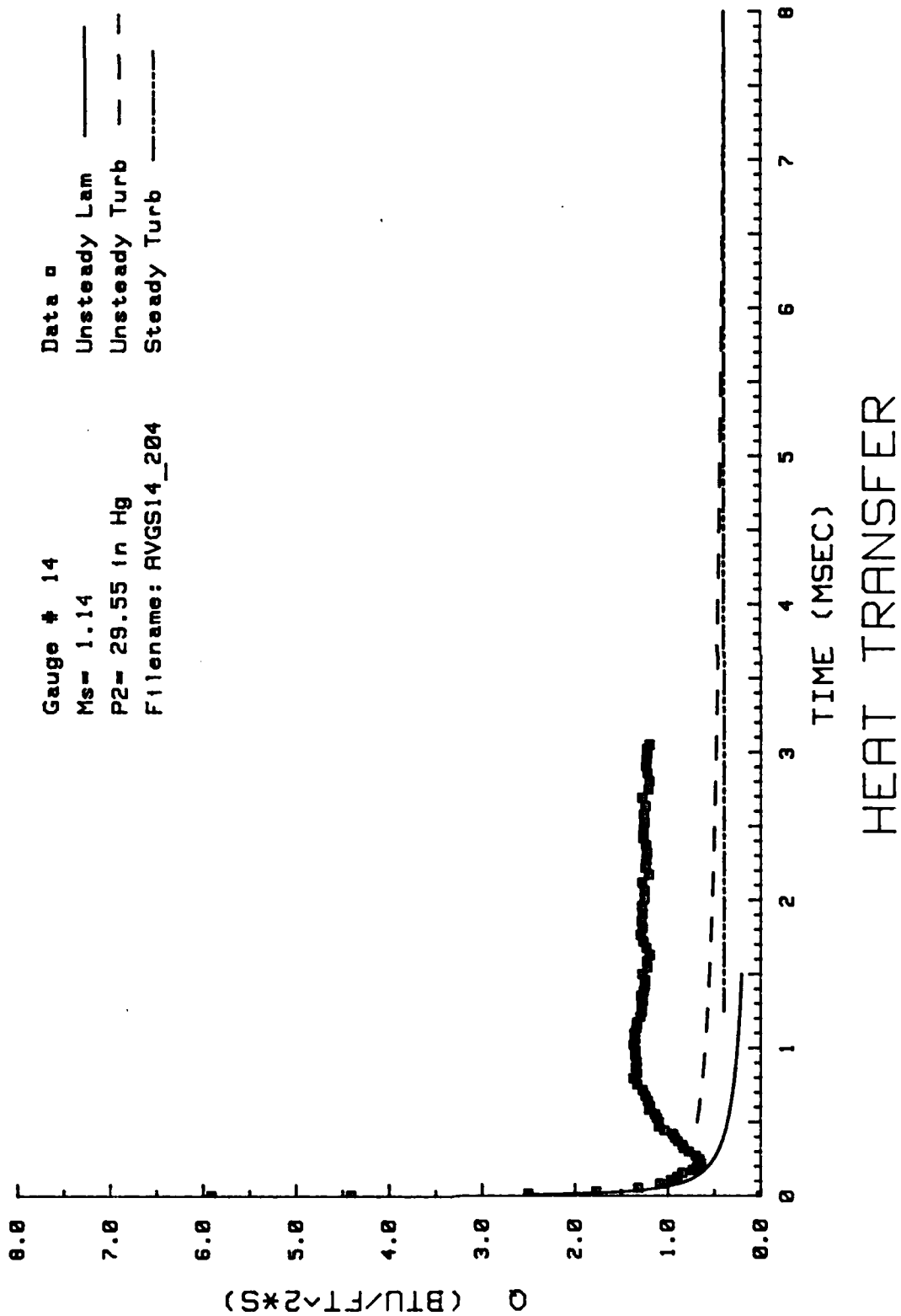
Figure 46. Heat Transfer: Data Set E Gage #14

95
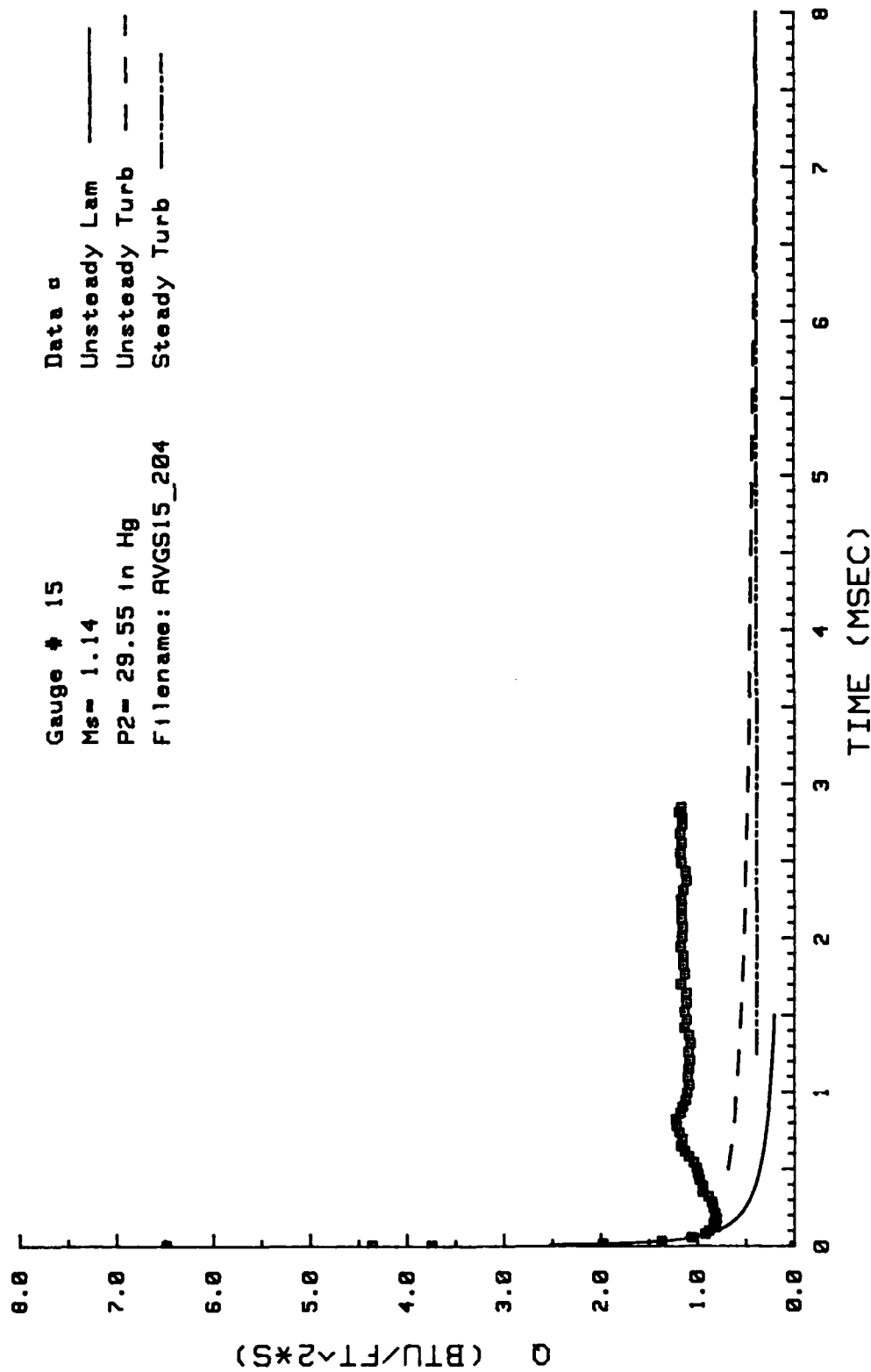
Figure 47. Heat Transfer: Data Set E Gage #15
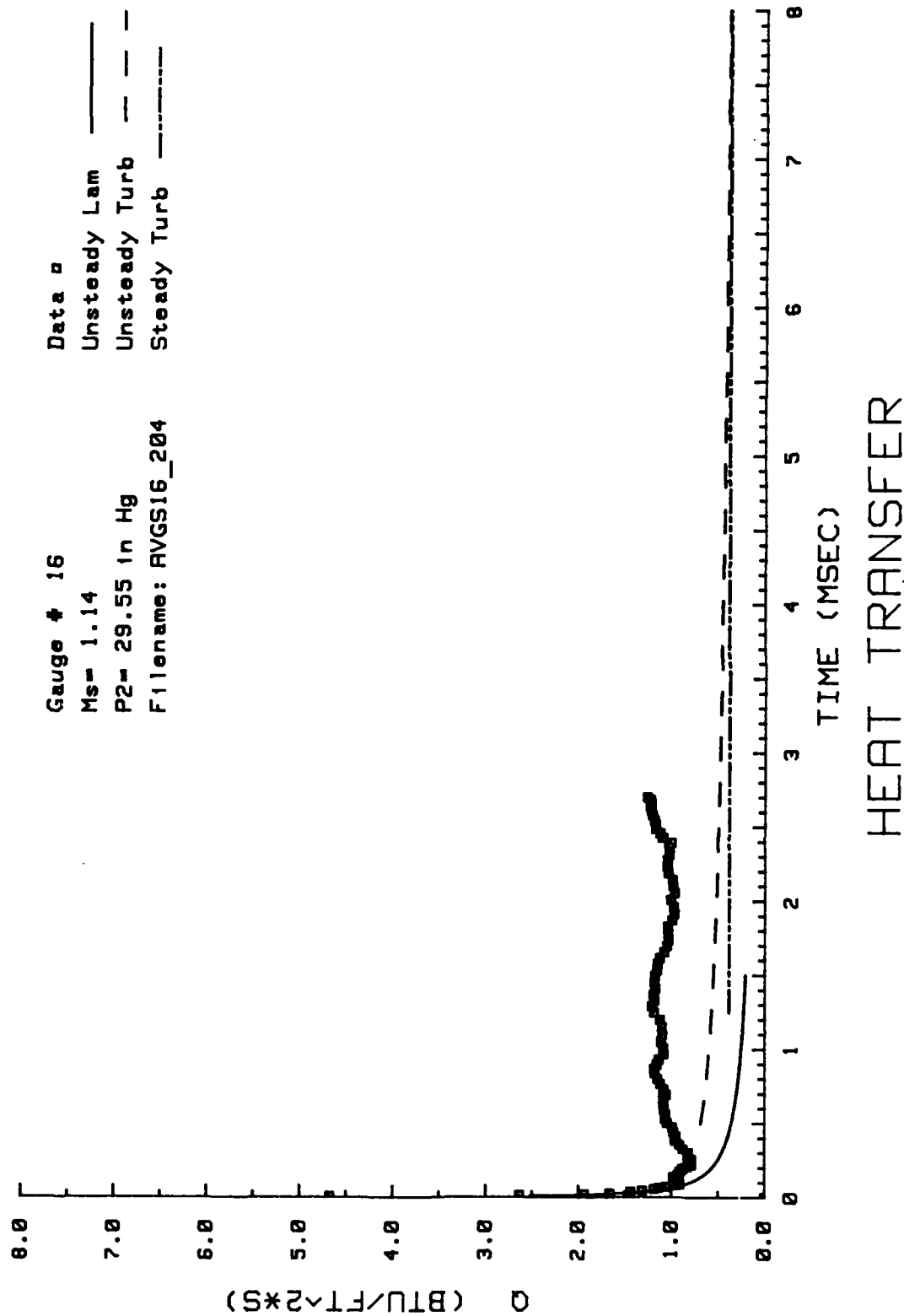
Figure 48. Heat Transfer: Data Set E Gage #16

97
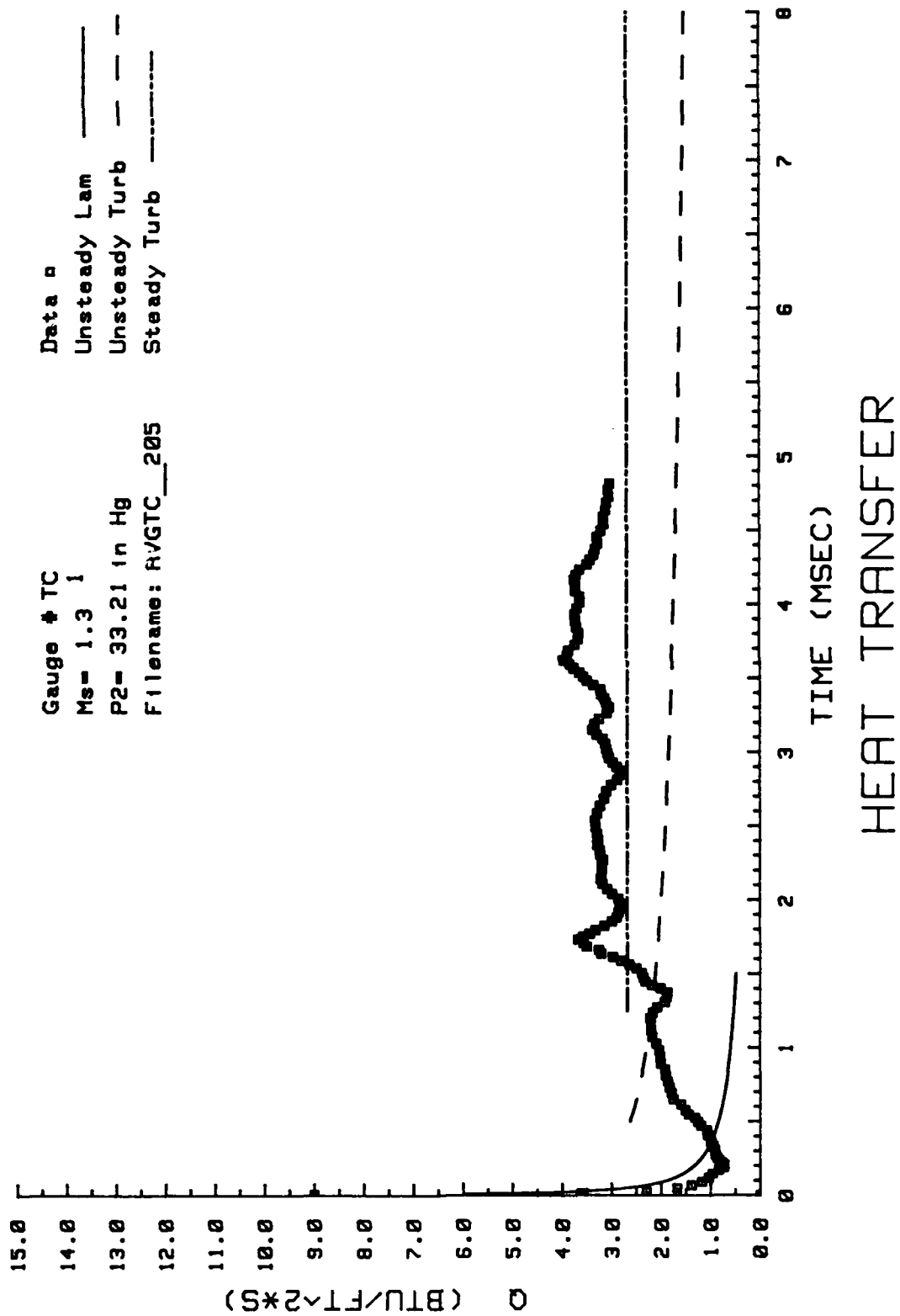
Figure 49. Heat Transfer: Data Set F Thermocouple
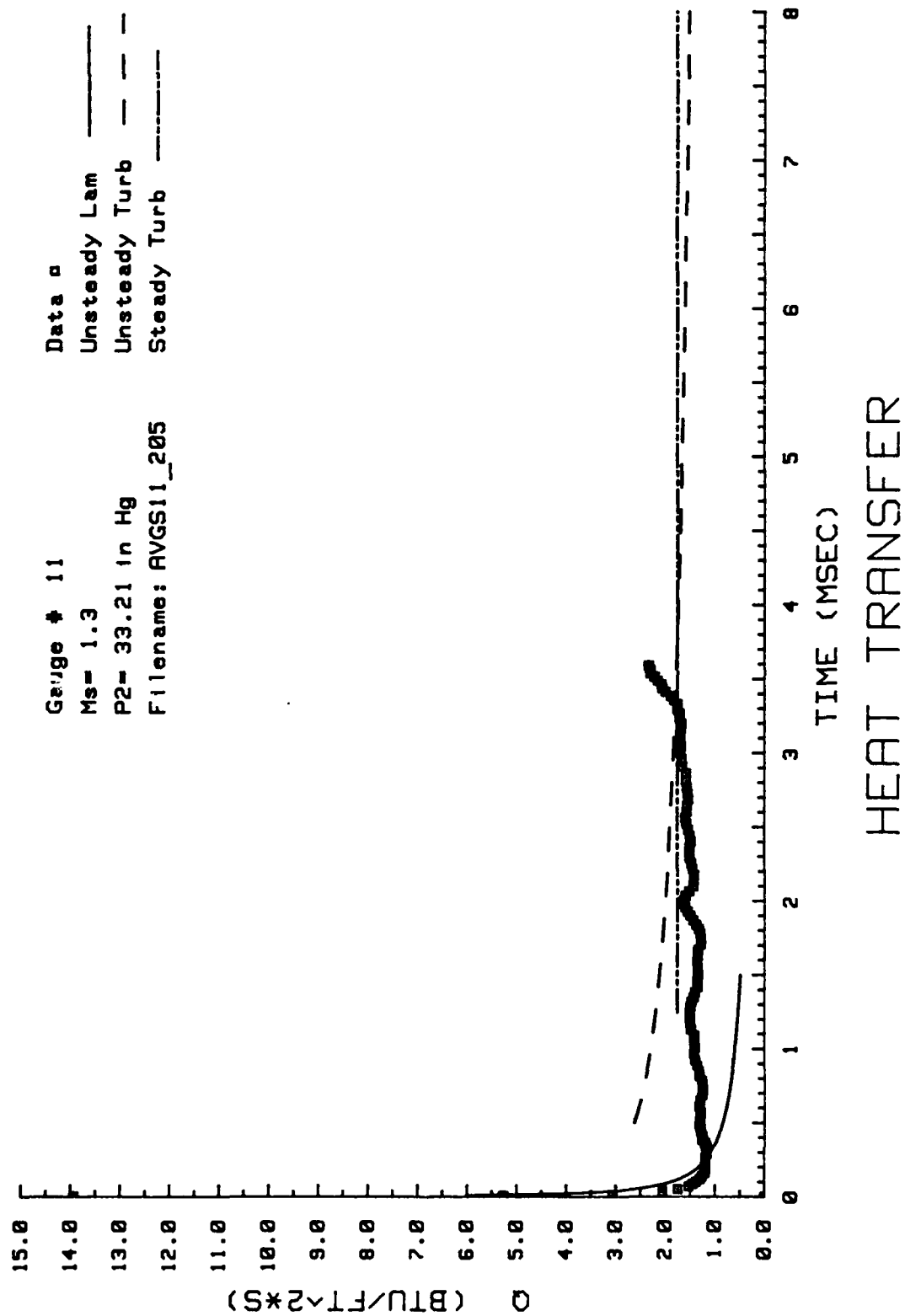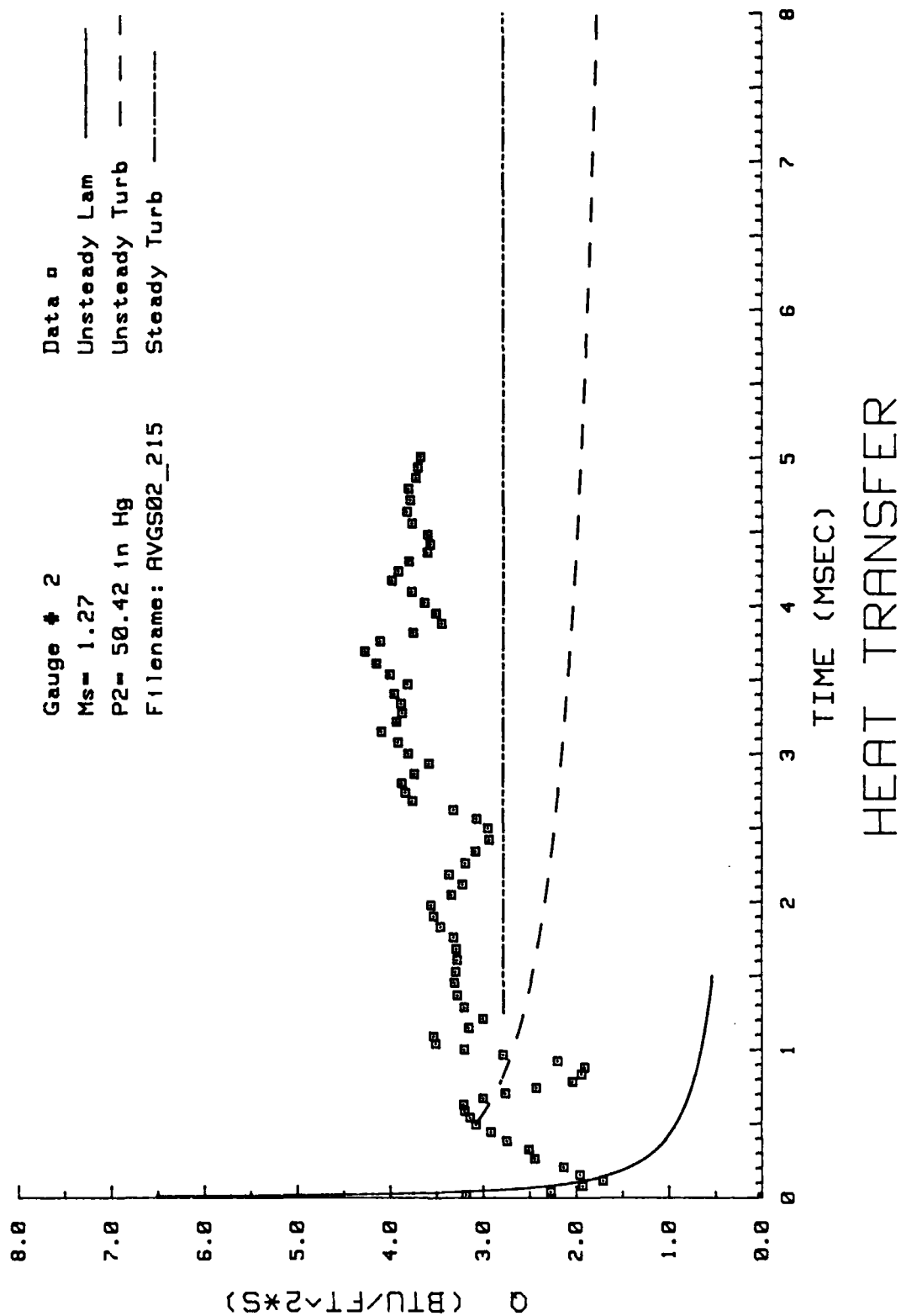
Figure 50. Heat Transfer: Data Set F Gage #11
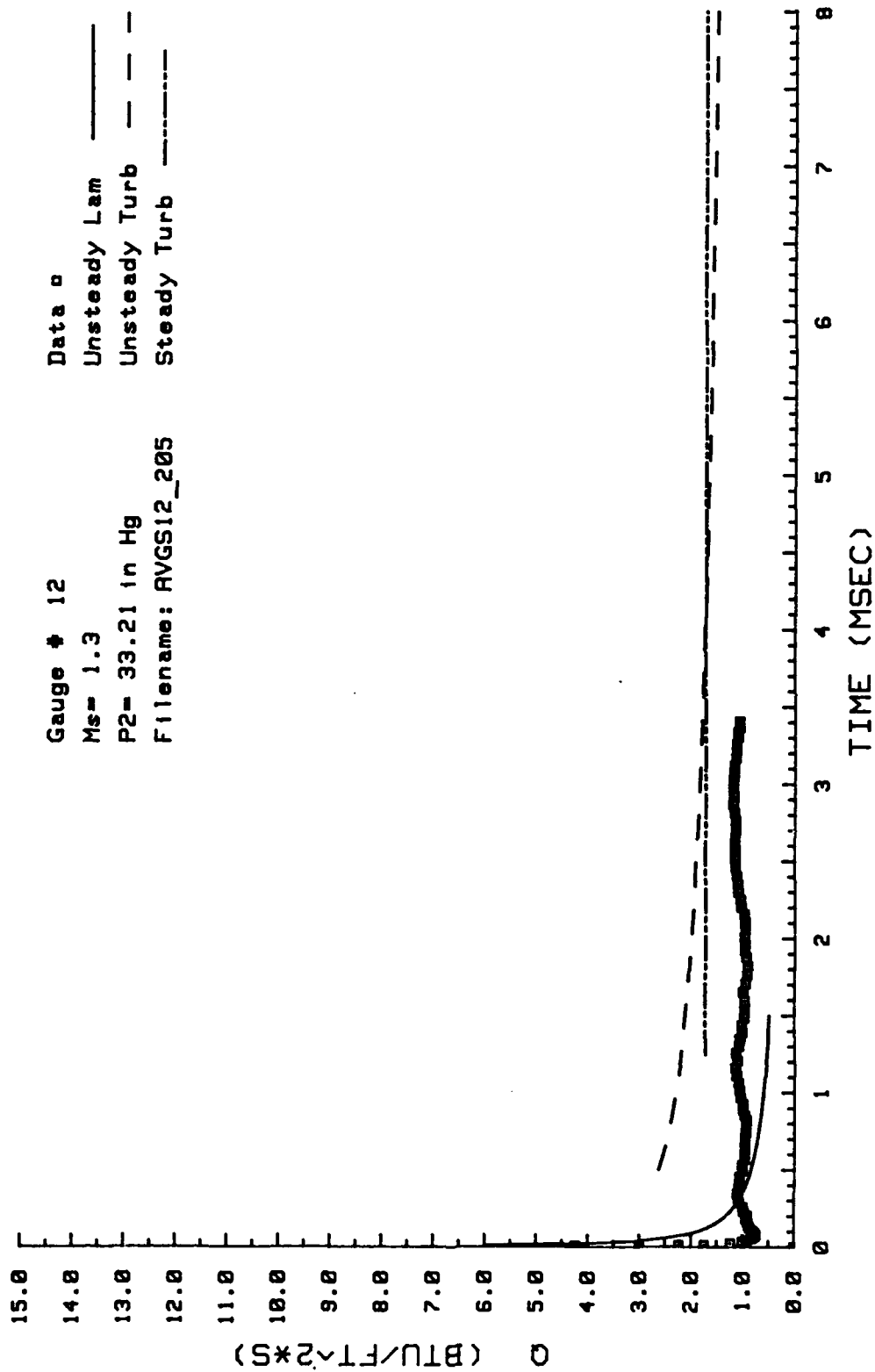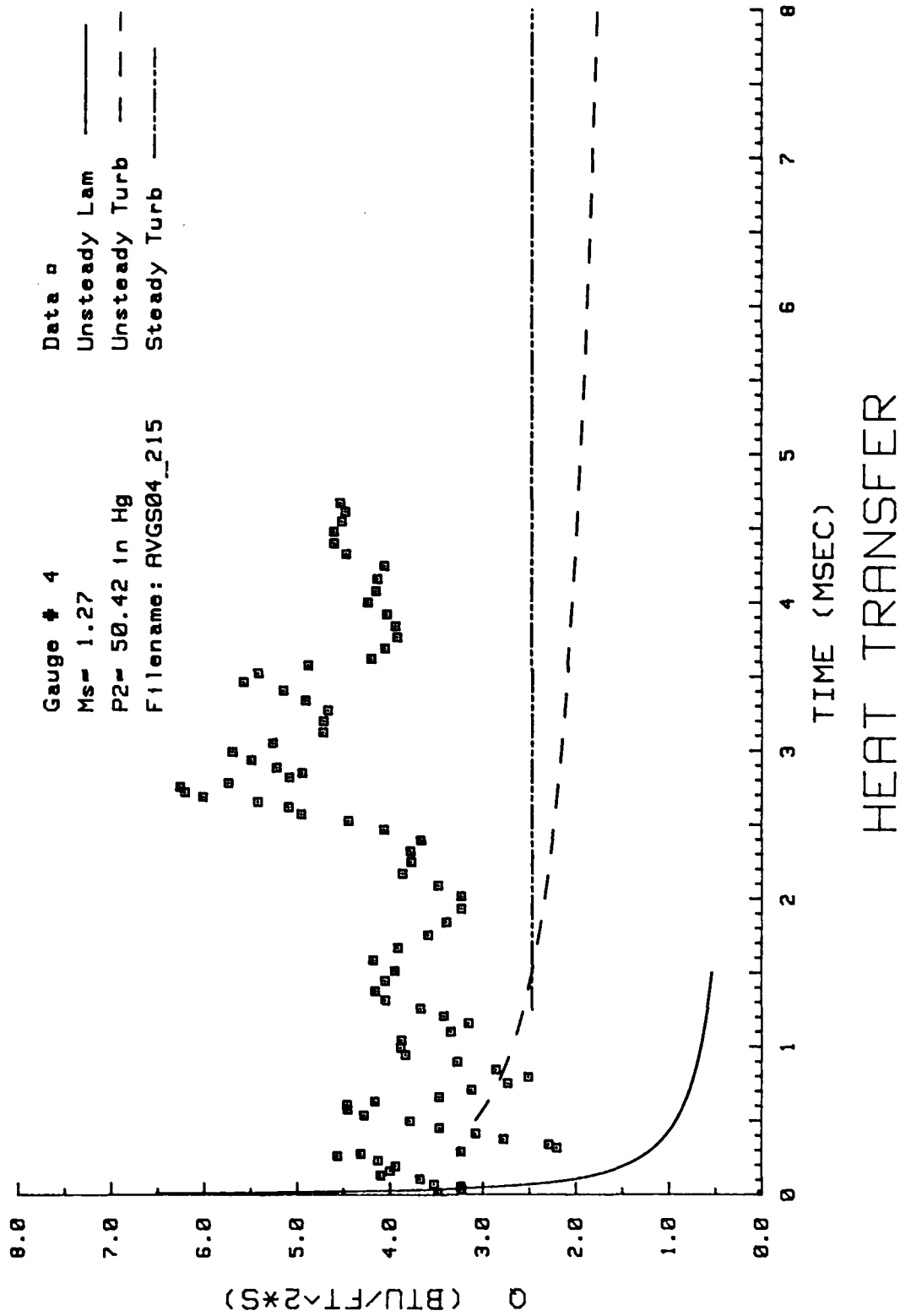
Figure 51. Heat Transfer: Data Set F Gage #12
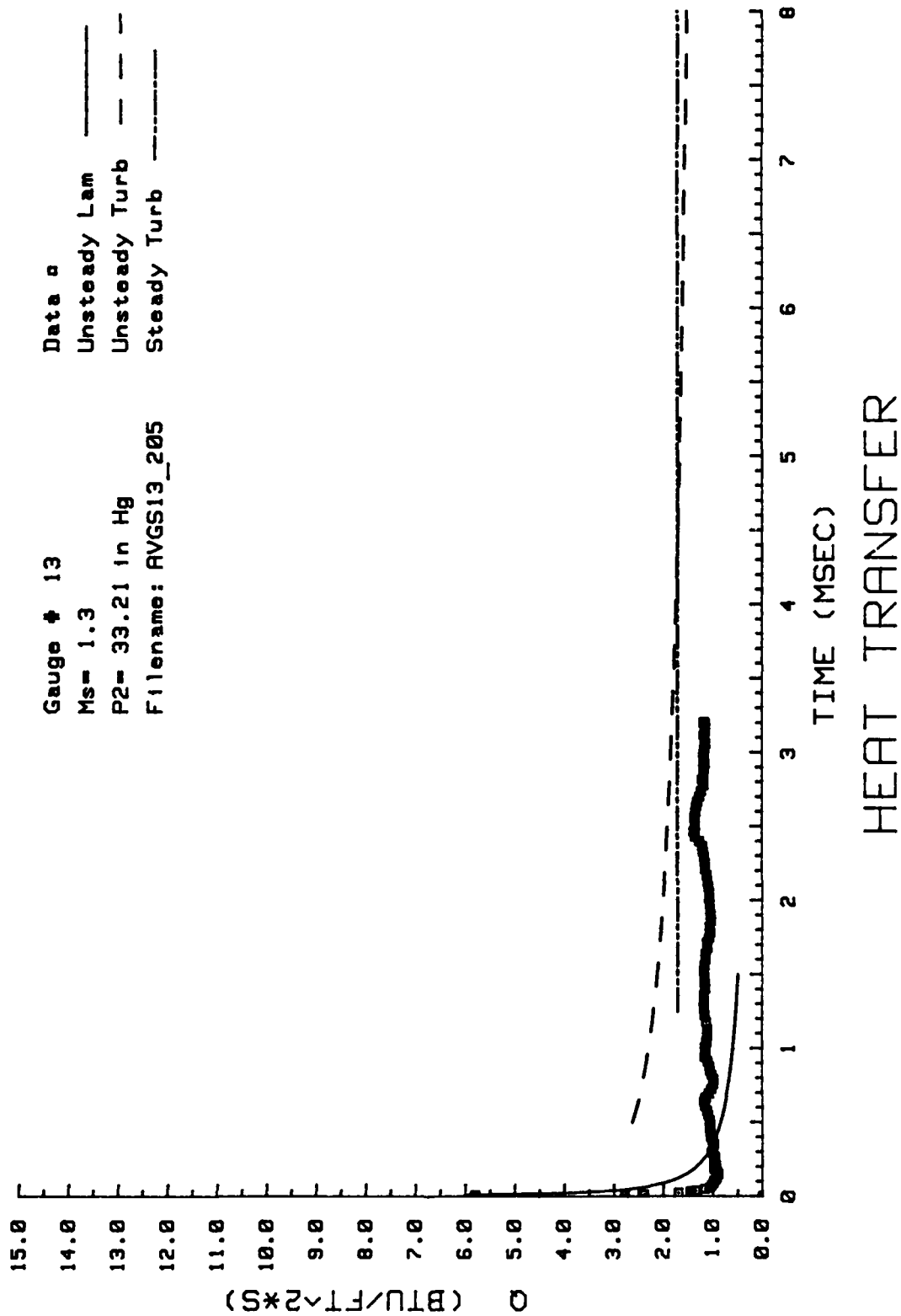
Figure 52. Heat Transfer: Data Set F Gage #13
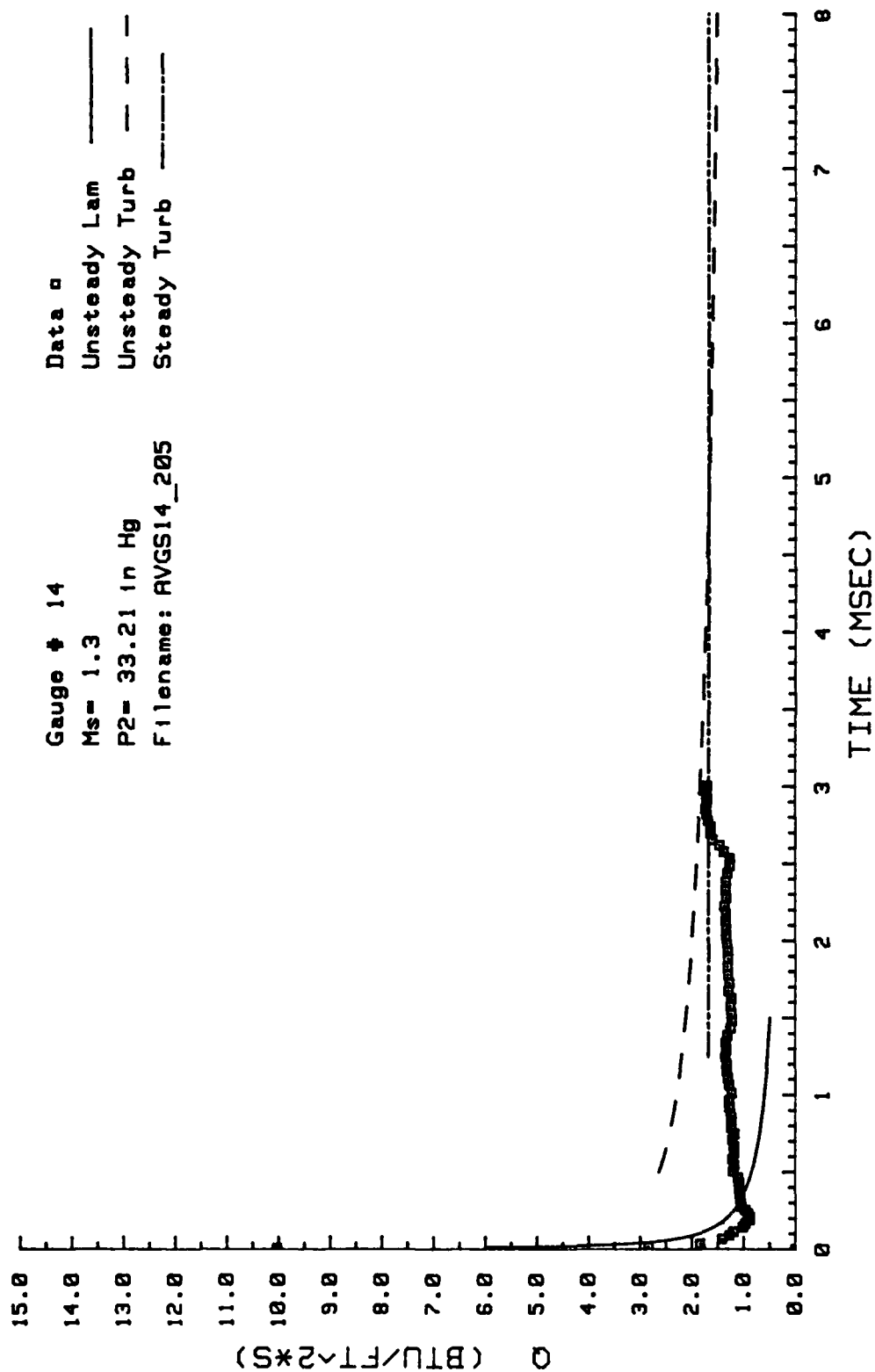
Figure 53. Heat Transfer: Data Set F Gage #14
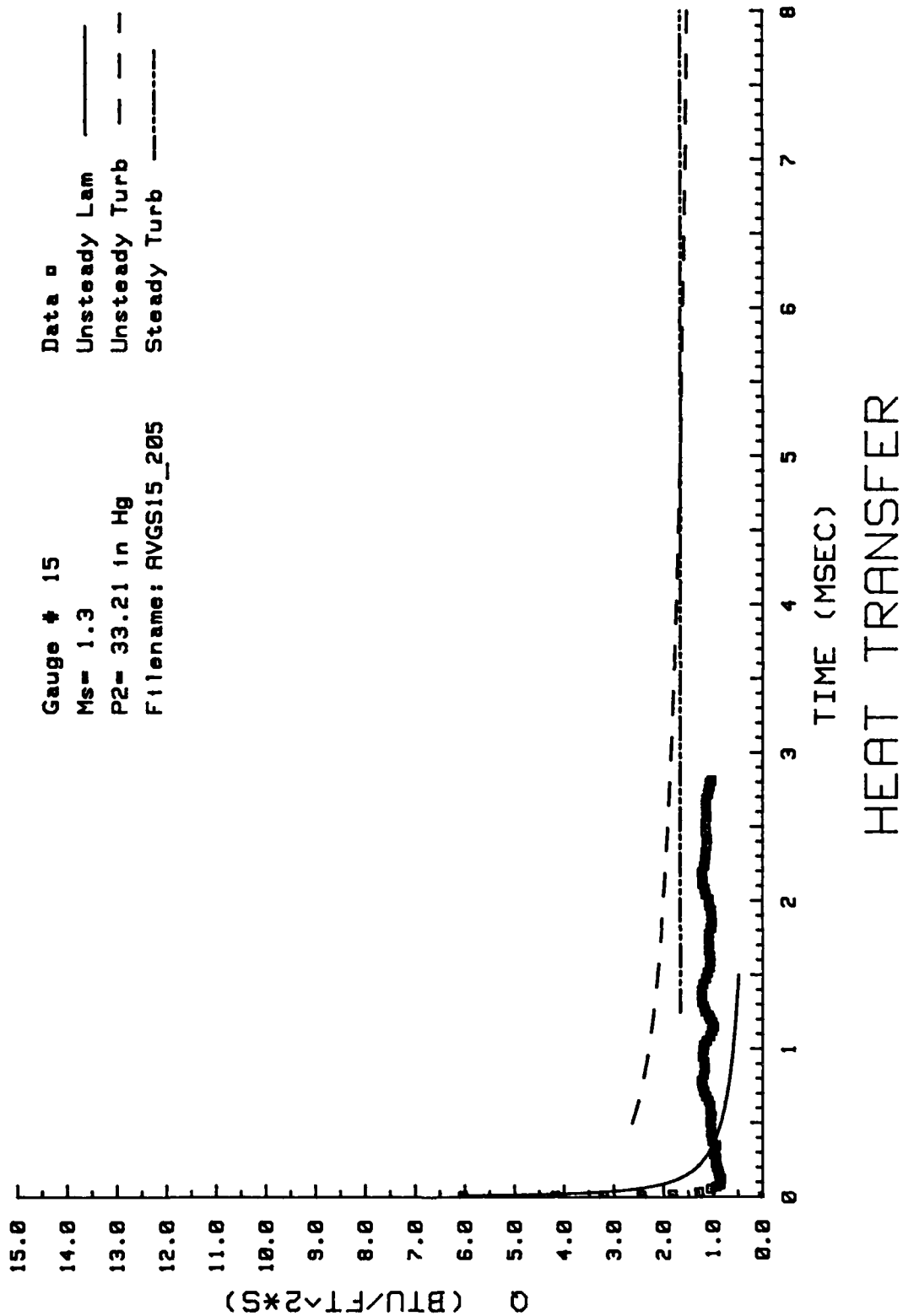
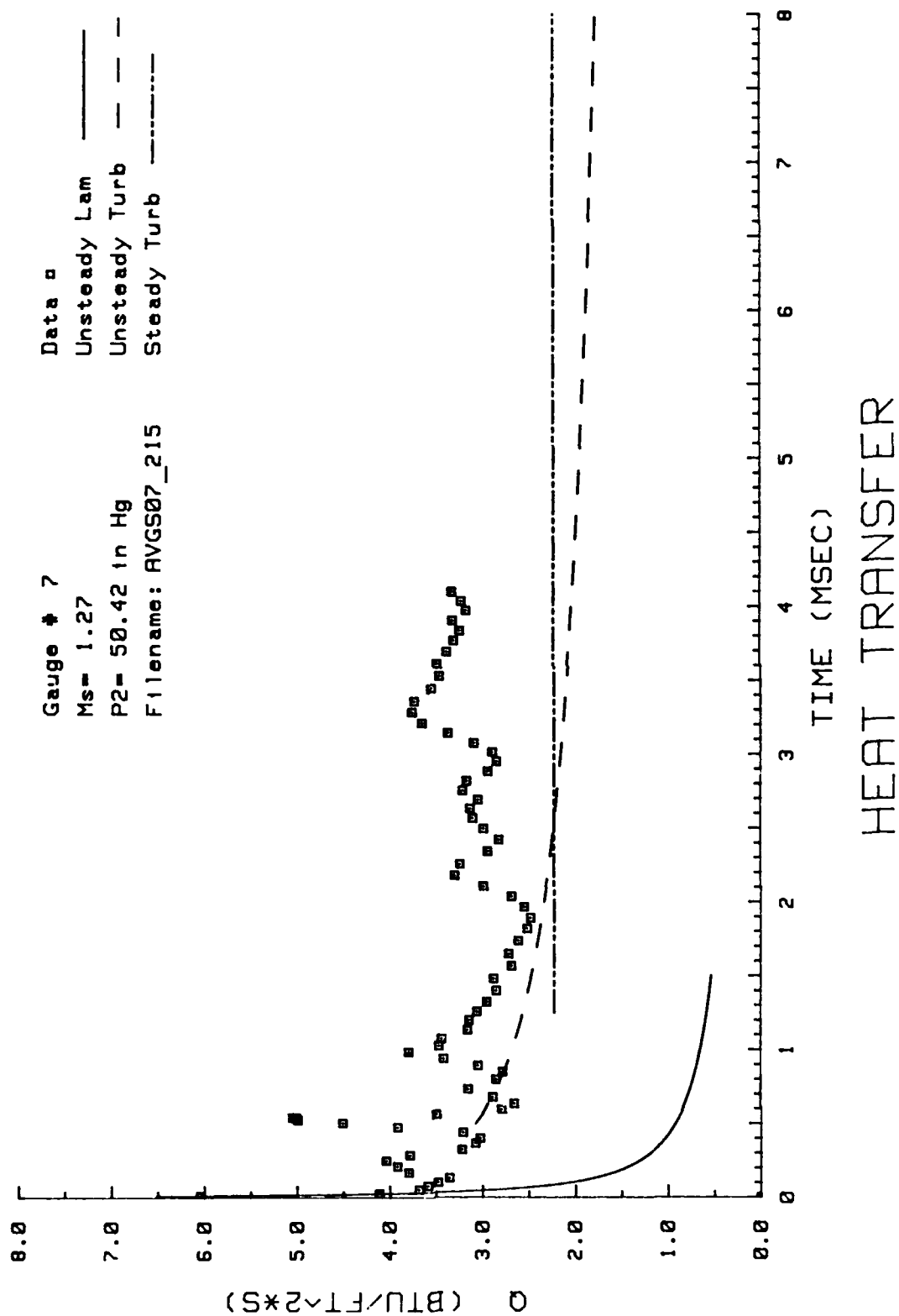Figure 54. Heat Transfer: Data Set F Gage #15

103
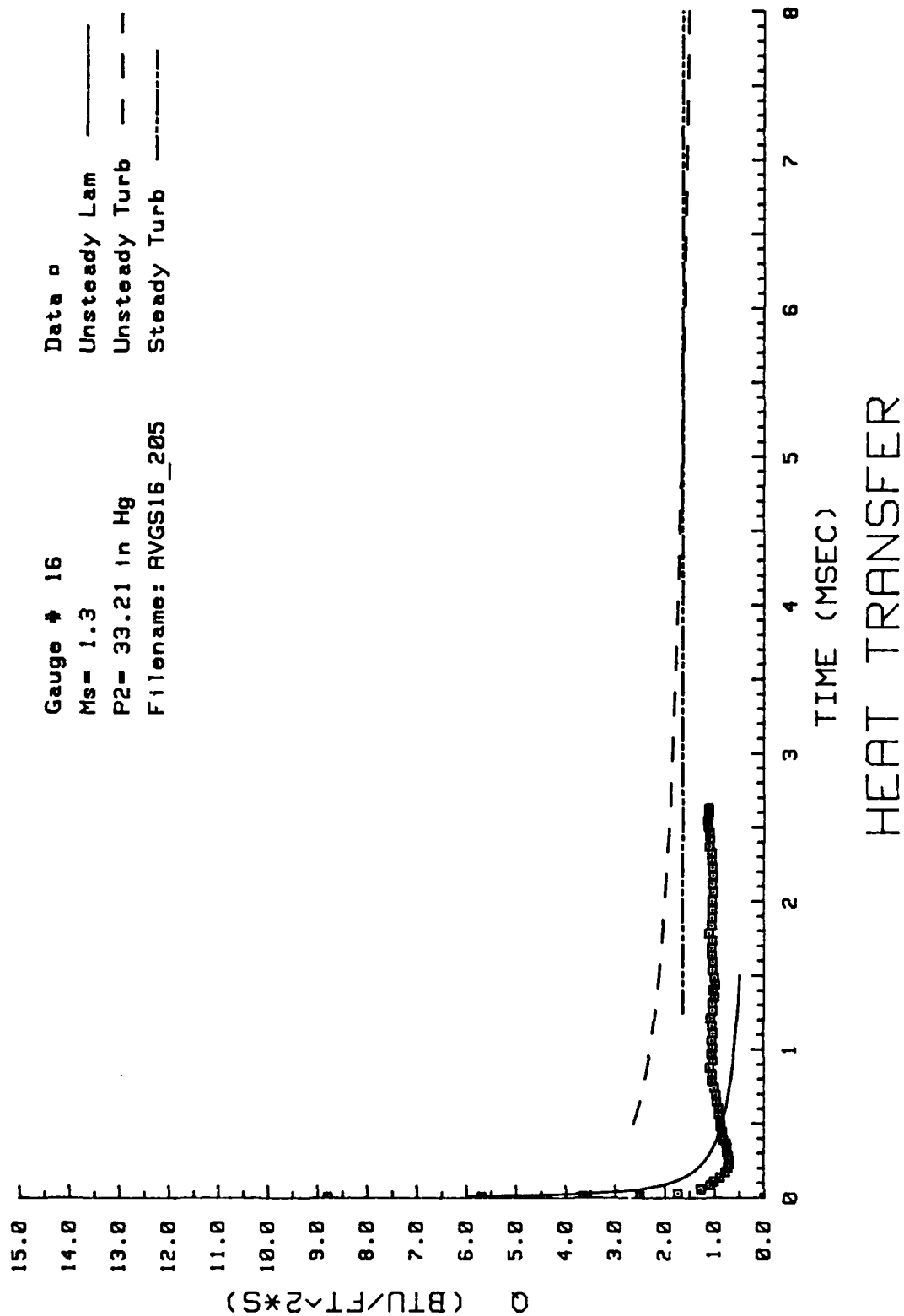
Figure 55. Heat Transfer: Data Set F Gage #16

104
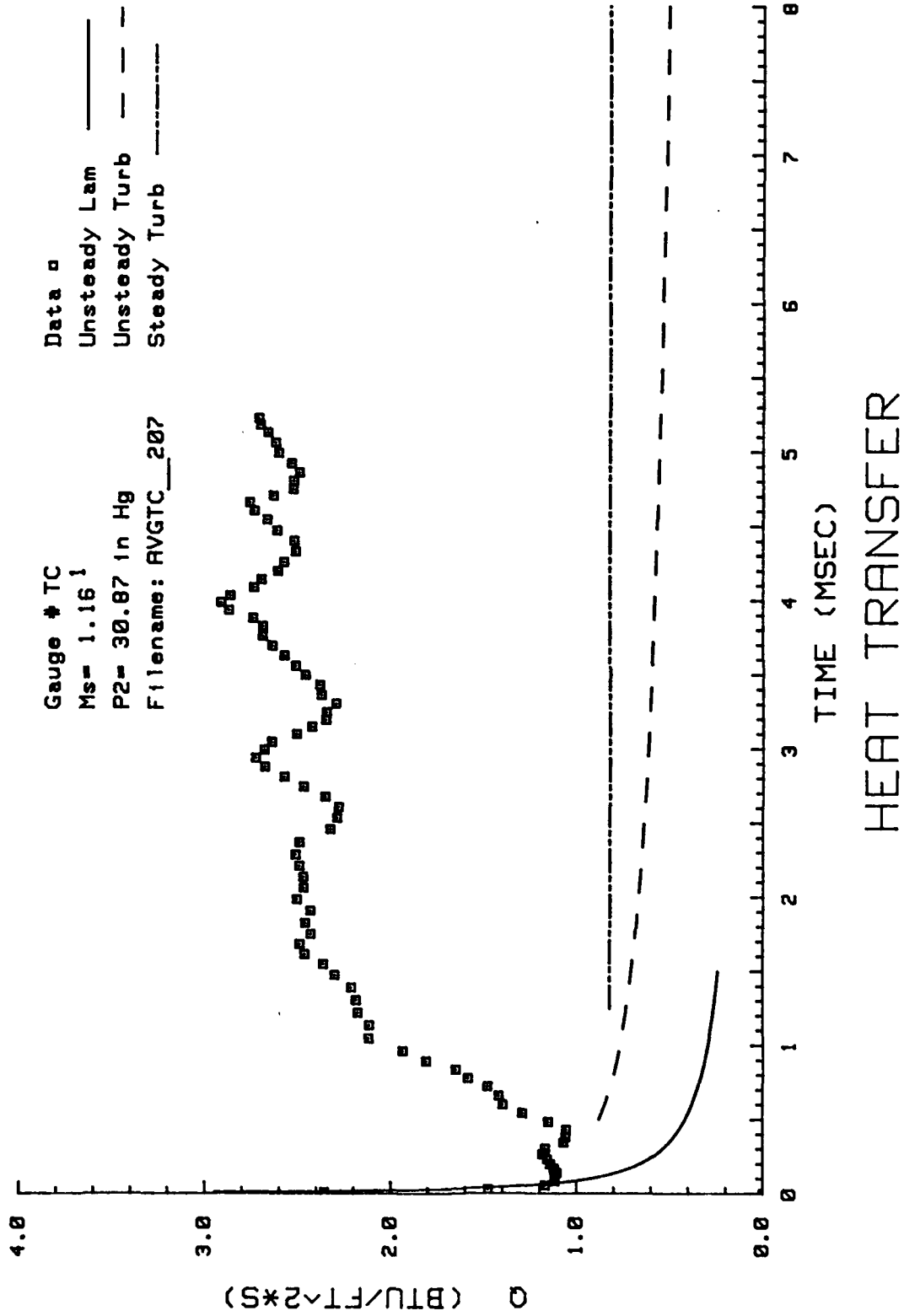
Figure 56. Heat Transfer: Data Set H Thermocouple
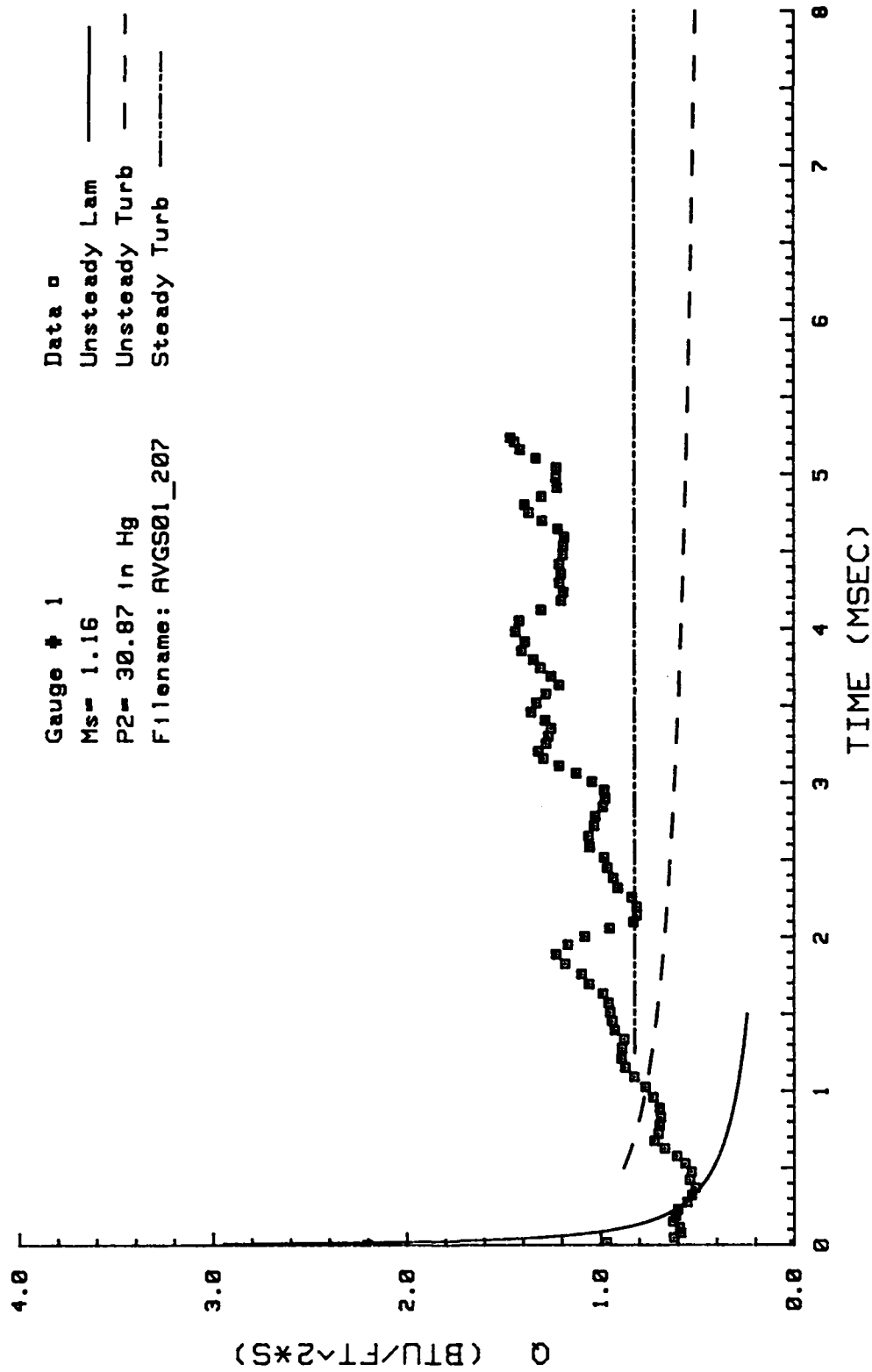
Figure 57. Heat Transfer: Data Set H Gage #1
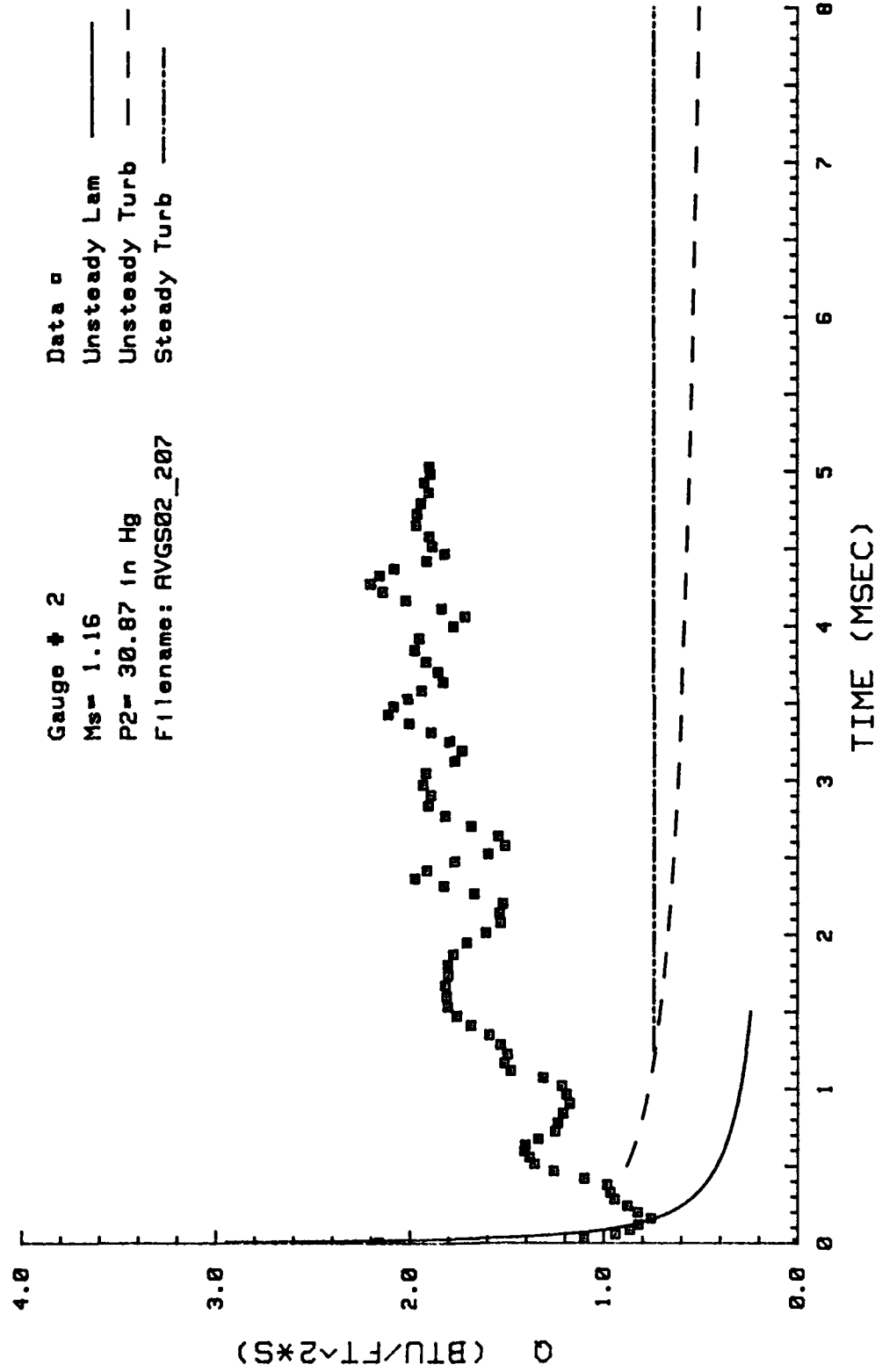
Figure 58. Heat Transfer: Data Set H Gage #2
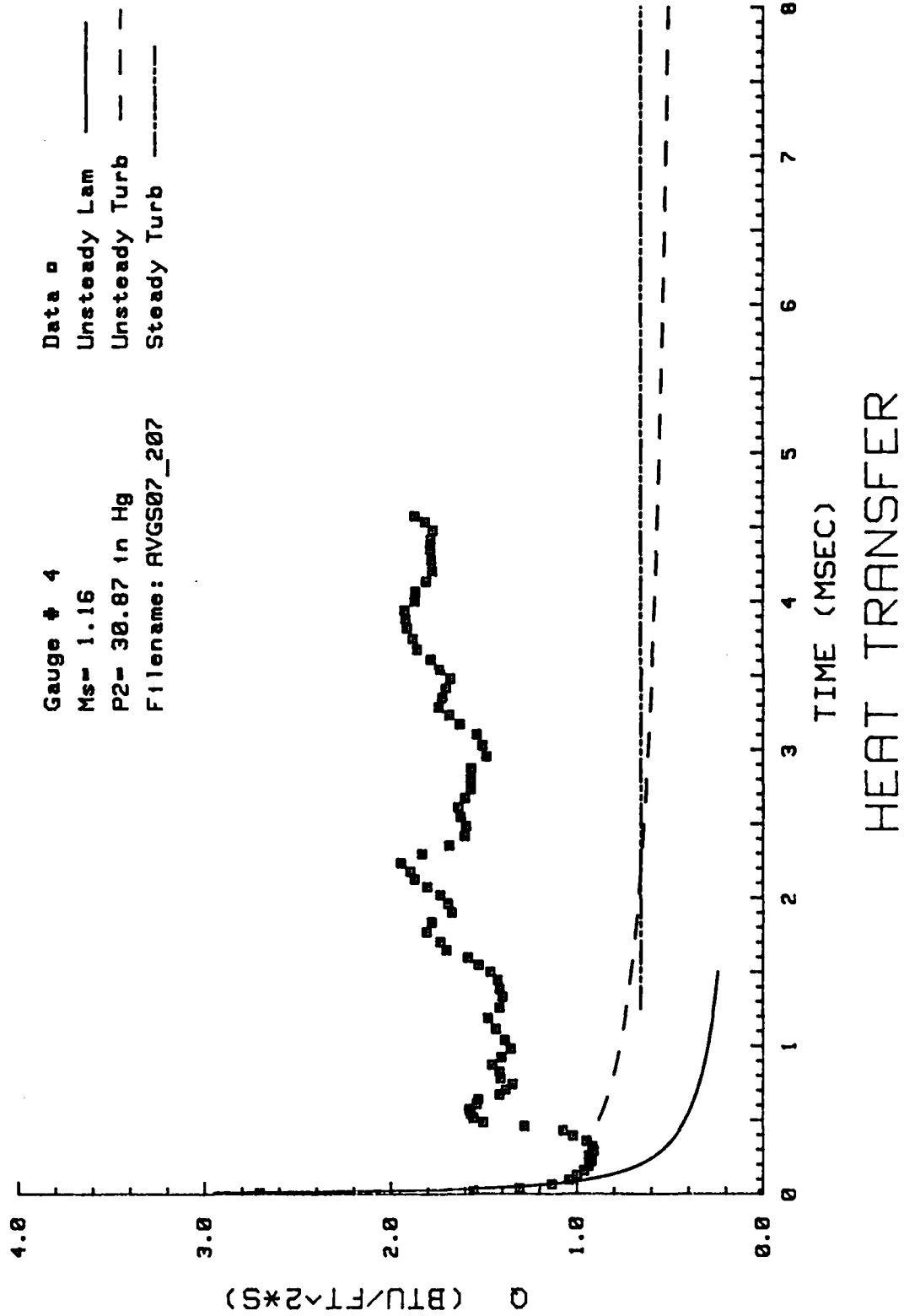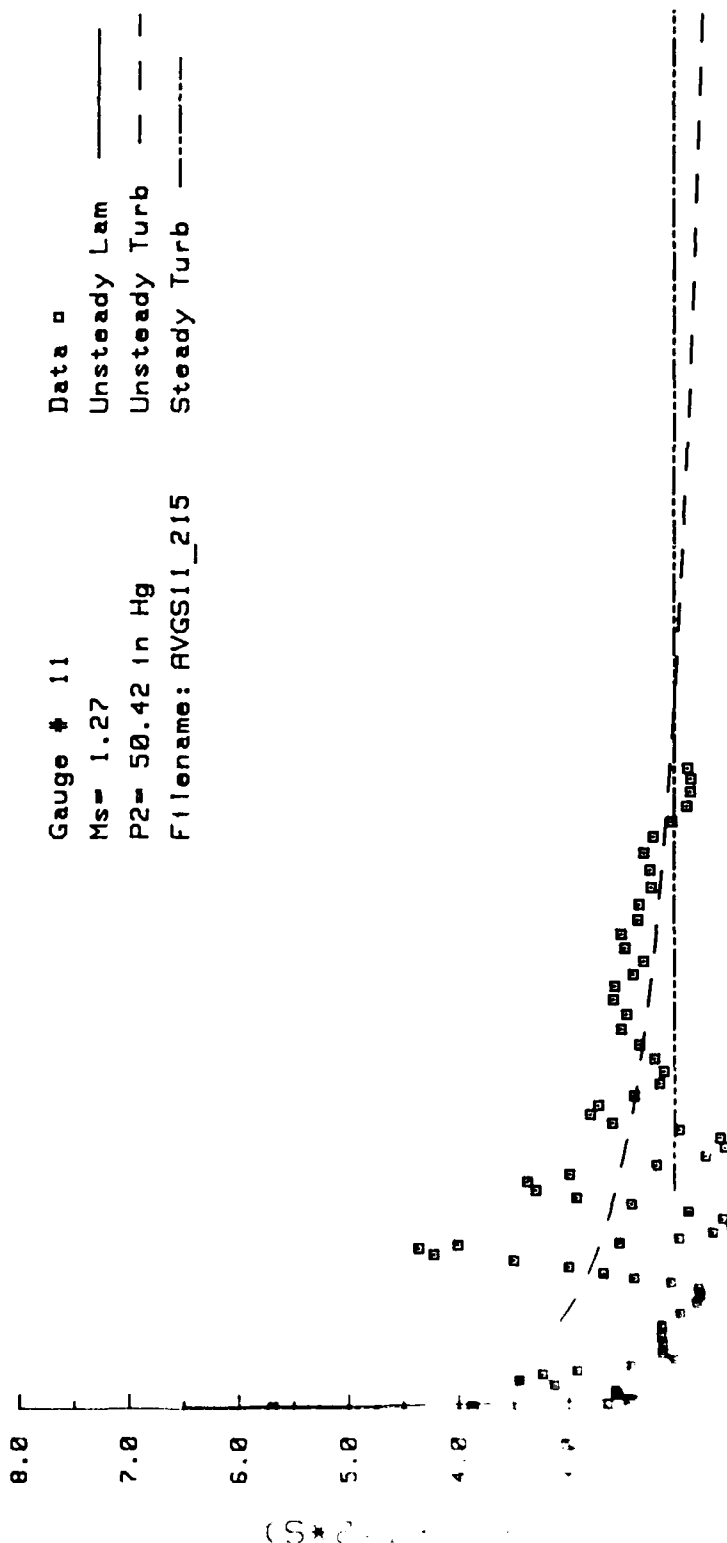
Figure 59. Heat Transfer: Data Set H Gage #4
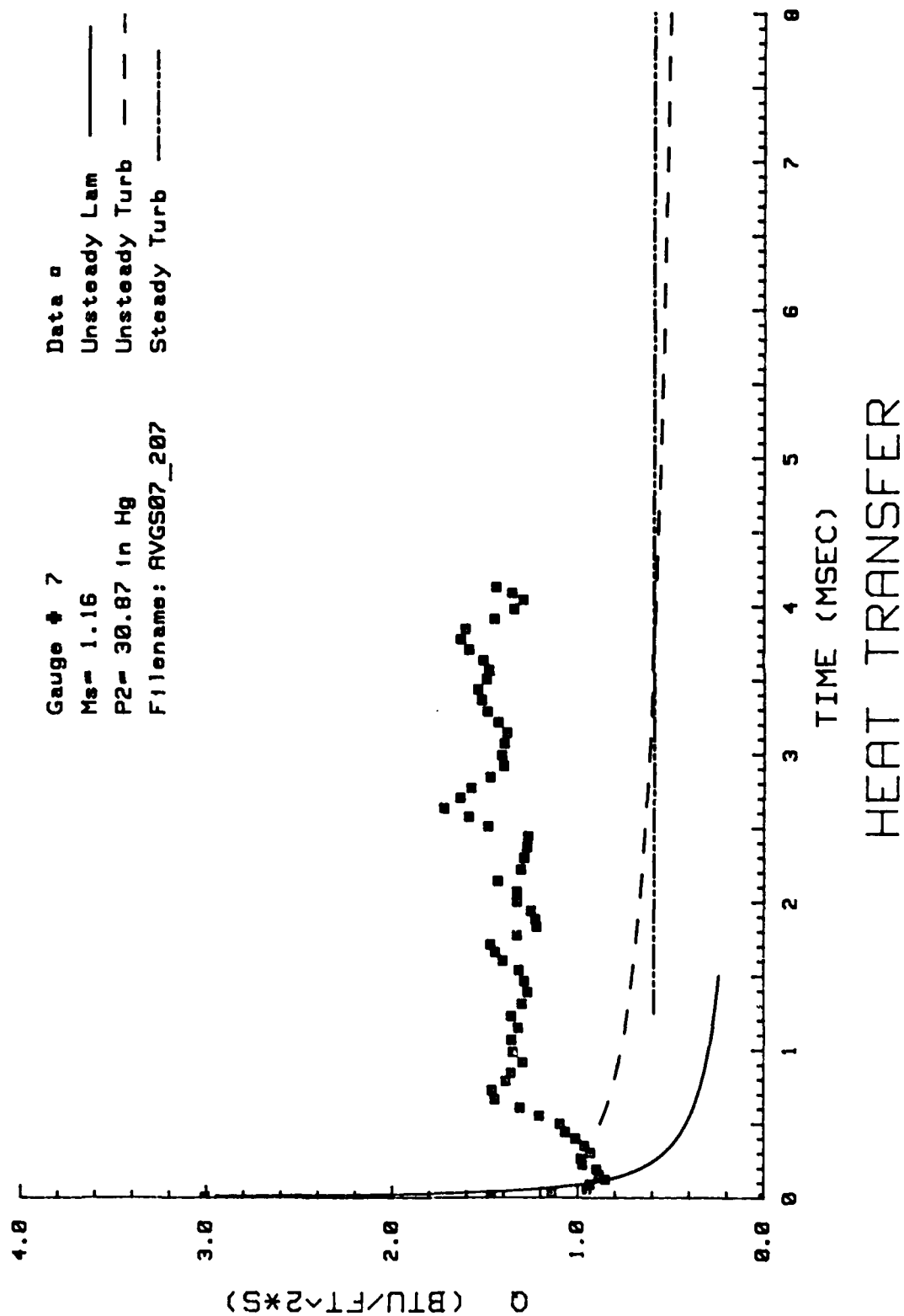
Figure 60. Heat Transfer: Data Set II Gage #7
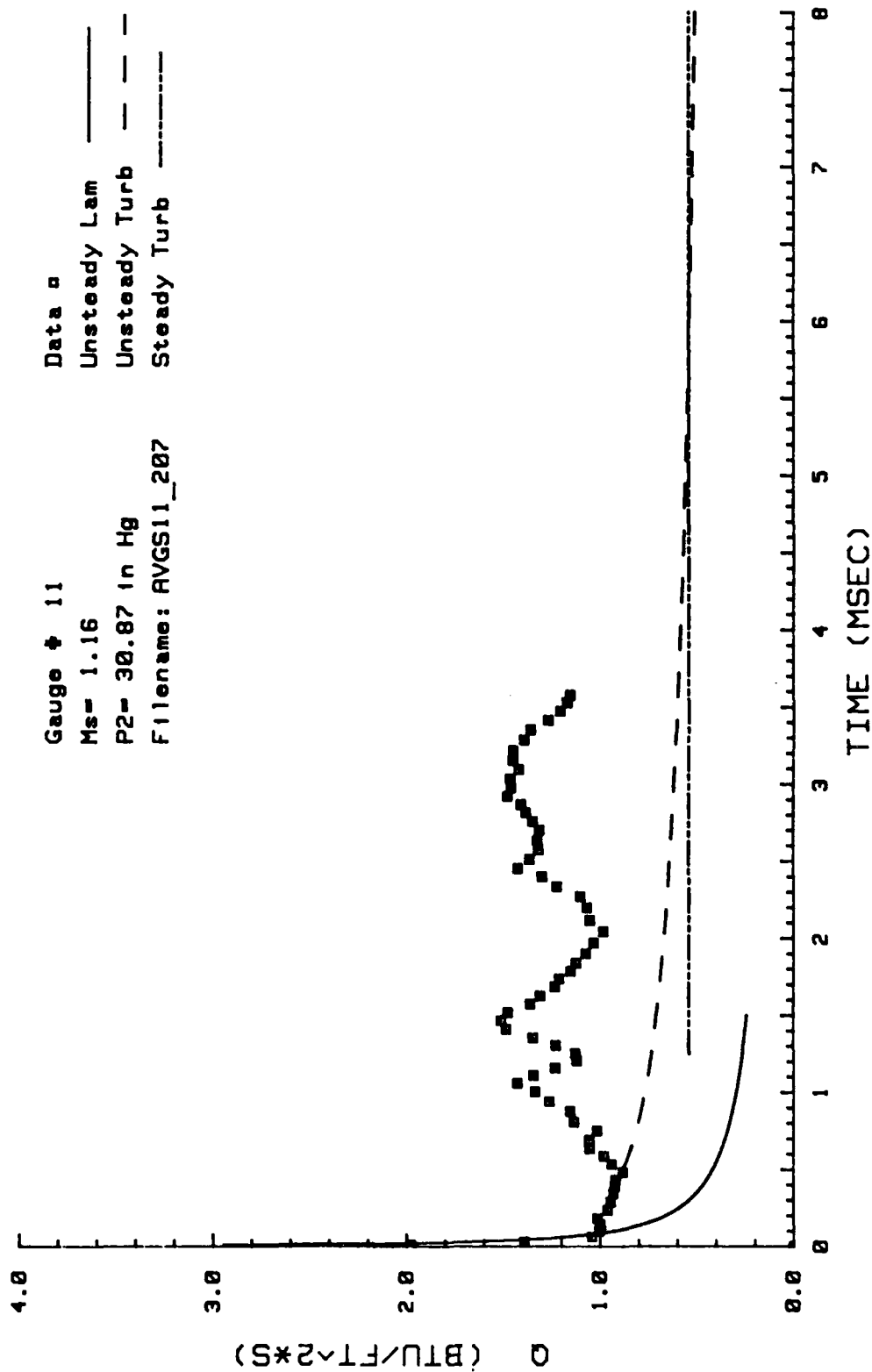
Figure 61. Heat Transfer: Data Set II Gage #11
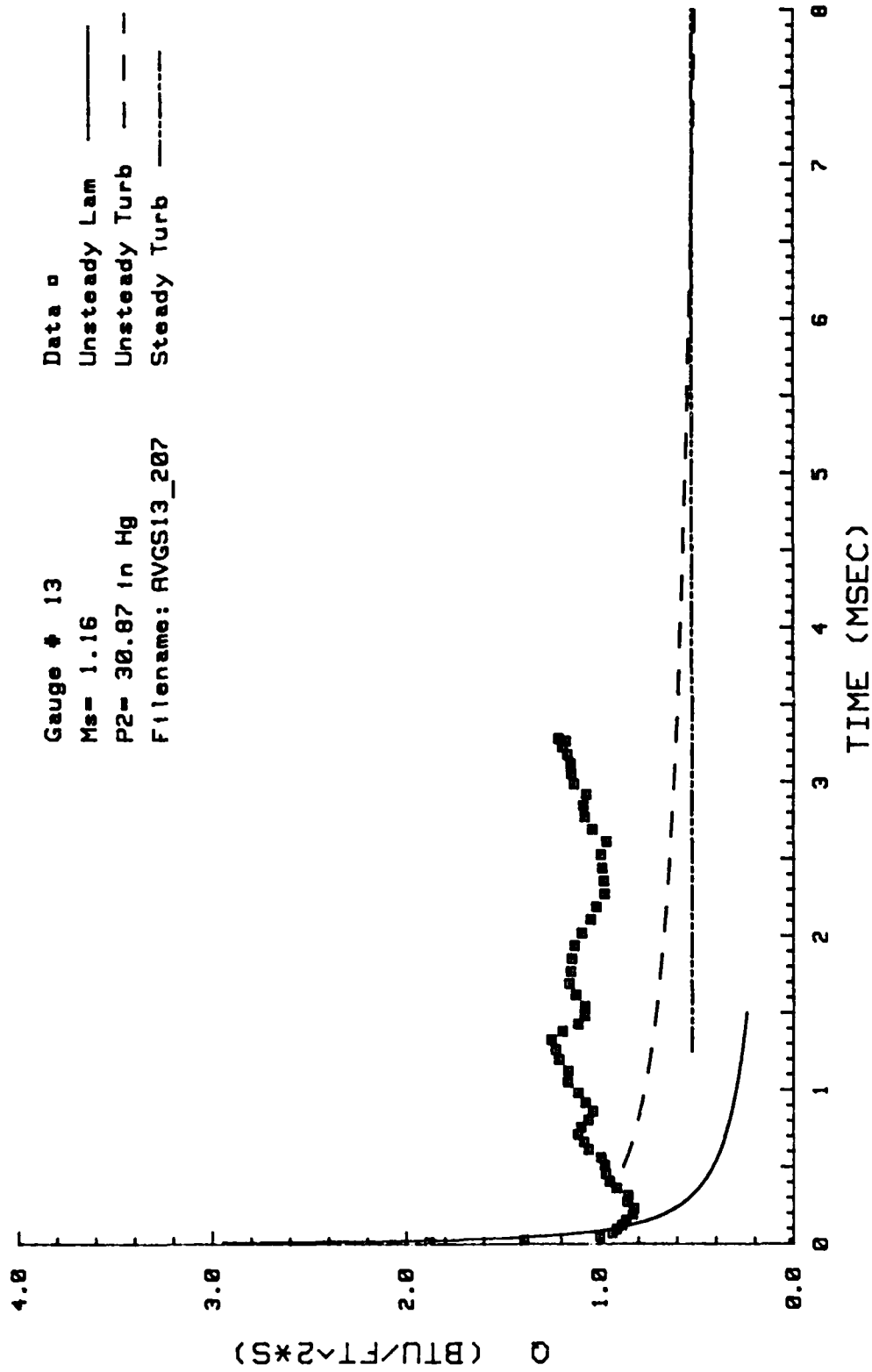
Figure 62.   Heat Transfer: Data Set H Gage #13
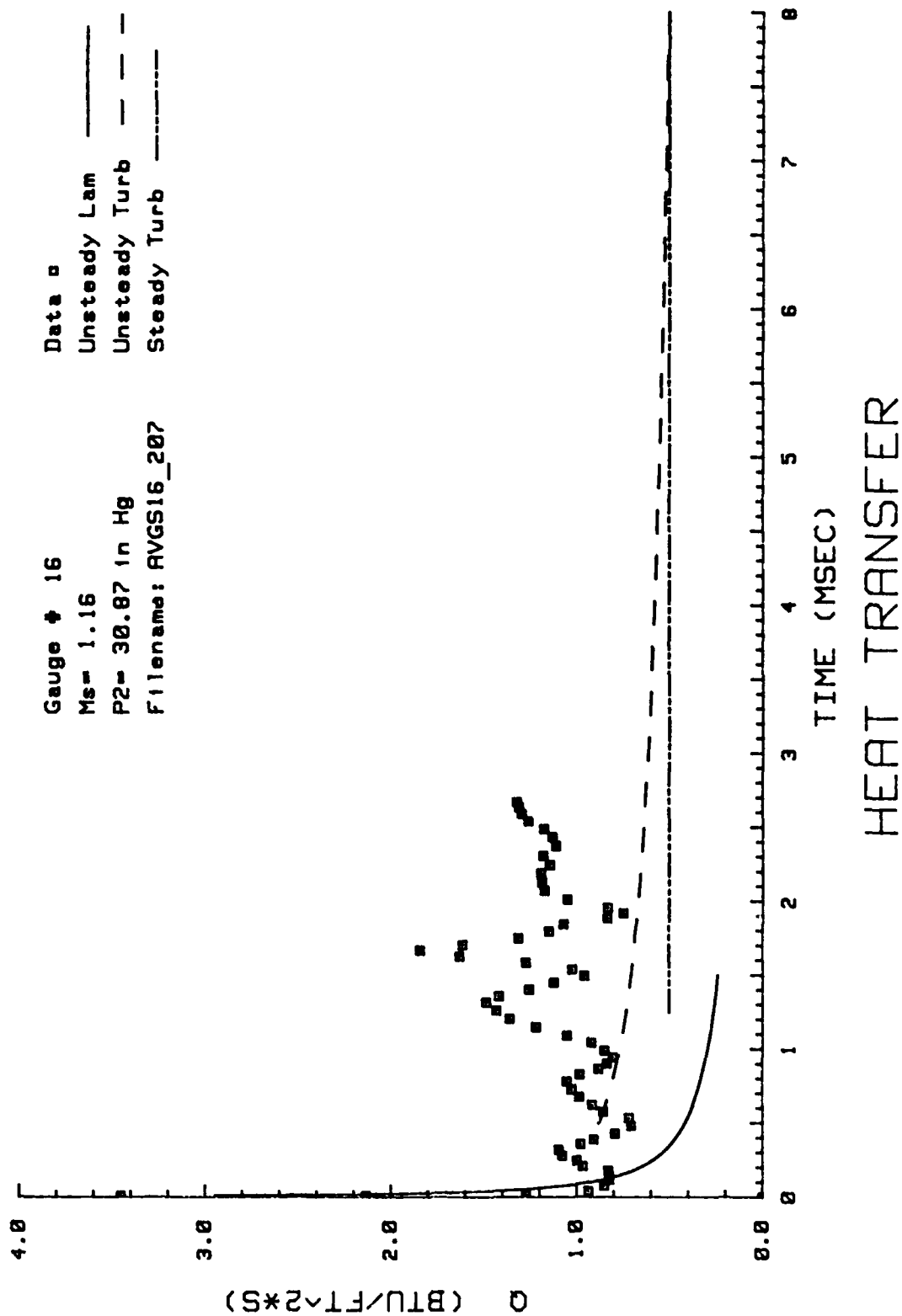
Figure 63. Heat Transfer: Data Set H Gage #16

112
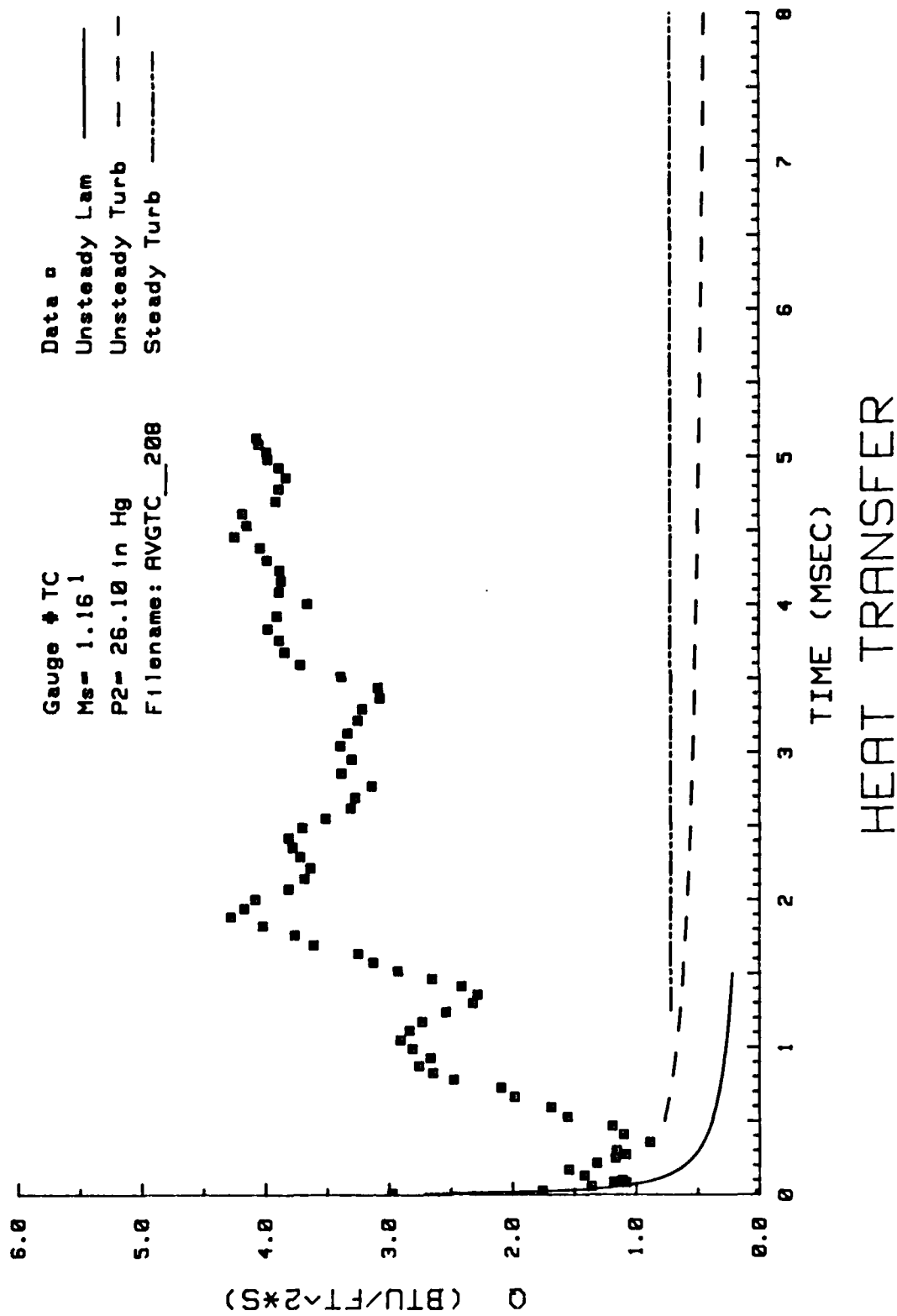
Figure 64. Heat Transfer: Data Set I Thermocouple
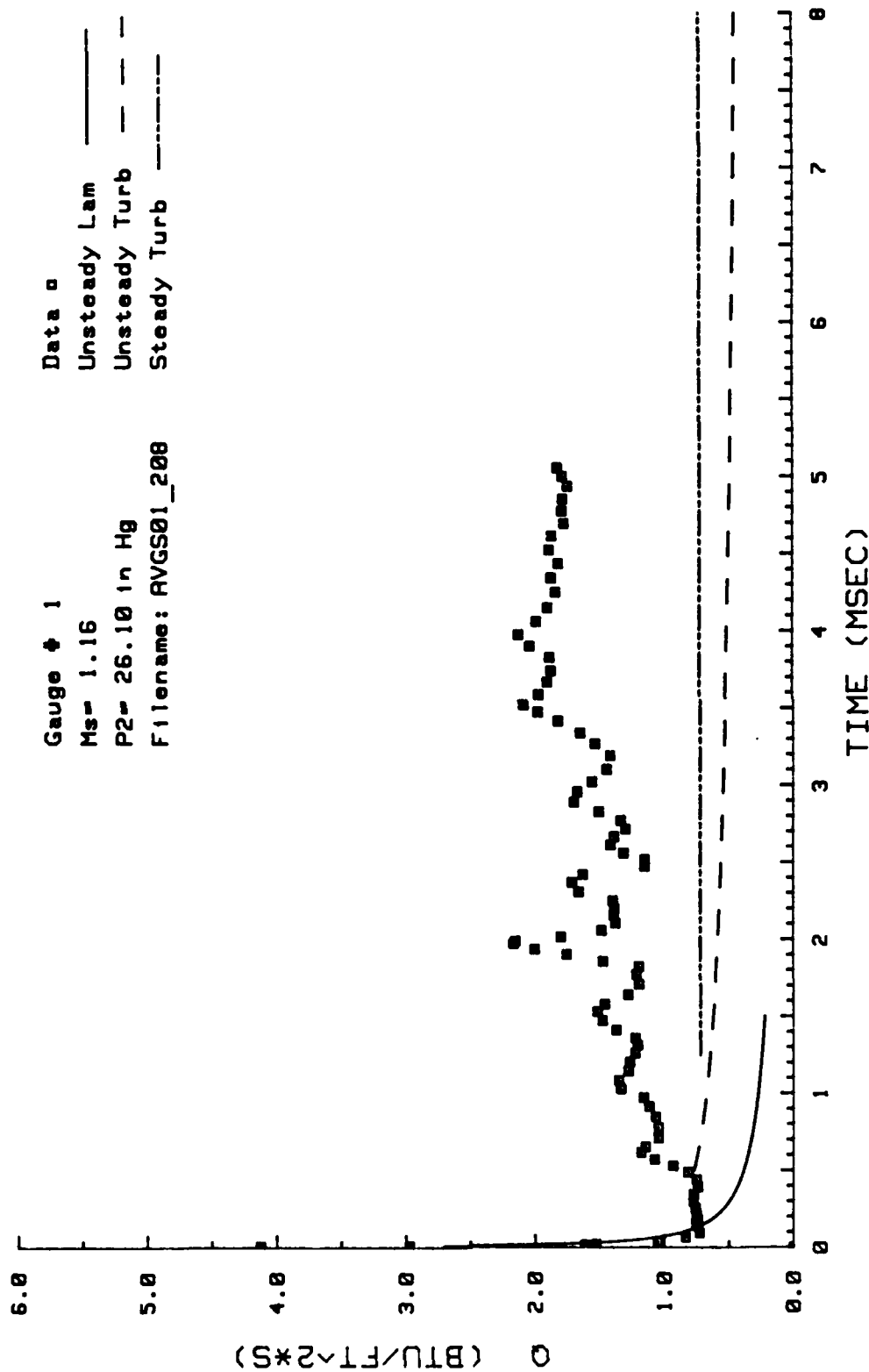
Figure 65. Heat Transfer: Data Set I Gage #1

114
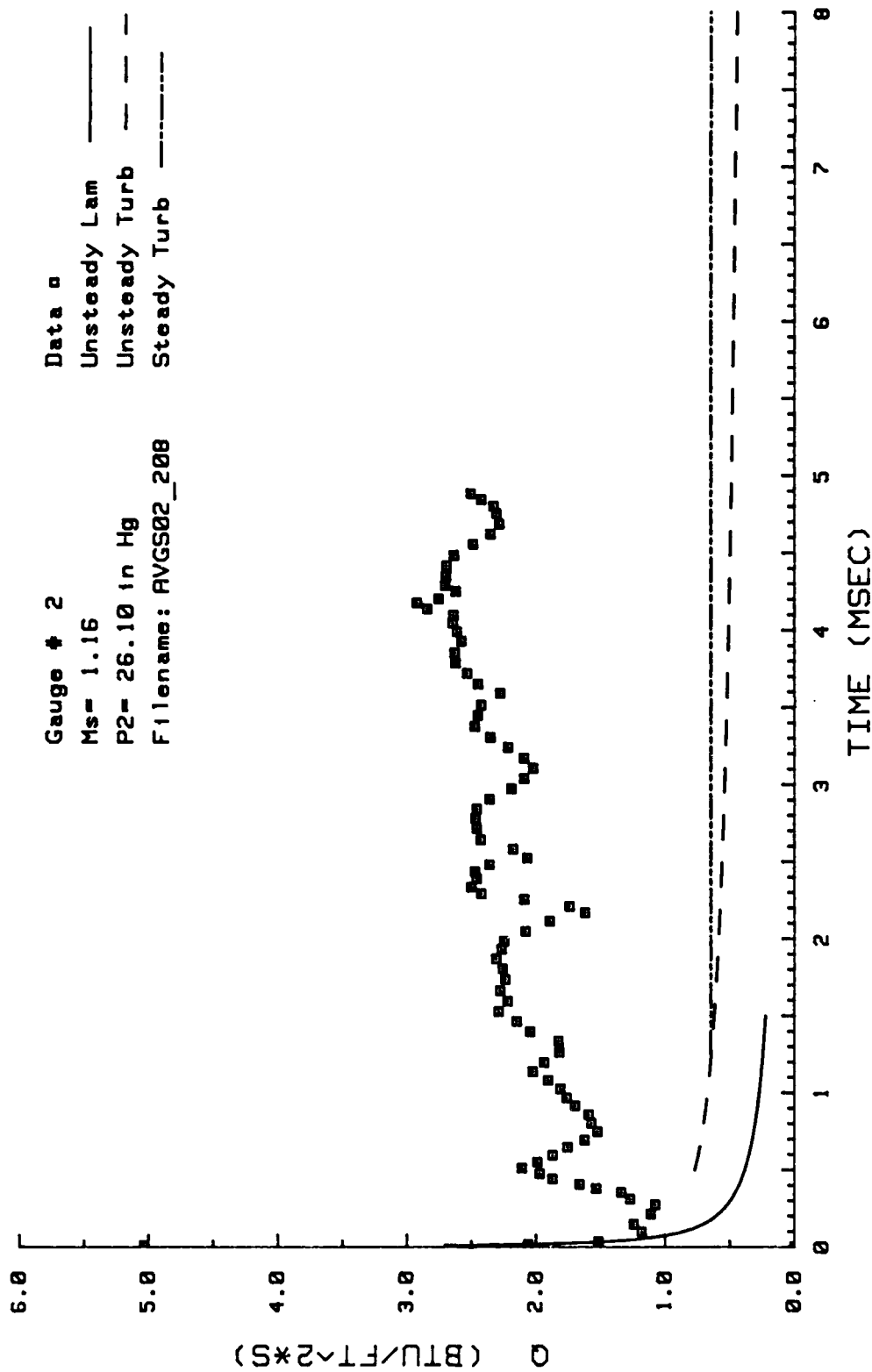
Figure 66. Heat Transfer: Data Set I Gage #2

115
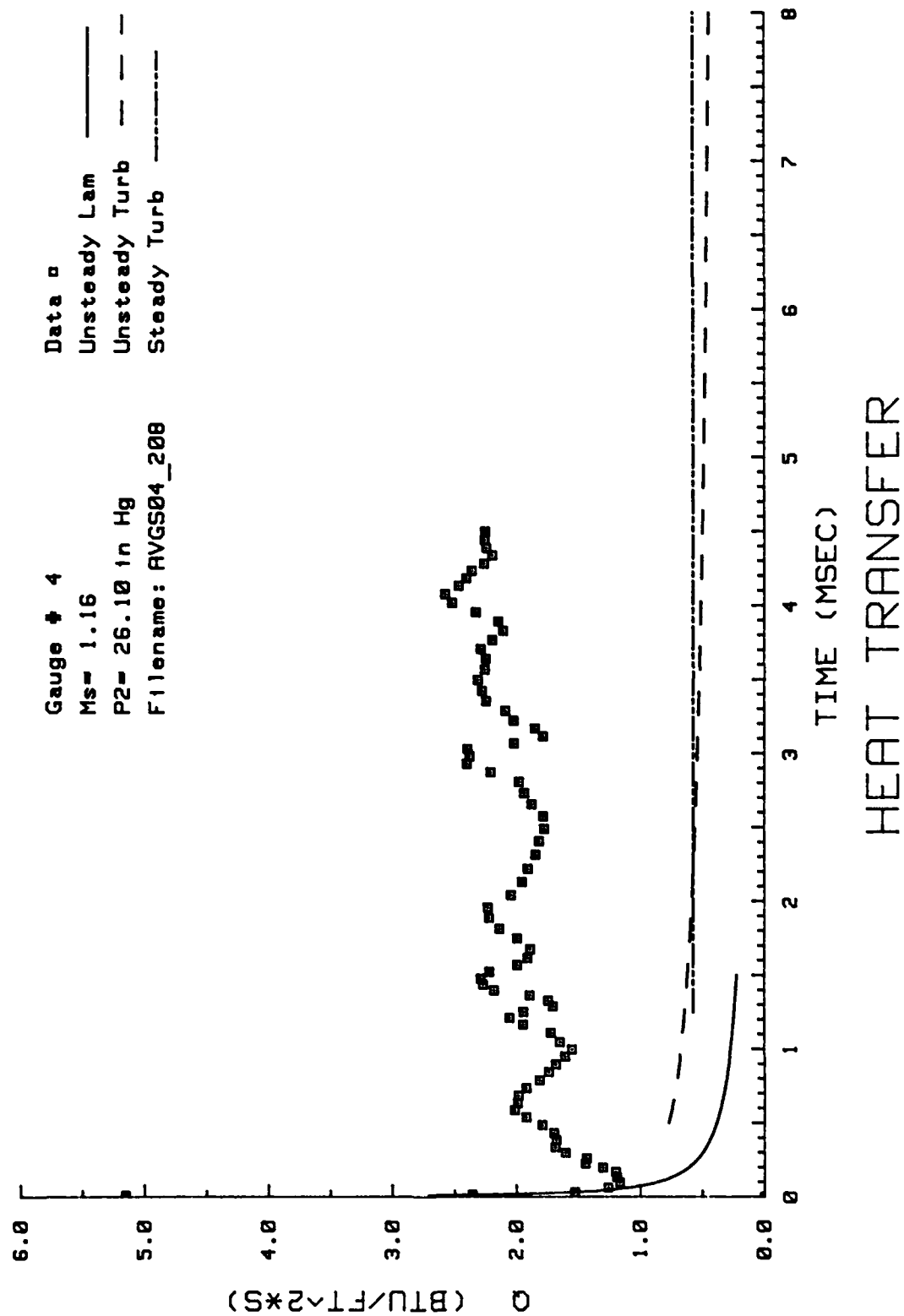
Figure 67.   Heat Transfer: Data Set I Gage #4
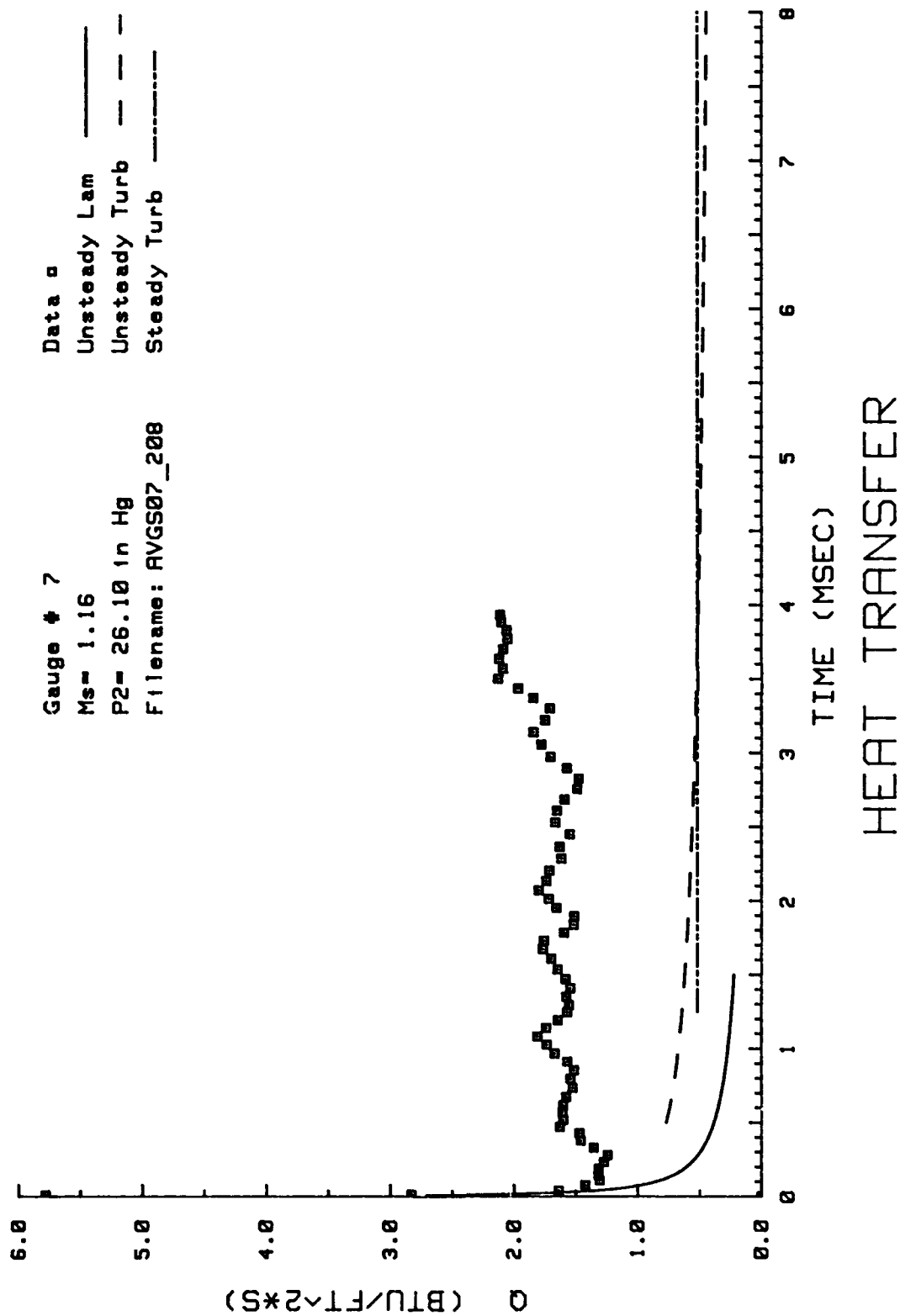
Figure 68. Heat Transfer: Data Set I Gage #7
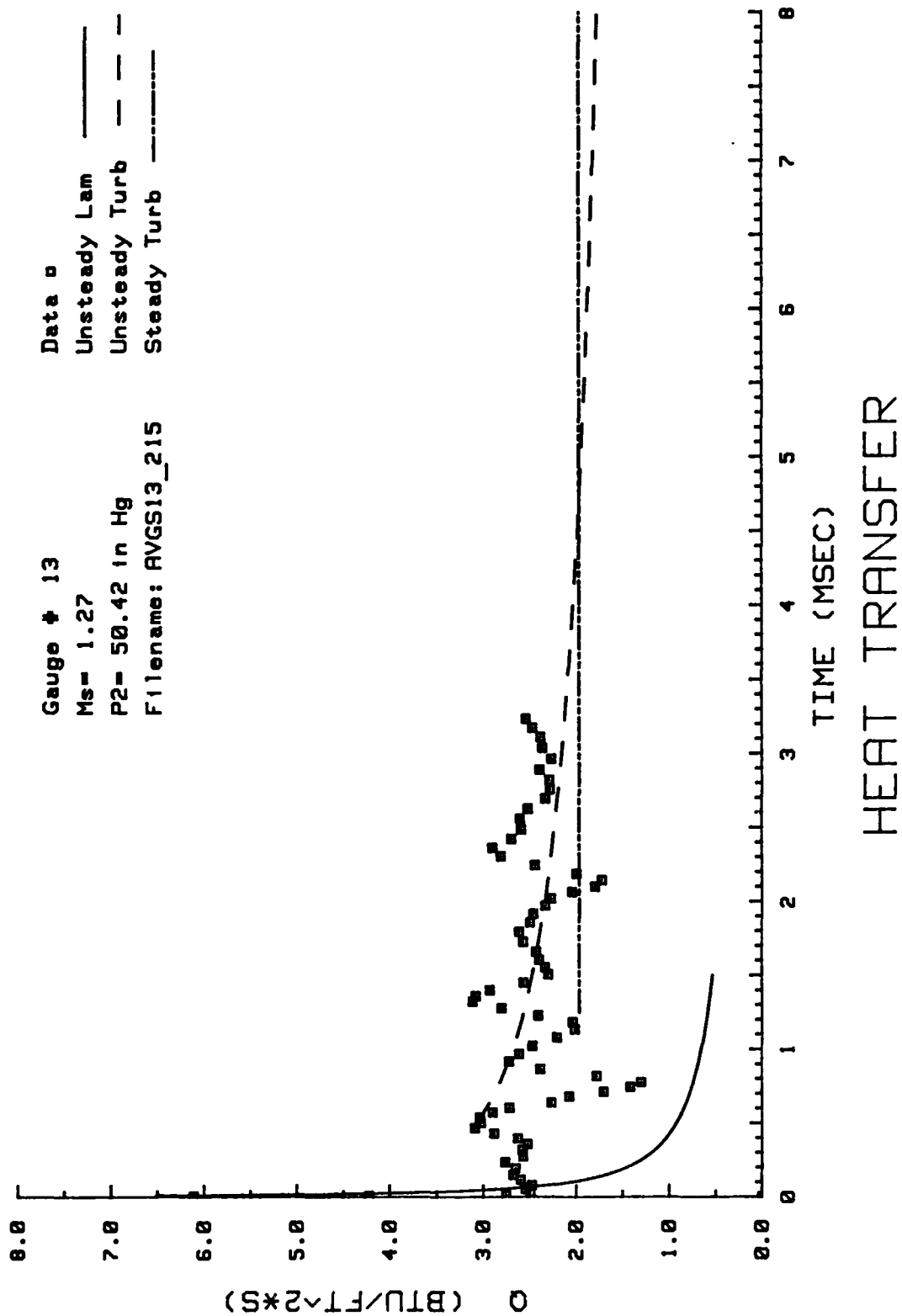
117
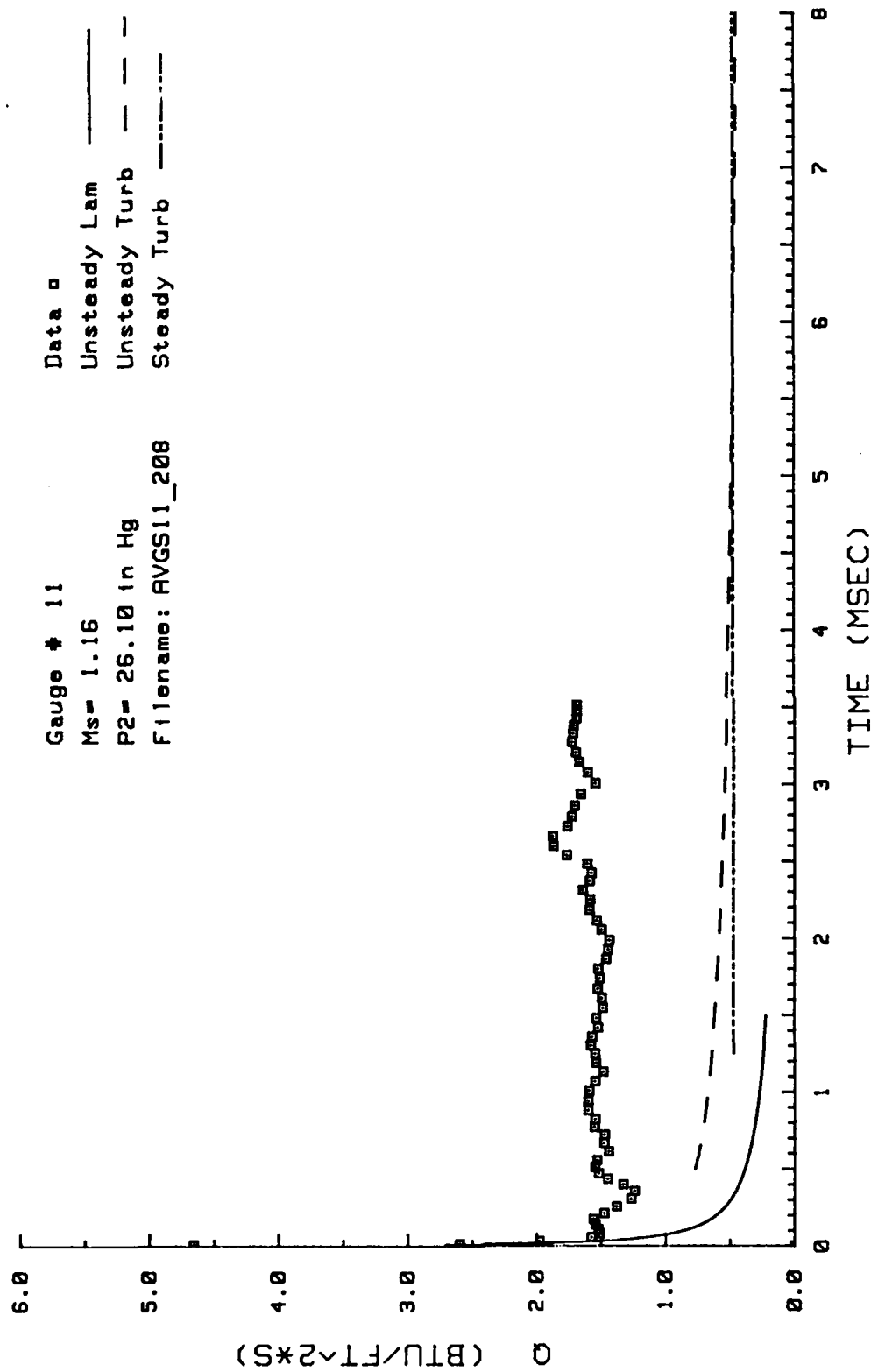
Figure 69. Heat Transfer: Data Set I Gage #11
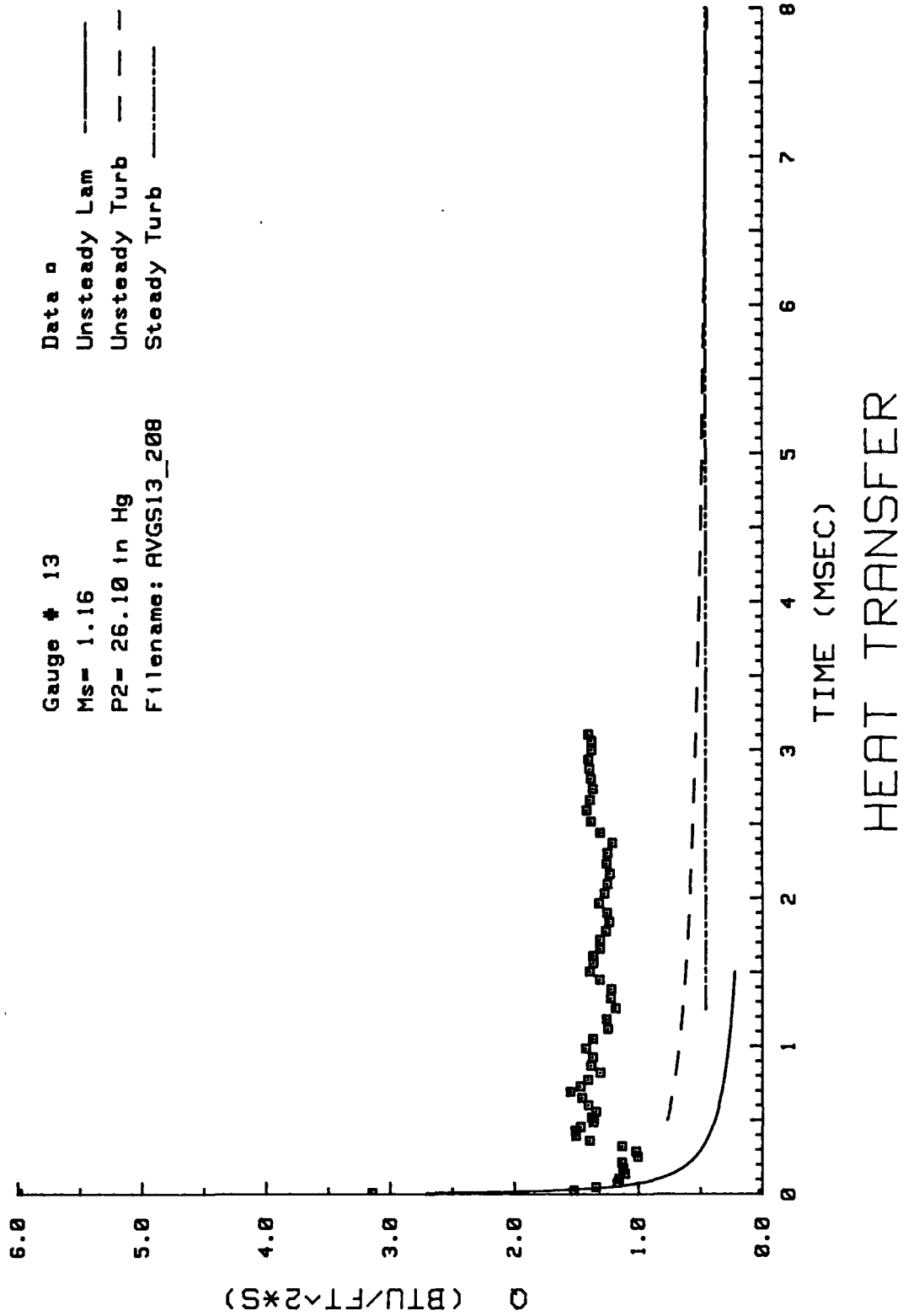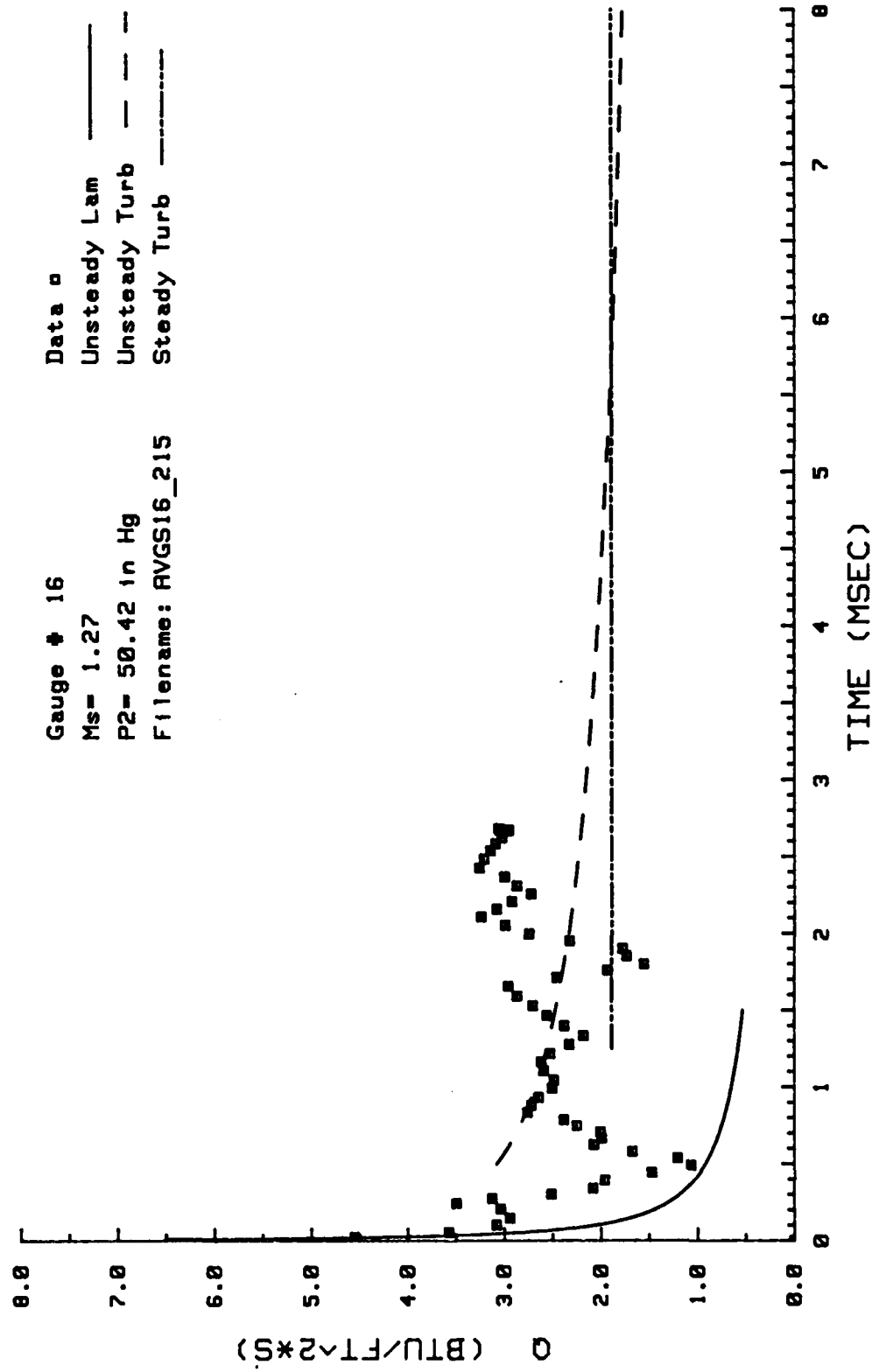
Figure 70. Heat Transfer: Data Set I Gage #13
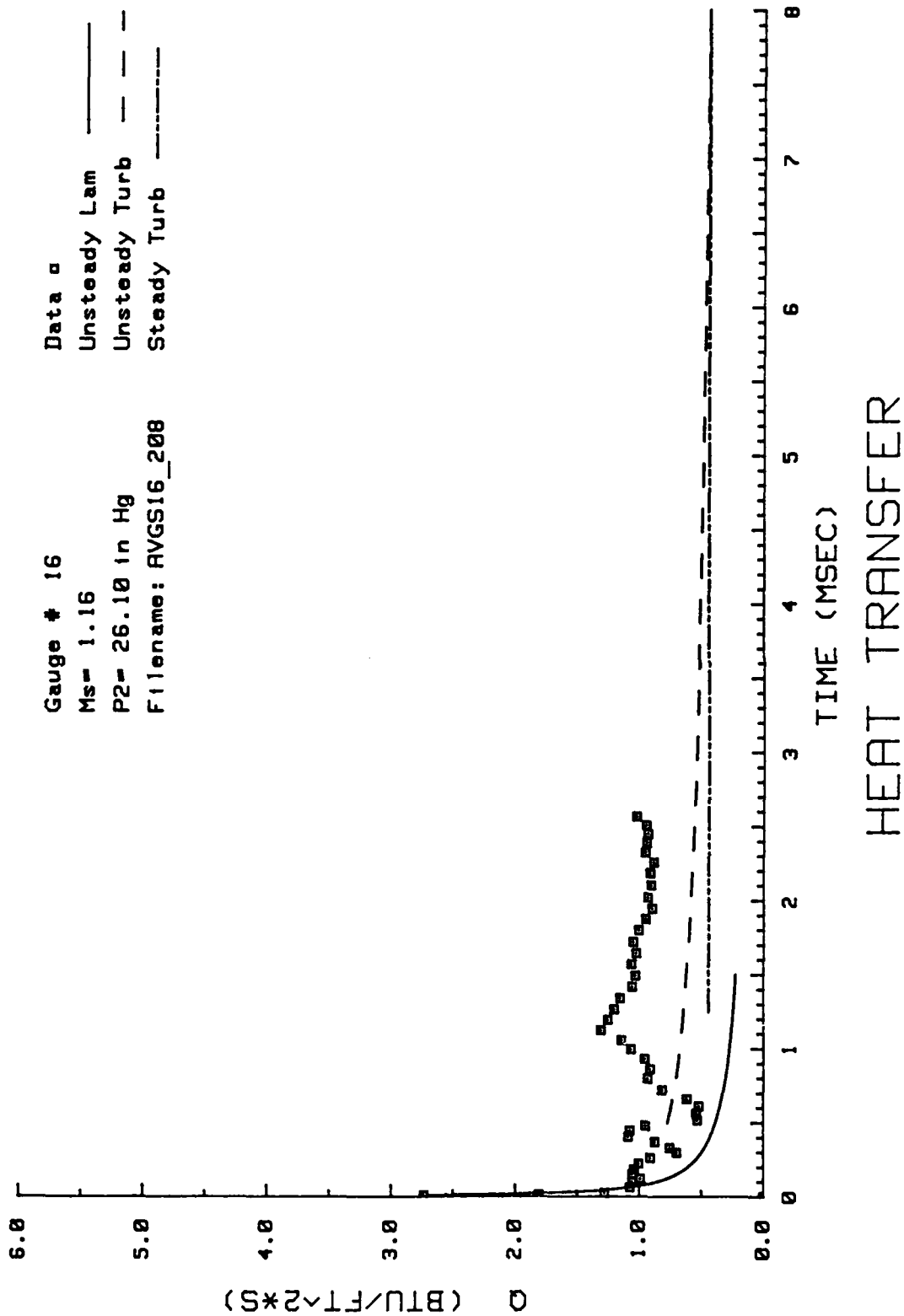
Figure 71. Heat Transfer: Data Set I Gage #16
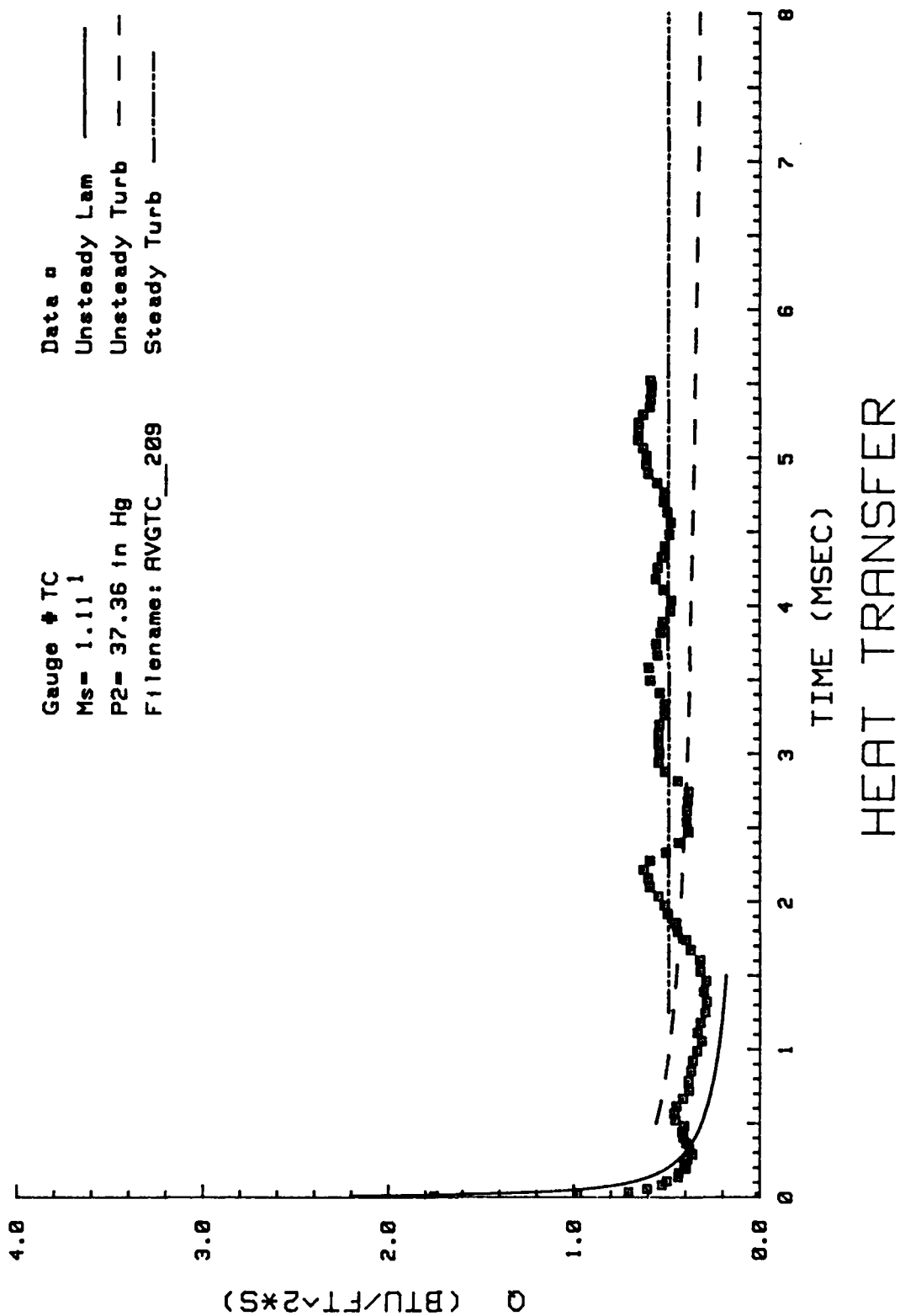
Figure 72. Heat Transfer: Data Set J Thermocouple
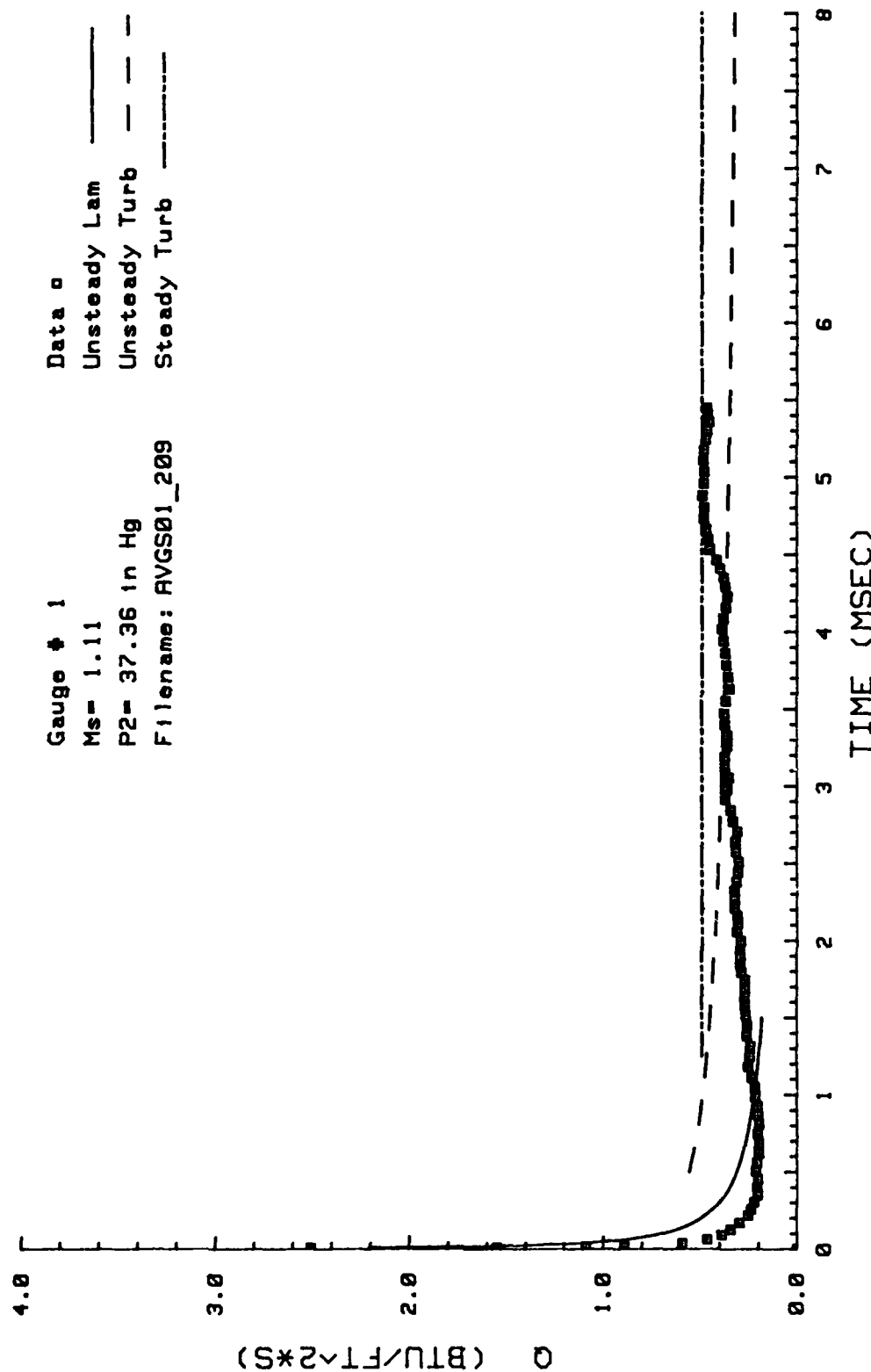
HEAT TRANSFER

Figure 73. Heat Transfer: Data Set J Gage #1
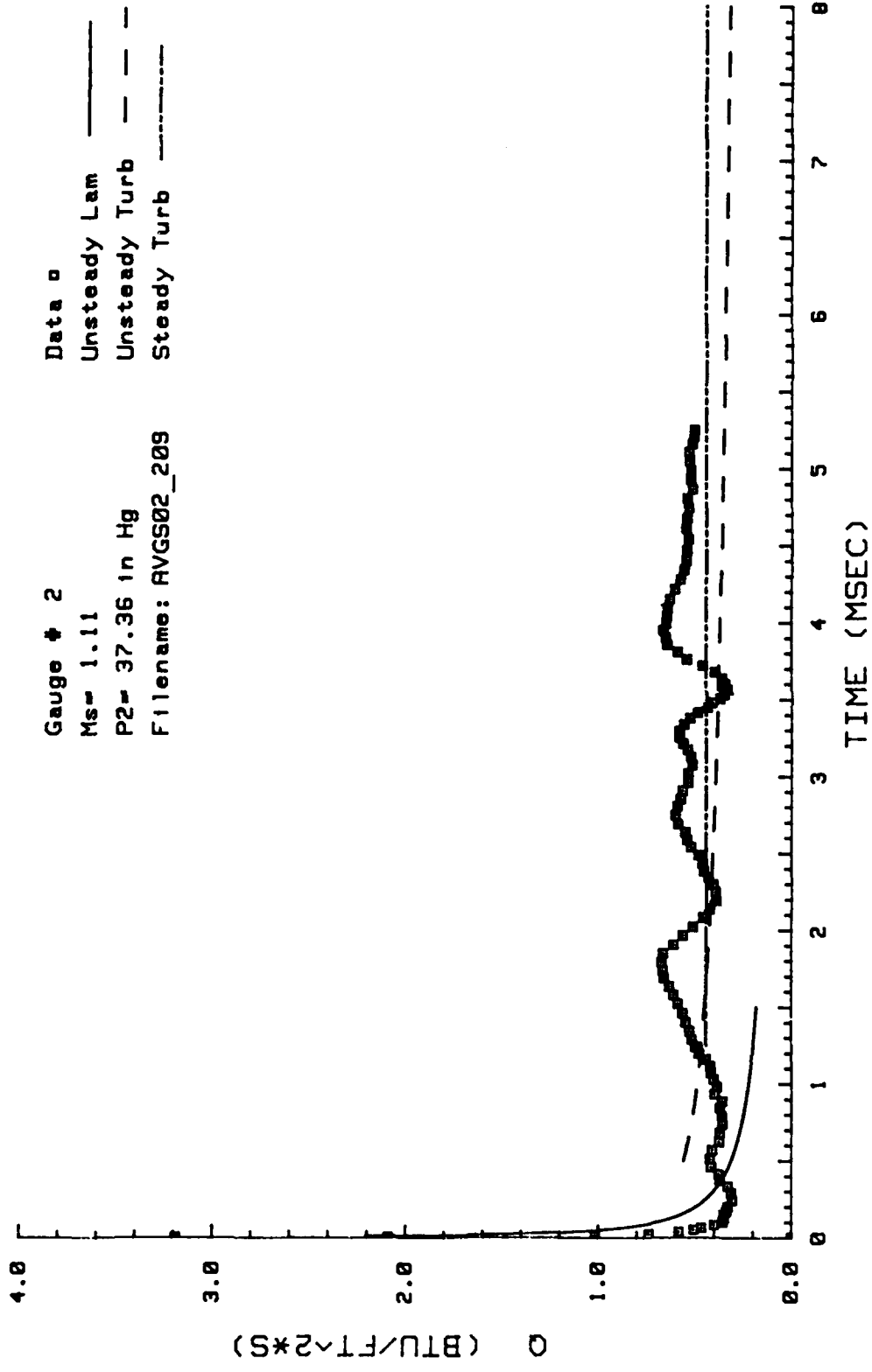
Figure 74. Heat Transfer: Data Set J Gage #2

123
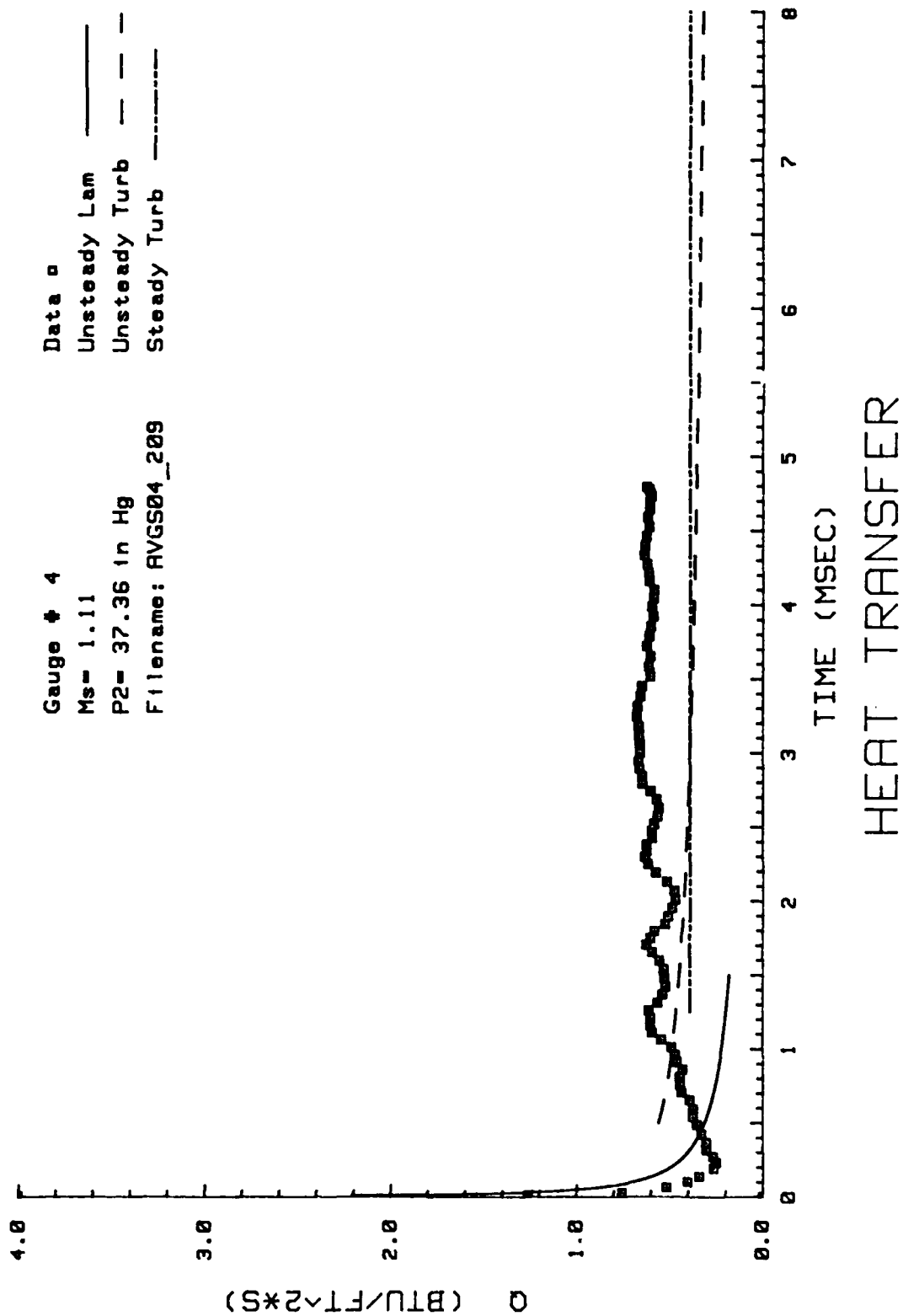
Figure 75. Heat Transfer: Data Set J Gage #4
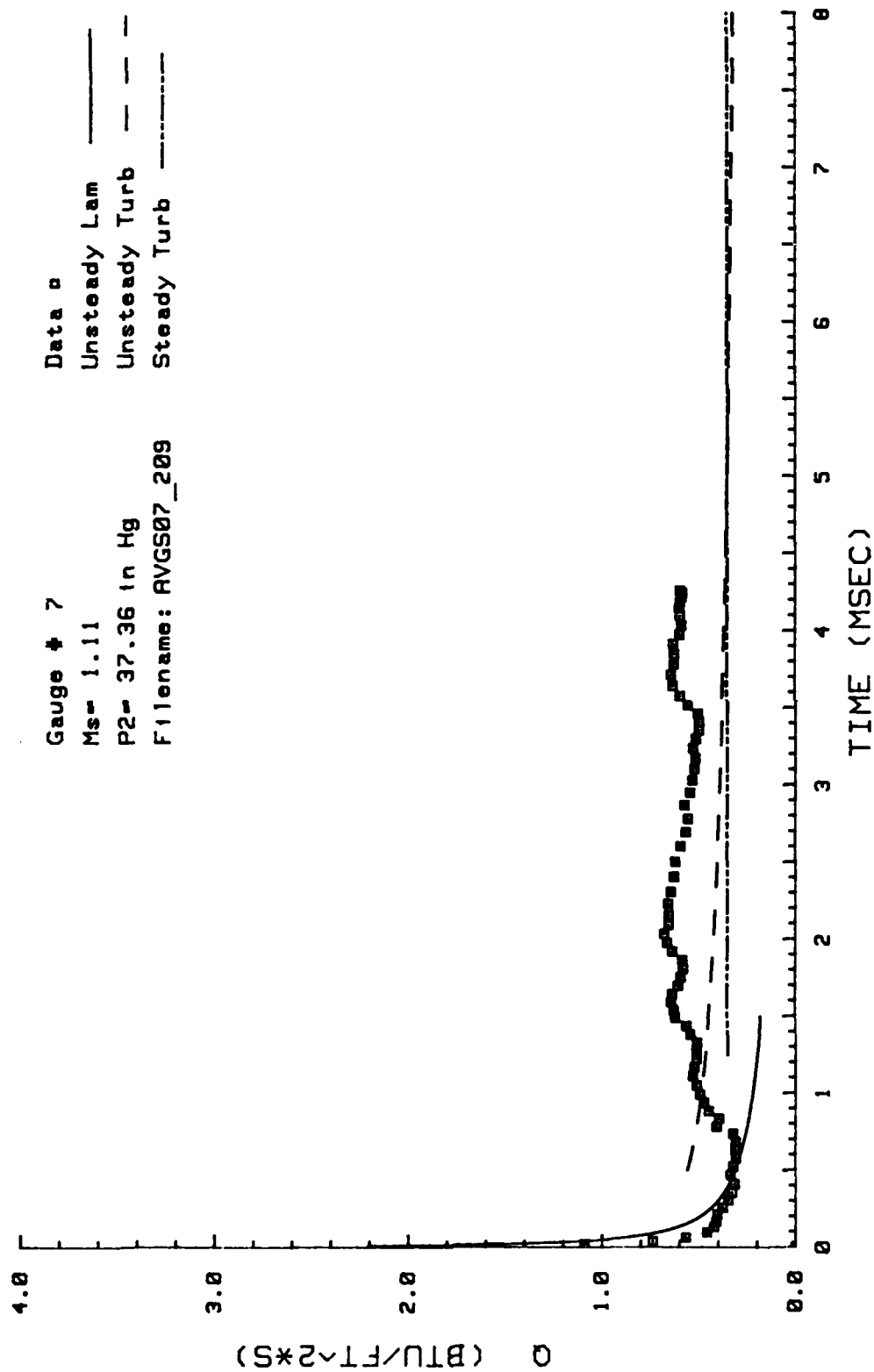
Figure 76. Heat Transfer: Data Set J Gage #7
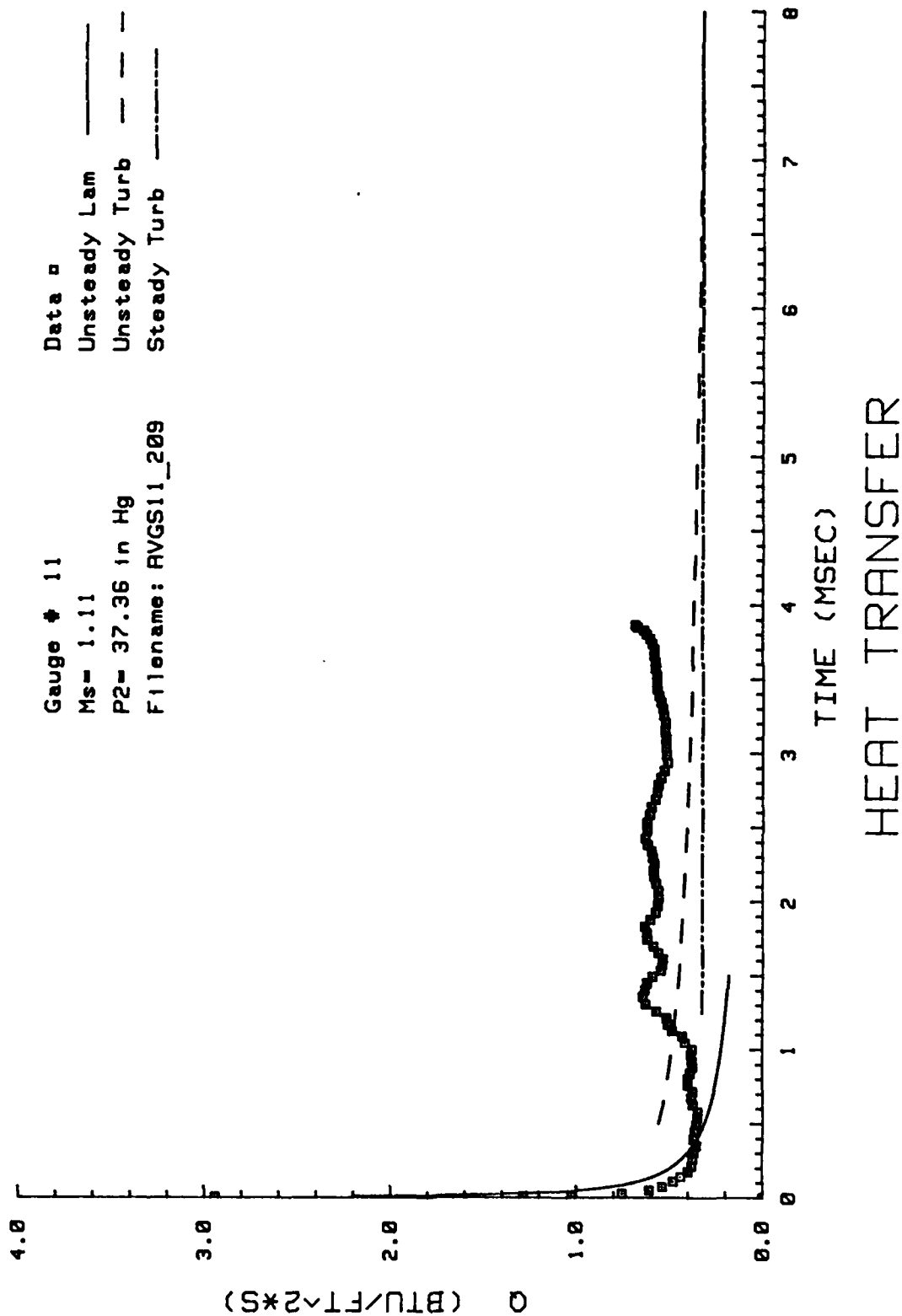
Figure 77. Heat Transfer: Data Set J Gage #11

126
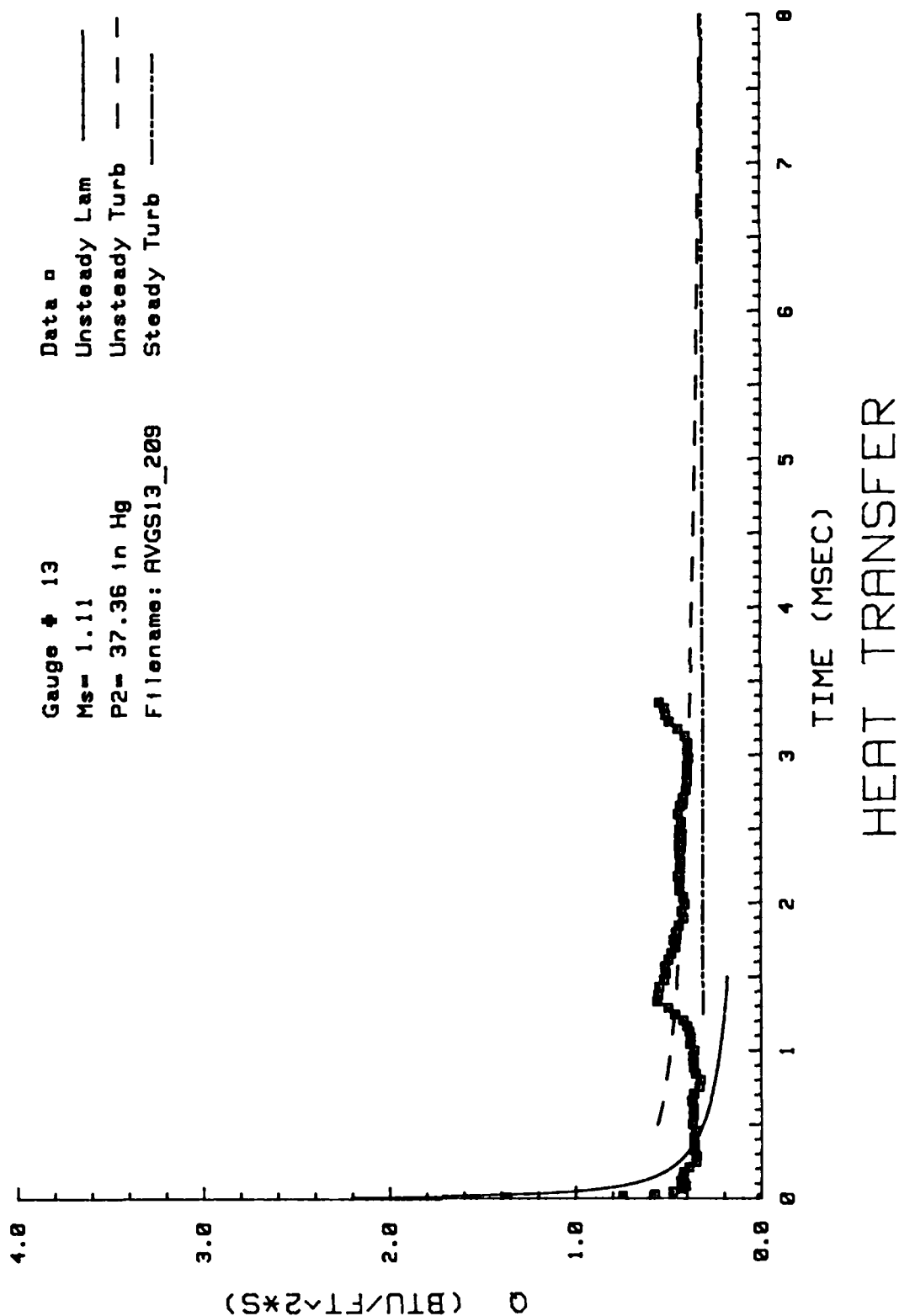
Figure 78. Heat Transfer: Data Set J Gage #13
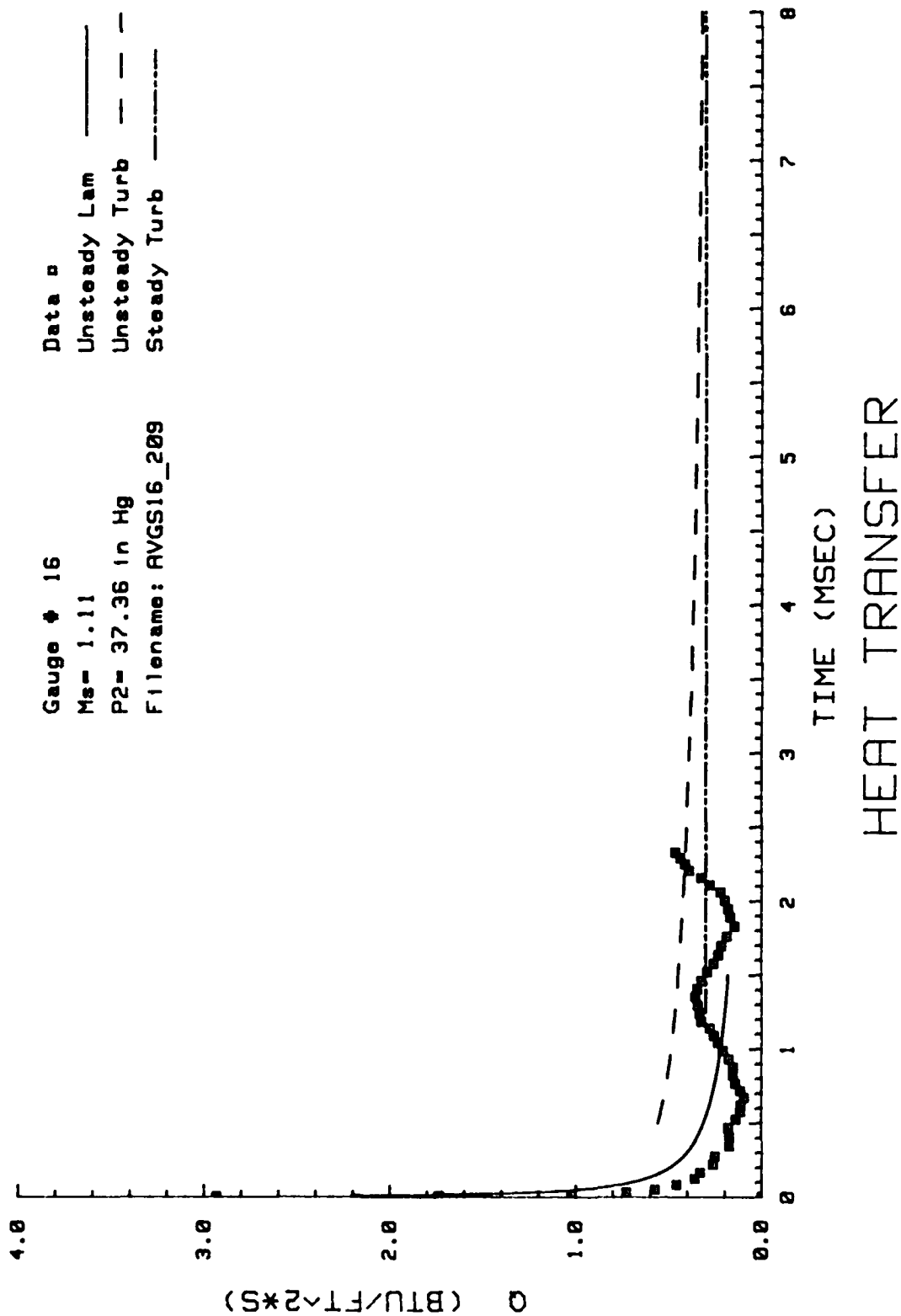
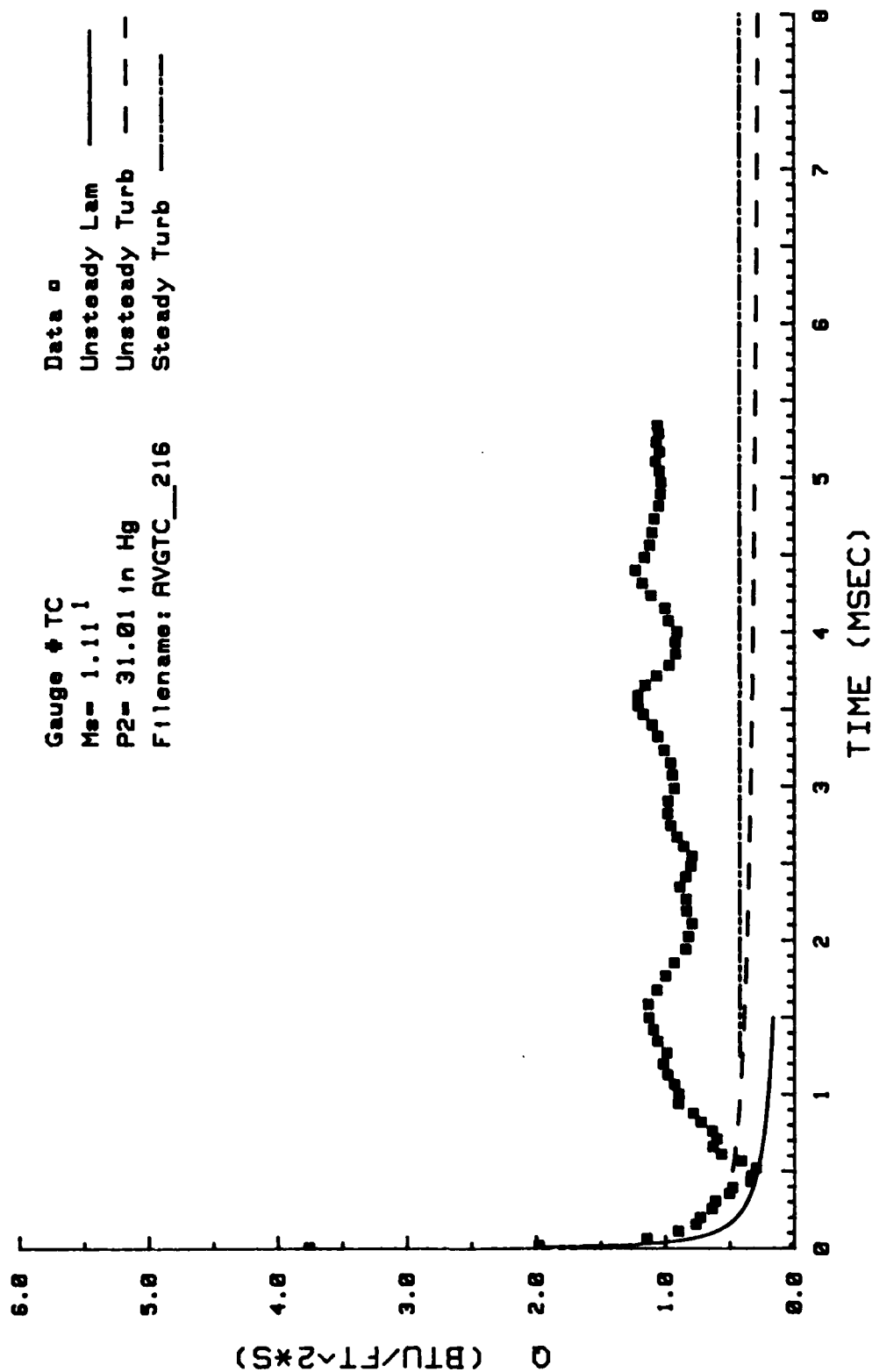Figure 79. Heat Transfer: Data Set J Gage #16
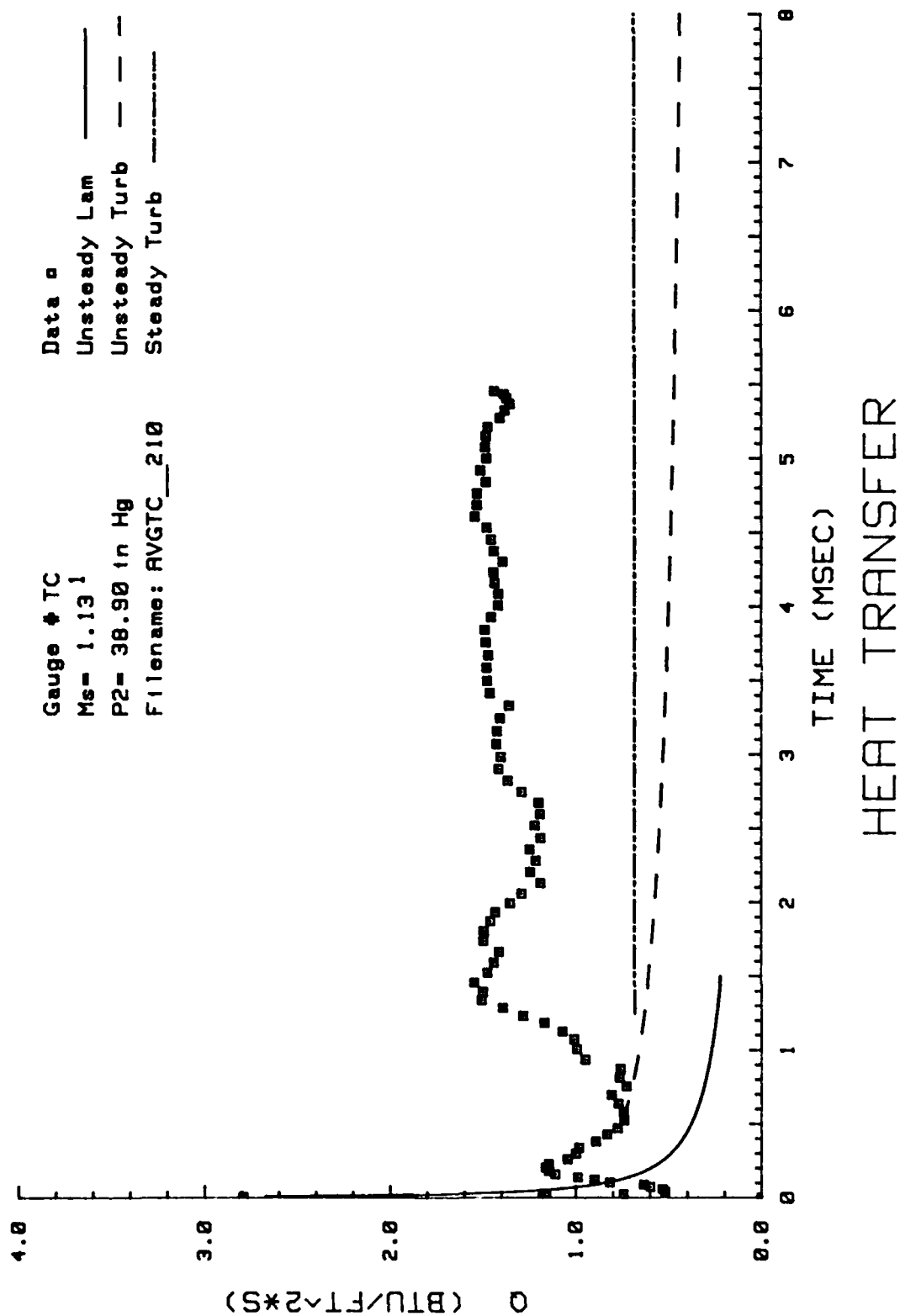
HEAT TRANSFER

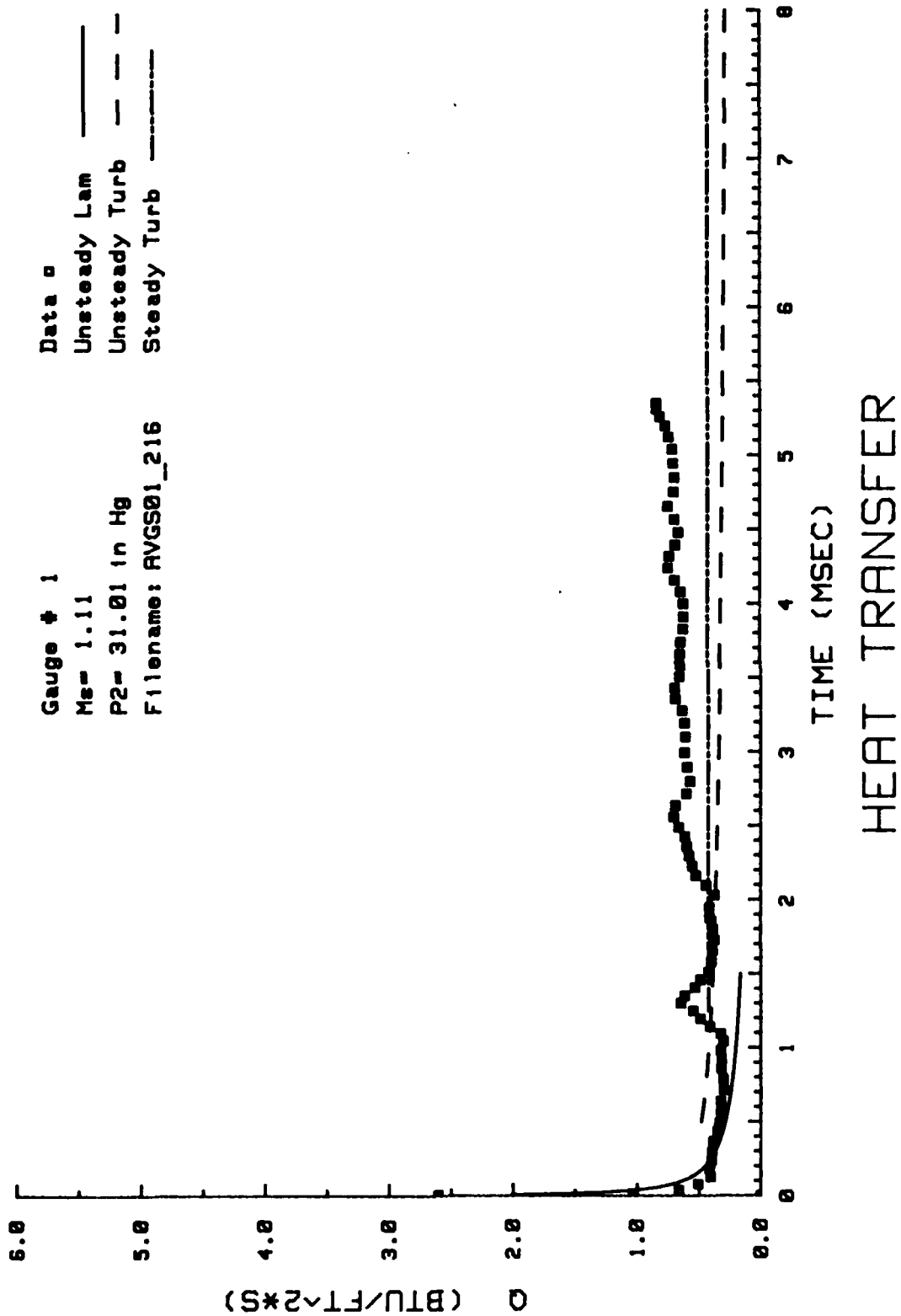Figure 80. Heat Transfer: Data Set K Thermocouple
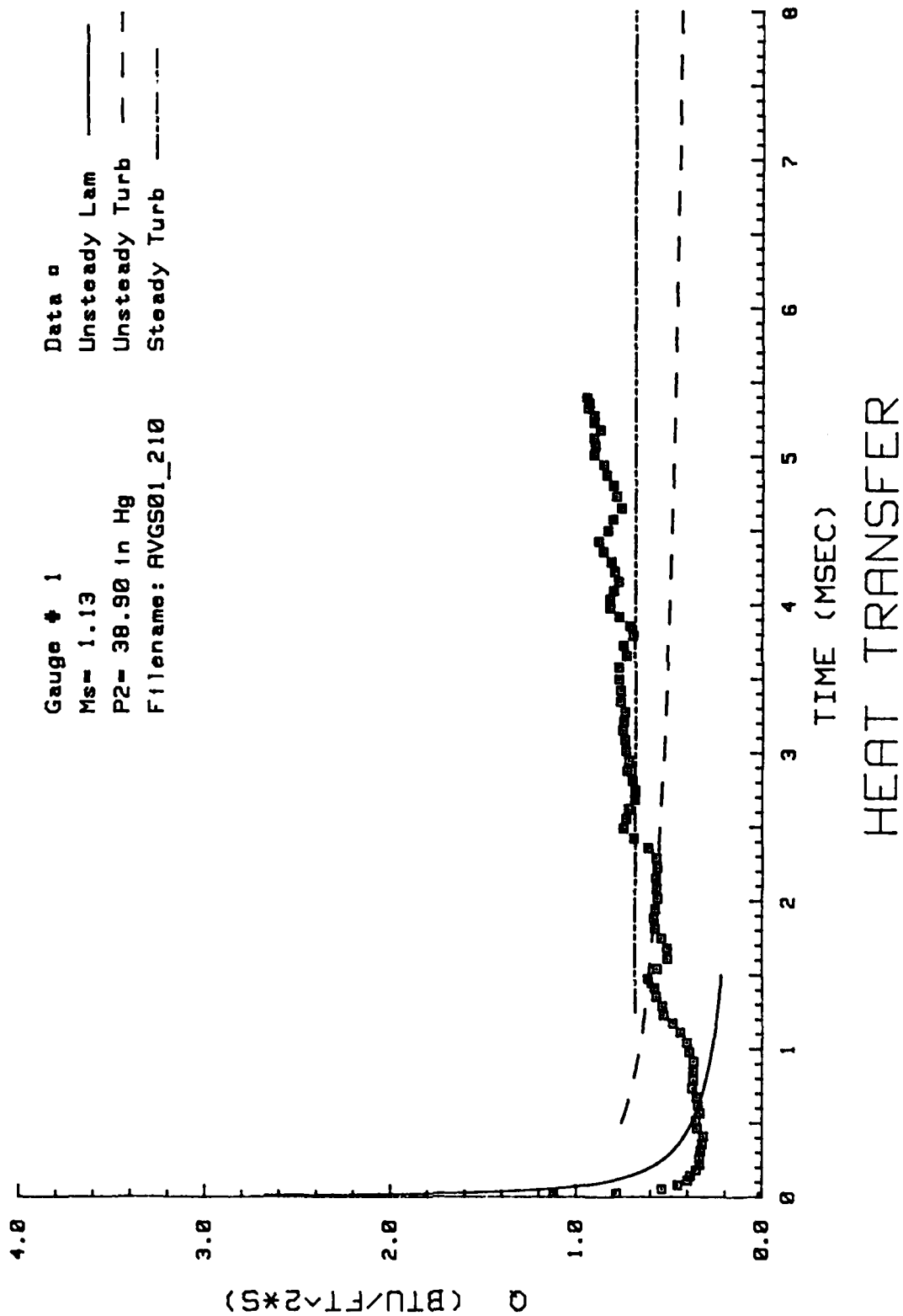
Figure 81. Heat Transfer: Data Set K Gage #1
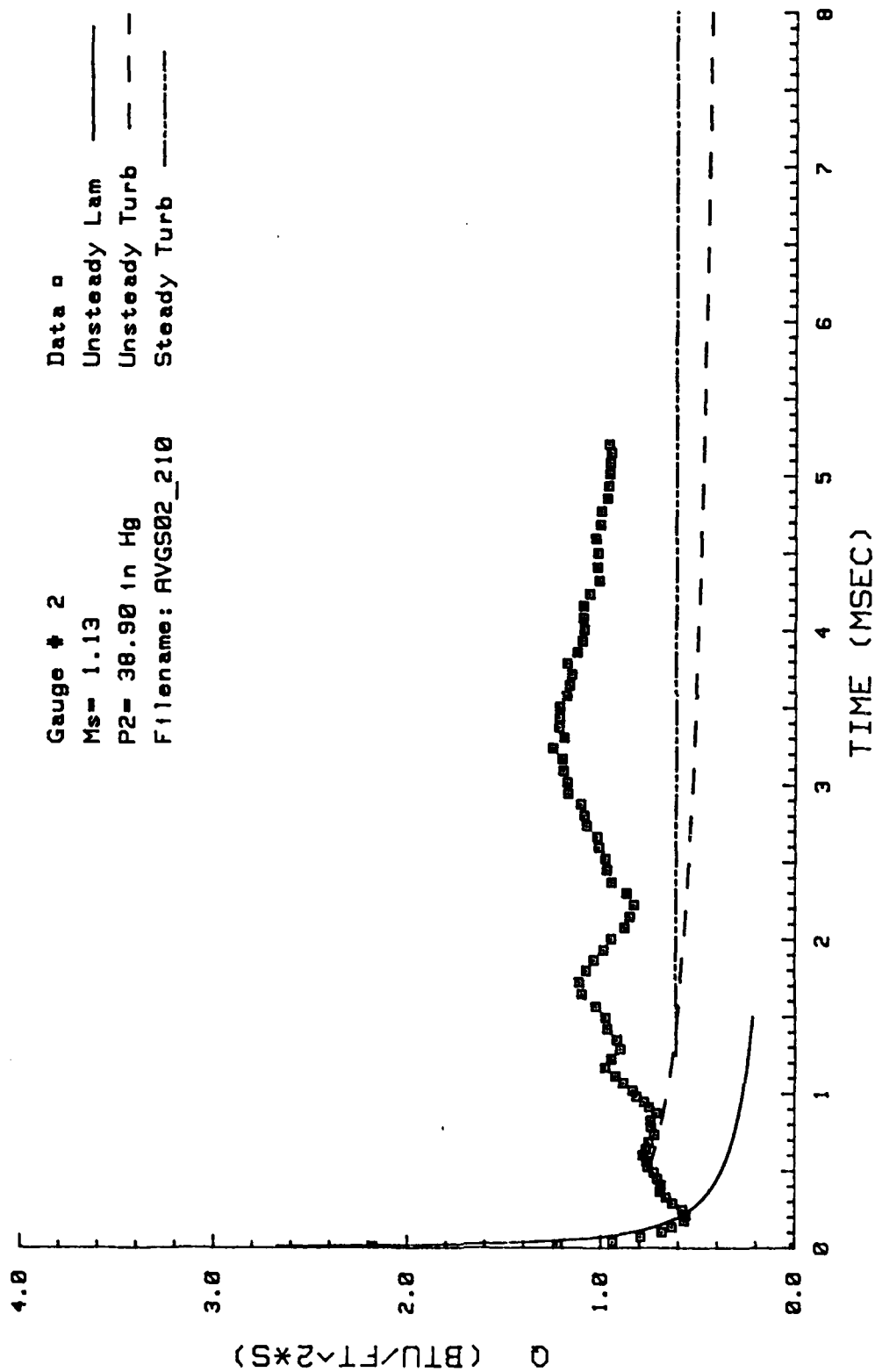
Figure 82. Heat Transfer: Data Set K Gage #2

131
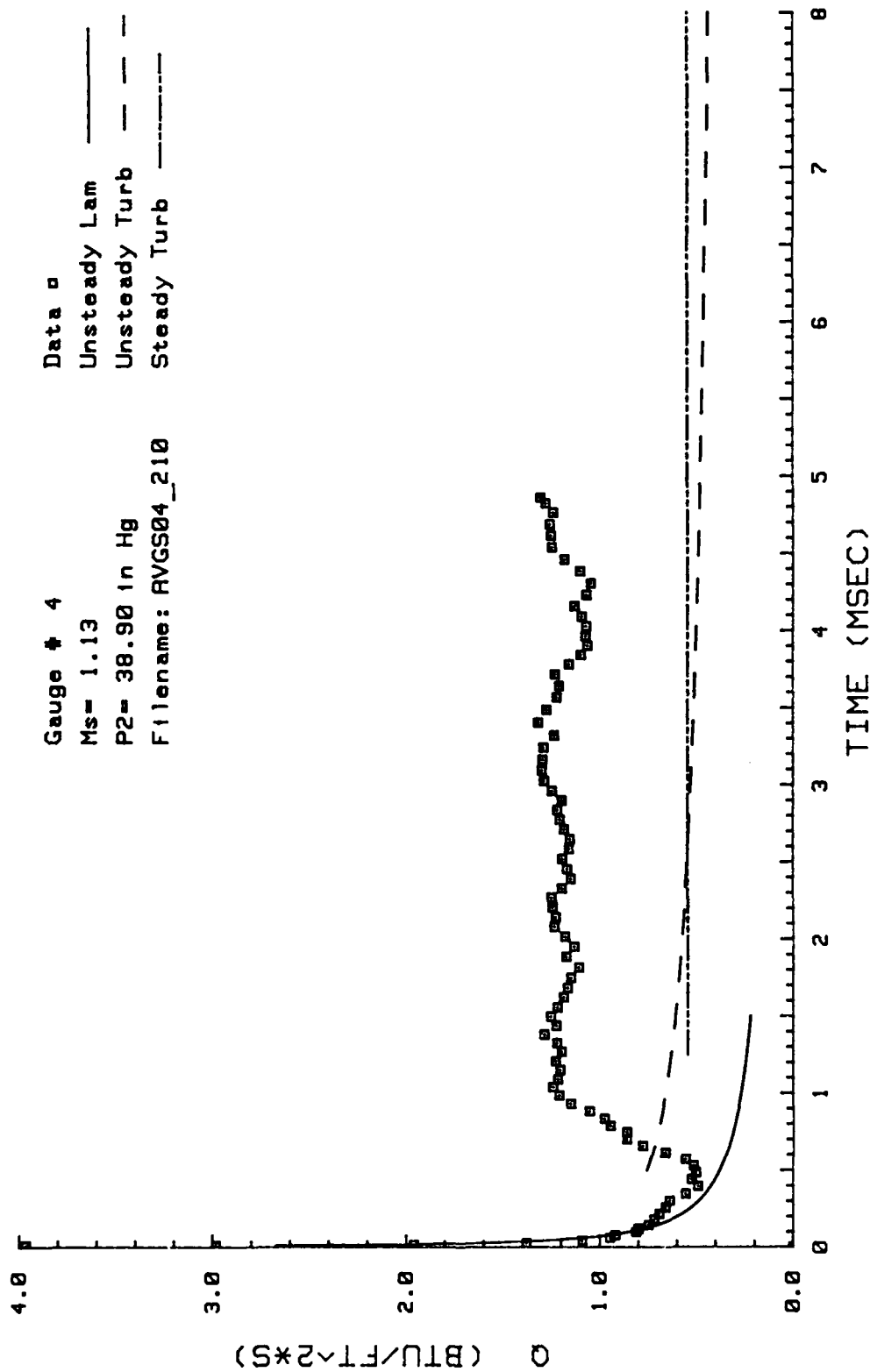
Figure 83. Heat Transfer: Data Set K Gage #4
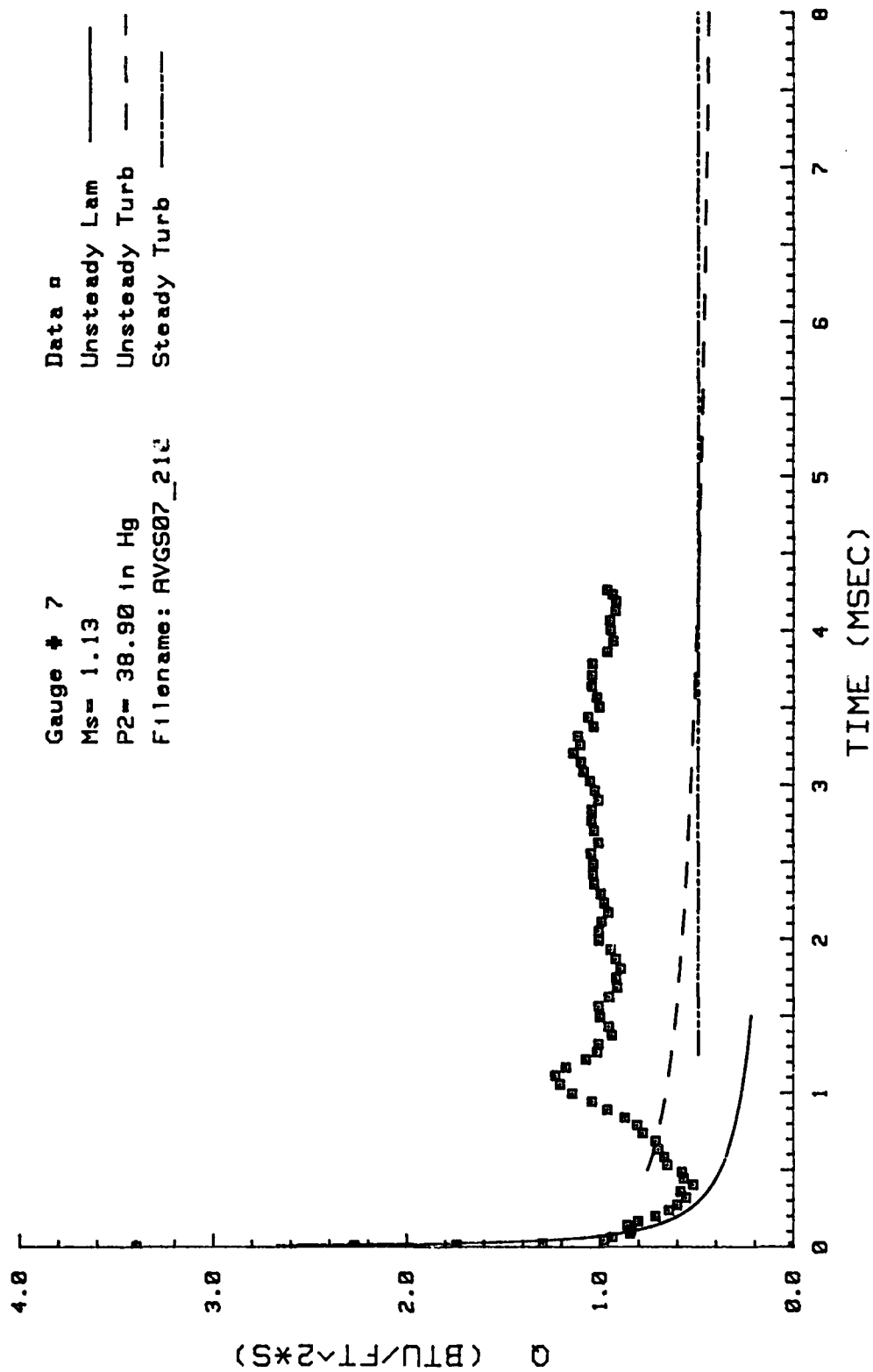
Figure 84.   Heat Transfer: Data Set K Gage #7
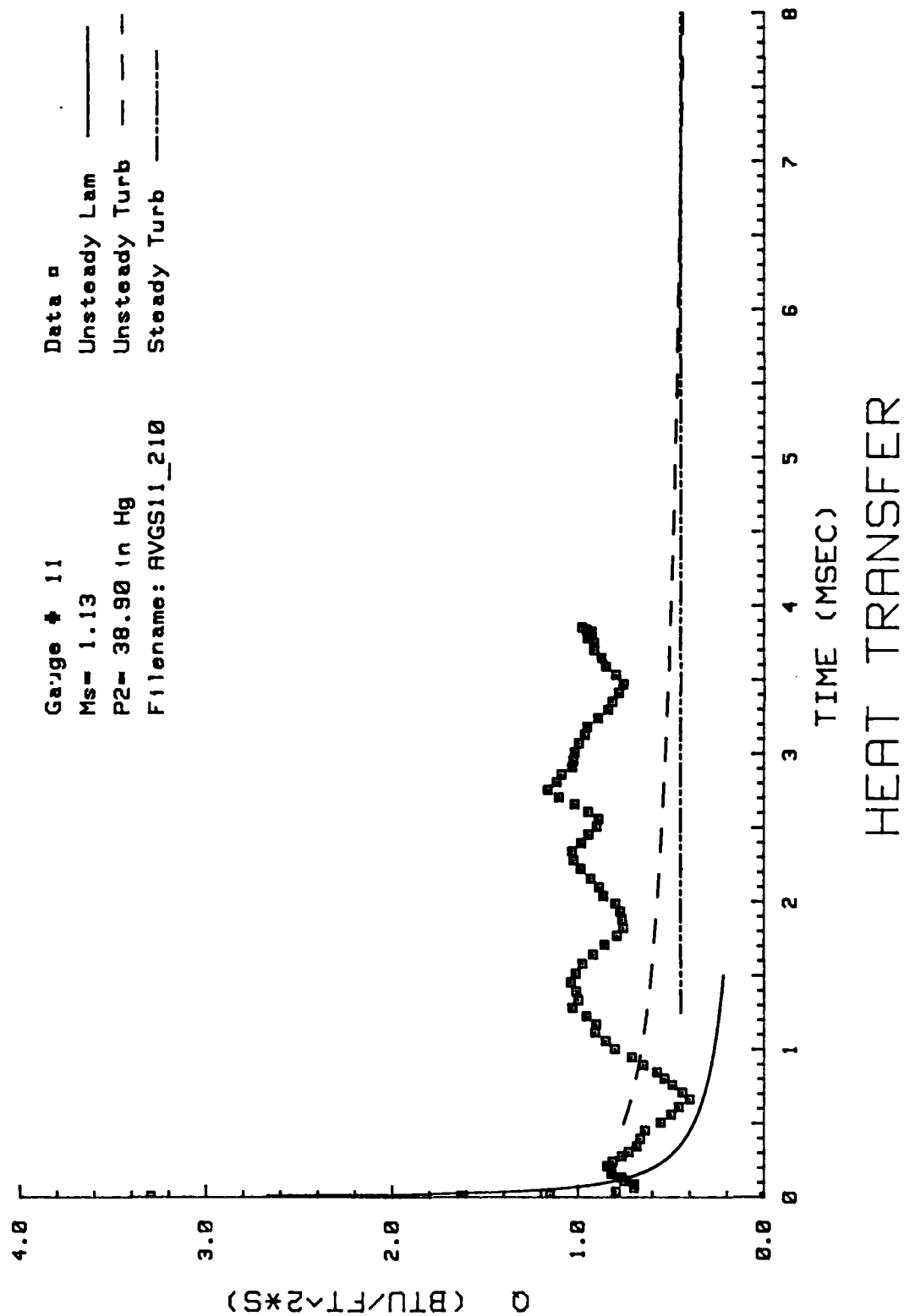
Figure 85. Heat Transfer: Data Set K Gage #11
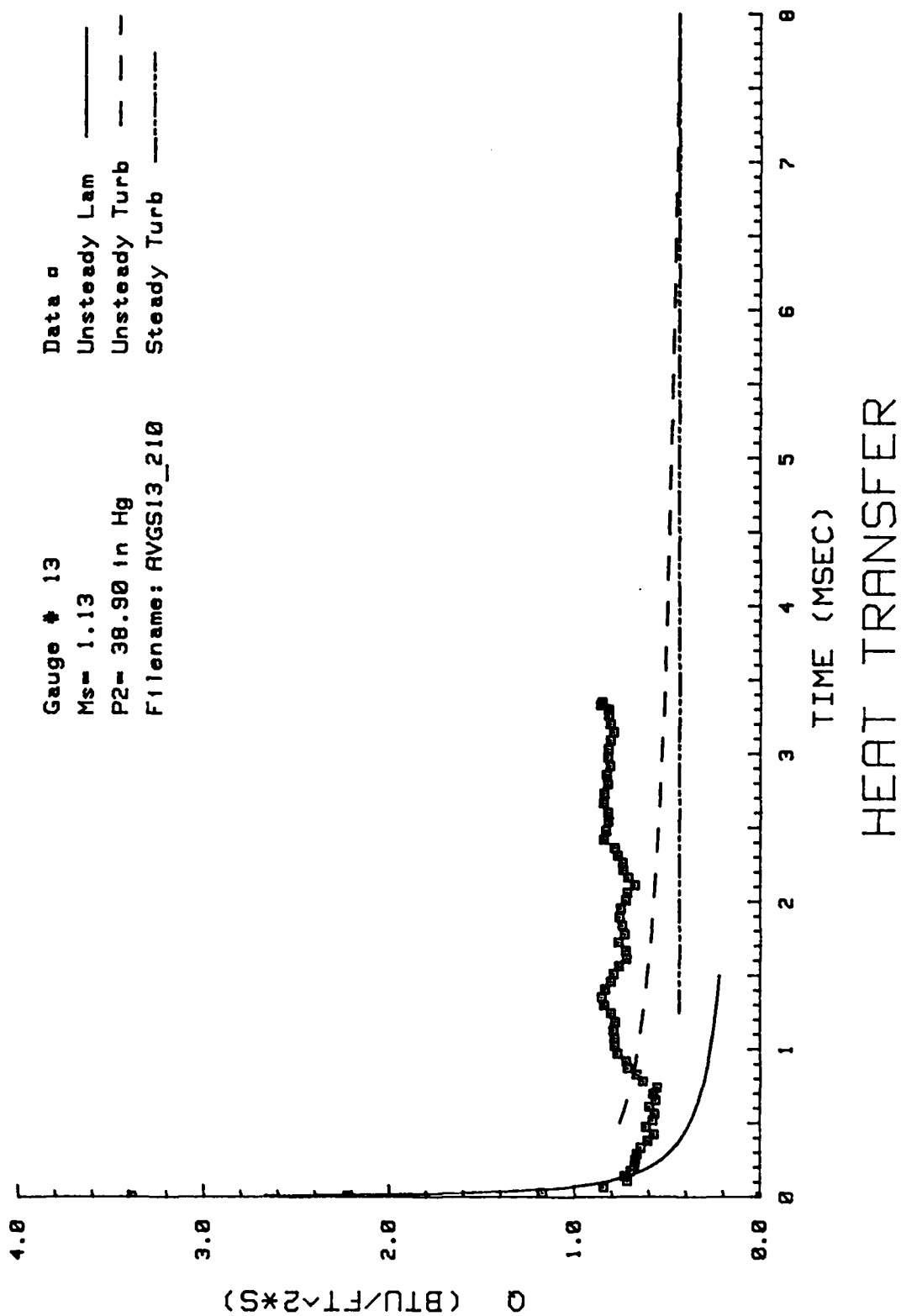
Figure 86. Heat Transfer: Data Set K Gage #13
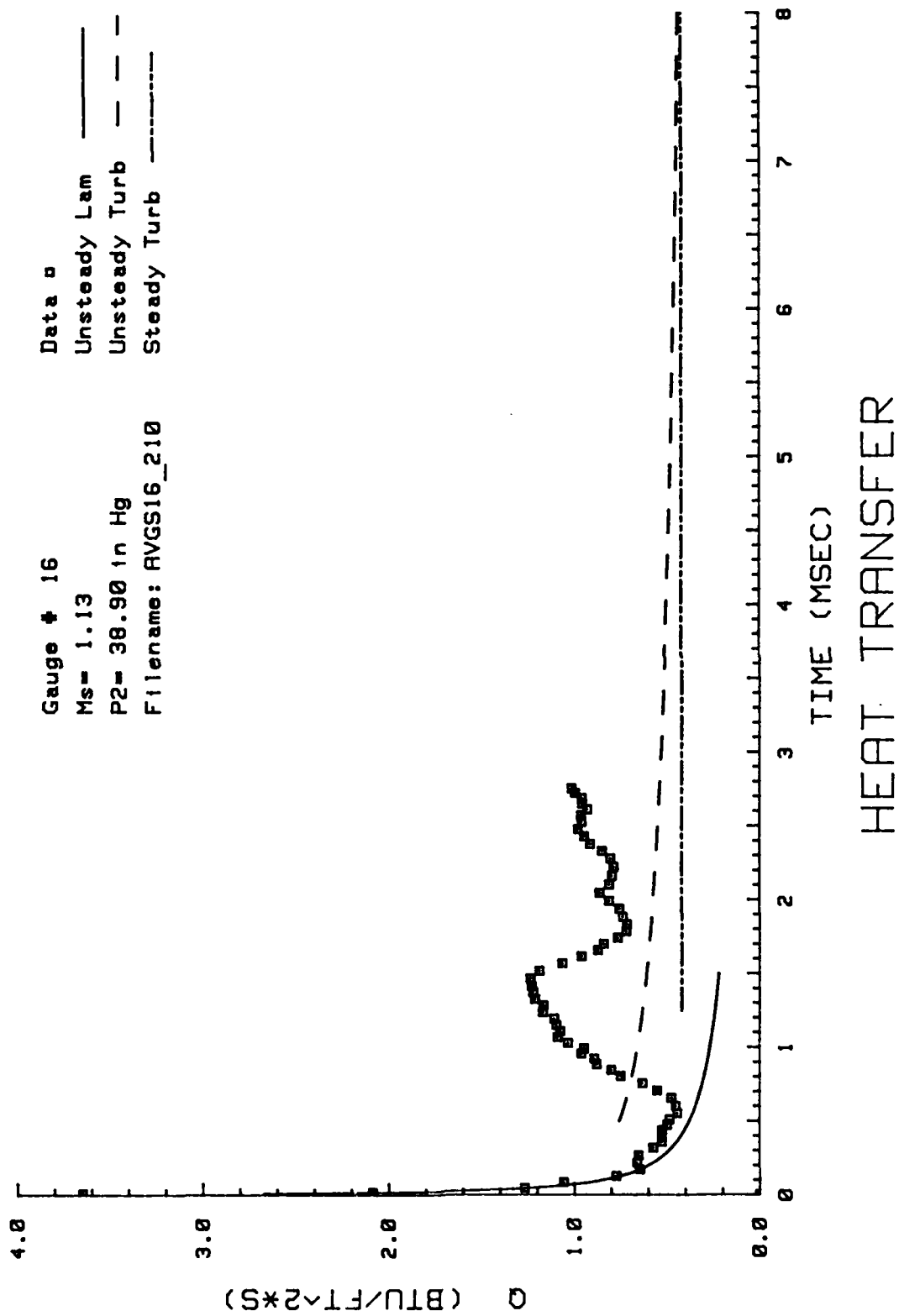
Figure 87. Heat Transfer: Data Set K Gage #16
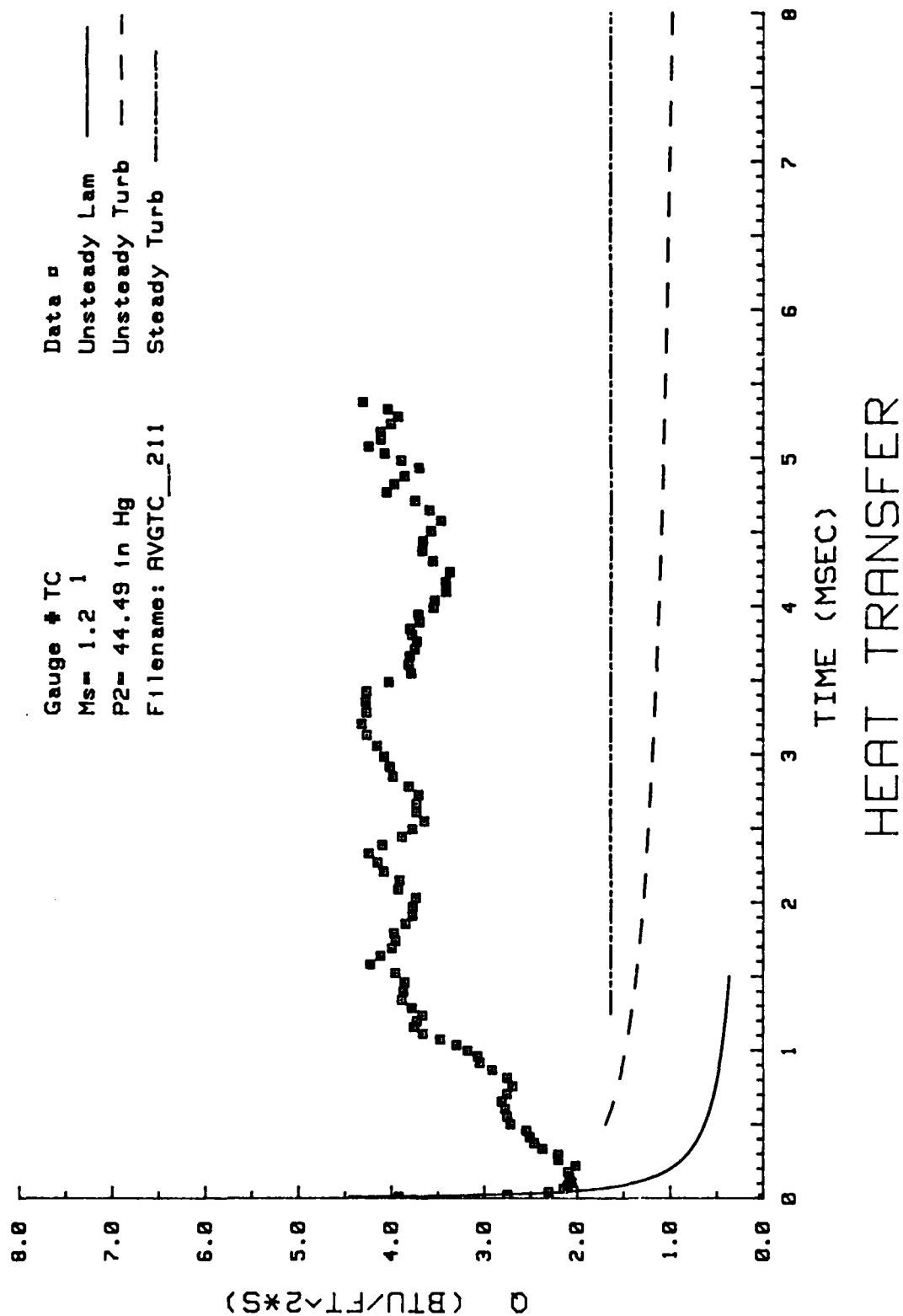
Figure 88. Heat Transfer: Data Set L Thermocouple
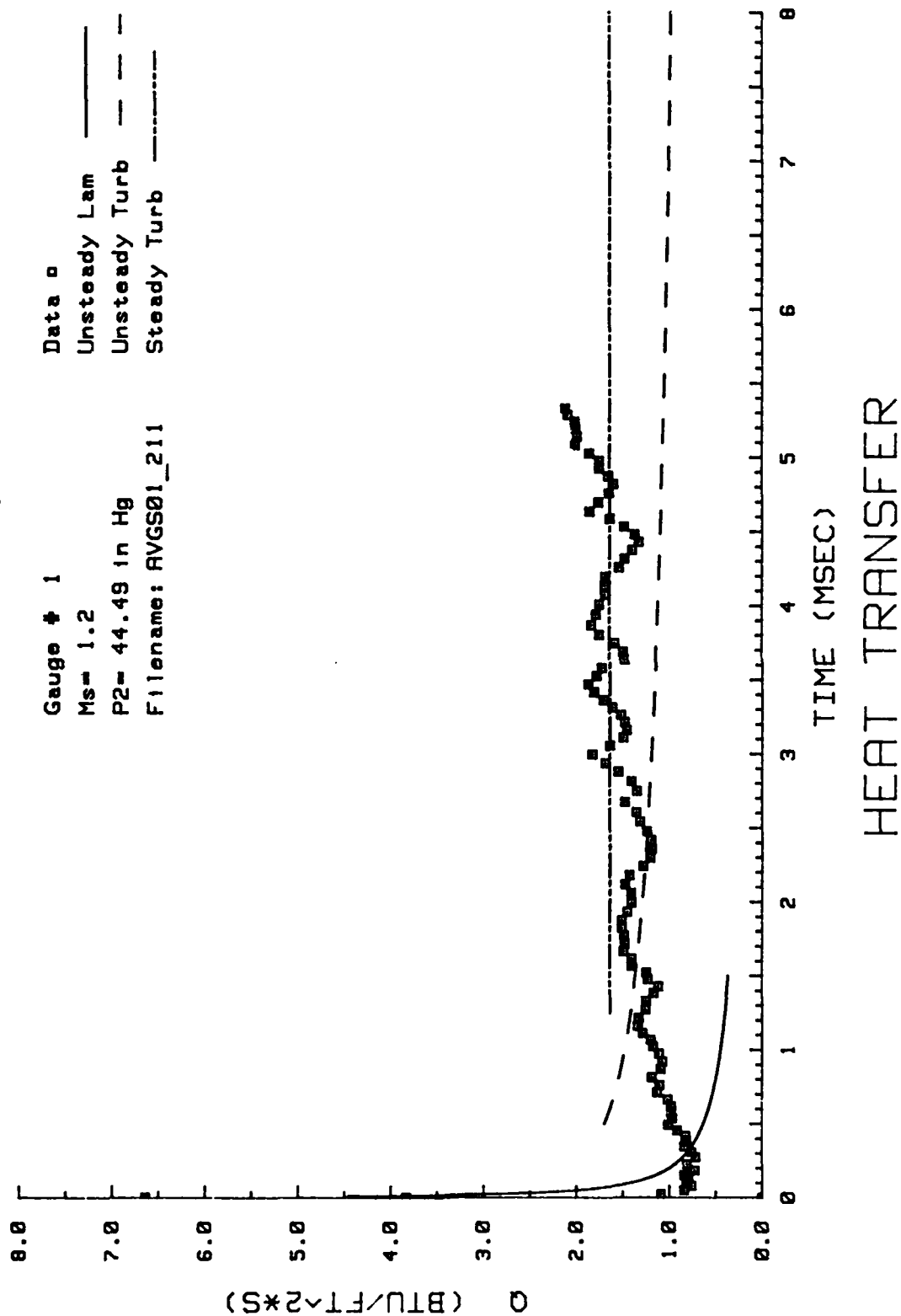
Figure 89. Heat Transfer: Data Set 1, Gage #1
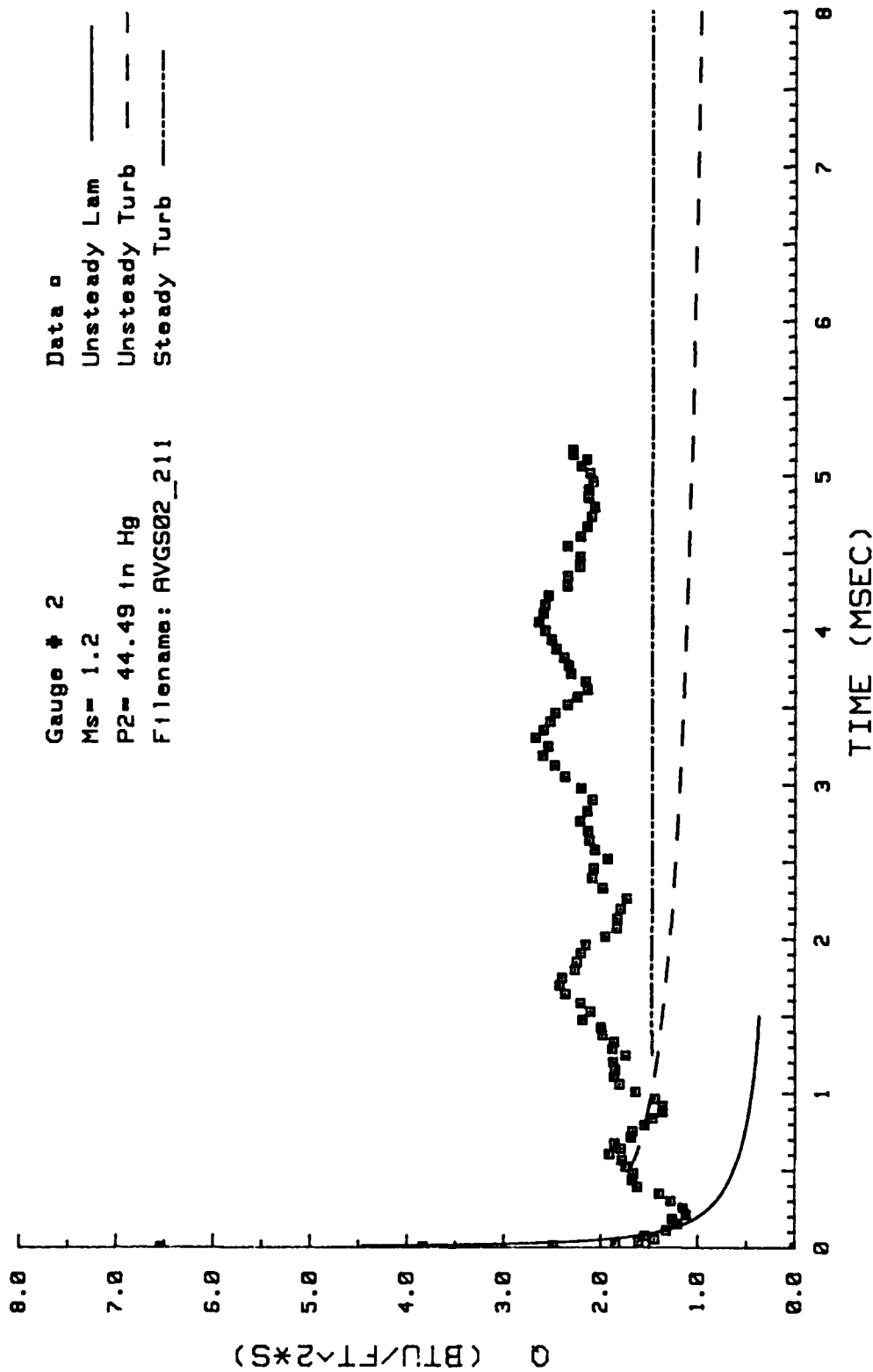
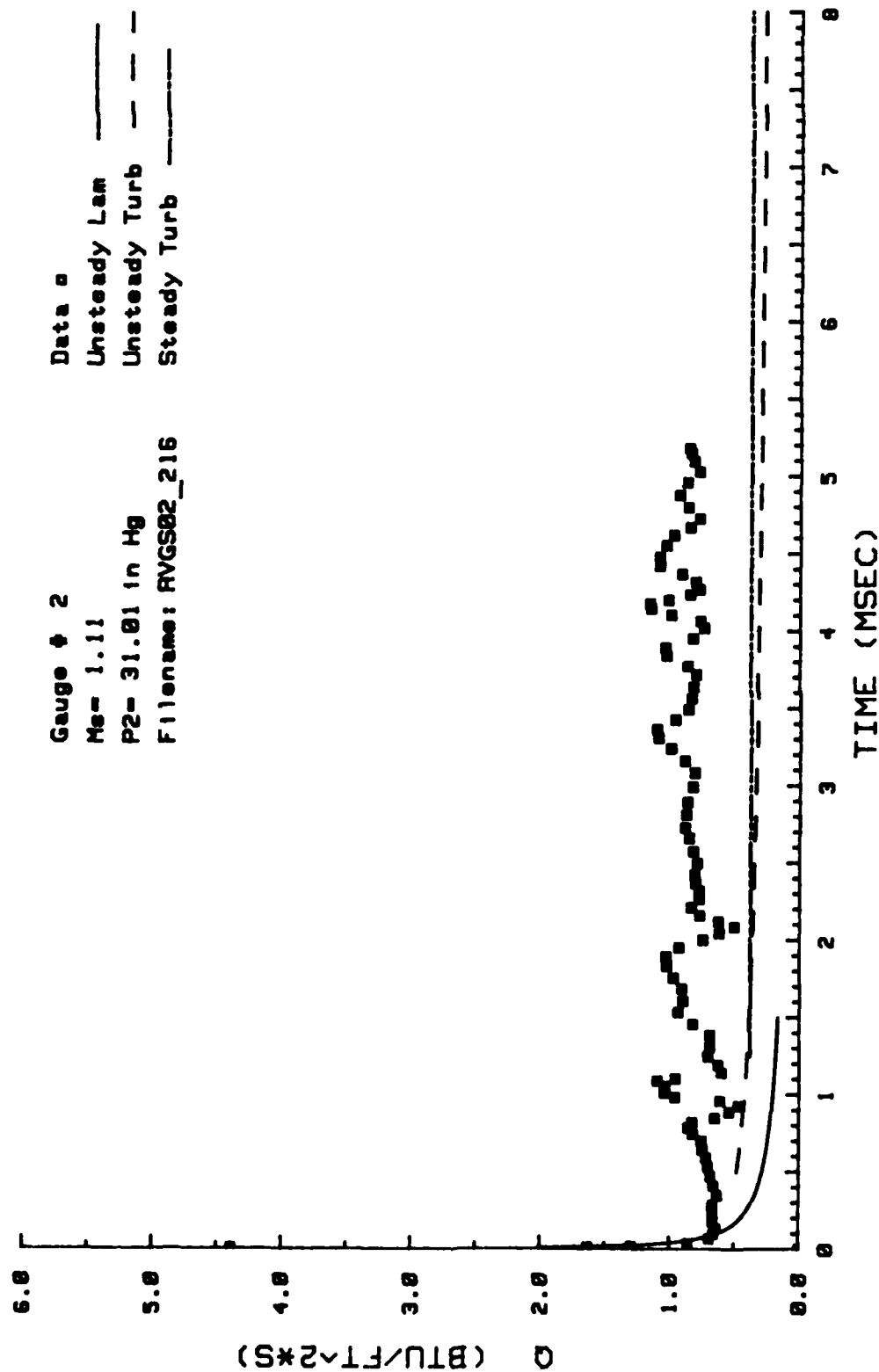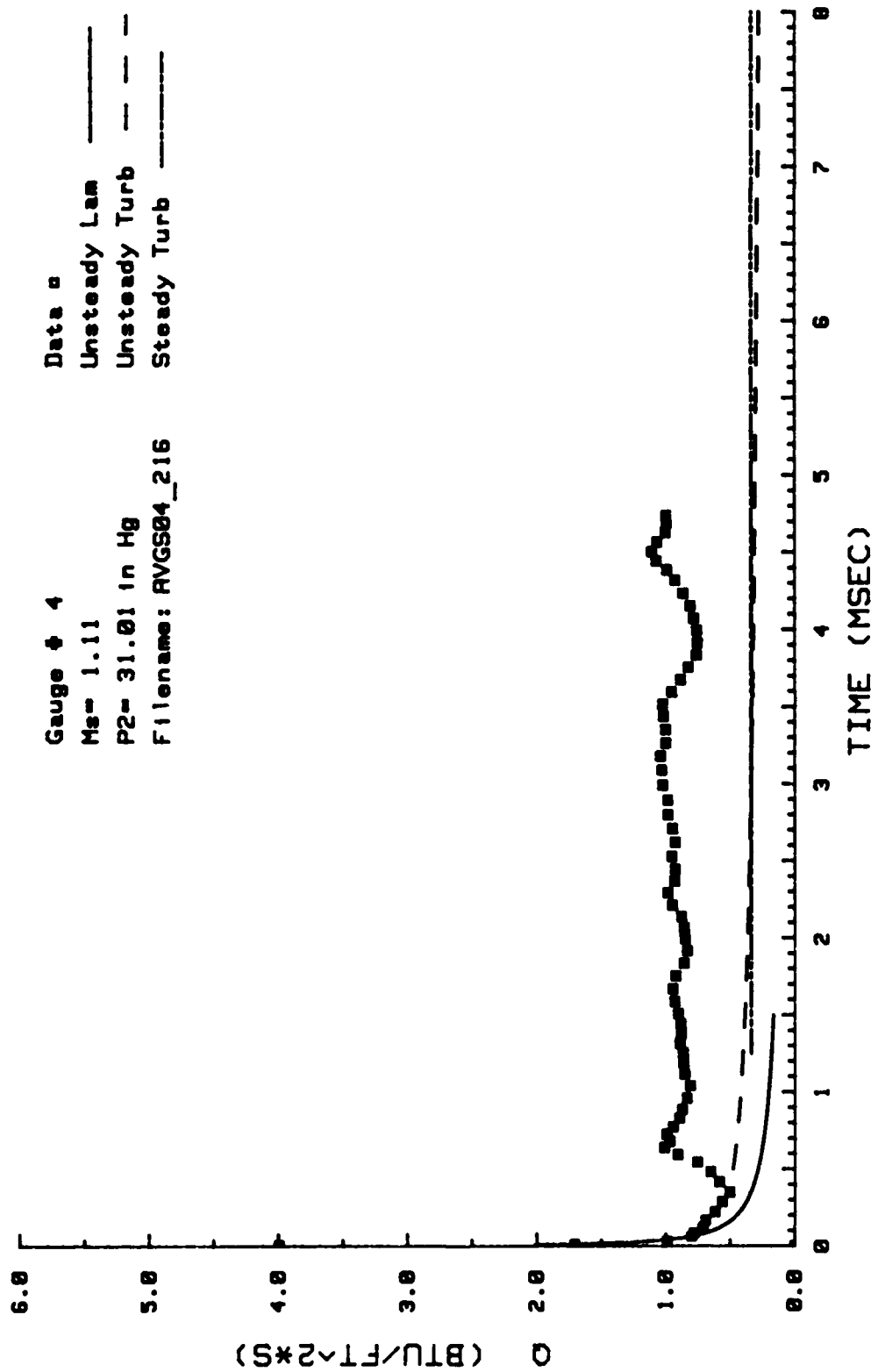Figure 90. Heat Transfer: Data Set L Gage #2
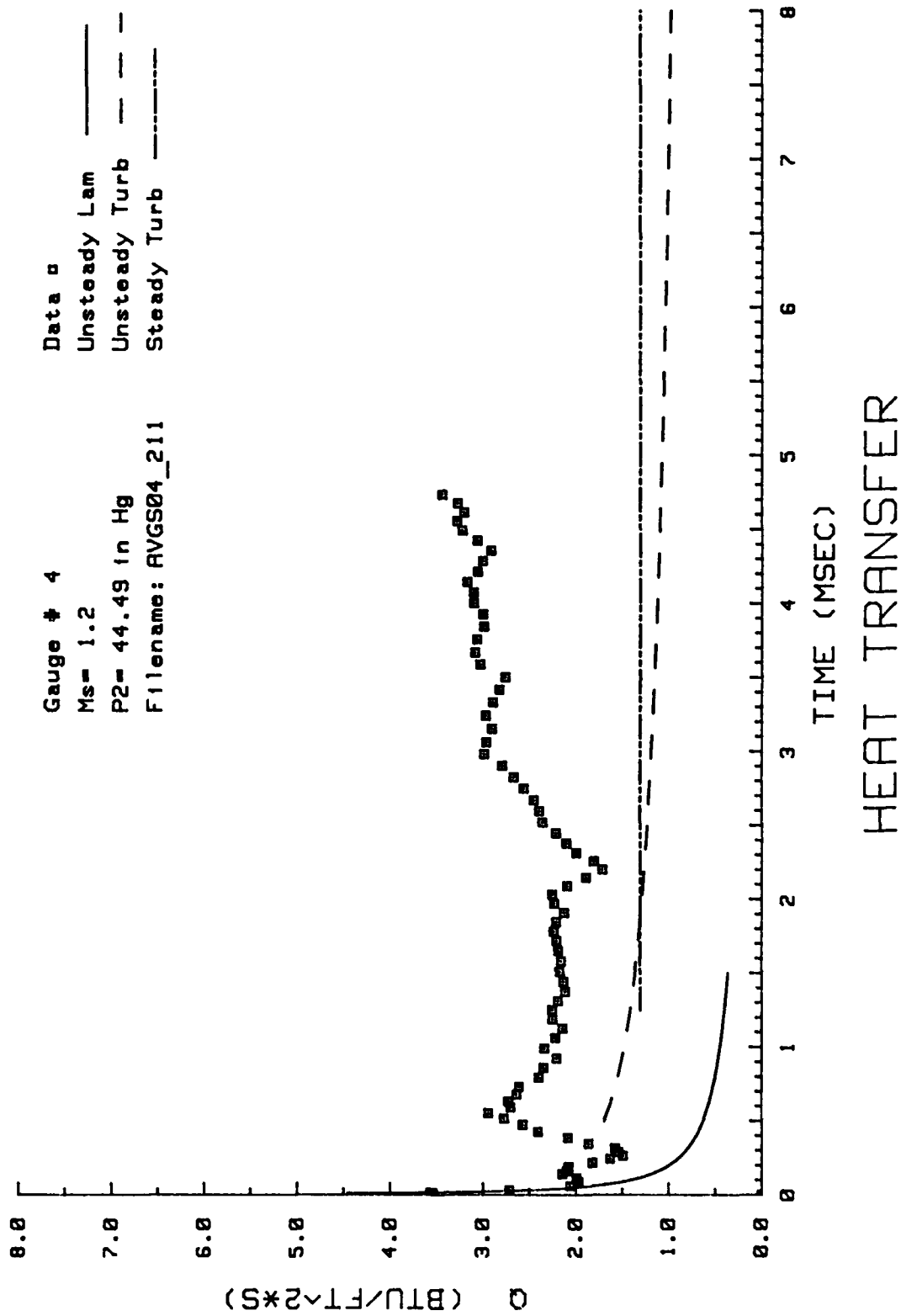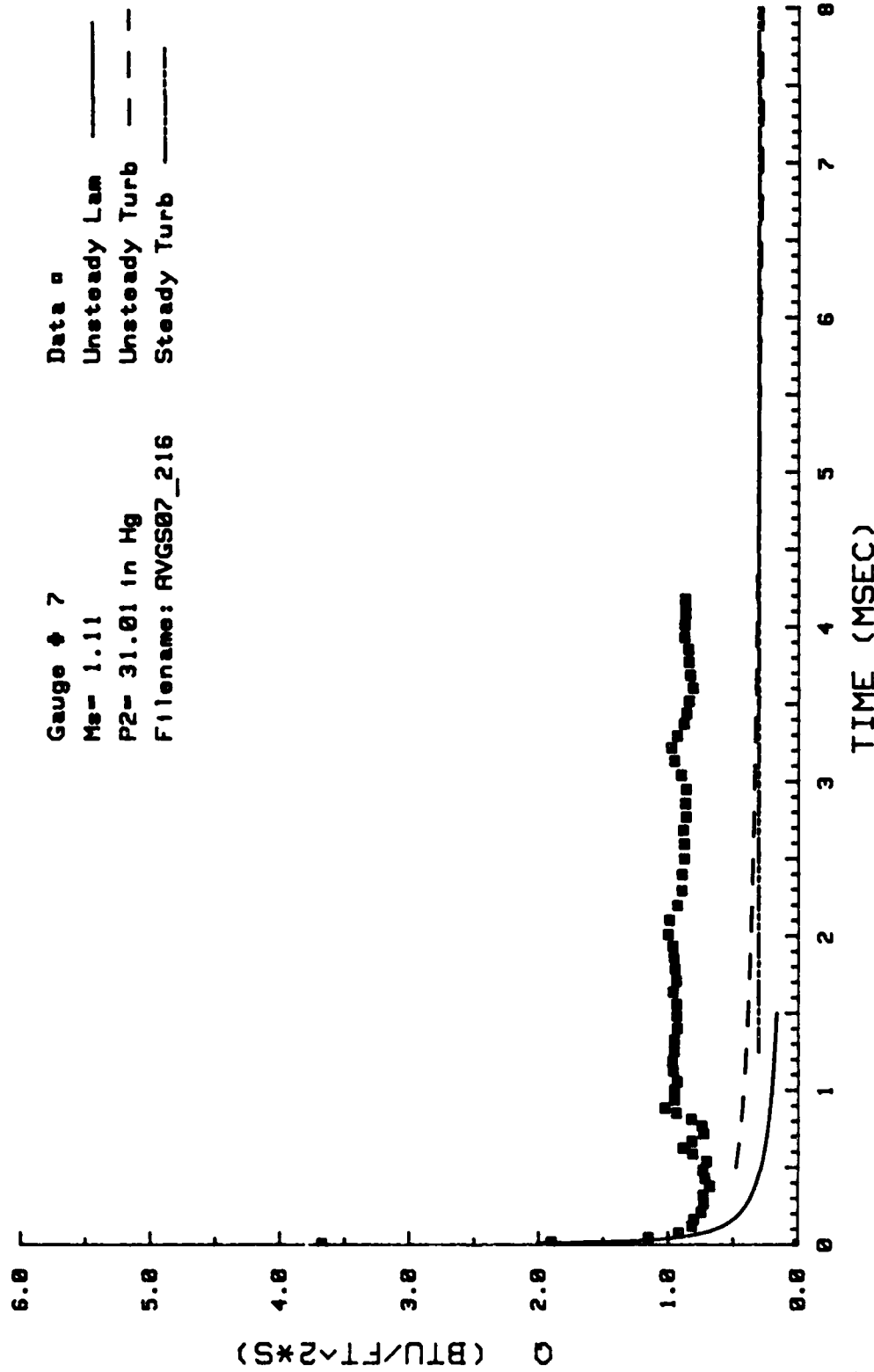
Figure 91. Heat Transfer: Data Set L Gage #4
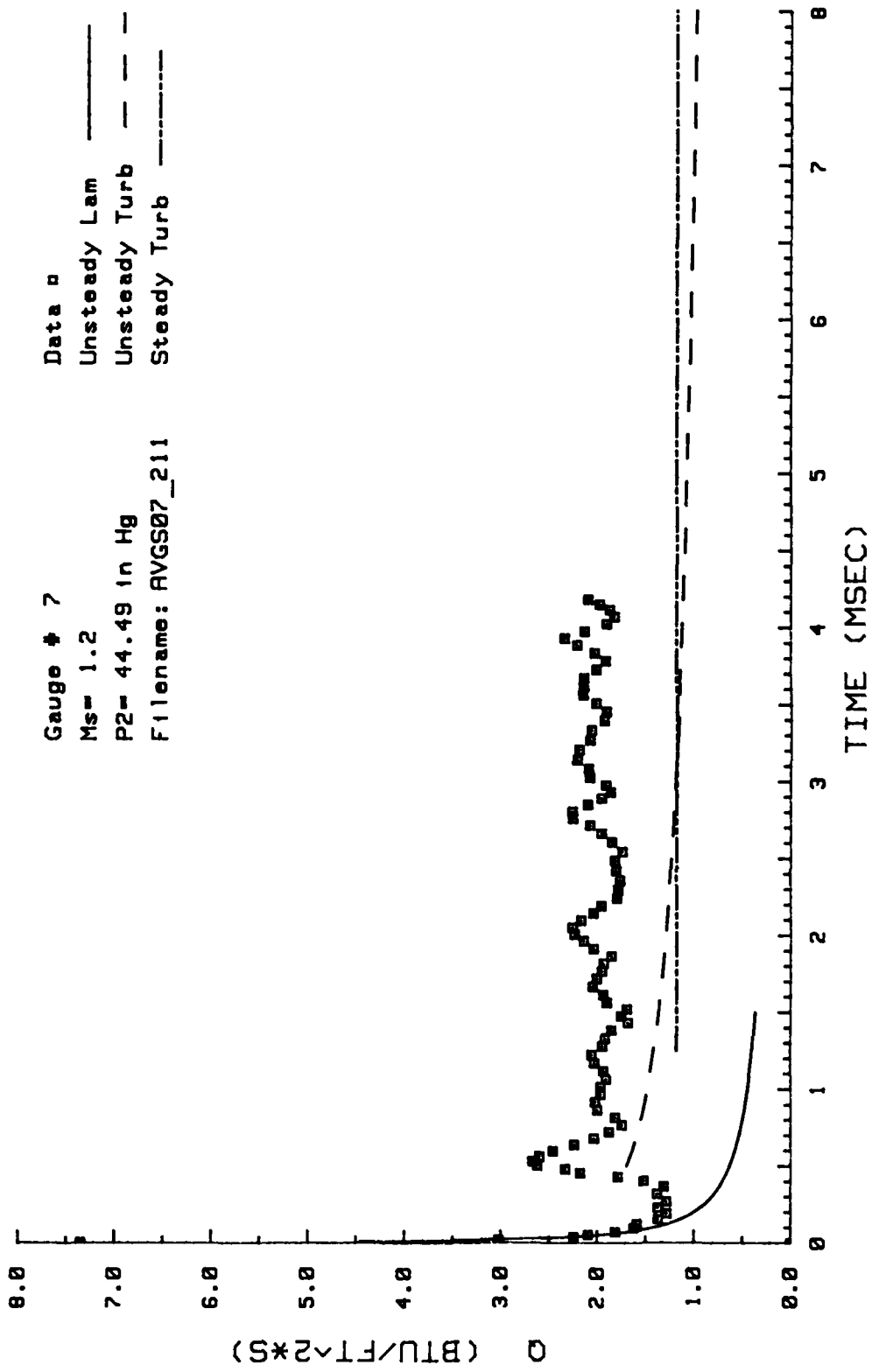
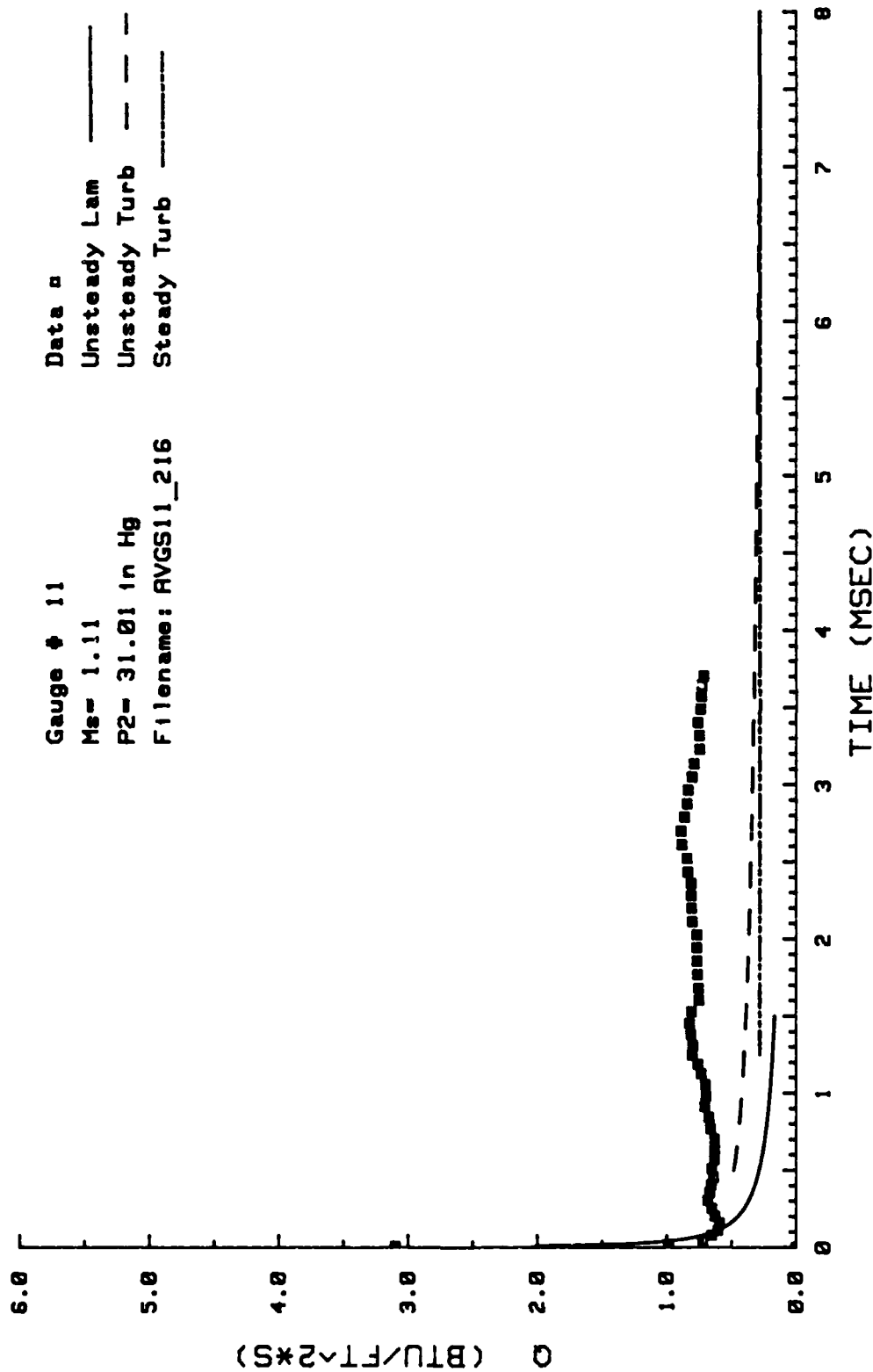Figure 92. Heat Transfer: Data Set L Gage #7
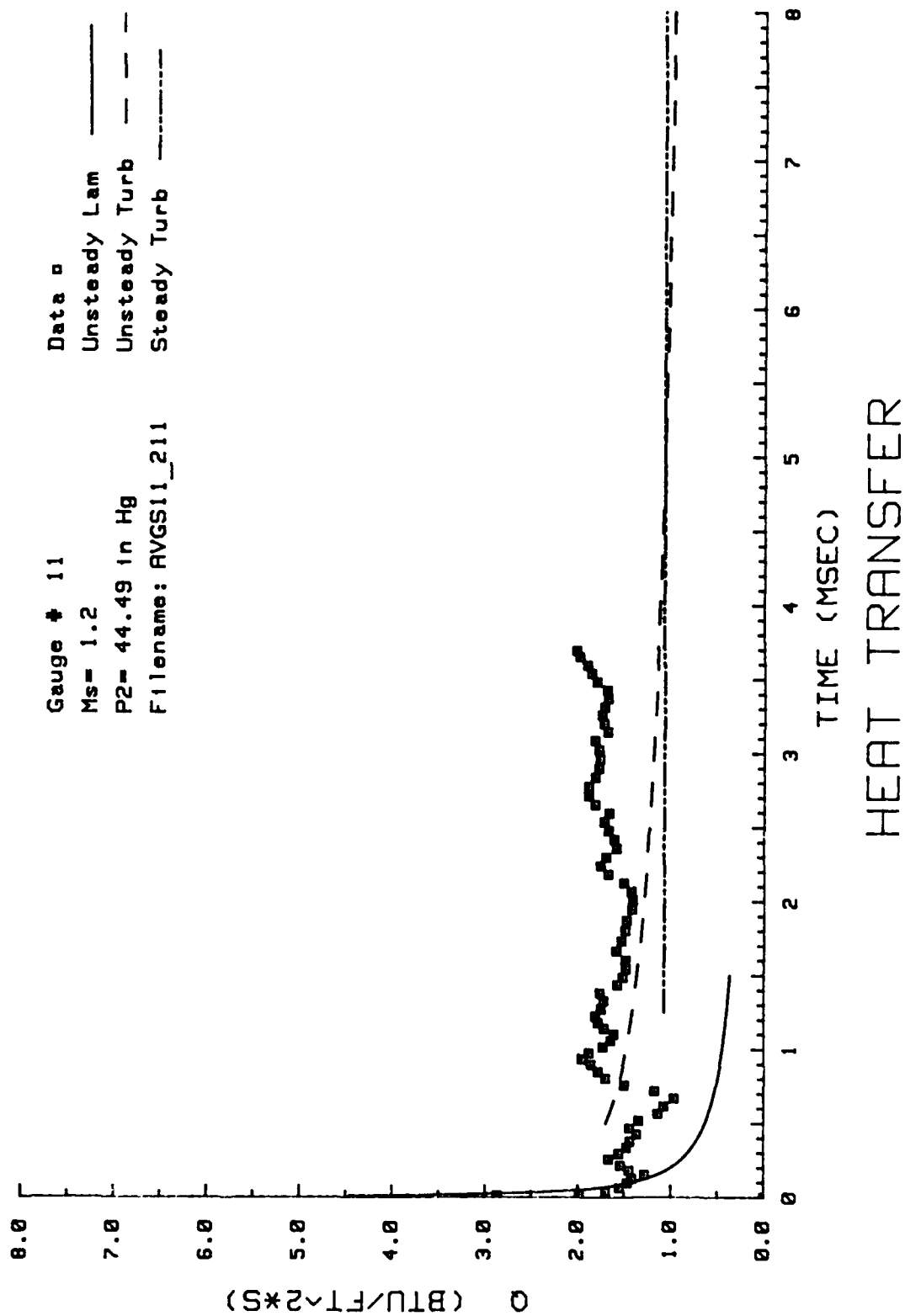
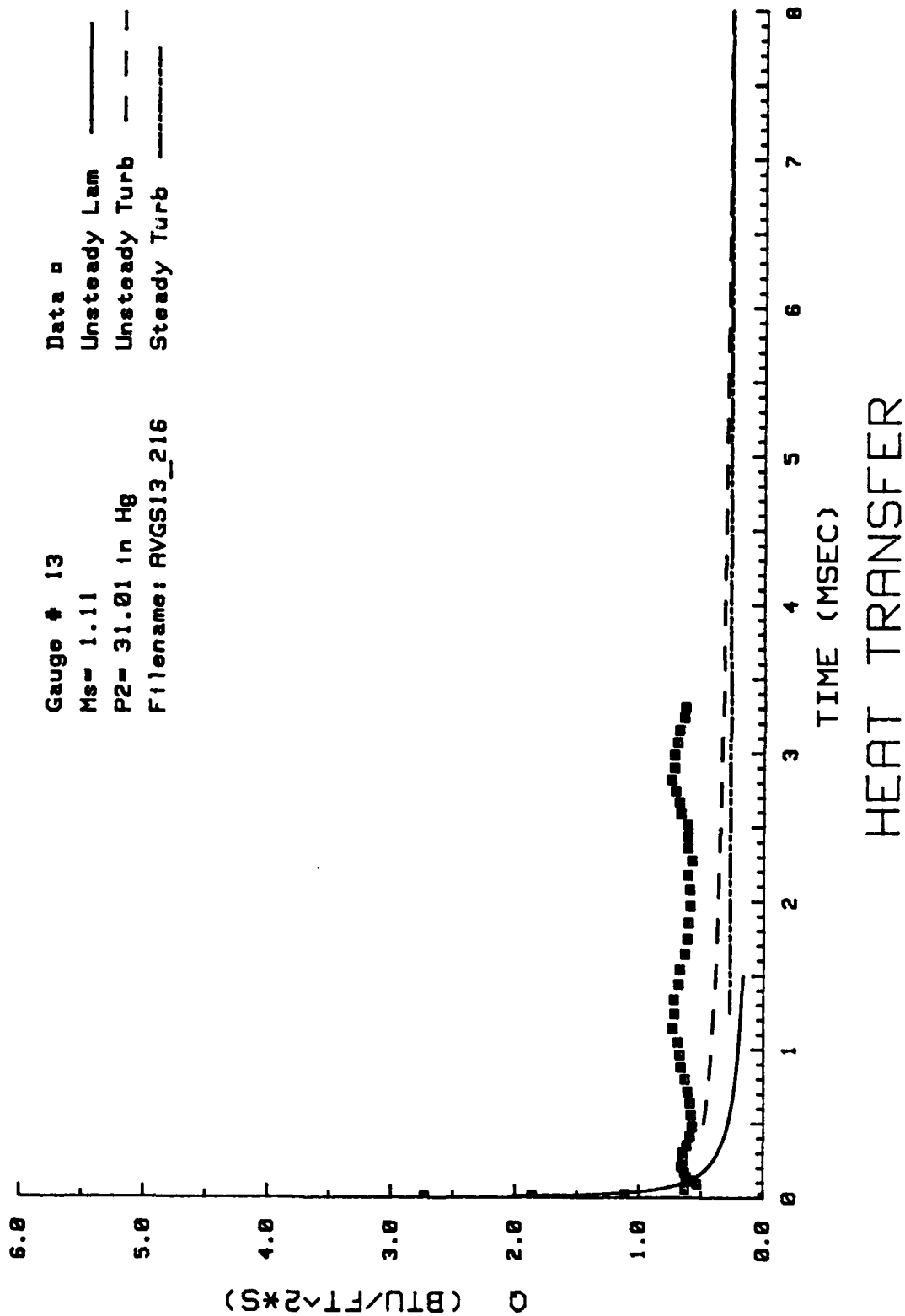Figure 93. Heat Transfer: Data Set 1, Gage #11
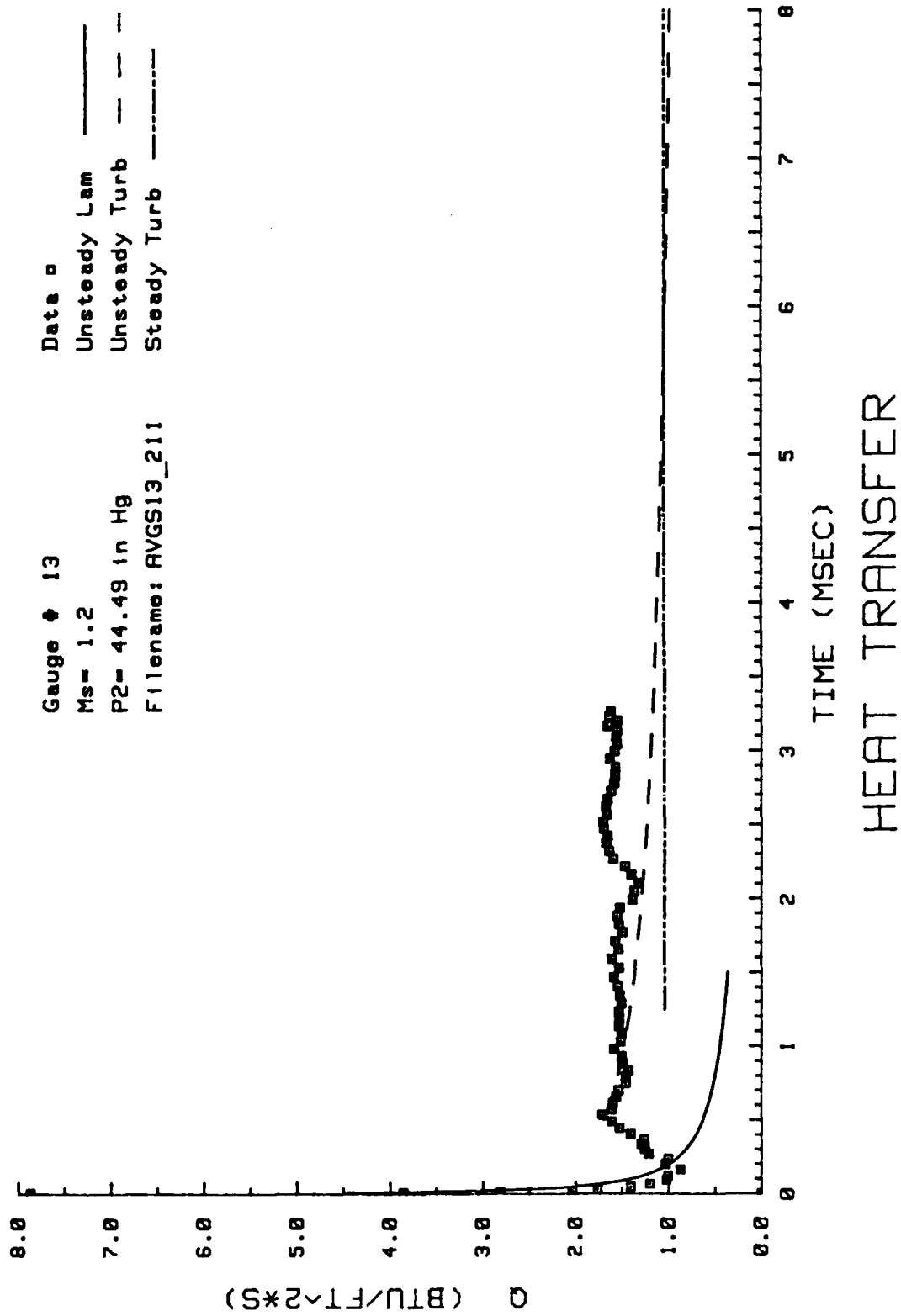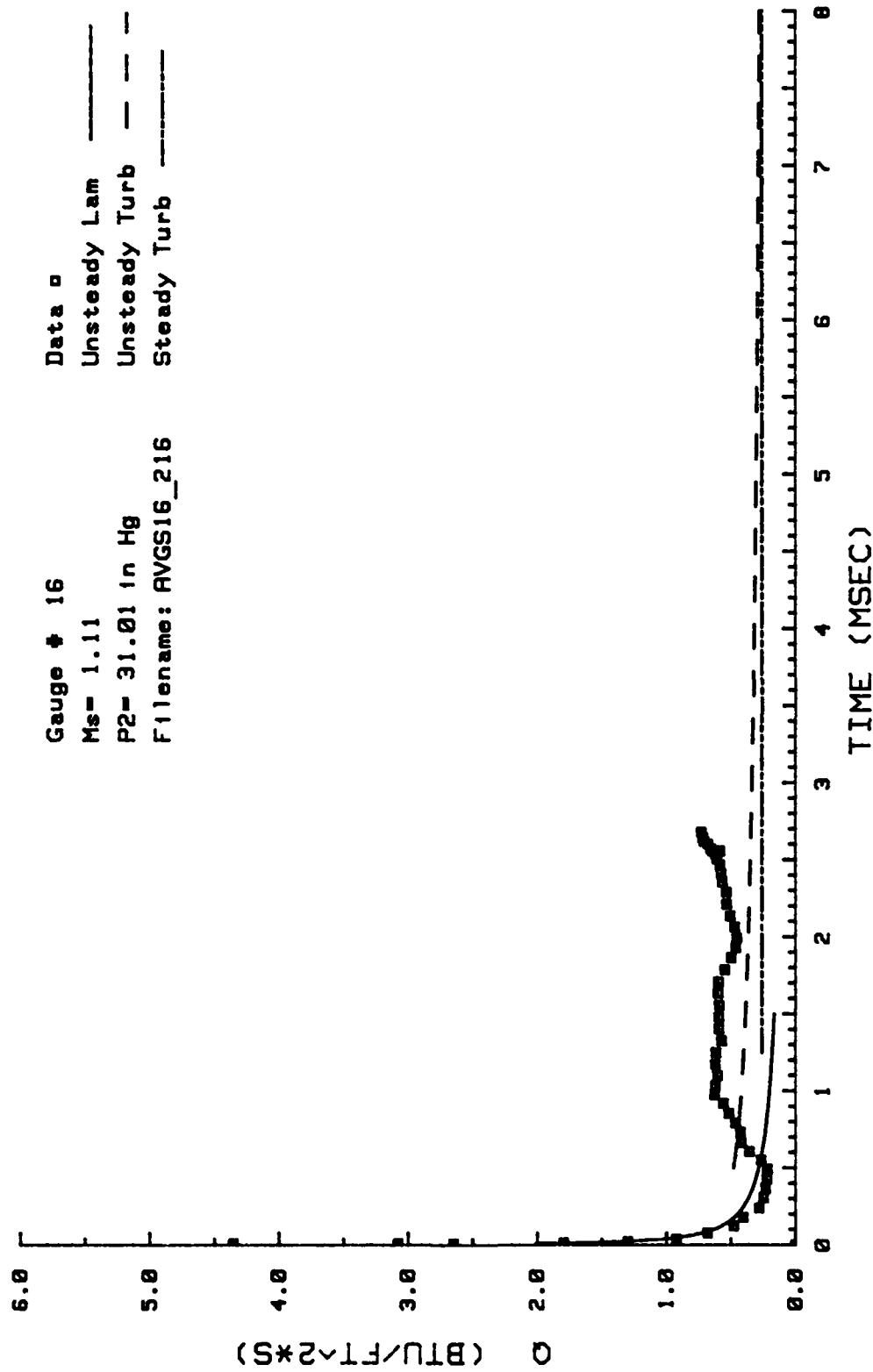
Figure 94. Heat Transfer: Data Set I, Gage #13
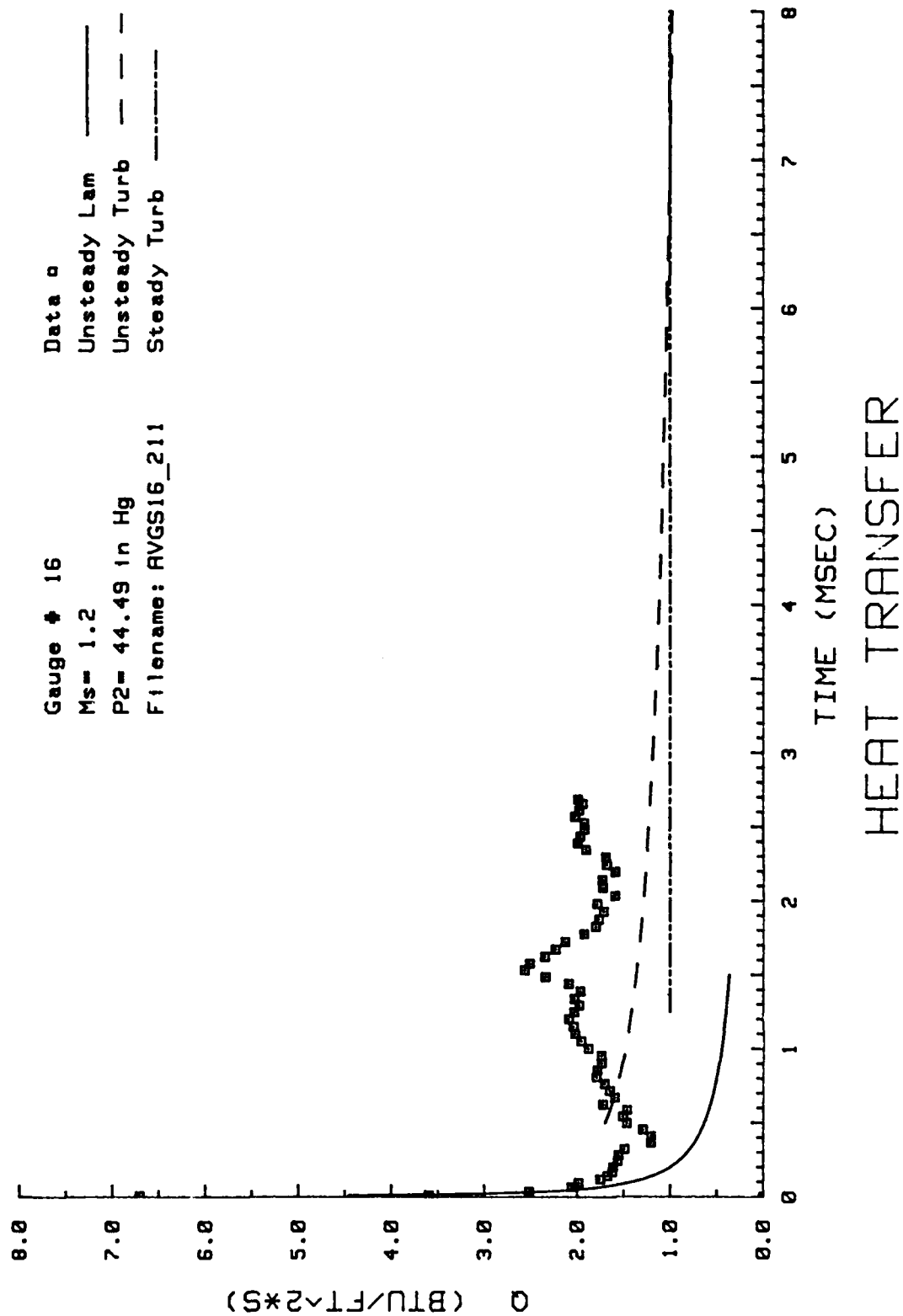
Figure 95. Heat Transfer: Data Set 1. Gage #16

144
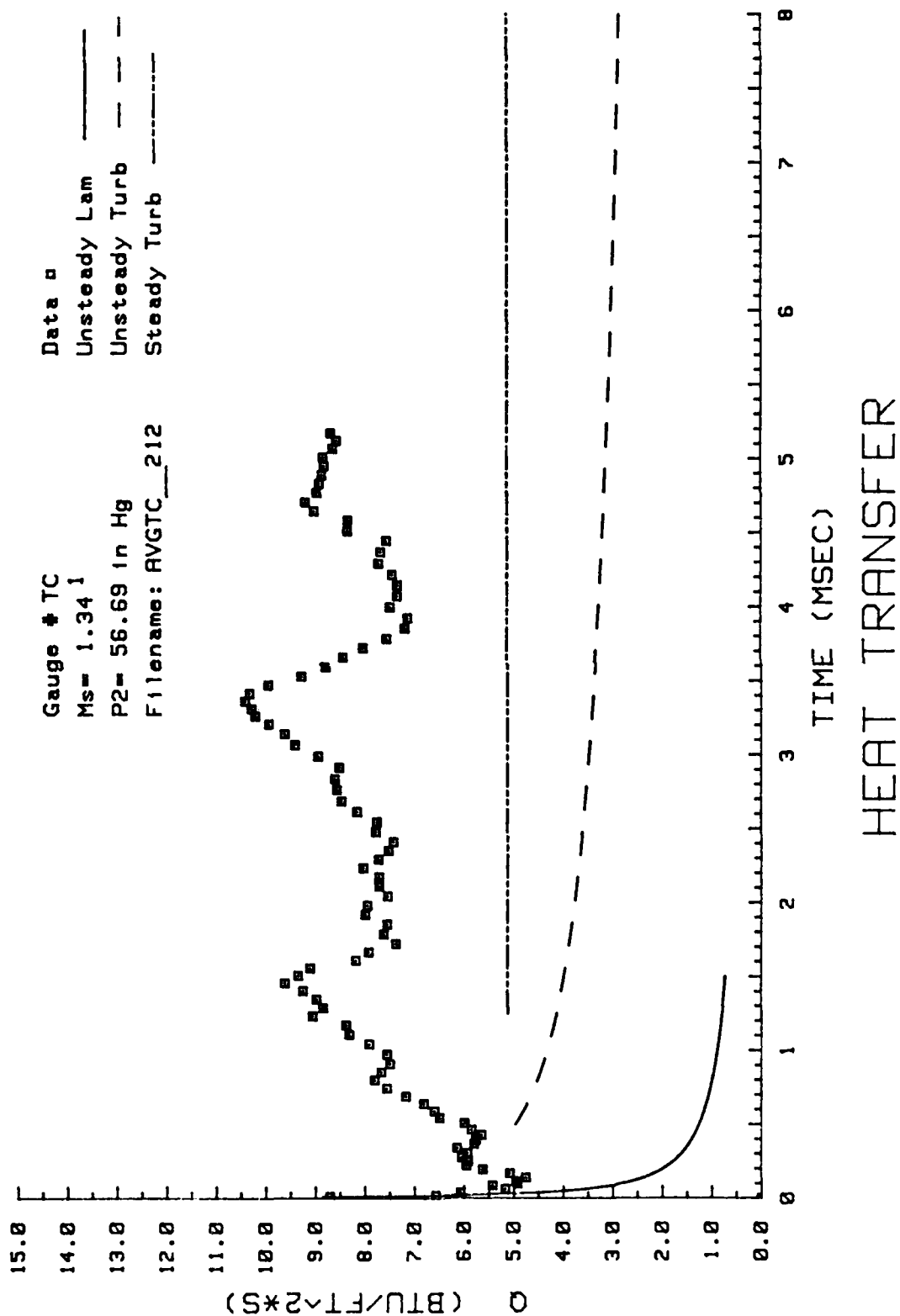
Figure 96. Heat Transfer: Data Set M Thermocouple

Figure 97. Heat Transfer: Data Set M Gage #1

Figure 98. Heat Transfer: Data Set M Gage #2

Figure 99. Heat Transfer: Data Set M Gage #4

148

Figure 100. Heat Transfer: Data Set M Gage #7

Figure 101. Heat Transfer: Data Set M Gage #11

Figure 102. Heat Transfer: Data Set M Gage #13

Figure 103. Heat Transfer: Data Set M Gage #16

152

Figure 104. Heat Transfer: Data Set N Thermocouple

Figure 105. Heat Transfer: Data Set N Gage #1

Figure 106. Heat Transfer: Data Set N Gage #2

155

Figure 107. Heat Transfer: Data Set N Gage #4

Figure 107. Heat Transfer: Data Set N Gage #7

Figure 109. Heat Transfer: Data Set N Gage #11
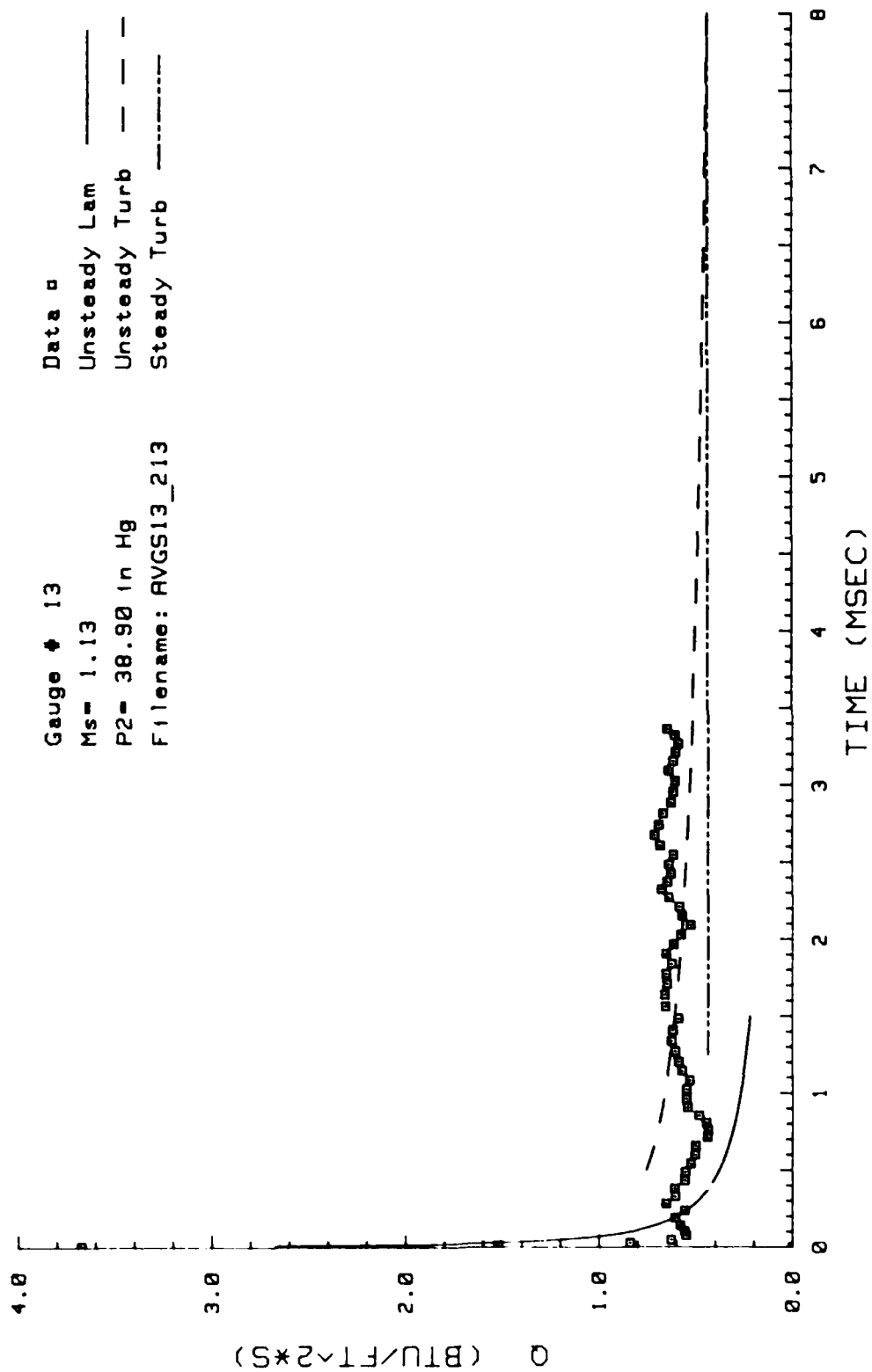
Figure 110. Heat Transfer: Data Set N Gage #13

Figure 111. Heat Transfer: Data Set N Gage #16

Figure 112. Heat Transfer: Data Set 0 Thermocouple

161

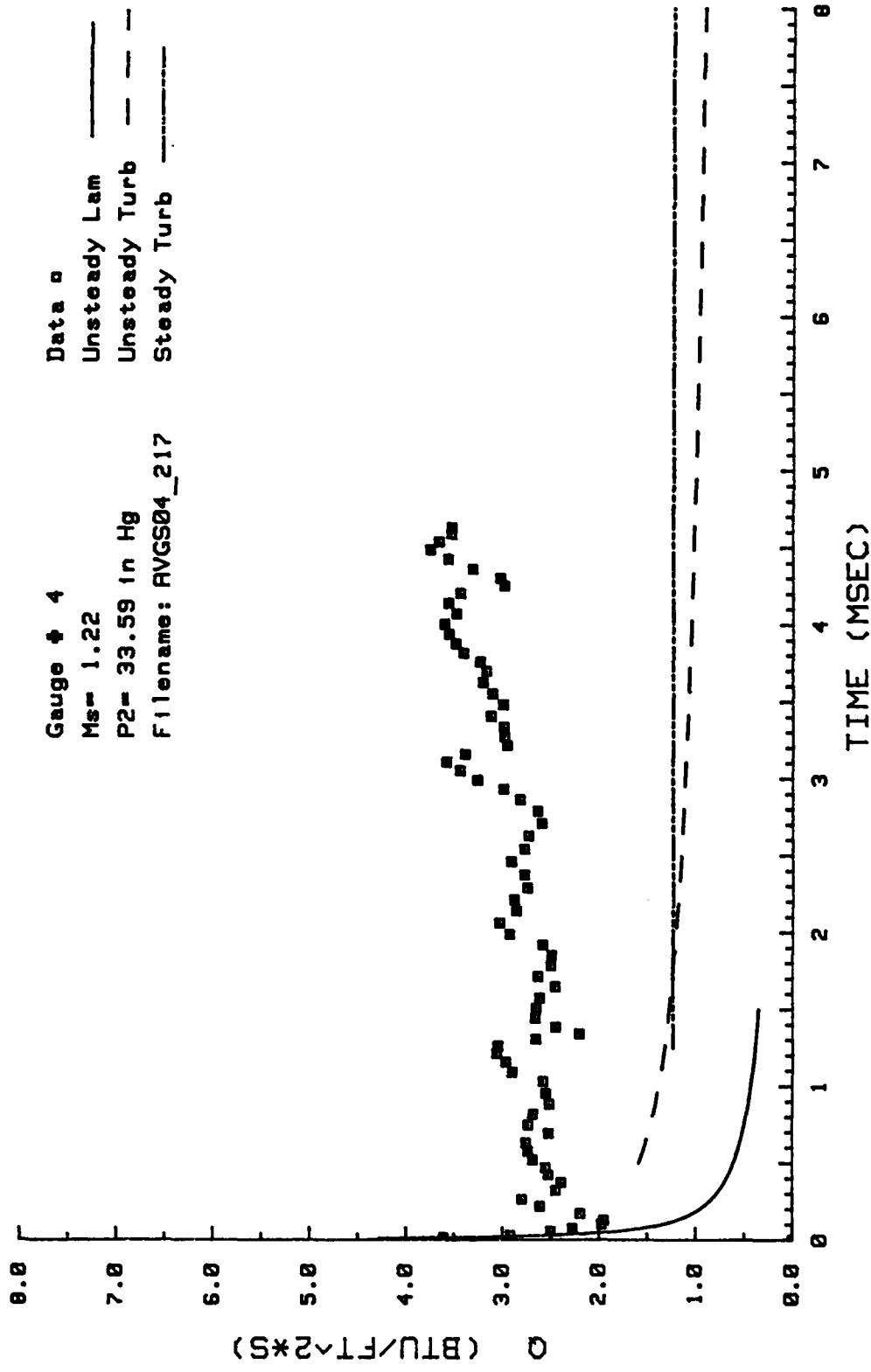Figure 113. Heat Transfer: Data Set 0 Gage #1

162
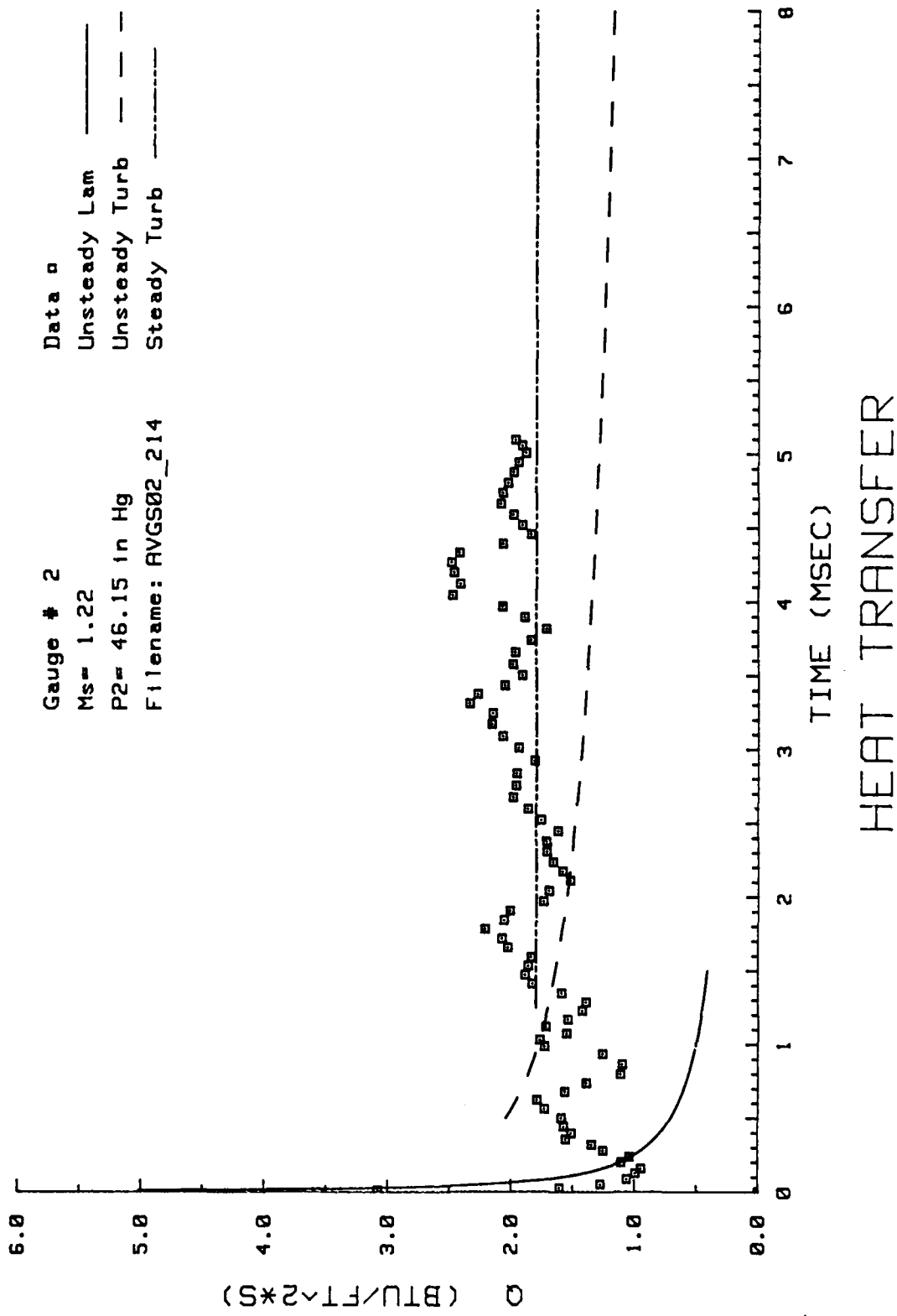
Figure 114. Heat Transfer: Data Set O Gage #2

163

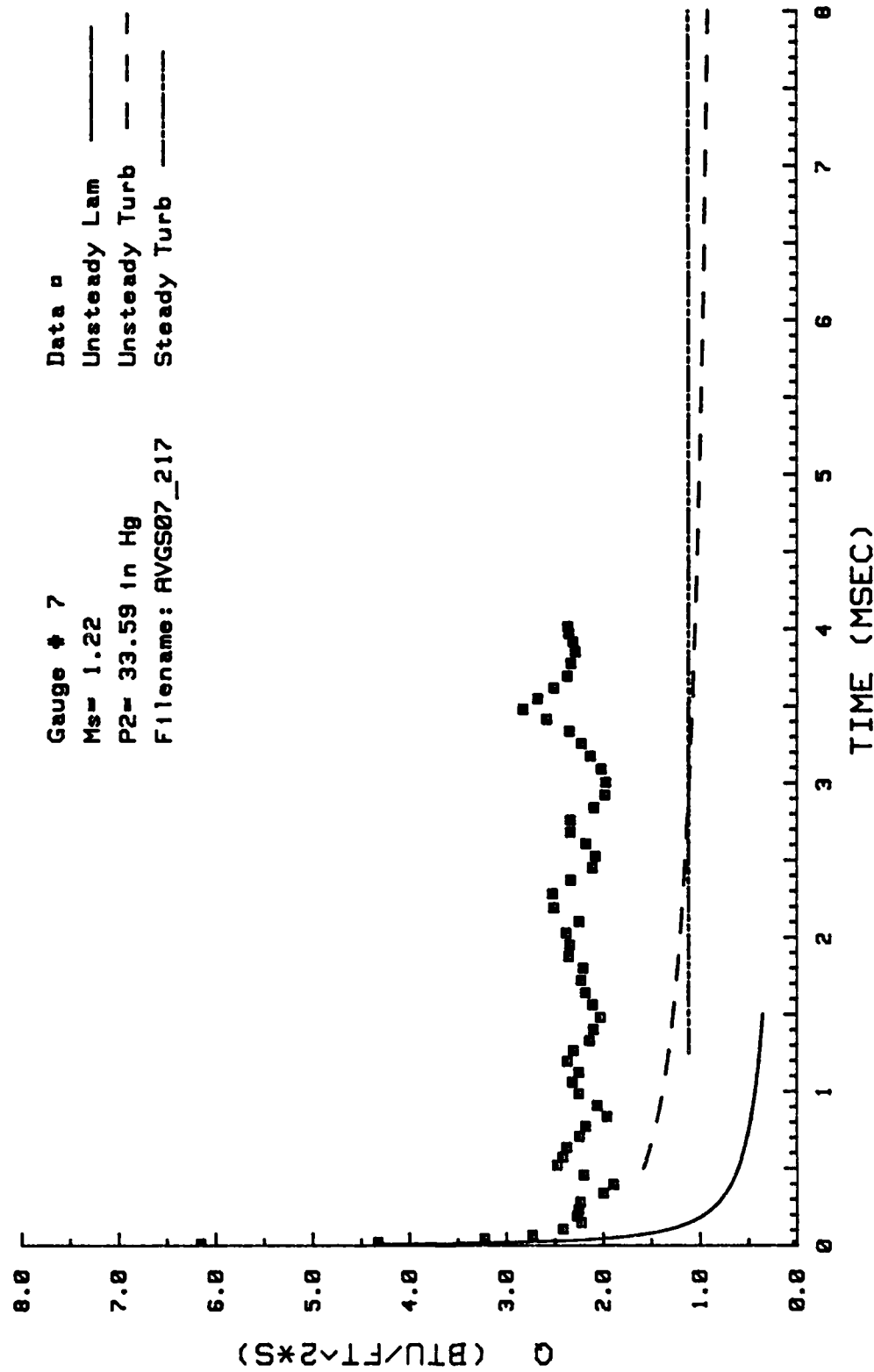Figure 115.   Heat Transfer: Data Set O Gage #4

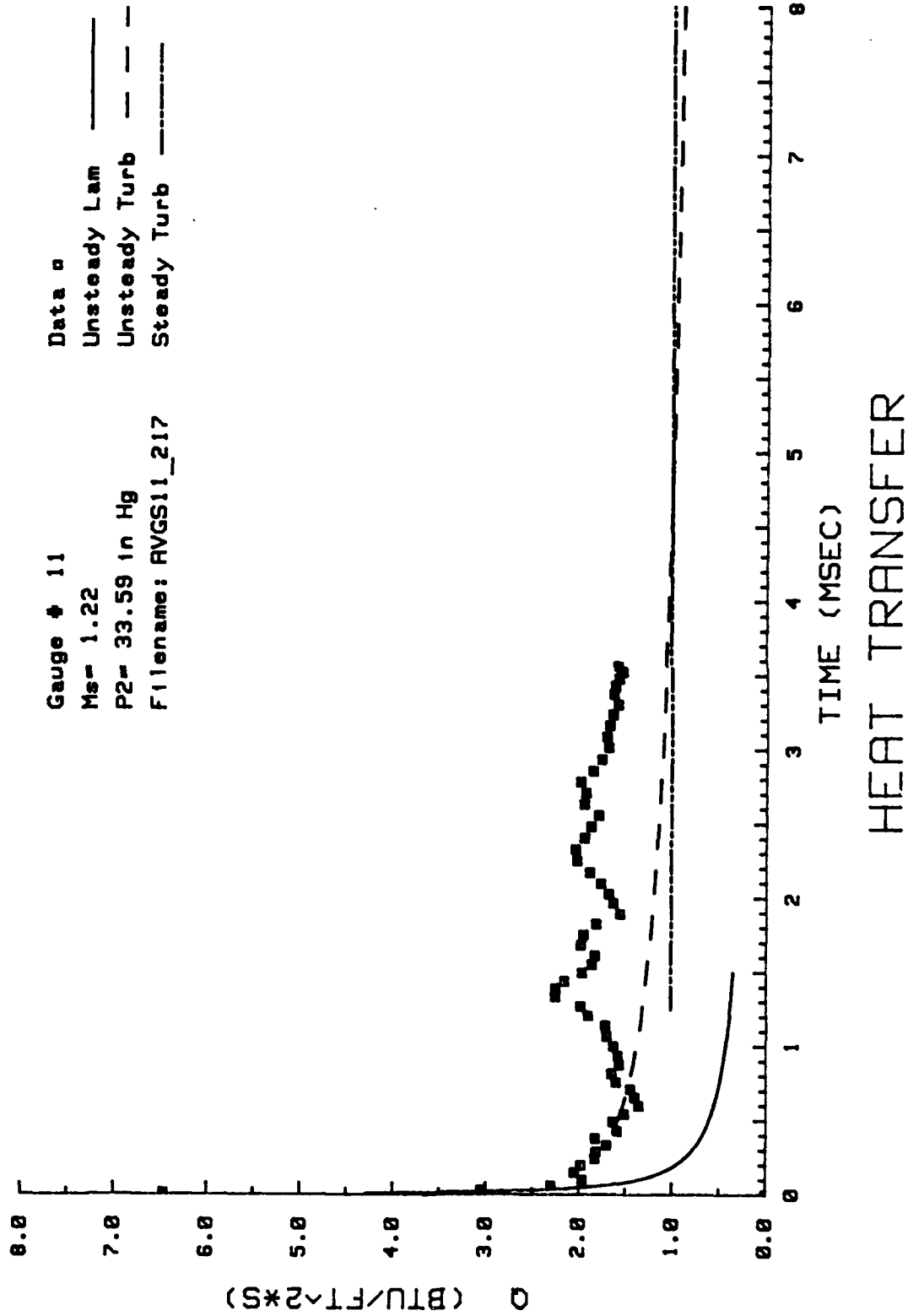Figure 116. Heat Transfer: Data Set O Gage #7

Figure 117.   Heat Transfer: Data Set 0 Gage #11

Figure 118. Heat Transfer: Data Set O Gage #13

Figure 119. Heat Transfer: Data Set 0 Gage #16

Figure 120. Heat Transfer: Data Set P Thermocouple
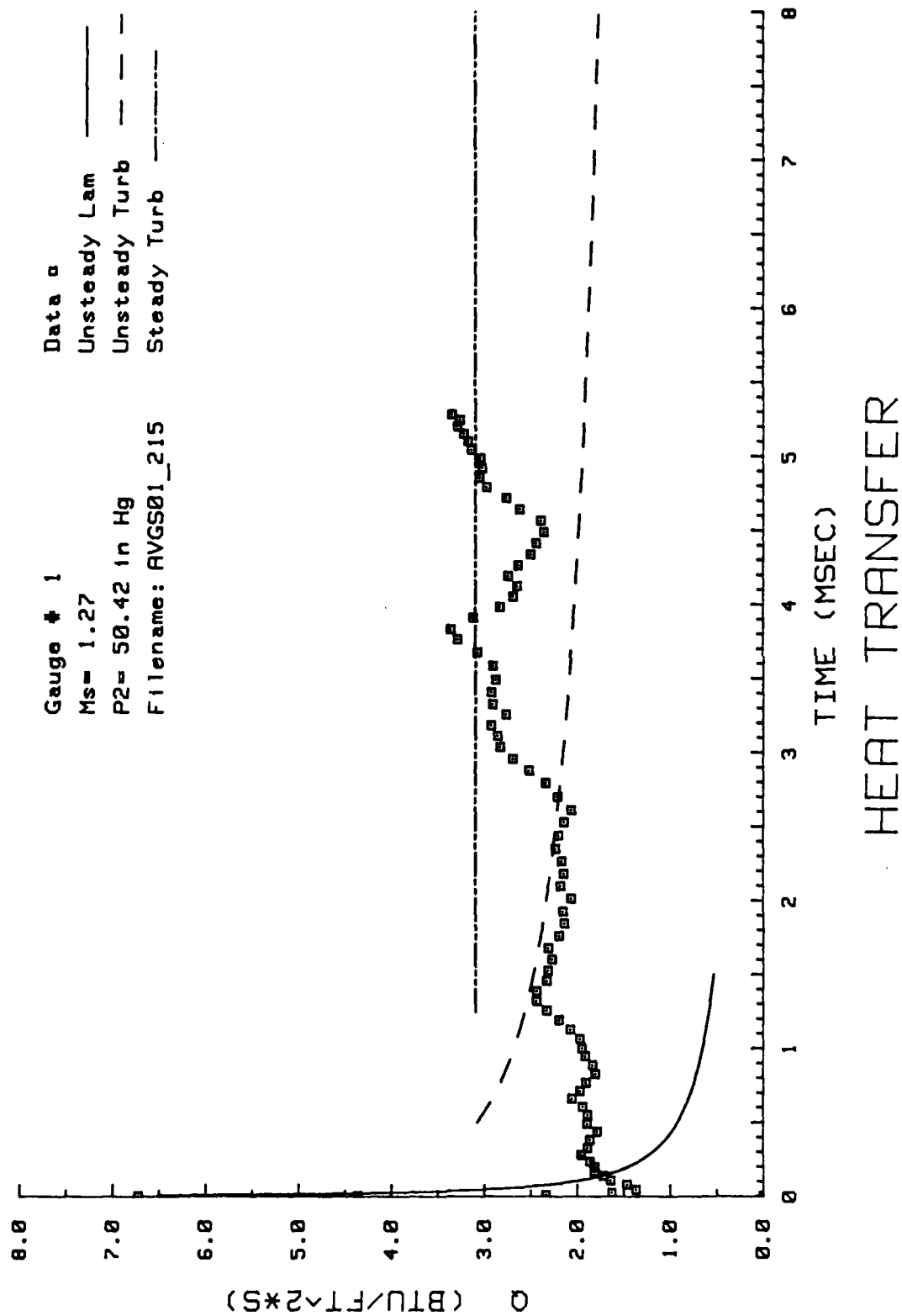
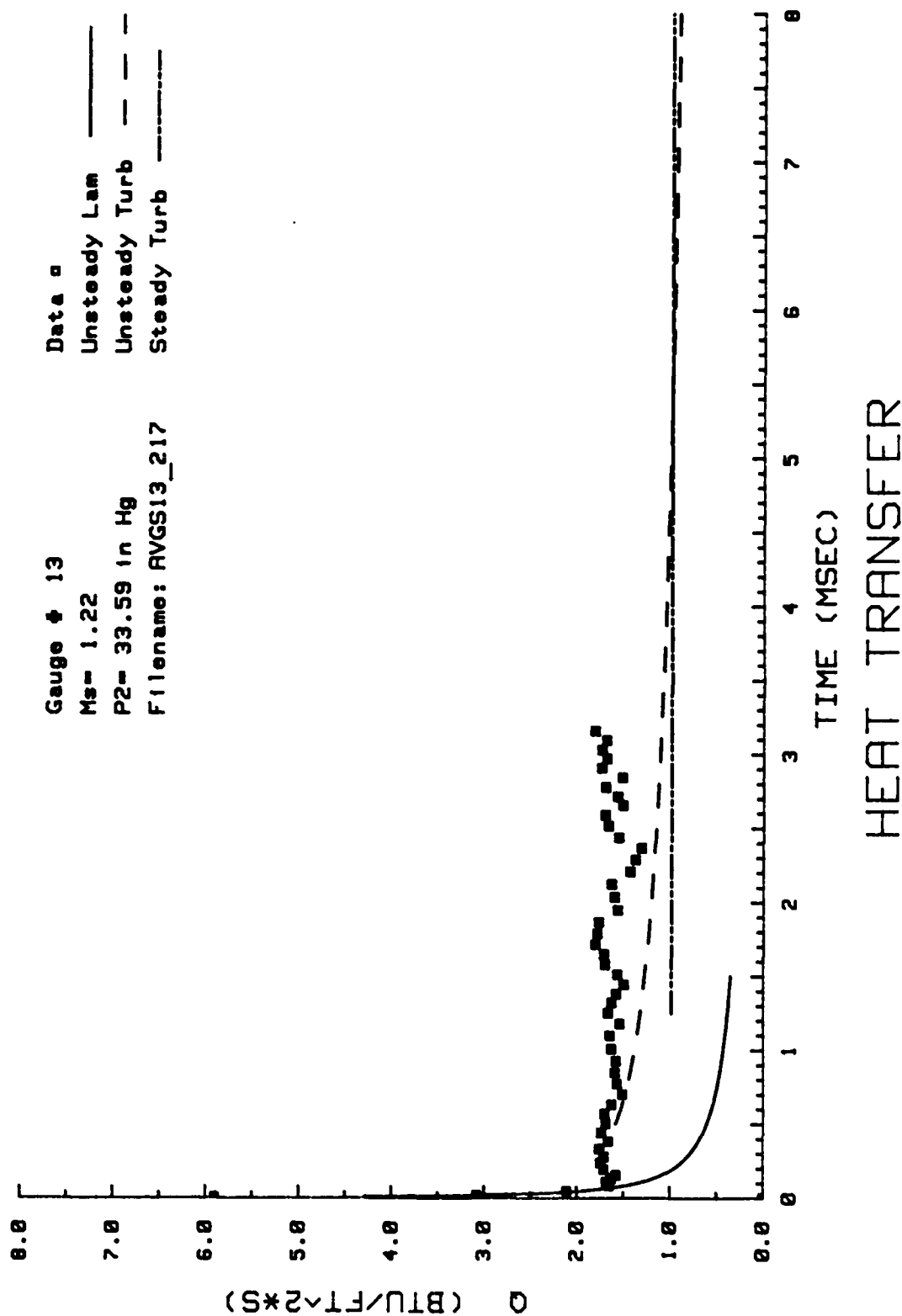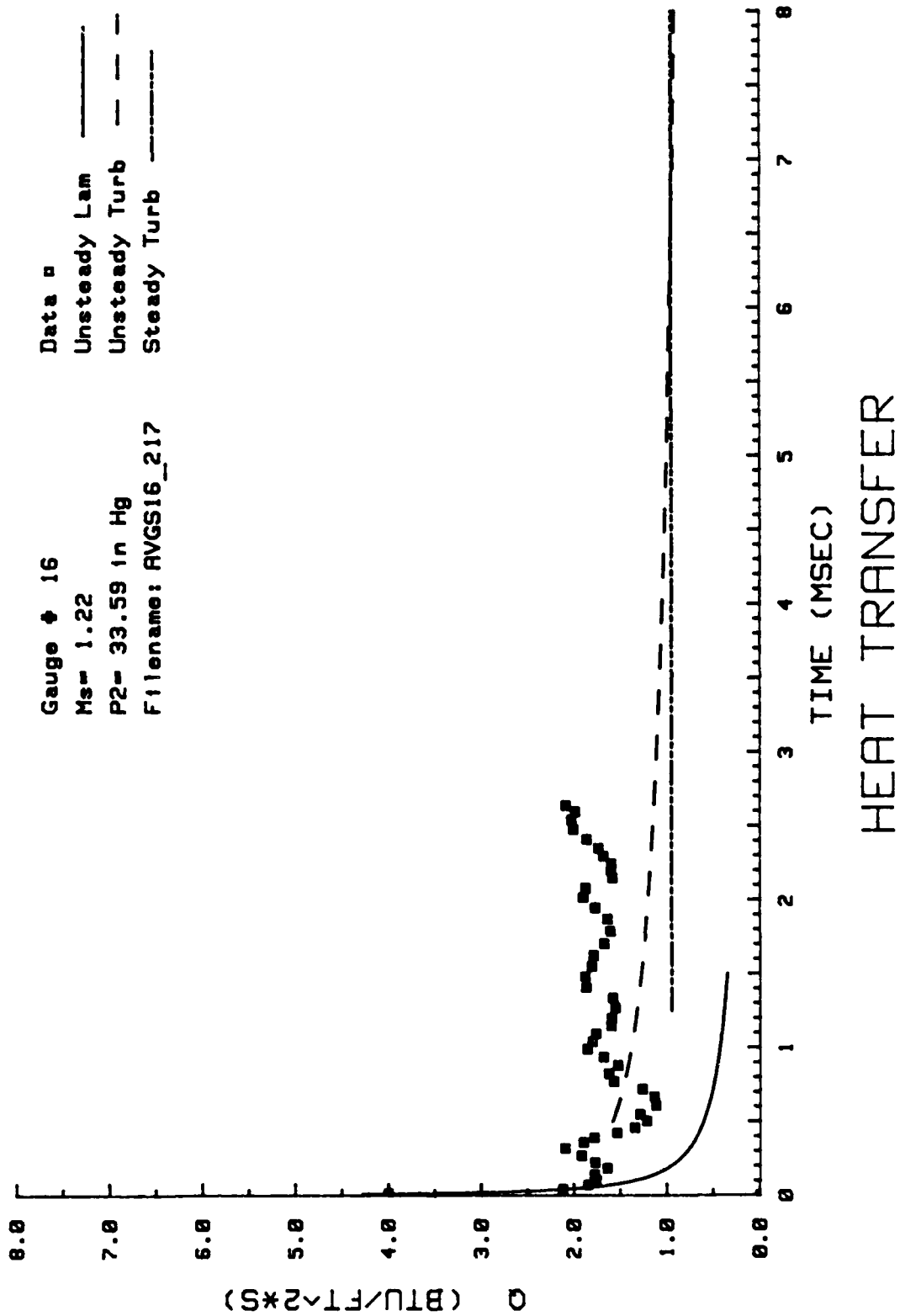Figure 121. Heat Transfer: Data Set P Gage #1

Figure 122. Heat Transfer: Data Set P Gage #2

171

Figure 123. Heat Transfer: Data Set P Gage #4

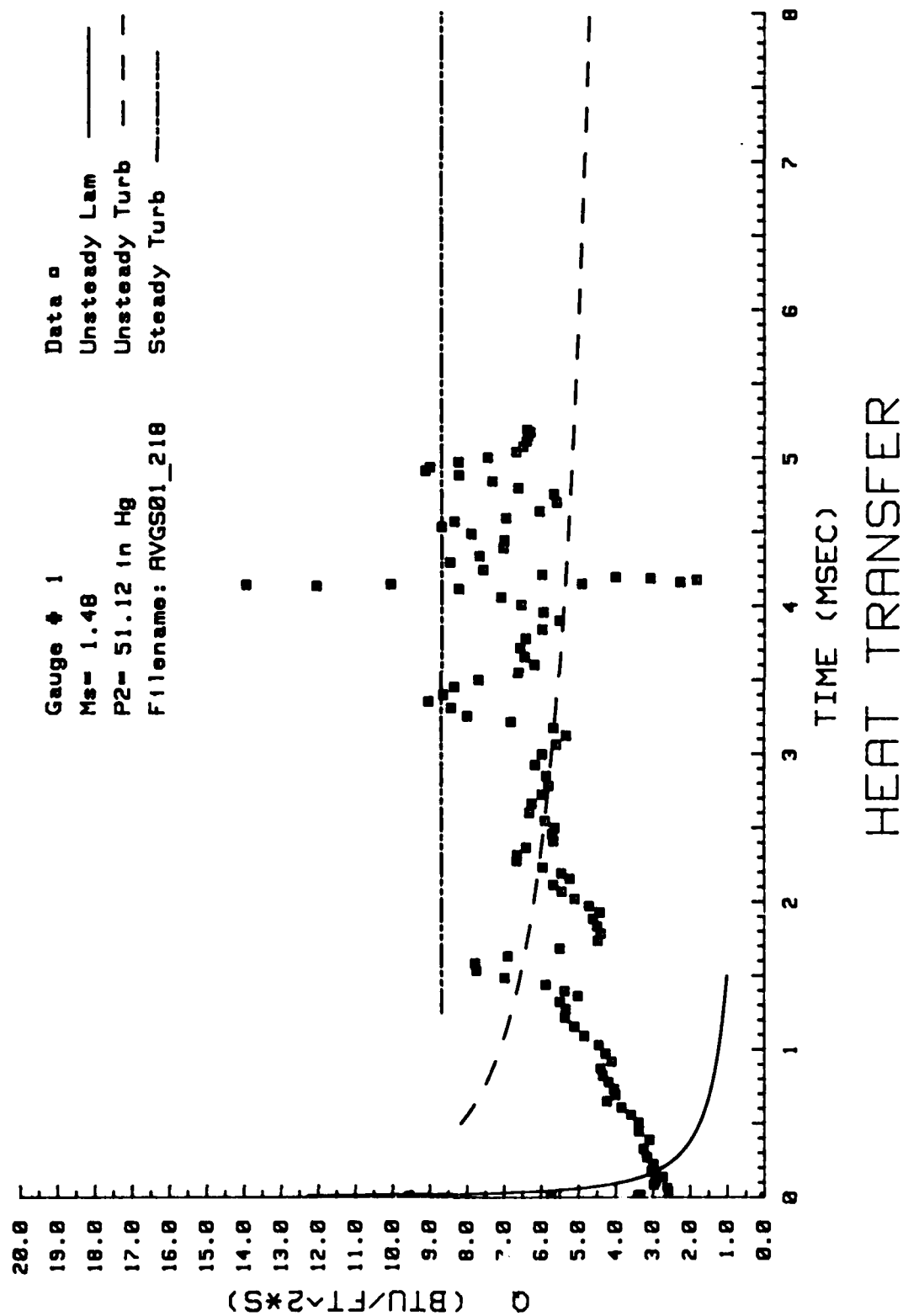Figure 124. Heat Transfer: Data Set P Gage #7

HEAT TRANSFER

TIME (MSEC)

Heat Transfer: Data Set P Gage #11

Gauge # 11
Ms= 1.27
P2= 50.42 in Hg
Filename: AVGS11_215

Data □
Unsteady Lam ——
Unsteady Turb — — —
Steady Turb ·······

MICROCOPY RESOLUTION TEST CHART

Figure 126. Heat Transfer: Data Set P Gage #13

175

Figure 127.   Heat Transfer: Data Set P Gage #16

Figure 128.   Heat Transfer: Data Set Q Thermocouple

177

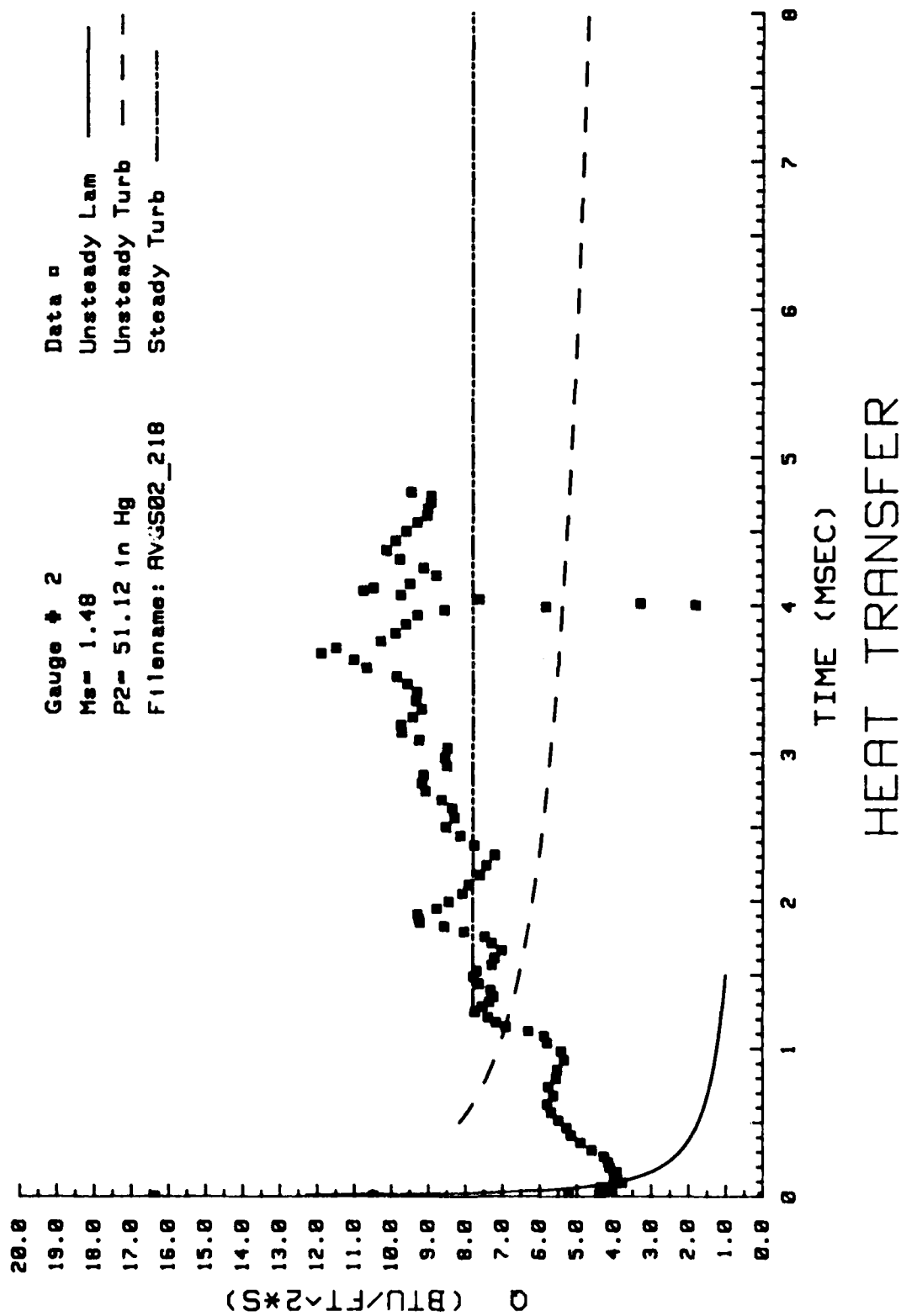Figure 129. Heat Transfer: Data Set Q Gage #1

178

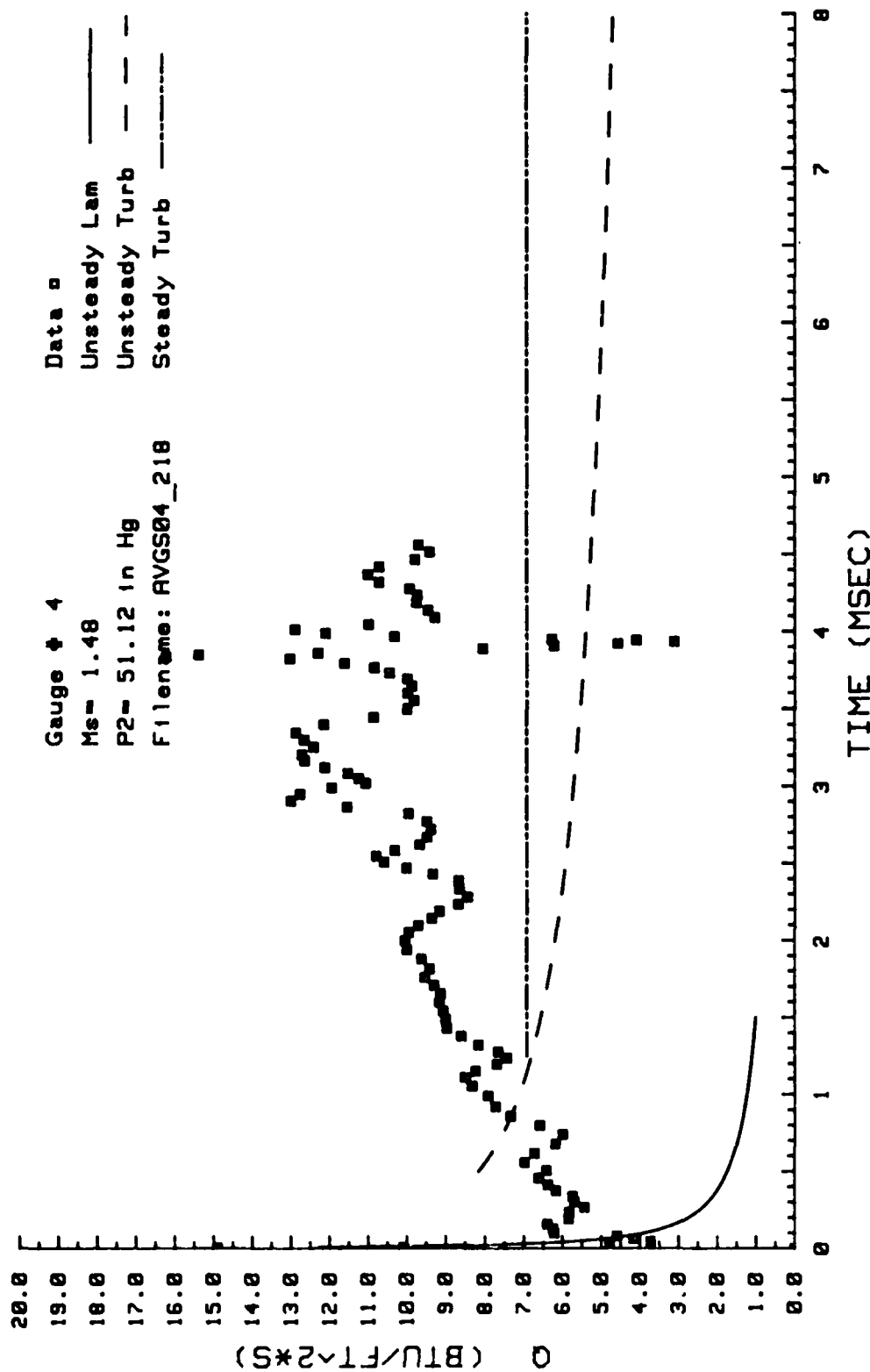Figure 130. Heat Transfer: Data Set Q Gage #2

179
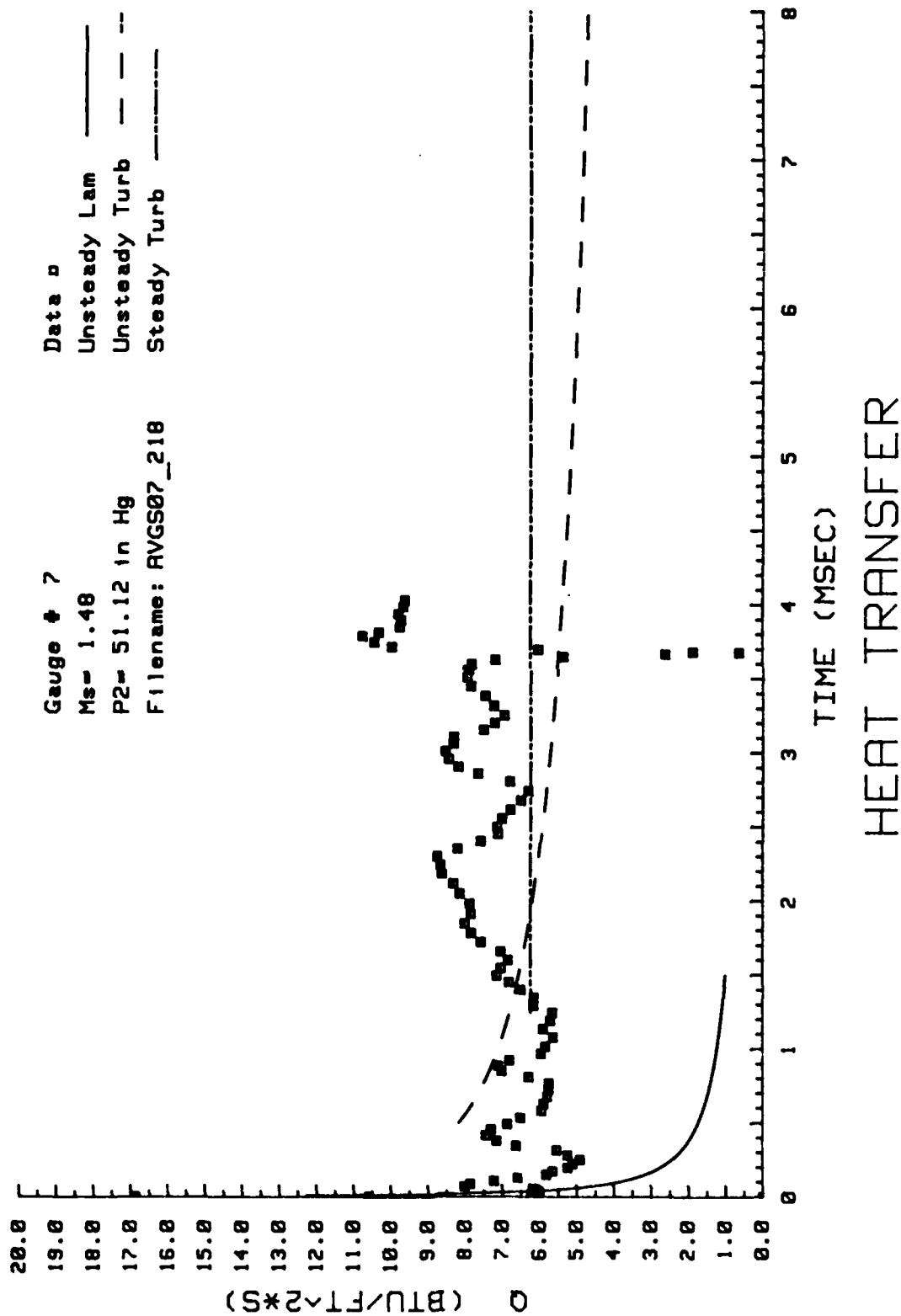
Figure 131. Heat Transfer: Data Set Q Gage #4

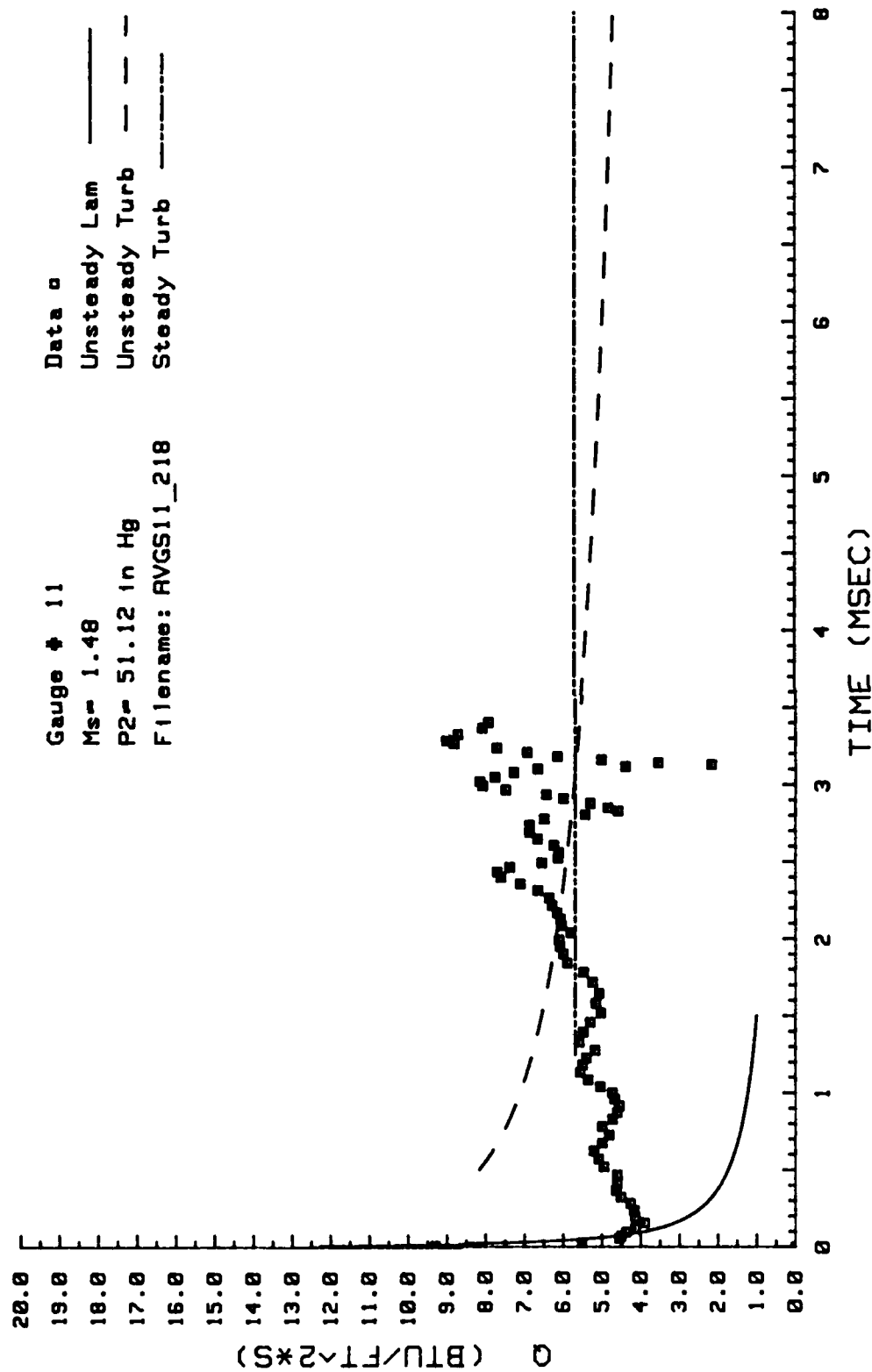Figure 132. Heat Transfer: Data Set Q Gage #7

181

Figure 133.   Heat Transfer: Data Set Q Gage #11

Figure 134. Heat Transfer: Data Set Q Gage #13

183

Figure 135. Heat Transfer: Data Set Q Gage #16
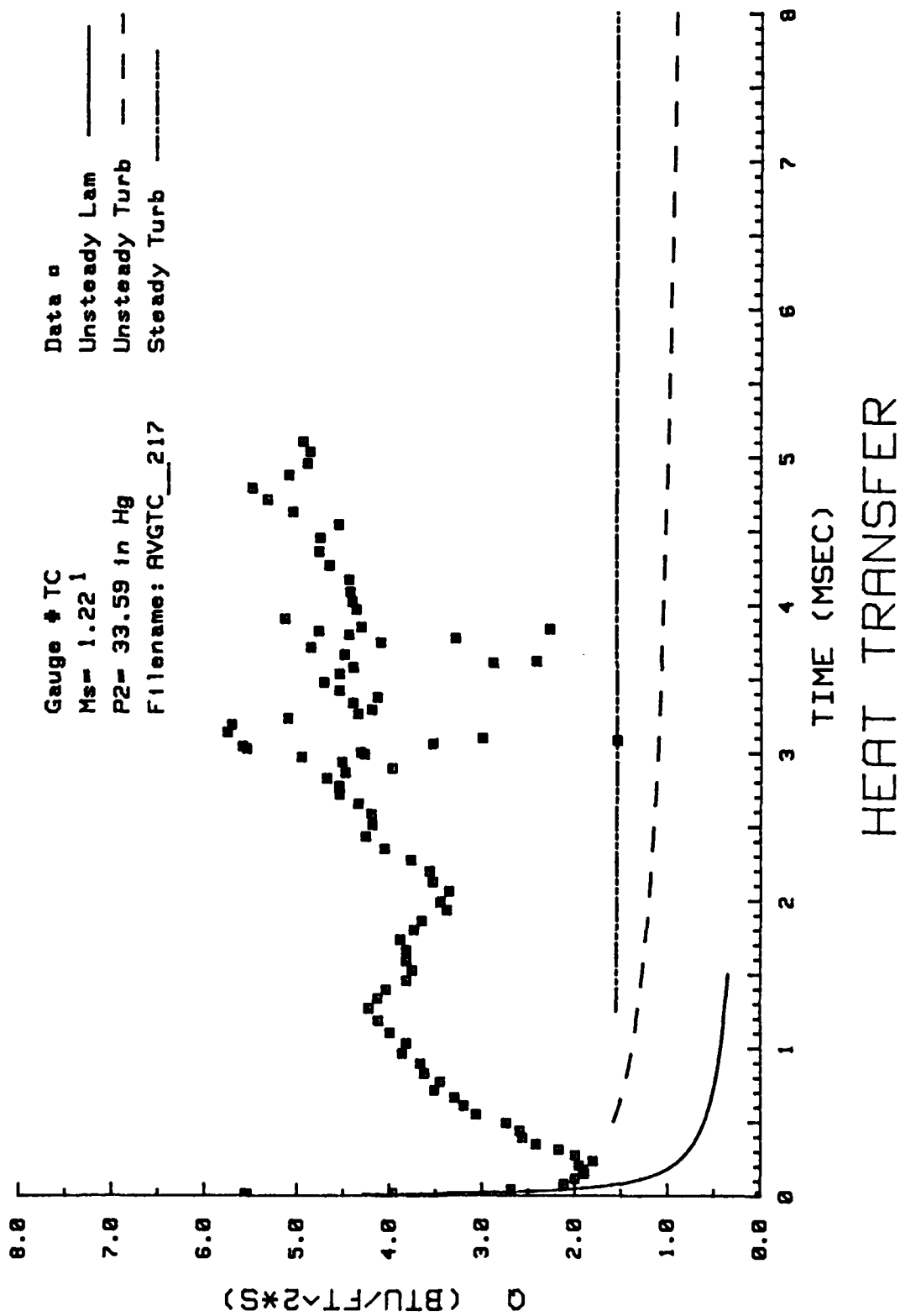
Figure 136. Heat Transfer: Data Set R Thermocouple
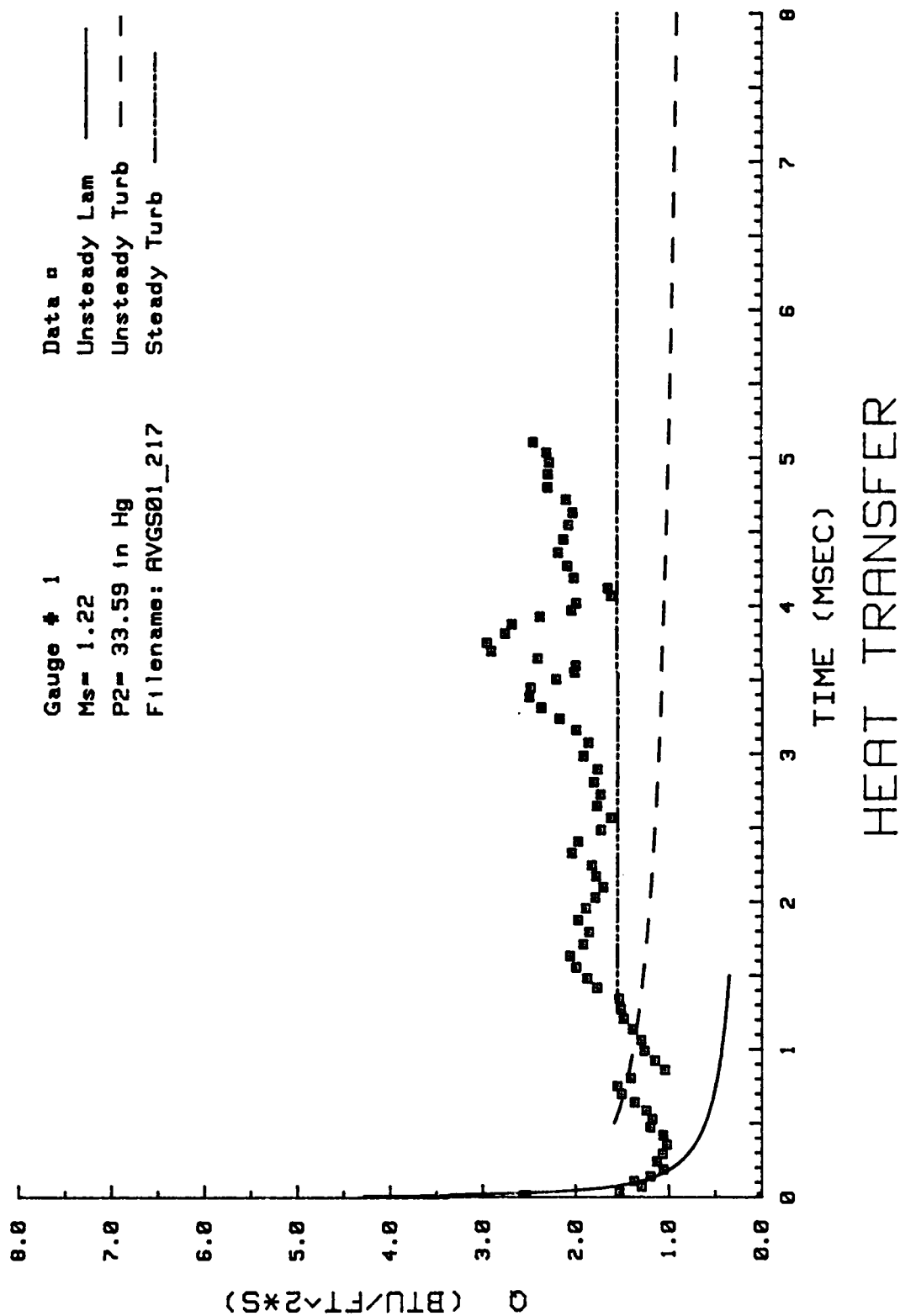
Figure 137. Heat Transfer: Data Set R Gage #1
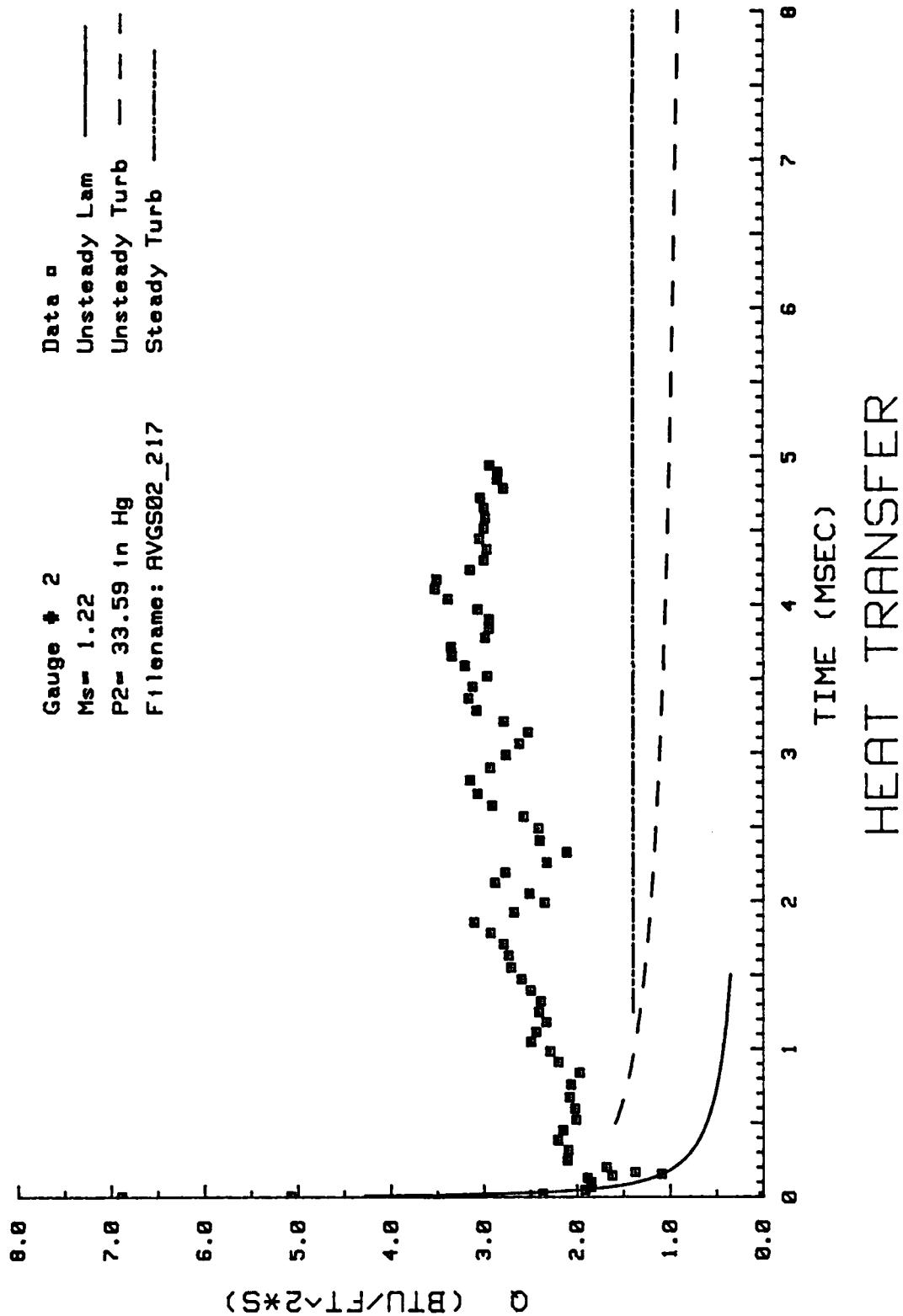
Figure 138. Heat Transfer: Data Set R Gage #2

Figure 139. Heat Transfer: Data Set R Gage #4

188

Figure 140. Heat Transfer: Data Set R Gage #7

189

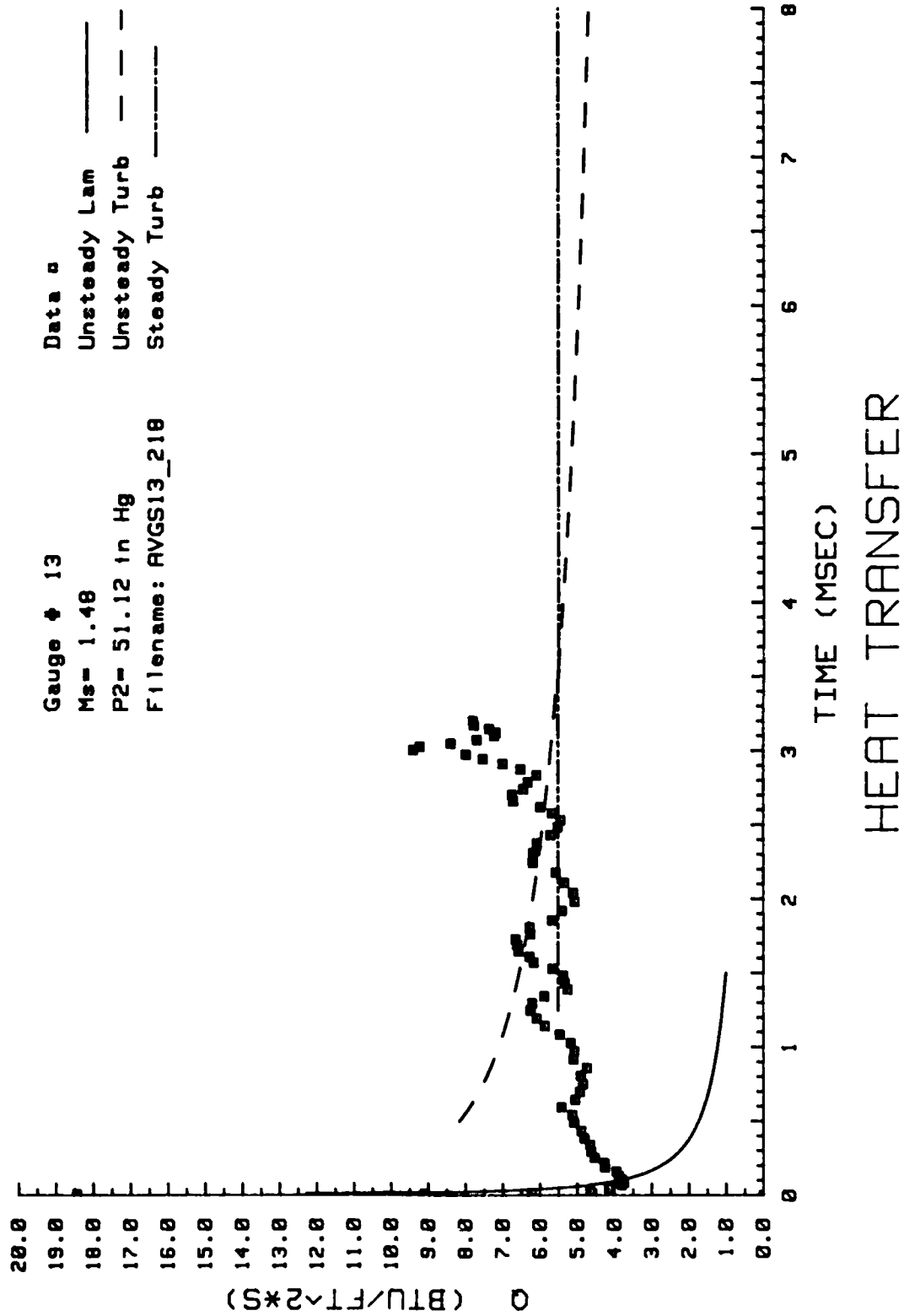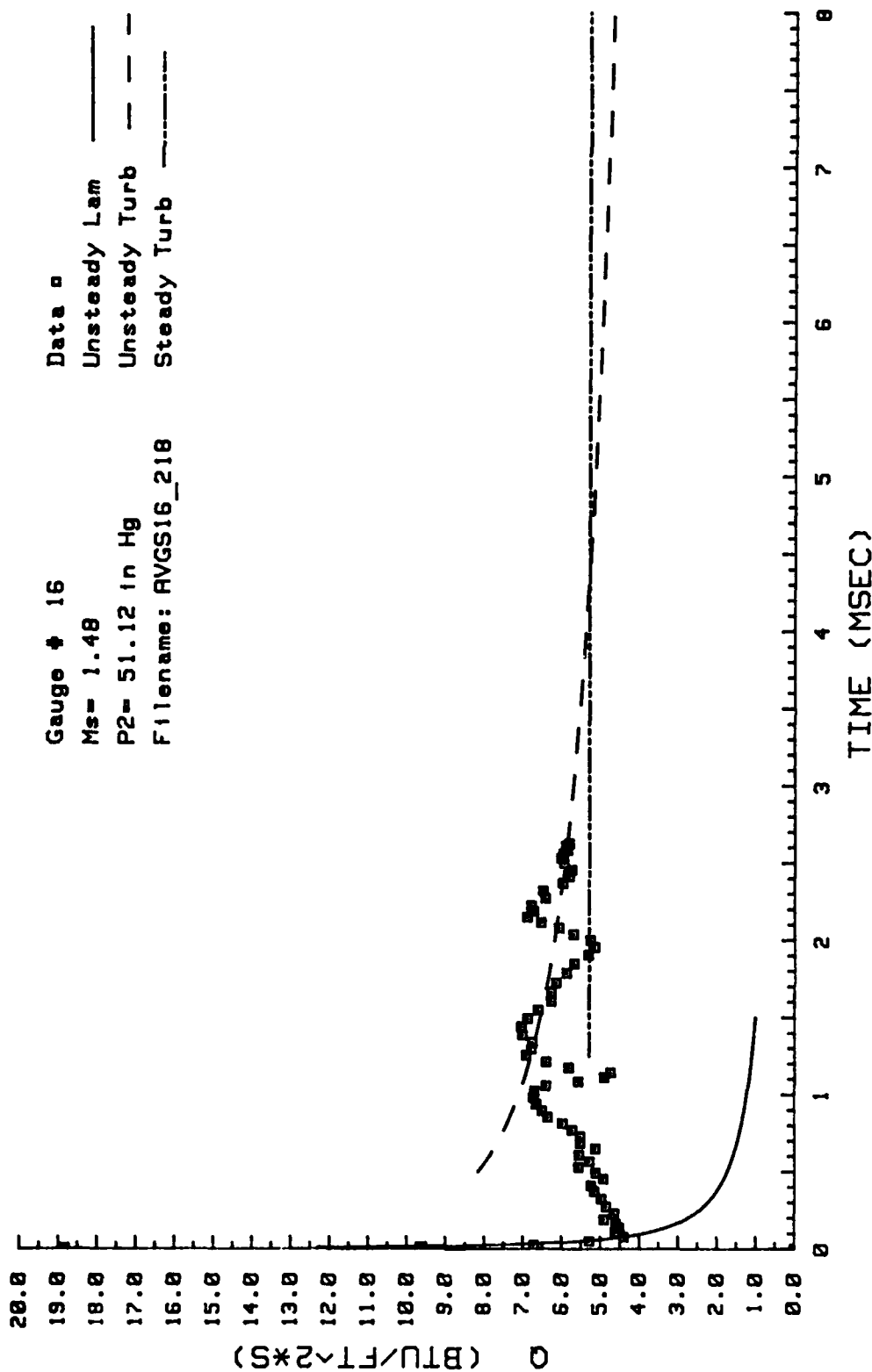Figure 141. Heat Transfer: Data Set R Gage #11

Figure 142. Heat Transfer: Data Set R Gage #13

Figure 143. Heat Transfer: Data Set R Gage #16

Figure 144.   Heat Transfer: Data Set S Gage #1
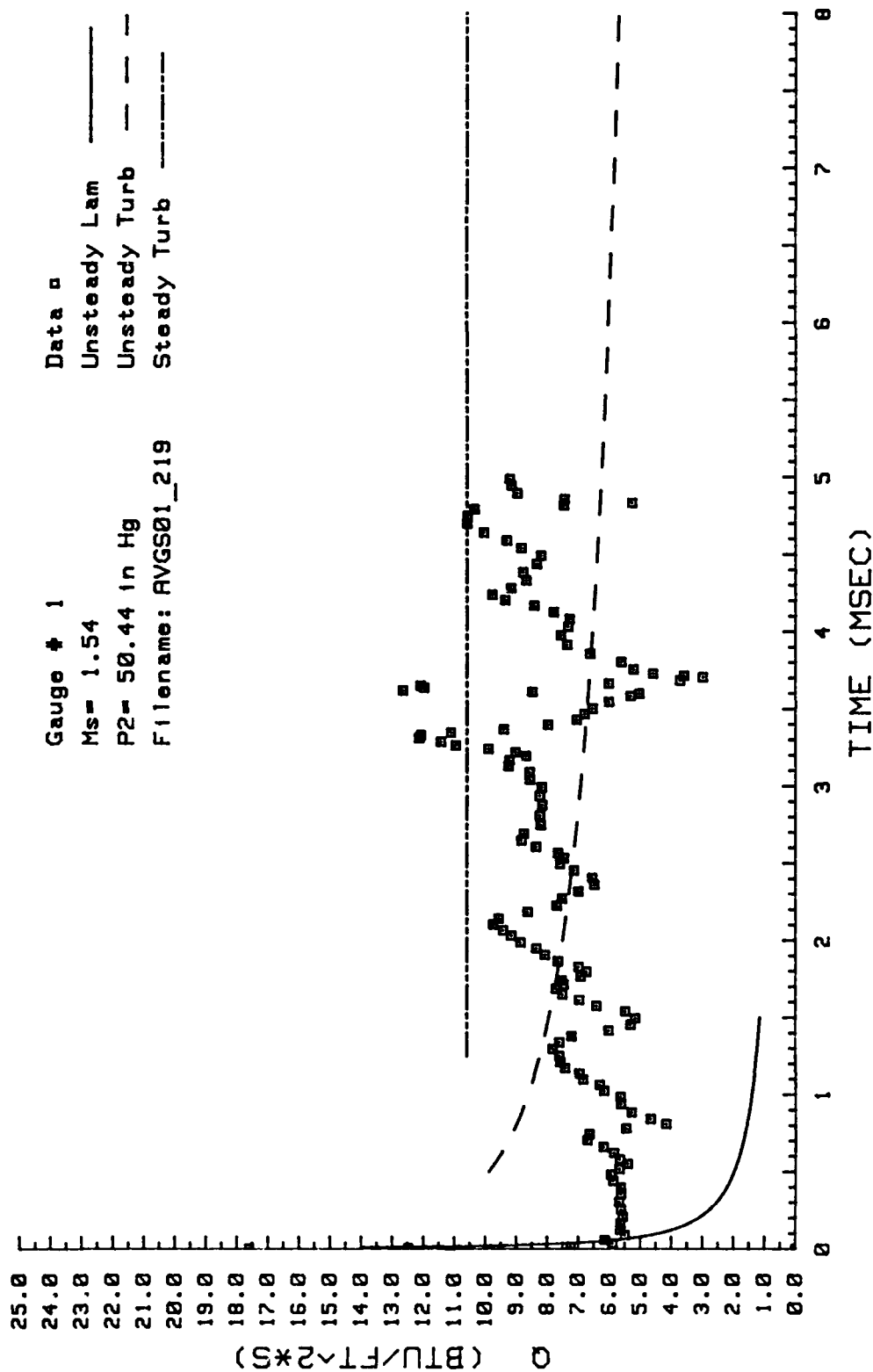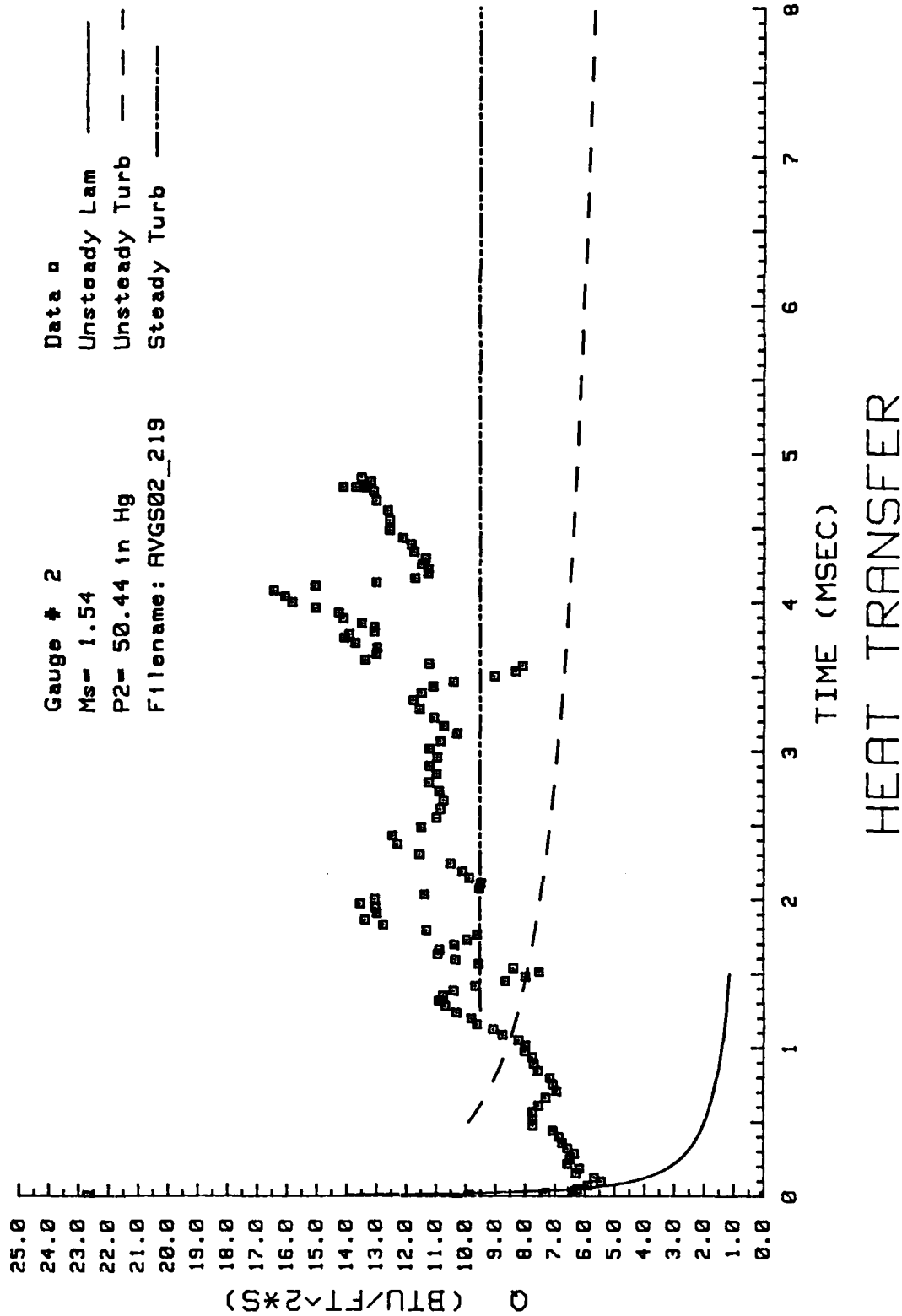
HEAT TRANSFER

Figure 145. Heat Transfer: Data Set S Gage #2

194

Figure 146. Heat Transfer: Data Set S Gage #4

Figure 147. Heat Transfer: Data Set S Gage #7

196

HEAT TRANSFER

Gauge # 11
Ms= 1.48
P2= 51.12 in Hg
Filename: AVGS11_218

Data □
Unsteady Lam
Unsteady Turb
Steady Turb

Q (BTU/FT^2*S)

20.0
19.0
18.0
17.0
16.0
15.0
14.0
13.0
12.0
11.0
10.0
9.0
8.0
7.0
6.0
5.0
4.0
3.0
2.0
1.0
0.0

0   1   2   3   4   5   6   7   8

TIME (MSEC)

Figure 148.   Heat Transfer: Data Set S Gage #11

197

Figure 149. Heat Transfer: Data Set S Gage #13

Figure 150. Heat Transfer: Data Set S Gage #16

199

Figure 151. Heat Transfer: Data Set T Gage #1

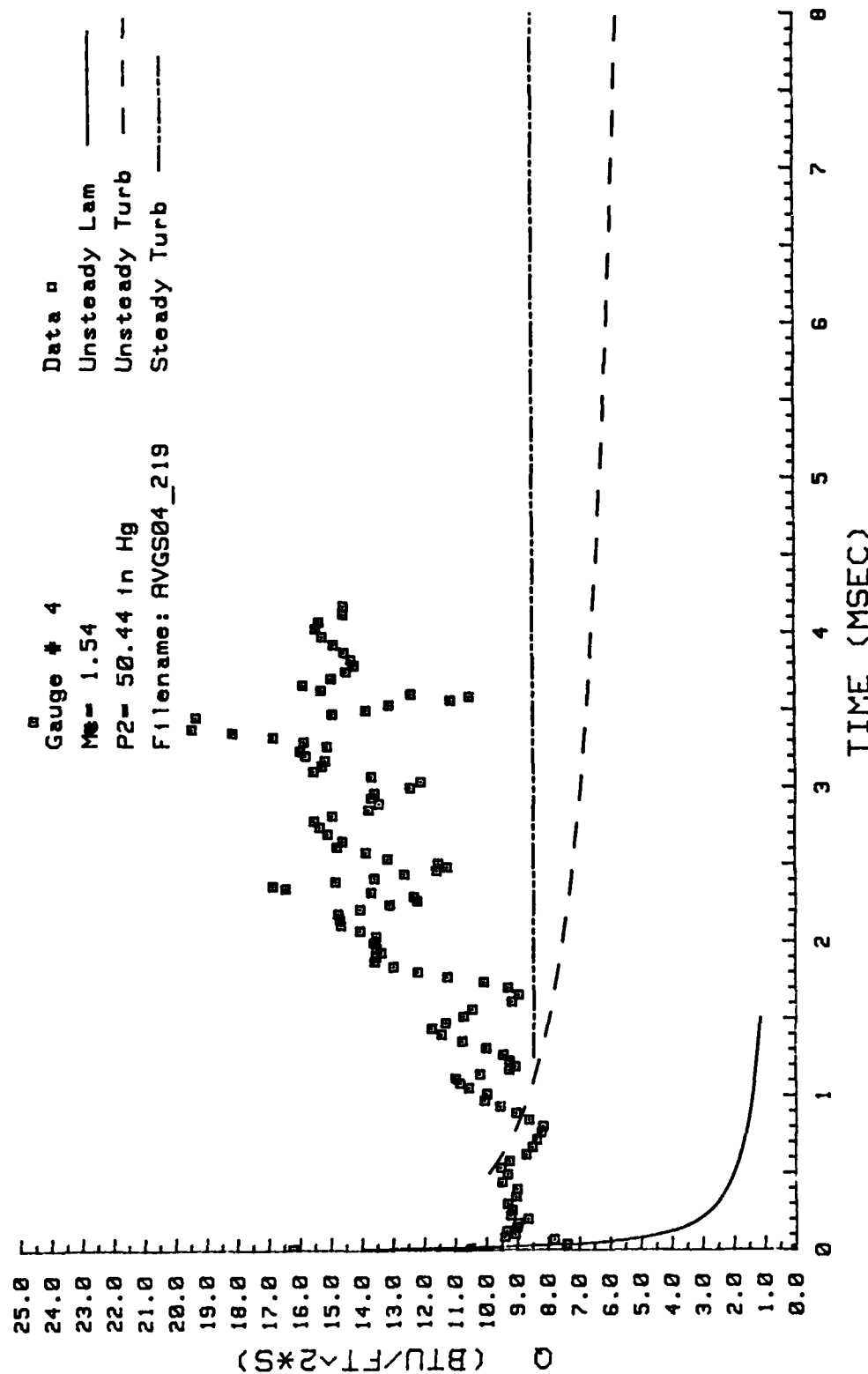Figure 152. Heat Transfer: Data Set T Gage #2
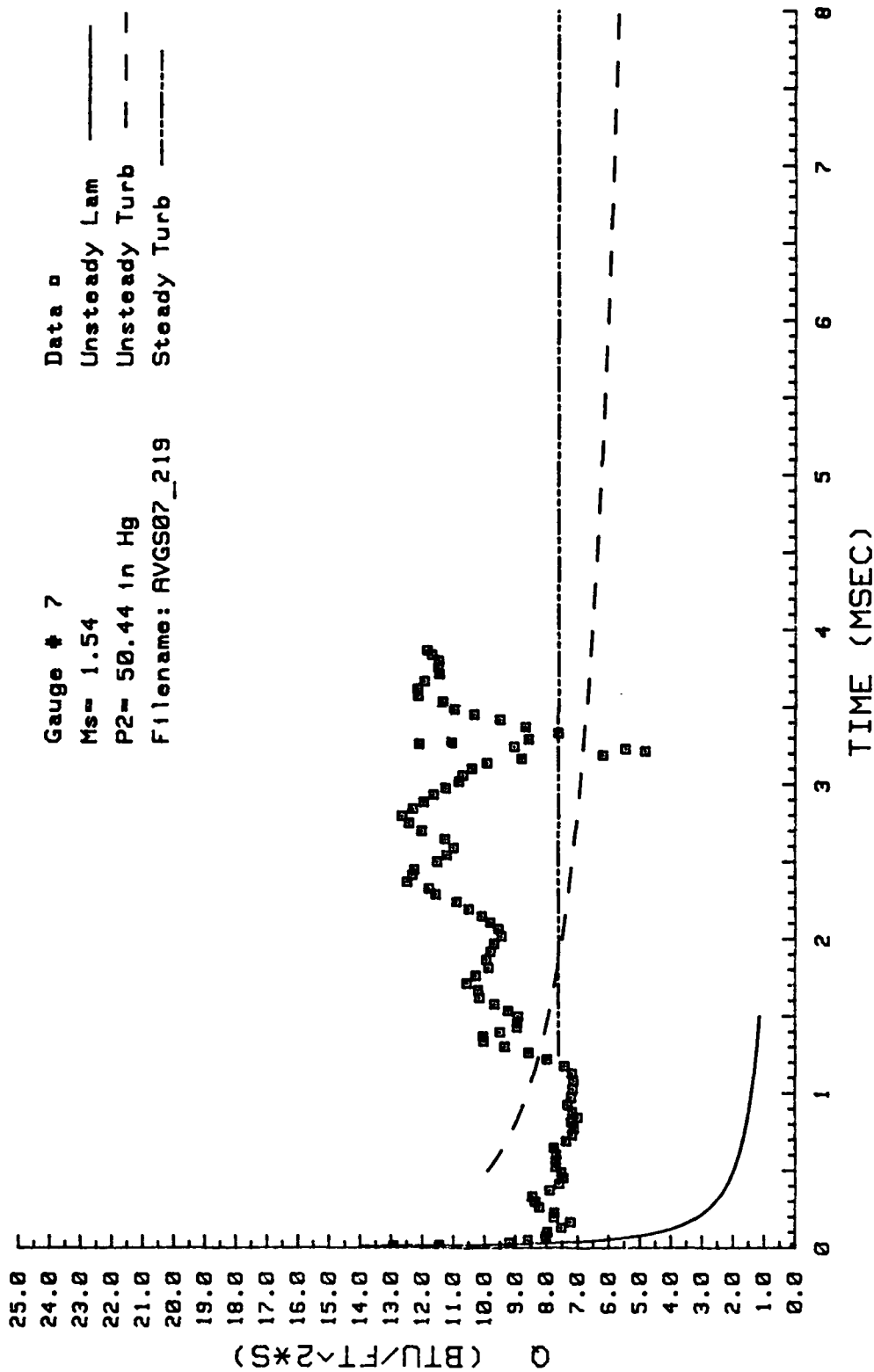
Figure 153. Heat Transfer: Data Set T Gage #4

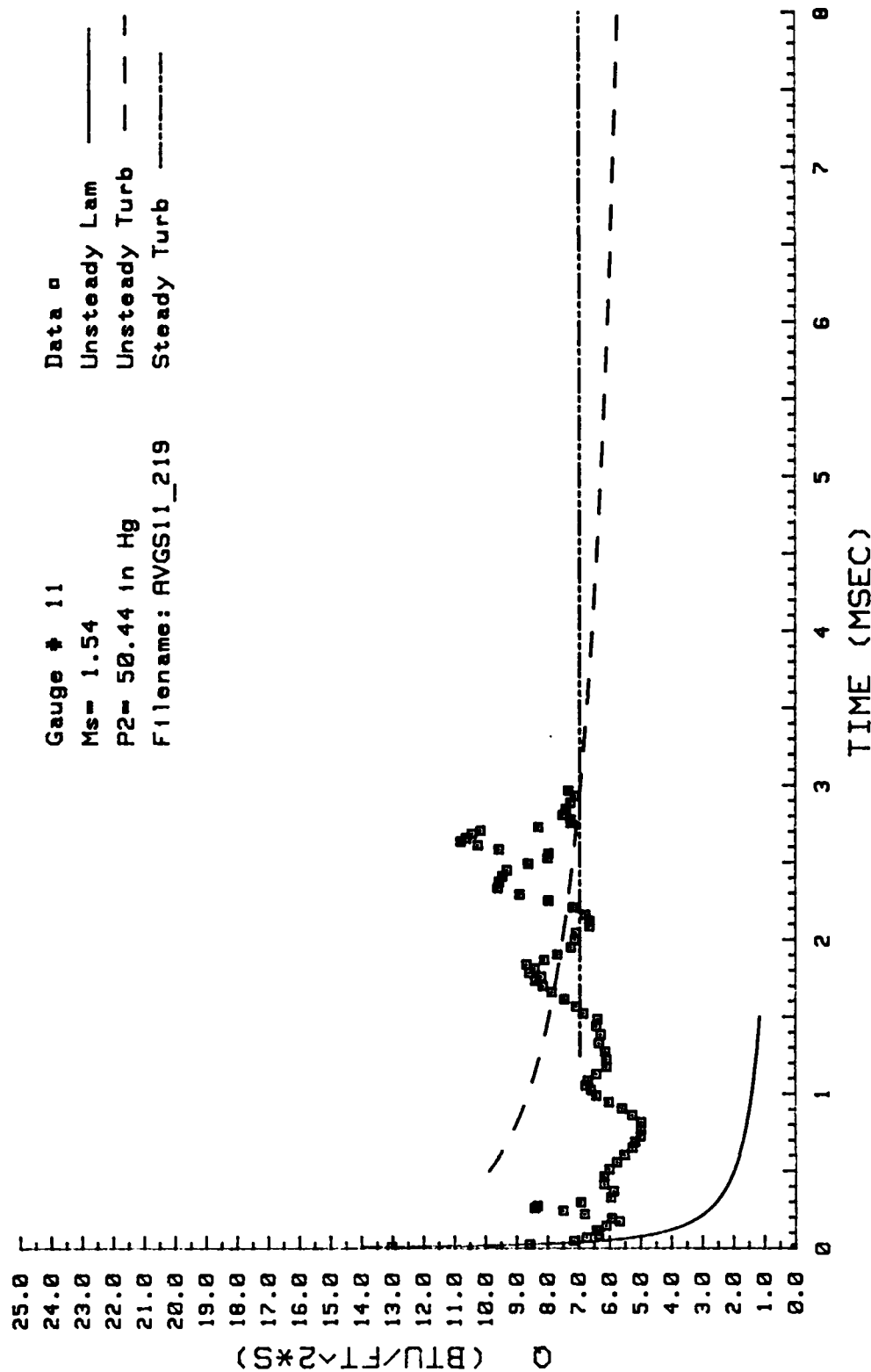Figure 154. Heat Transfer: Data Set T Gage #7
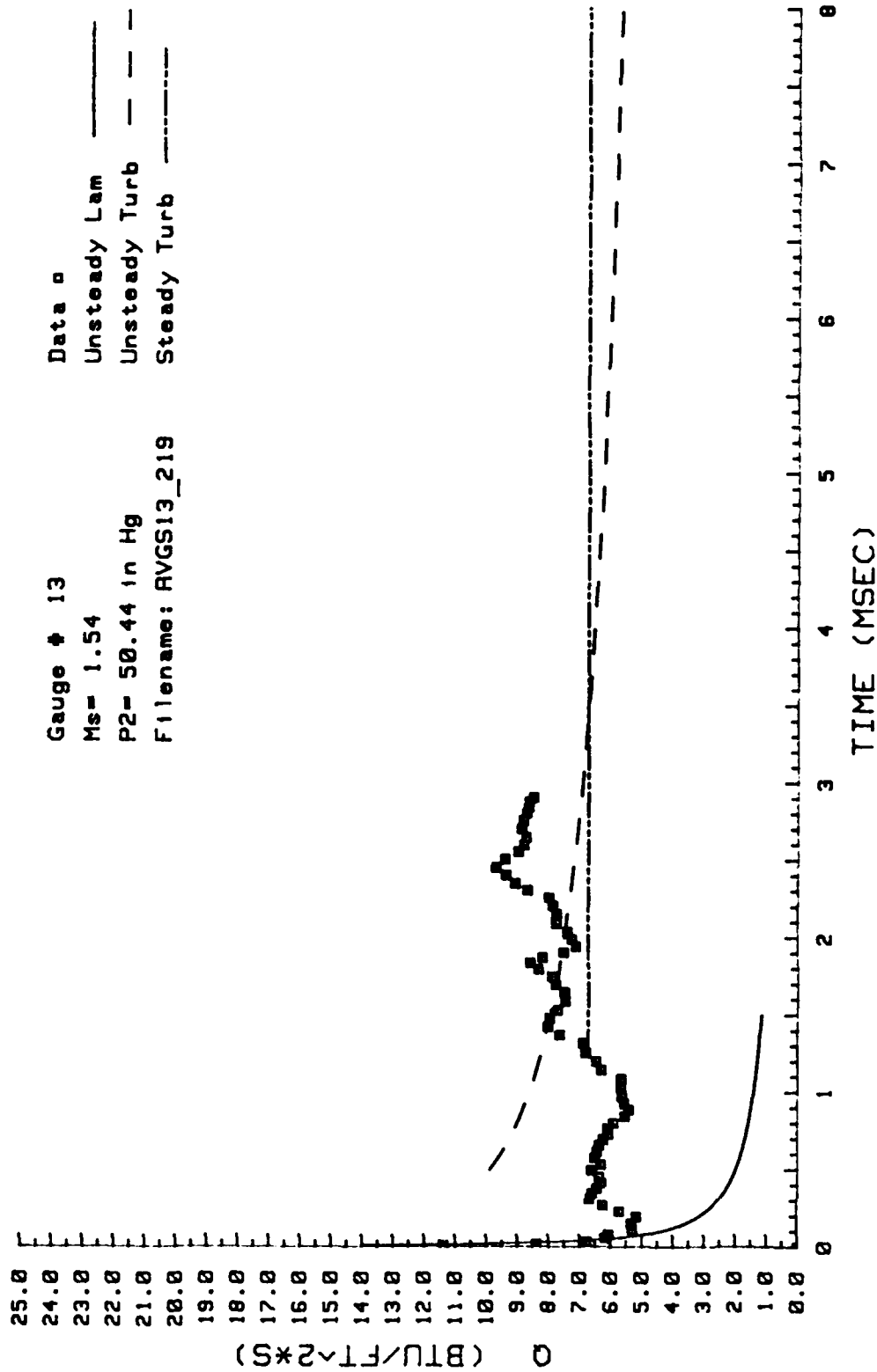
Figure 155. Heat Transfer: Data Set T Gage #11

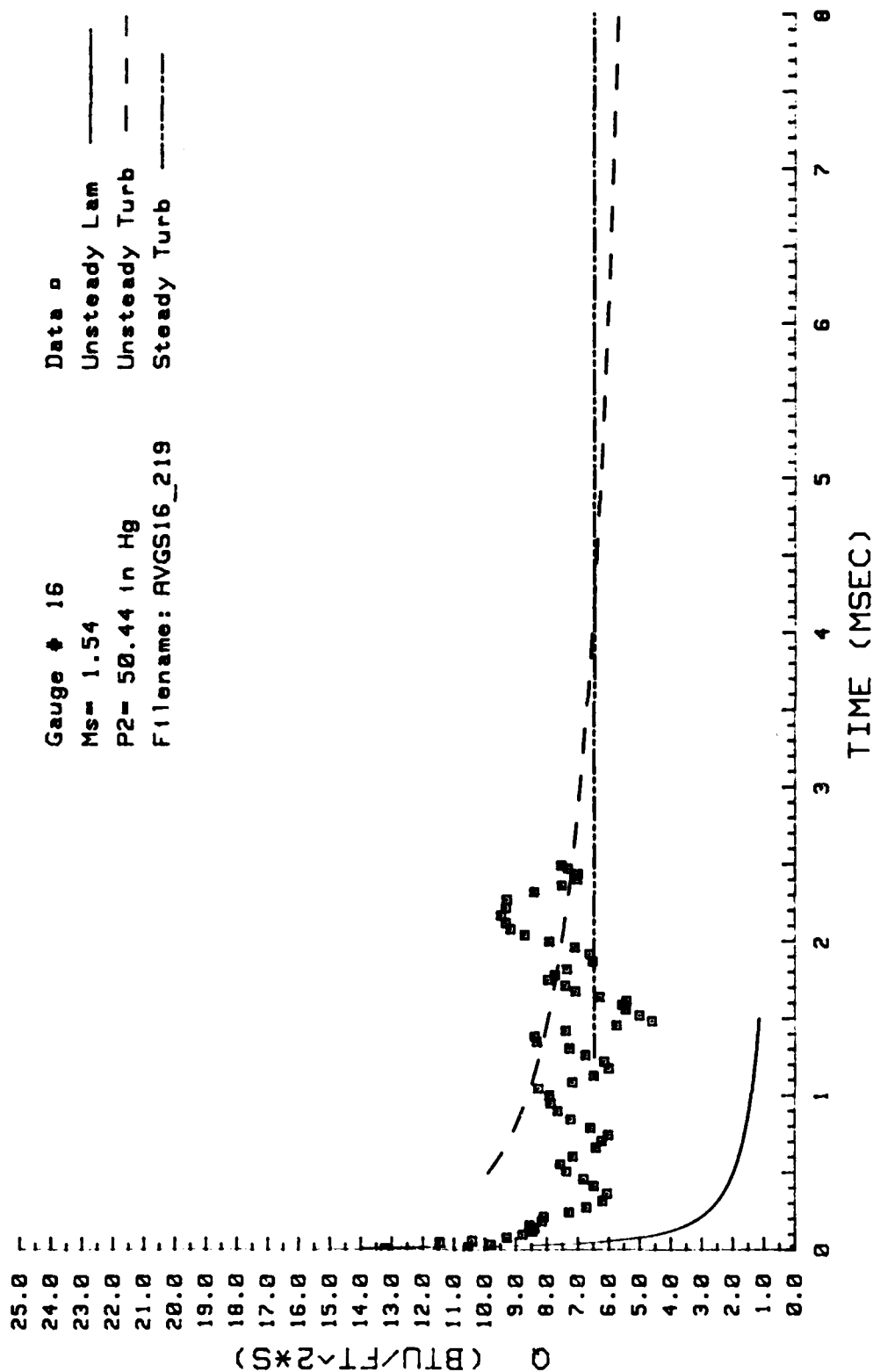Figure 156. Heat Transfer: Data Set T Gage #13

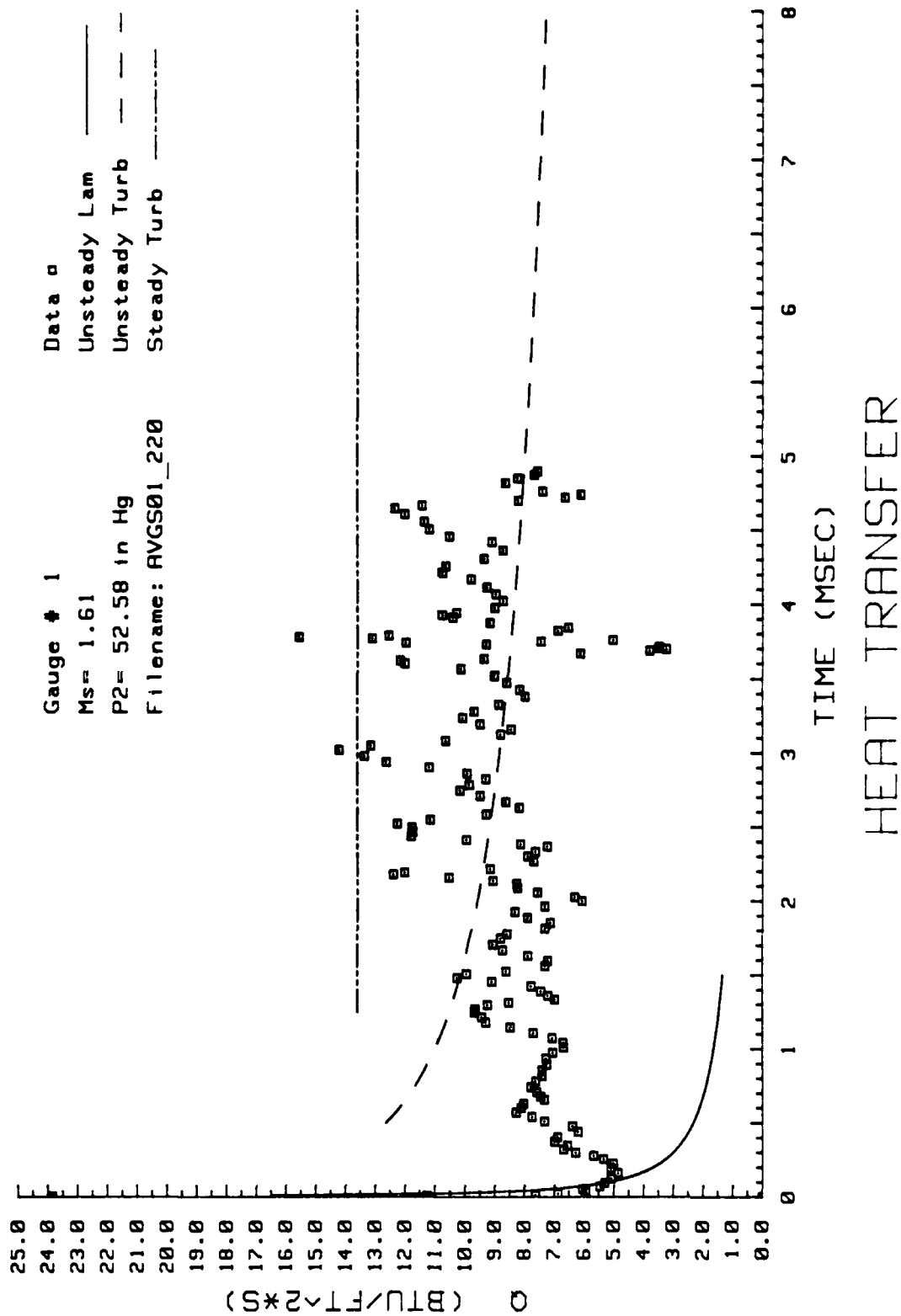Figure 157. Heat Transfer: Data Set T Gage #16

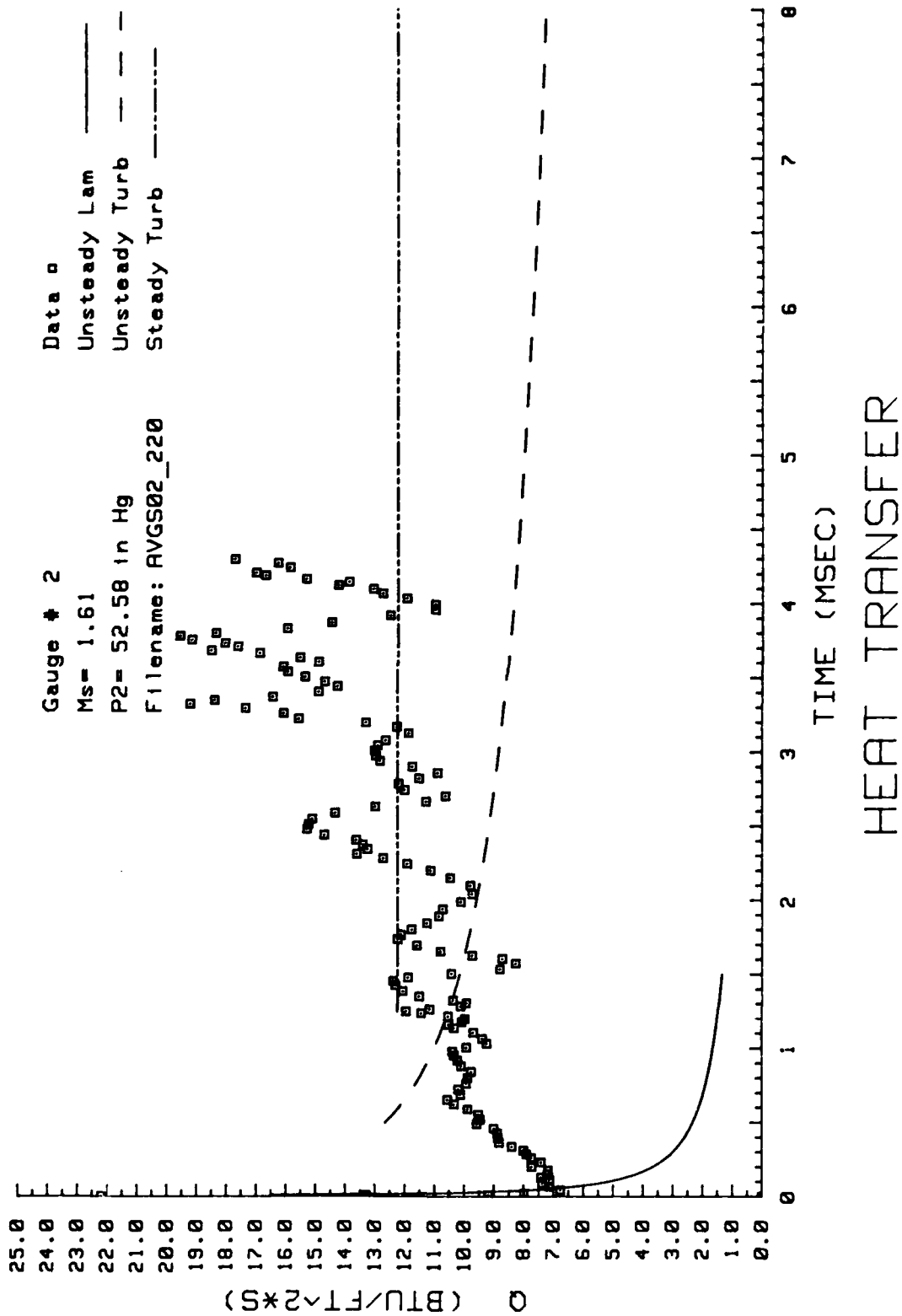Figure 158.   Heat Transfer: Data Set U Gage #1

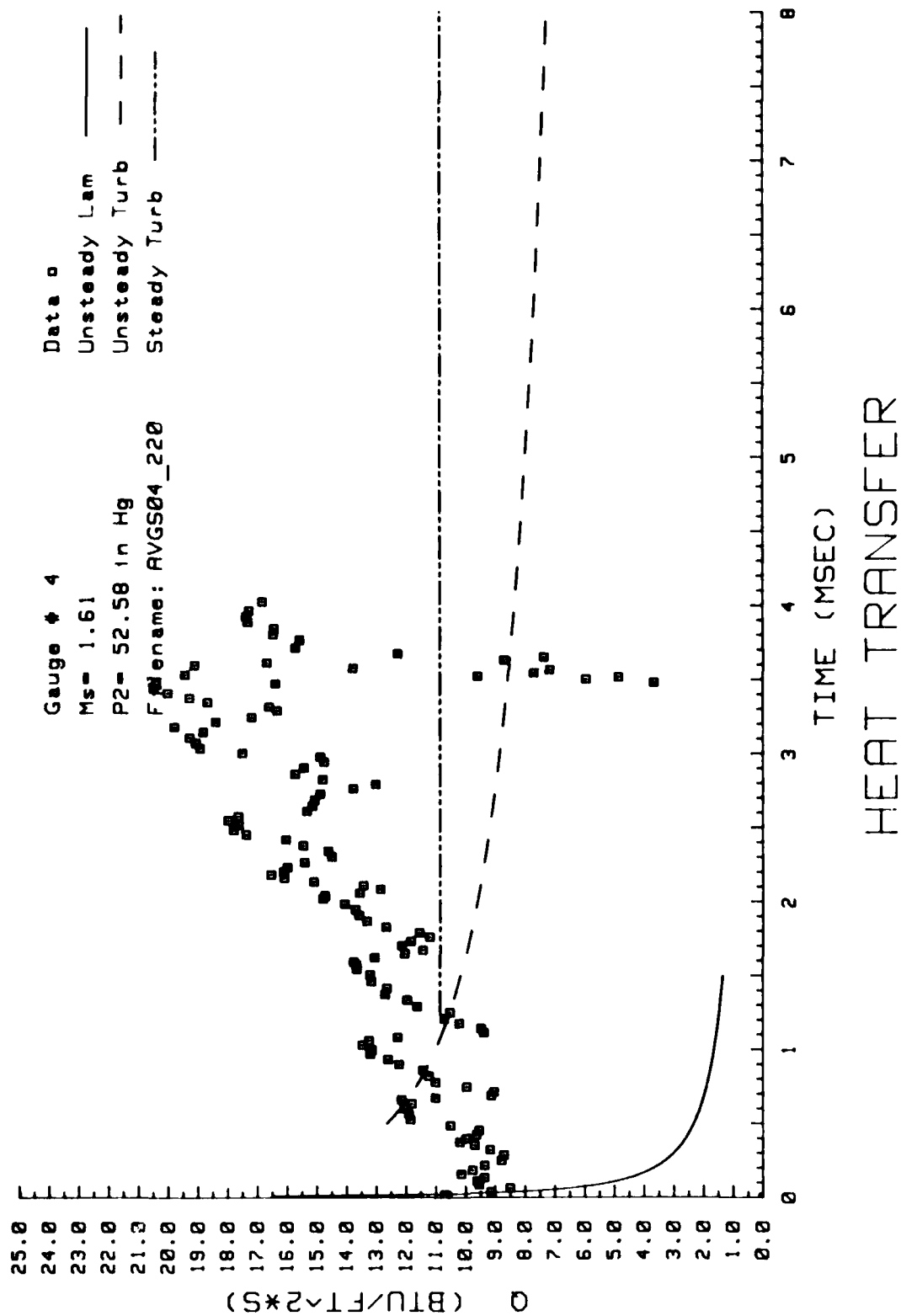Figure 159. Heat Transfer: Data Set U Gage #2
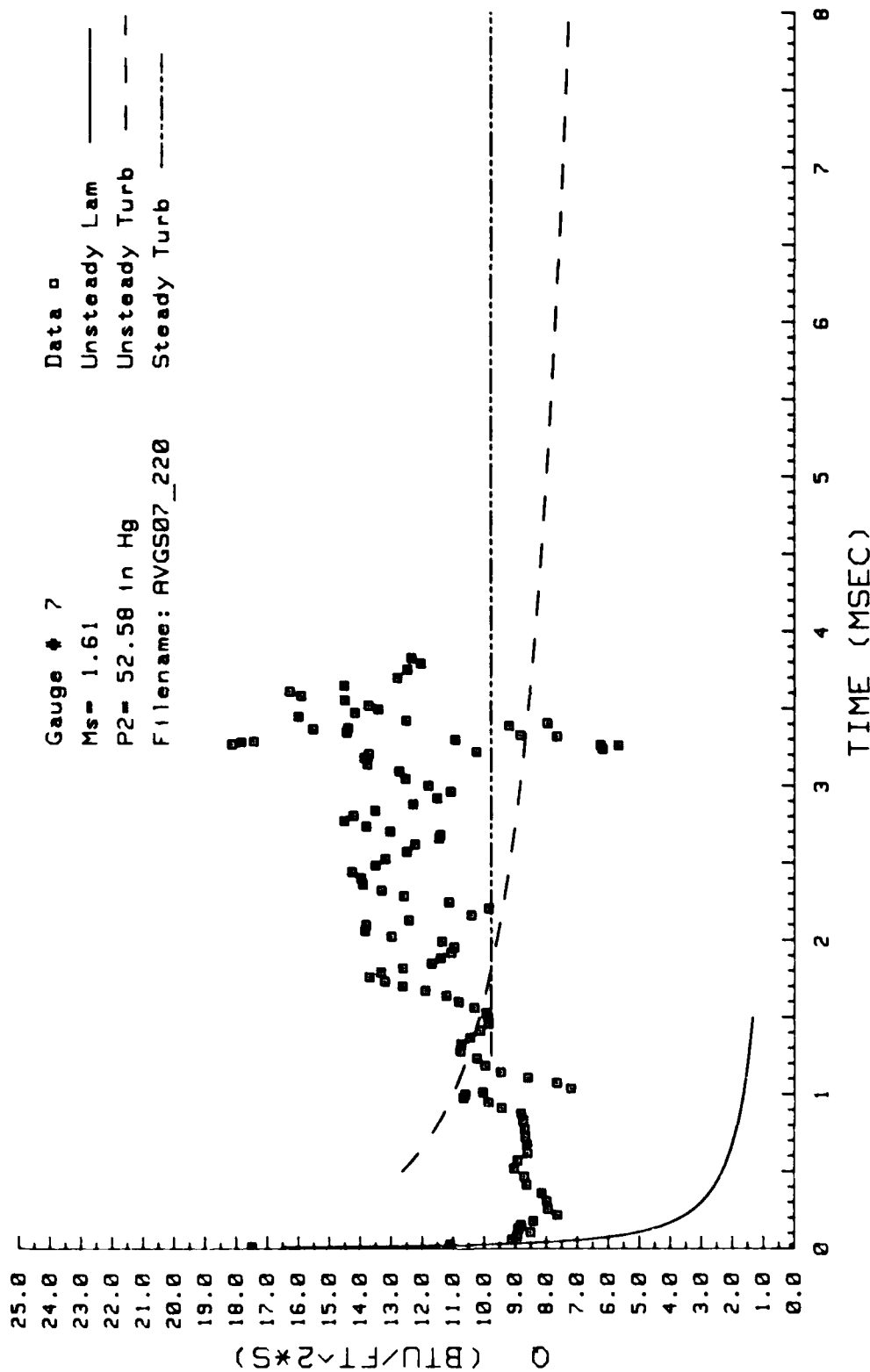
Figure 160. Heat Transfer: Data Set U Gage #4

Figure 161. Heat Transfer: Data Set U Gage #7

210

Figure 162.   Heat Transfer: Data Set U Gage #11

211

Figure 163. Heat Transfer: Data Set U Gage #13

HEAT TRANSFER

Figure 164. Heat Transfer: Data Set U Gage #16

Gauge # 16
Ms= 1.61
P2= 52.58 in Hg
Filename: AVGS16_220

Data □
Unsteady Lam ———
Unsteady Turb — —
Steady Turb ·····

TIME (MSEC)

Q (BTU/FT^2*S)

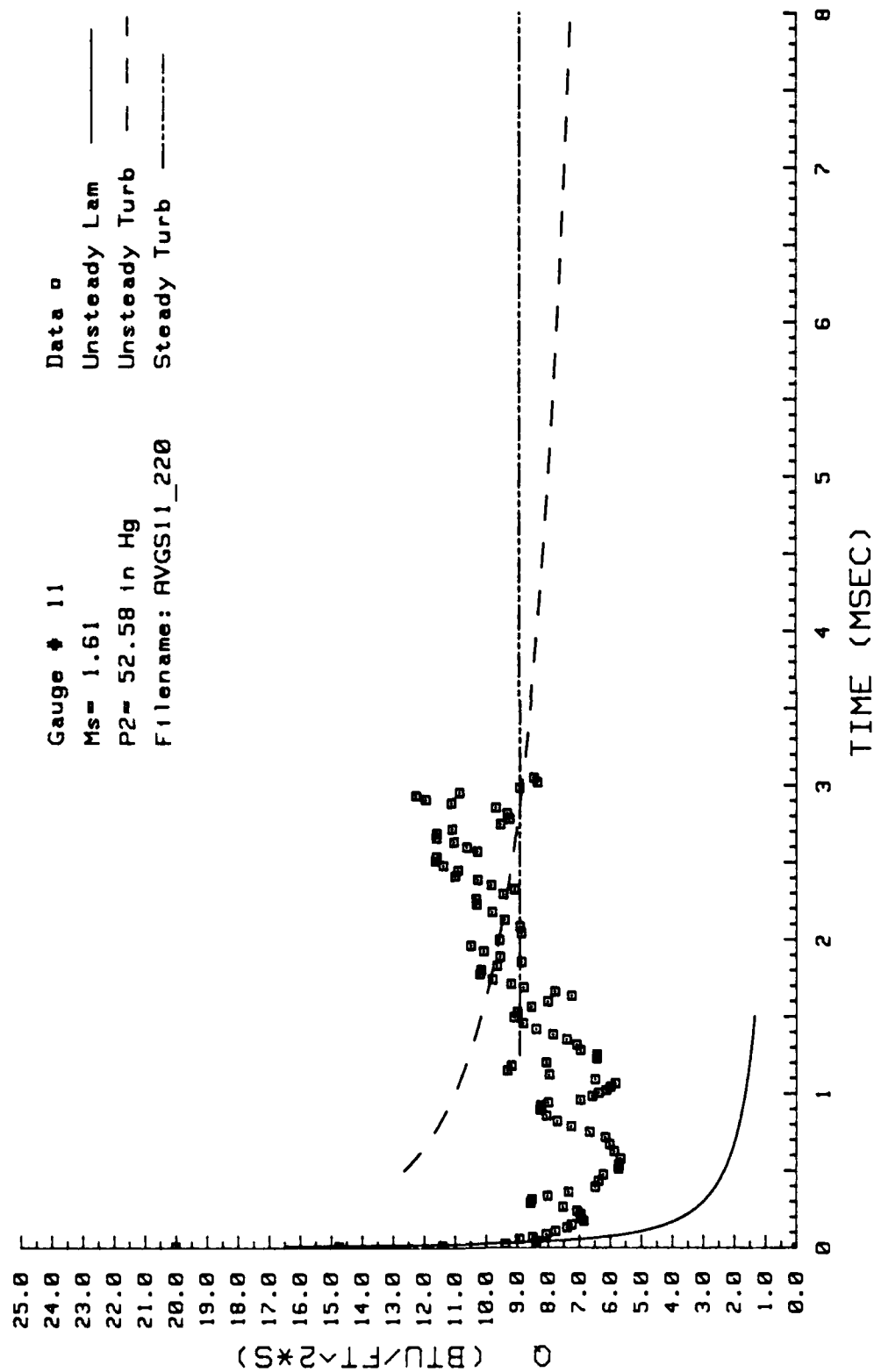Figure 165. Heat Transfer: Data Set V Gage #14

214

Figure 166. Heat Transfer: Data Set V Gage #12

215

Figure 167. Heat Transfer: Data Set V Gage #9

Figure 168. Heat Transfer: Data Set V Gage #6

217

Figure 169. Heat Transfer: Data Set V Gage #4
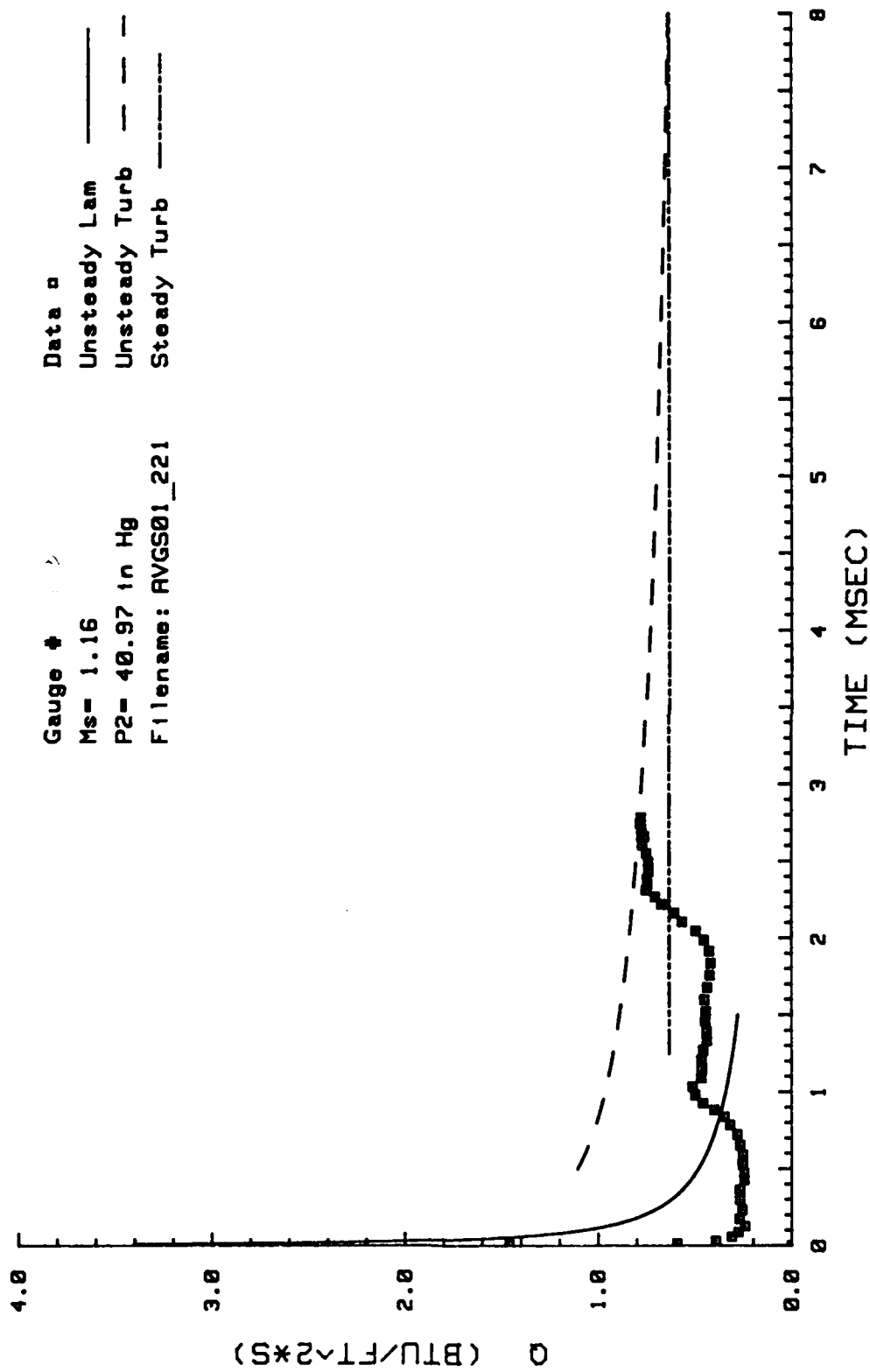
Figure 170. Heat Transfer: Data Set V Gage #1
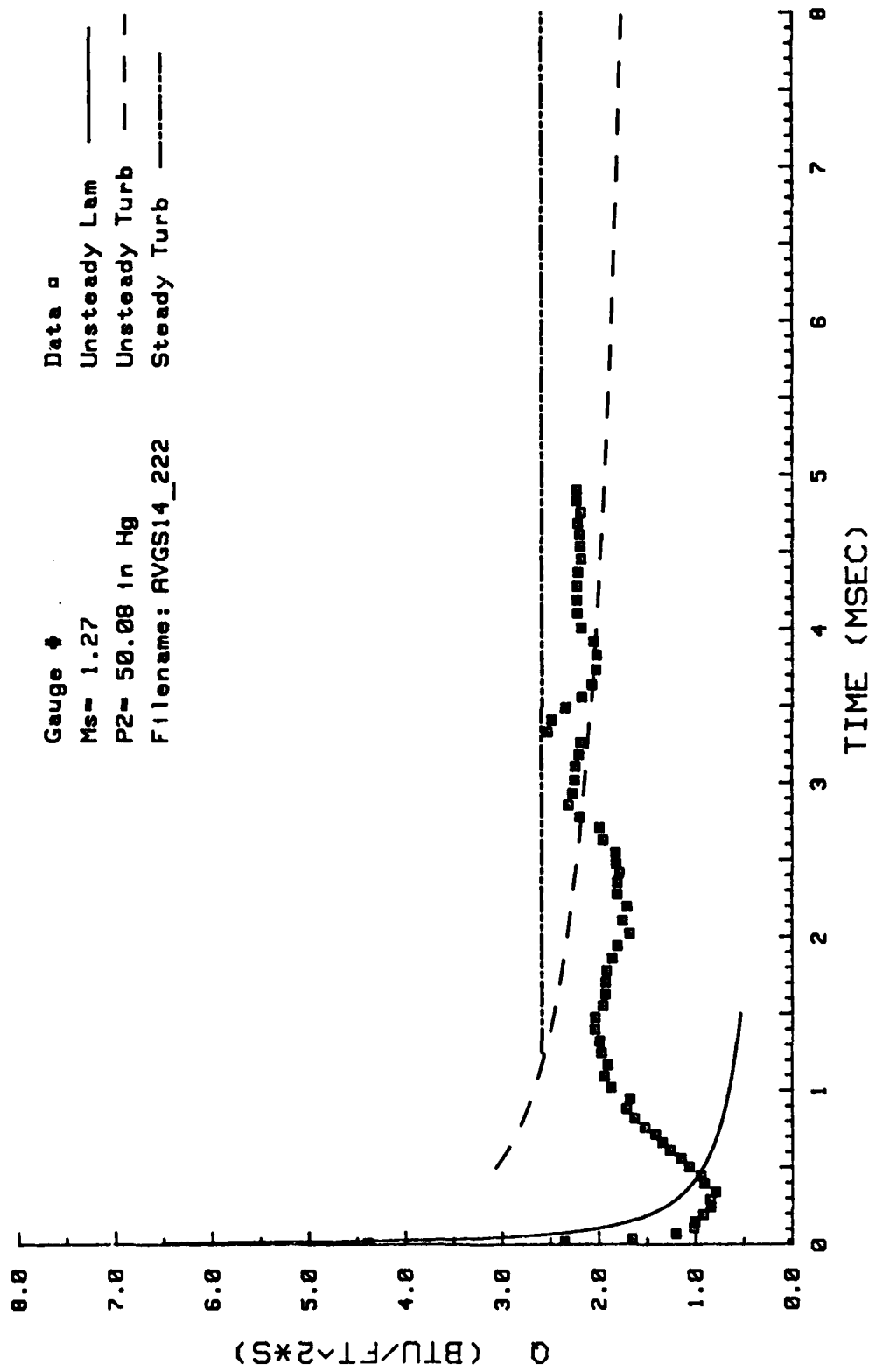
Figure 171. Heat Transfer: Data Set W Gage #14
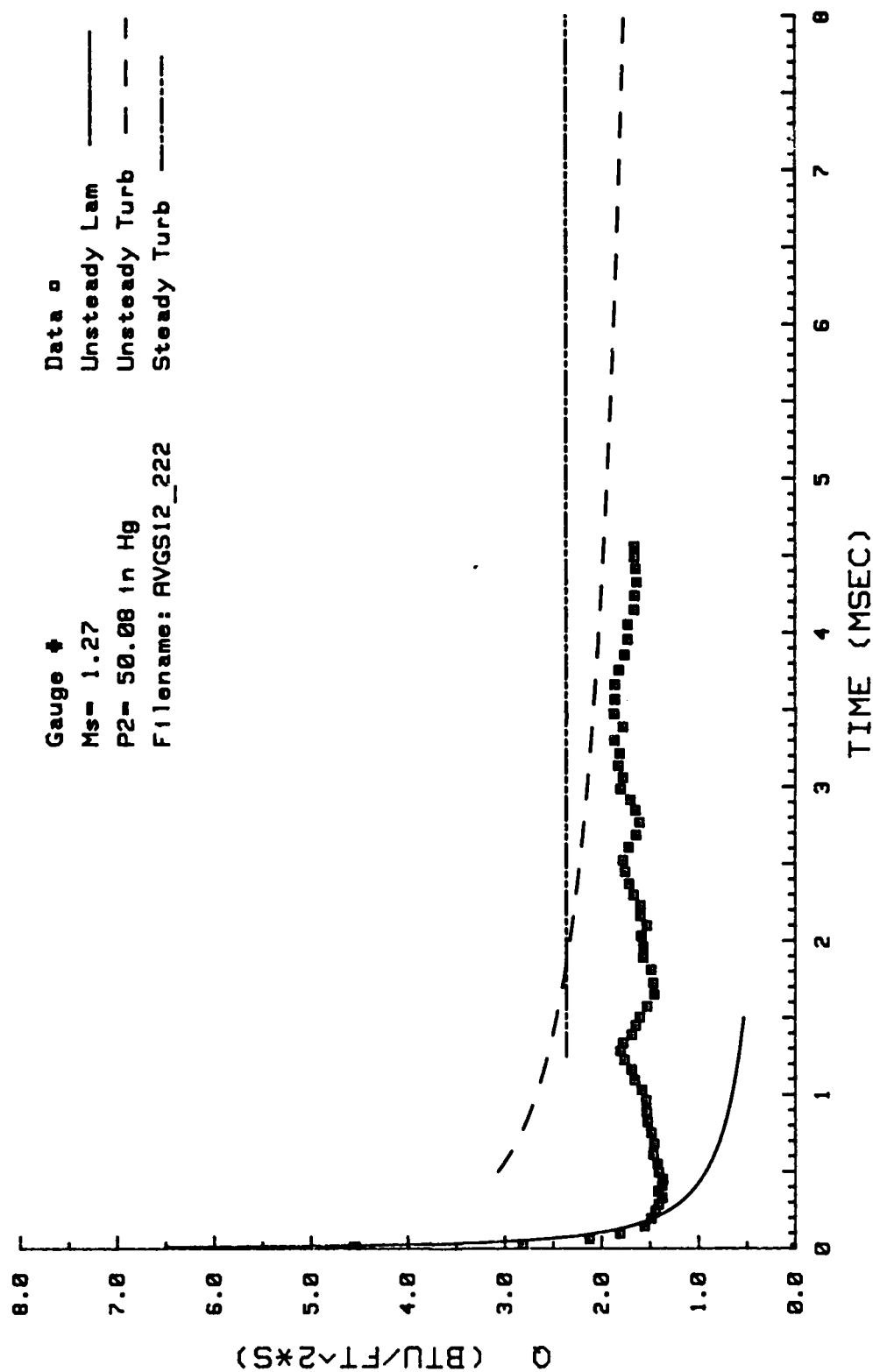
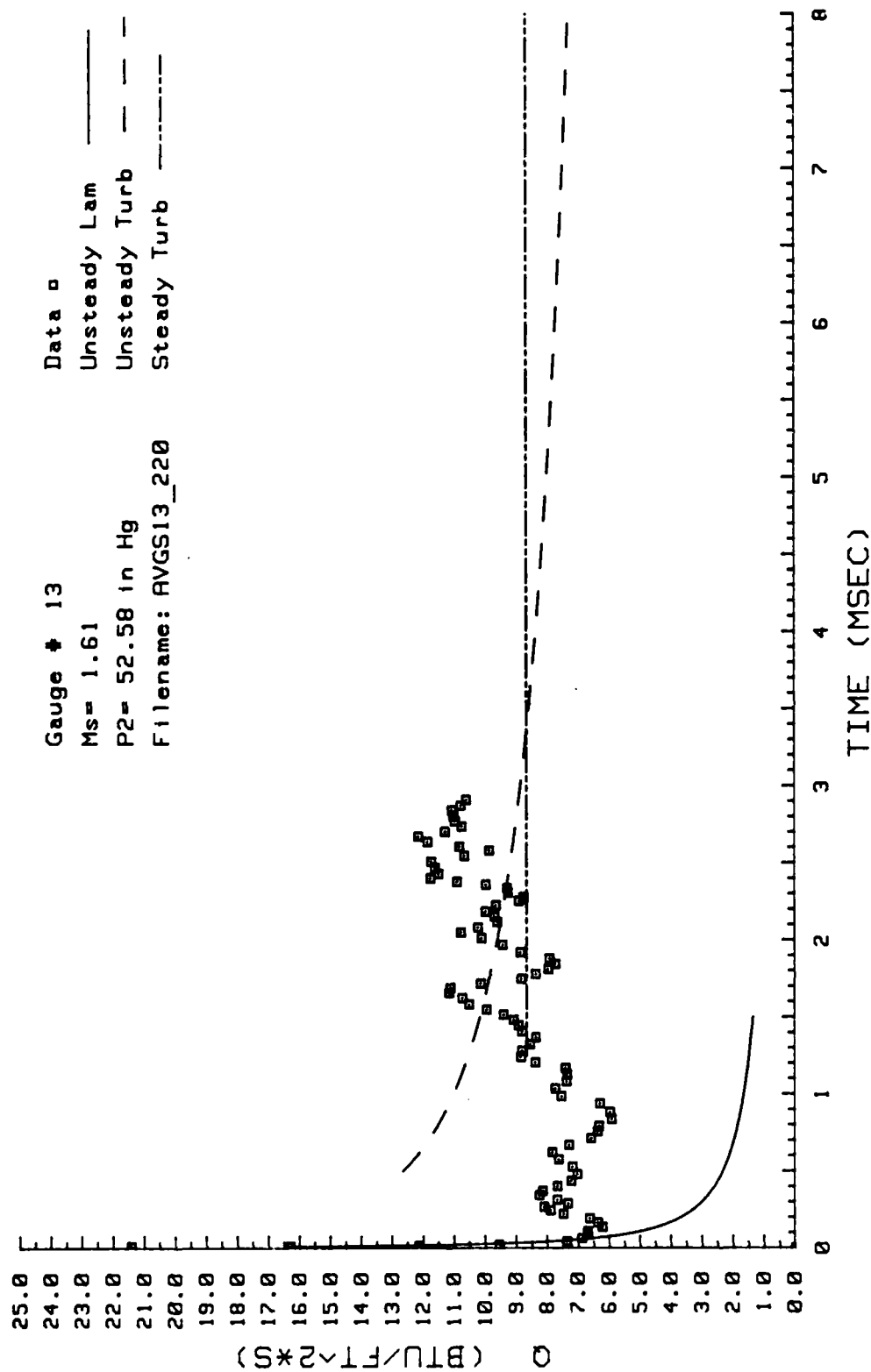Figure 172. Heat Transfer: Data Set W Gage #12
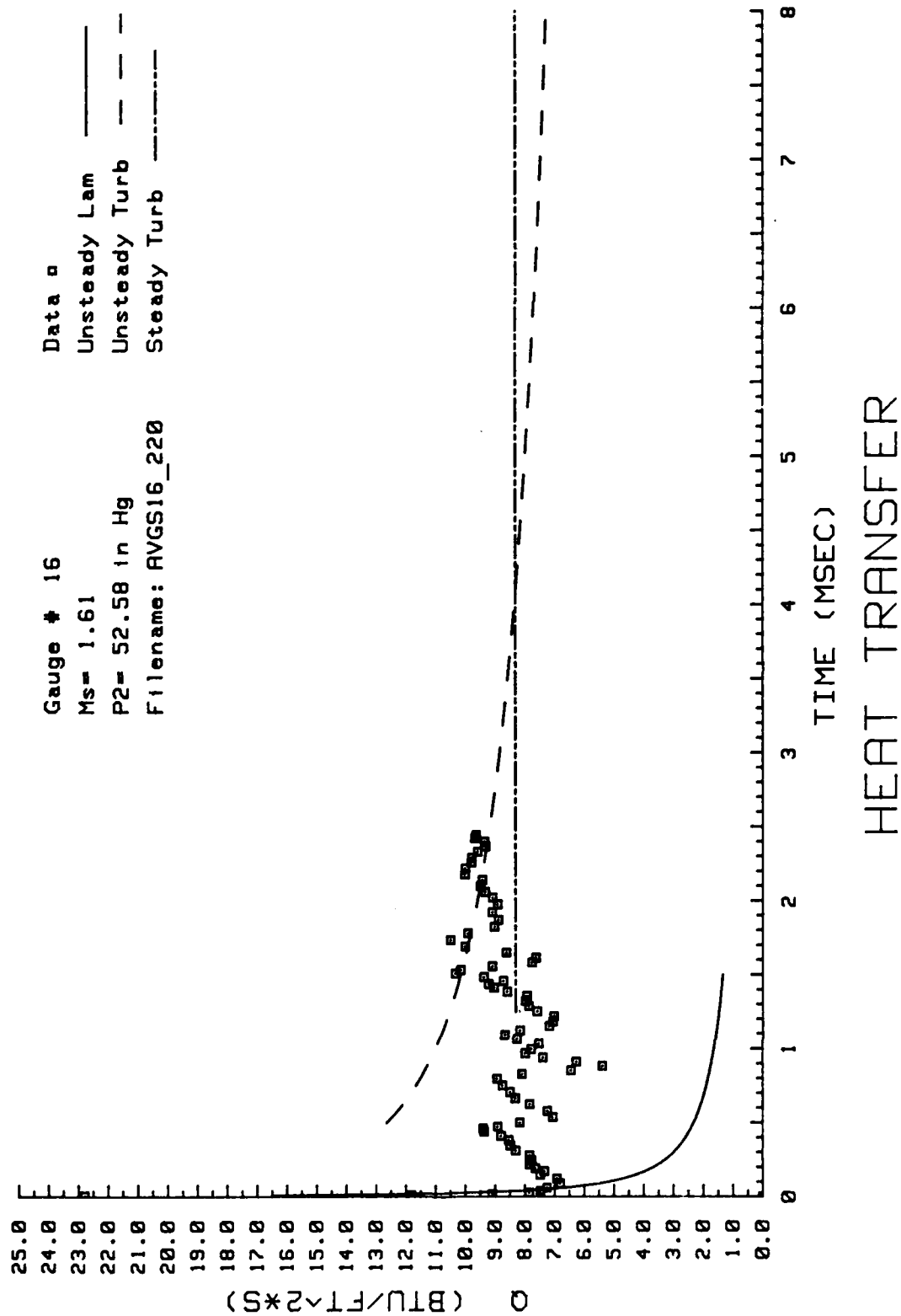
221
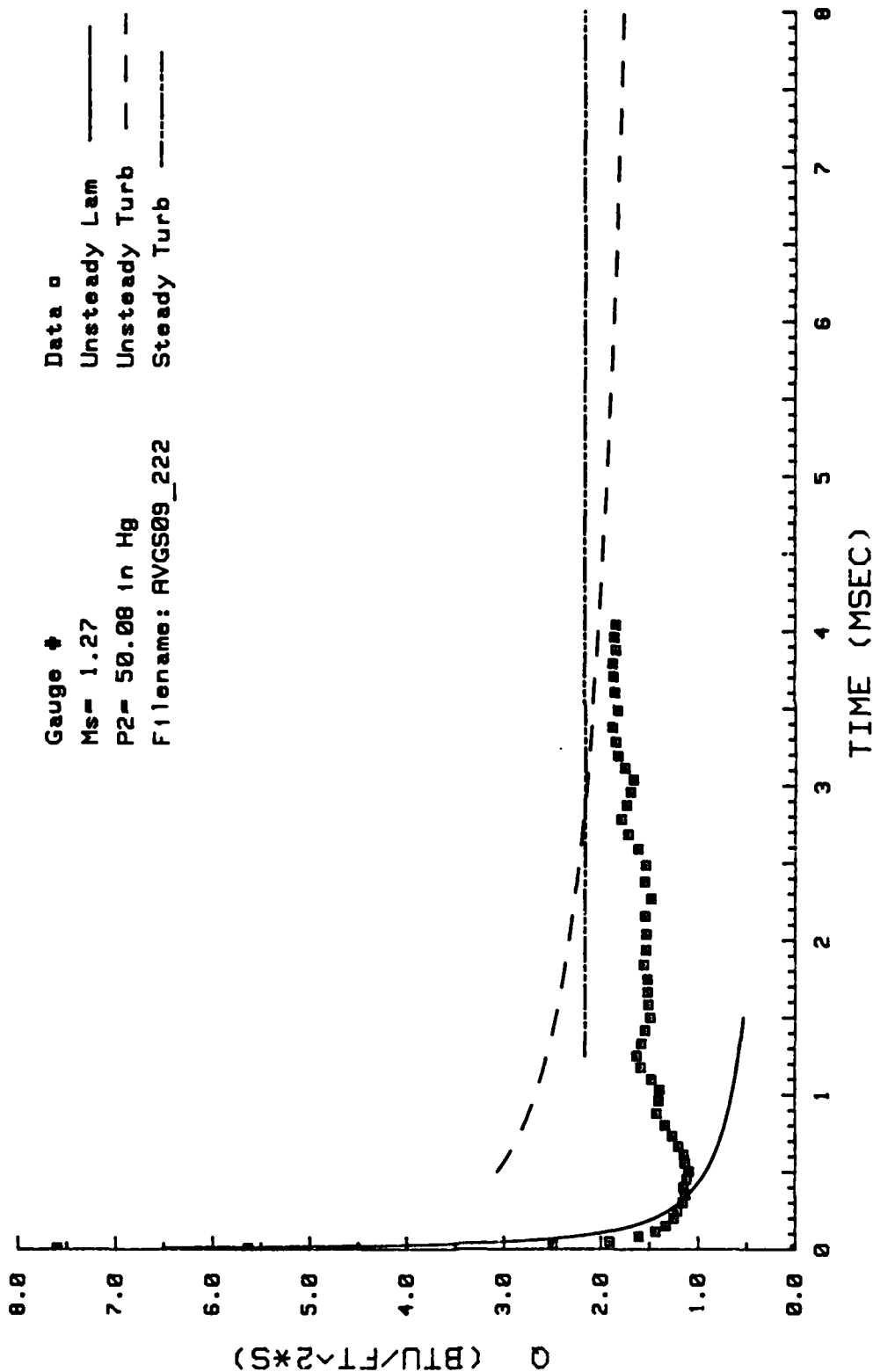
Figure 173. Heat Transfer: Data Set W Gage #9
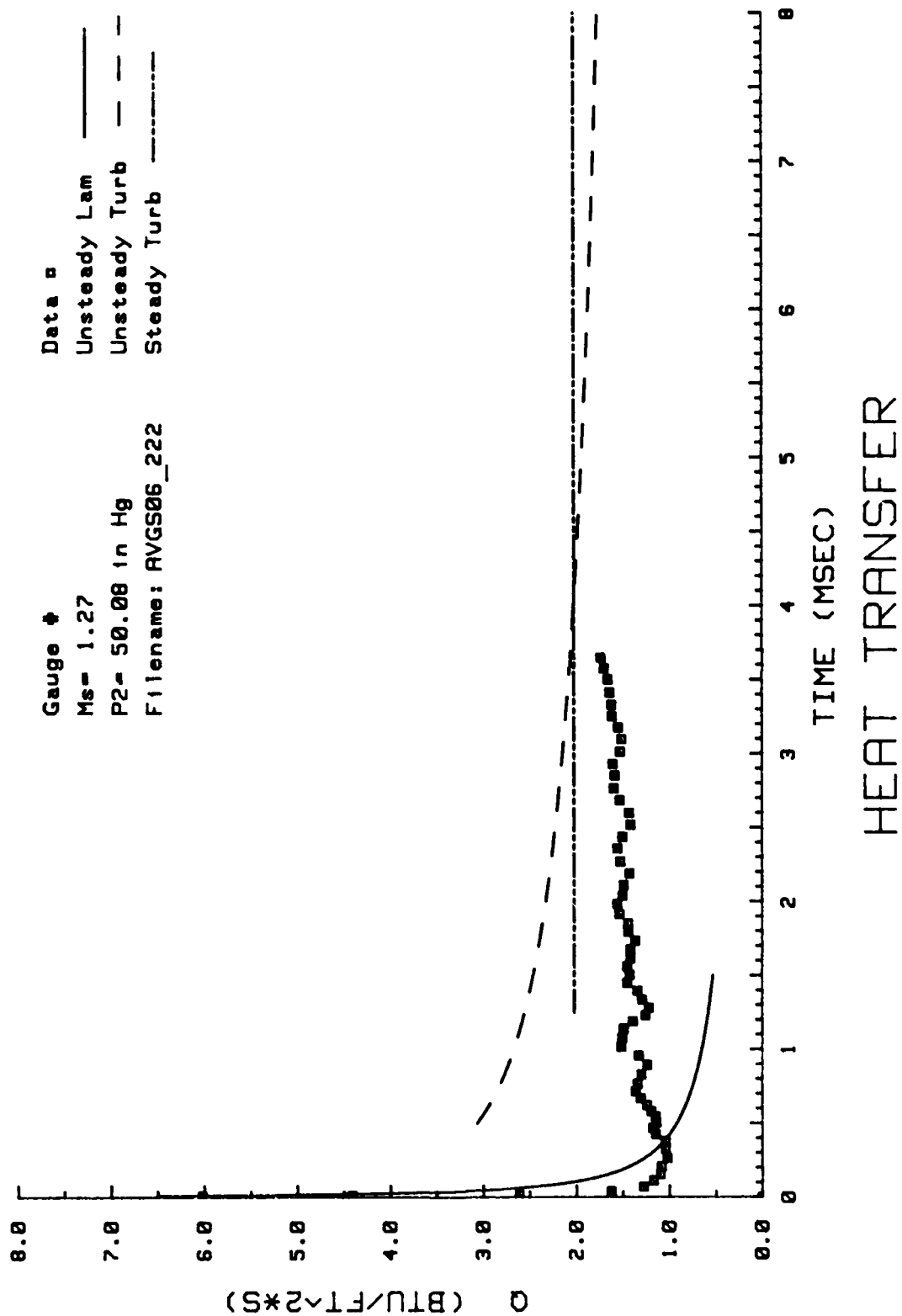
Figure 174. Heat Transfer: Data Set W Gage #6

223
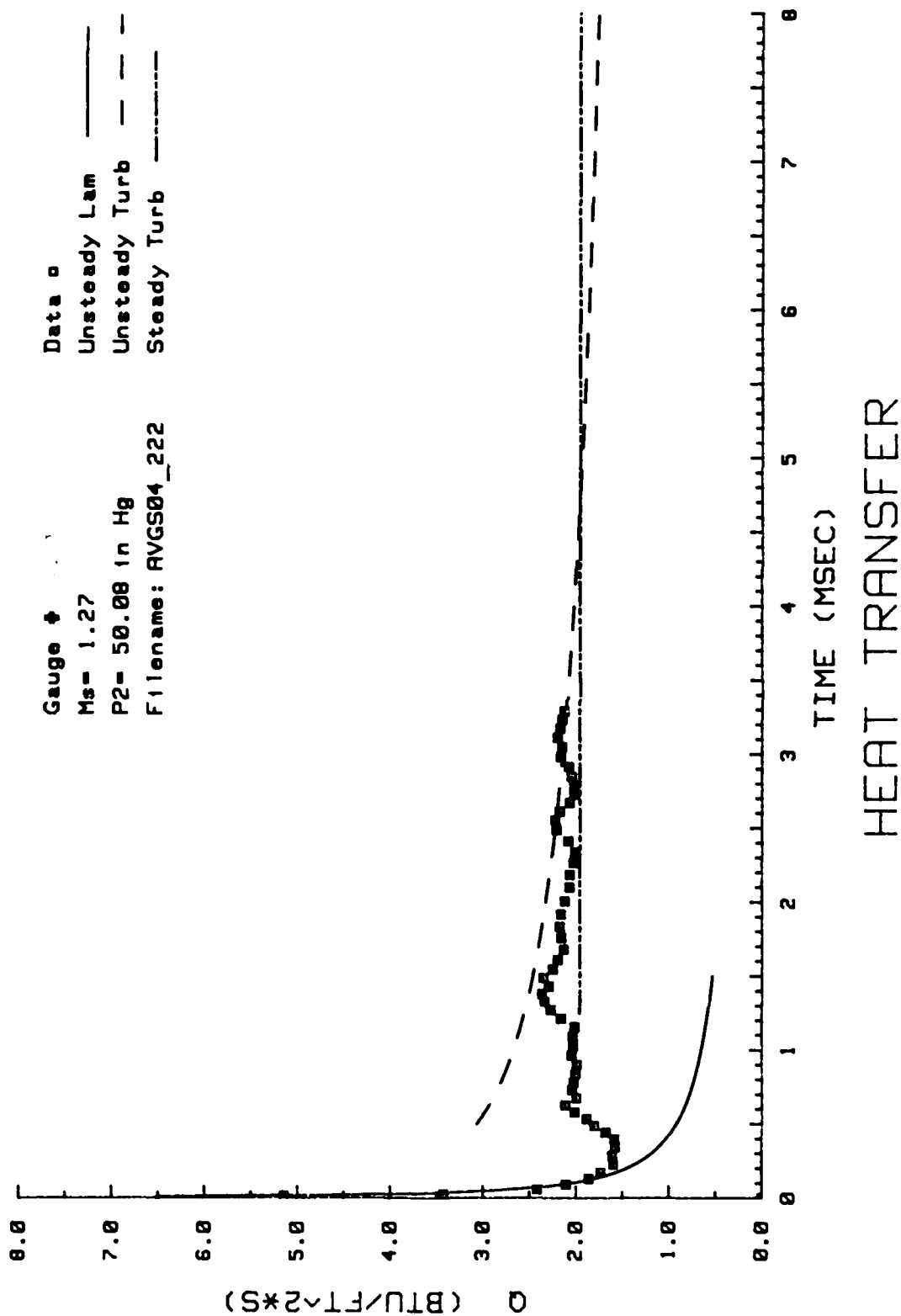
Figure 175. Heat Transfer: Data Set W Gage #4
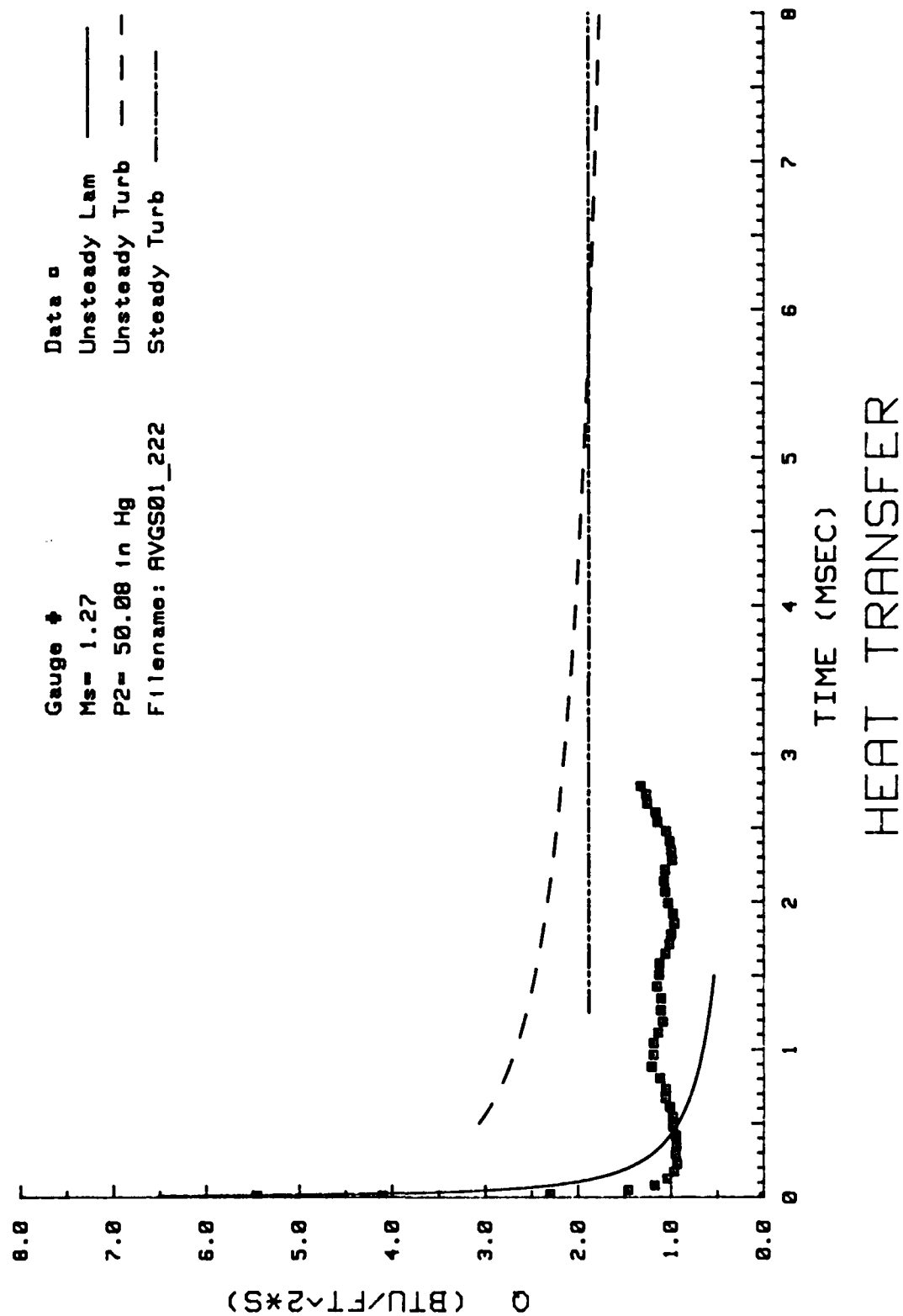
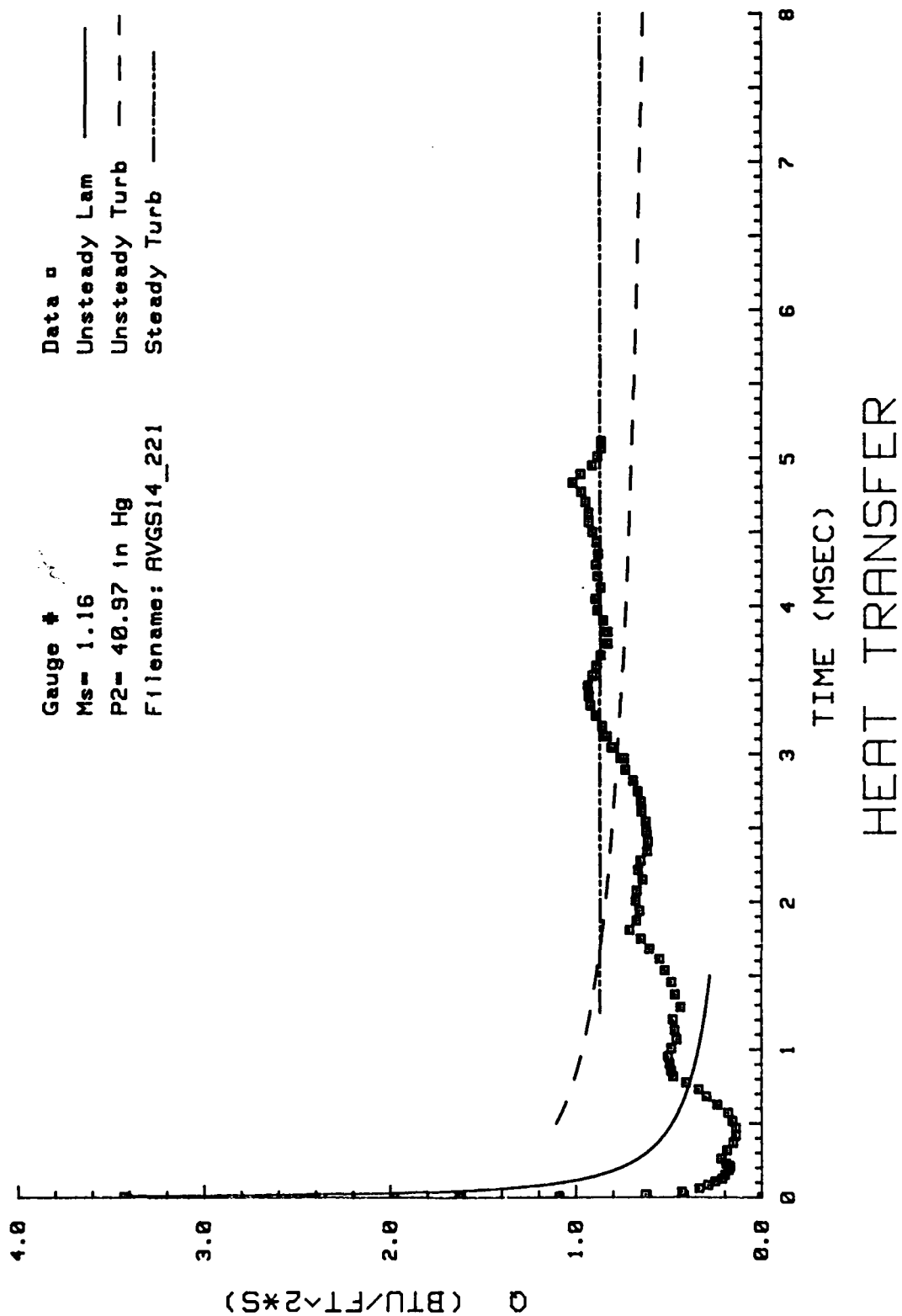Figure 176. Heat Transfer: Data Set W Gage #1

225
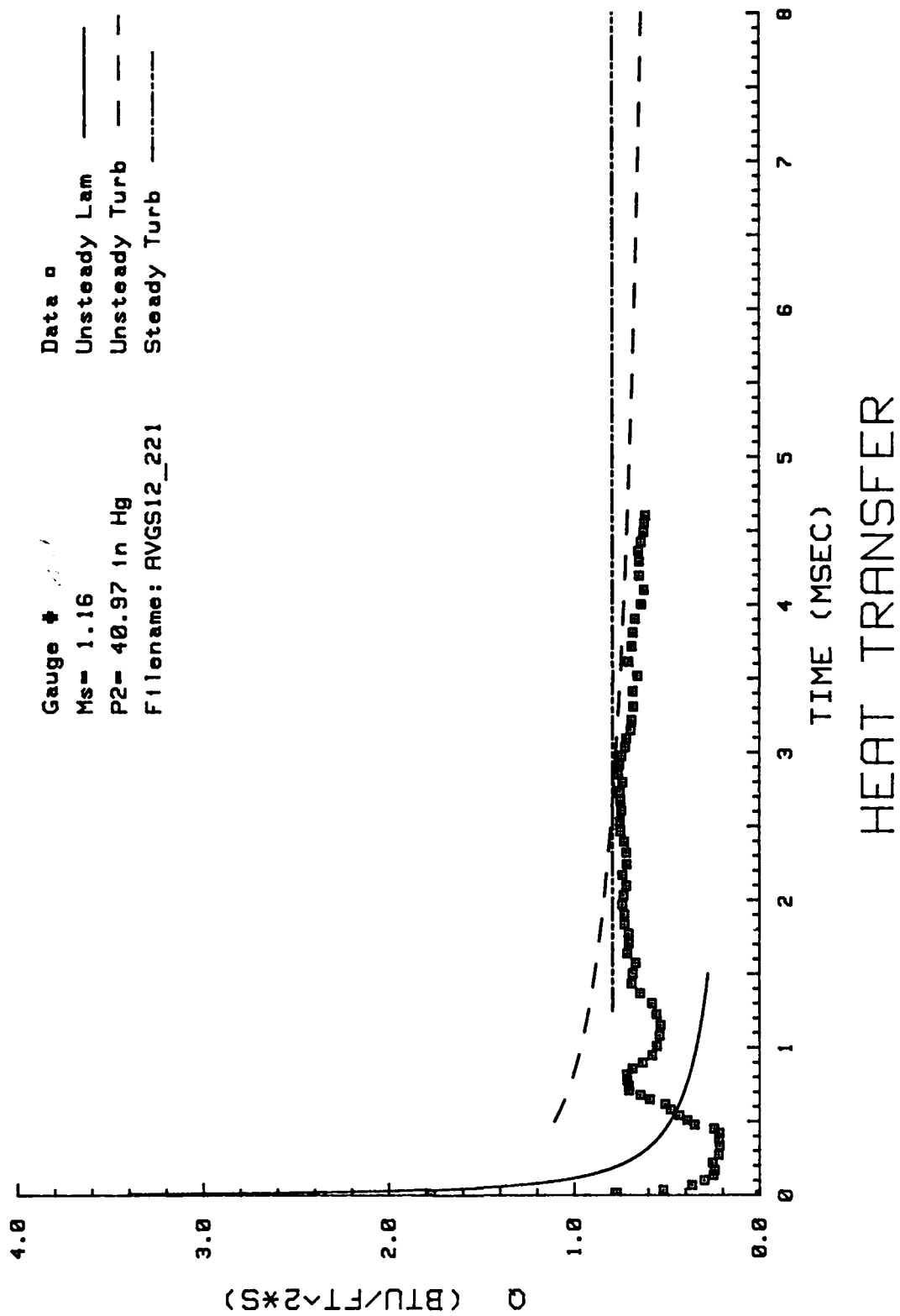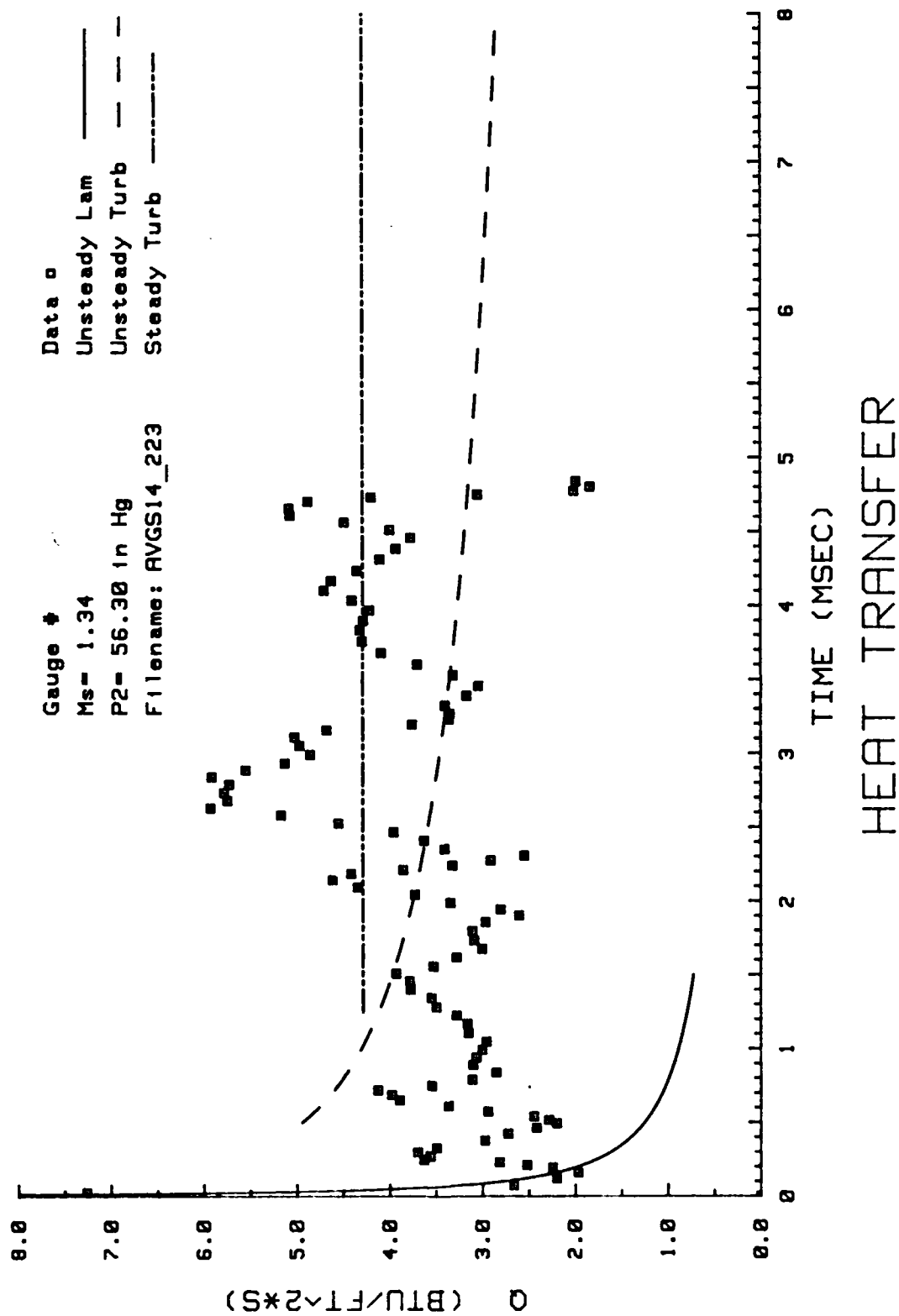
Figure 177. Heat Transfer: Data Set X Gage #14
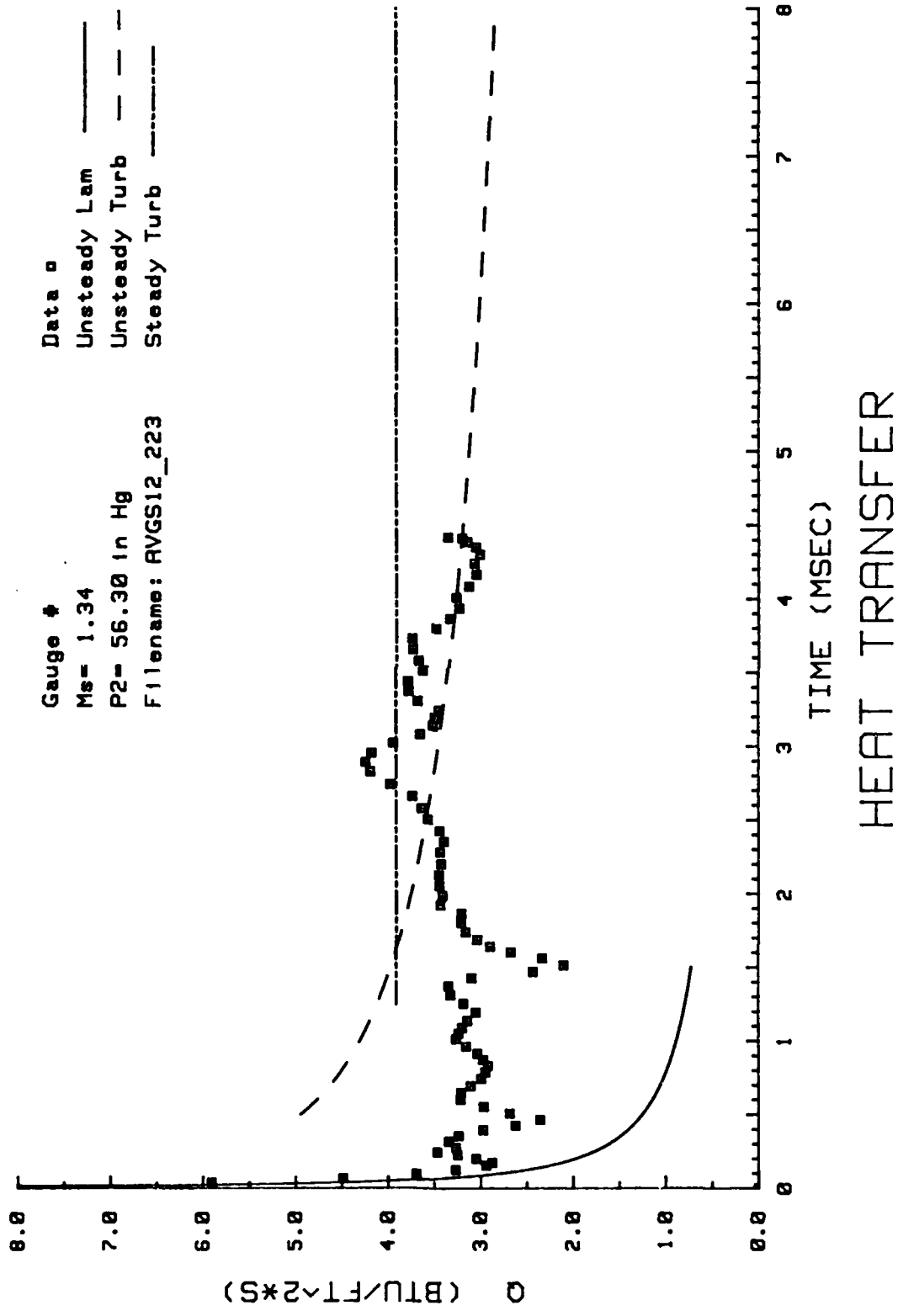
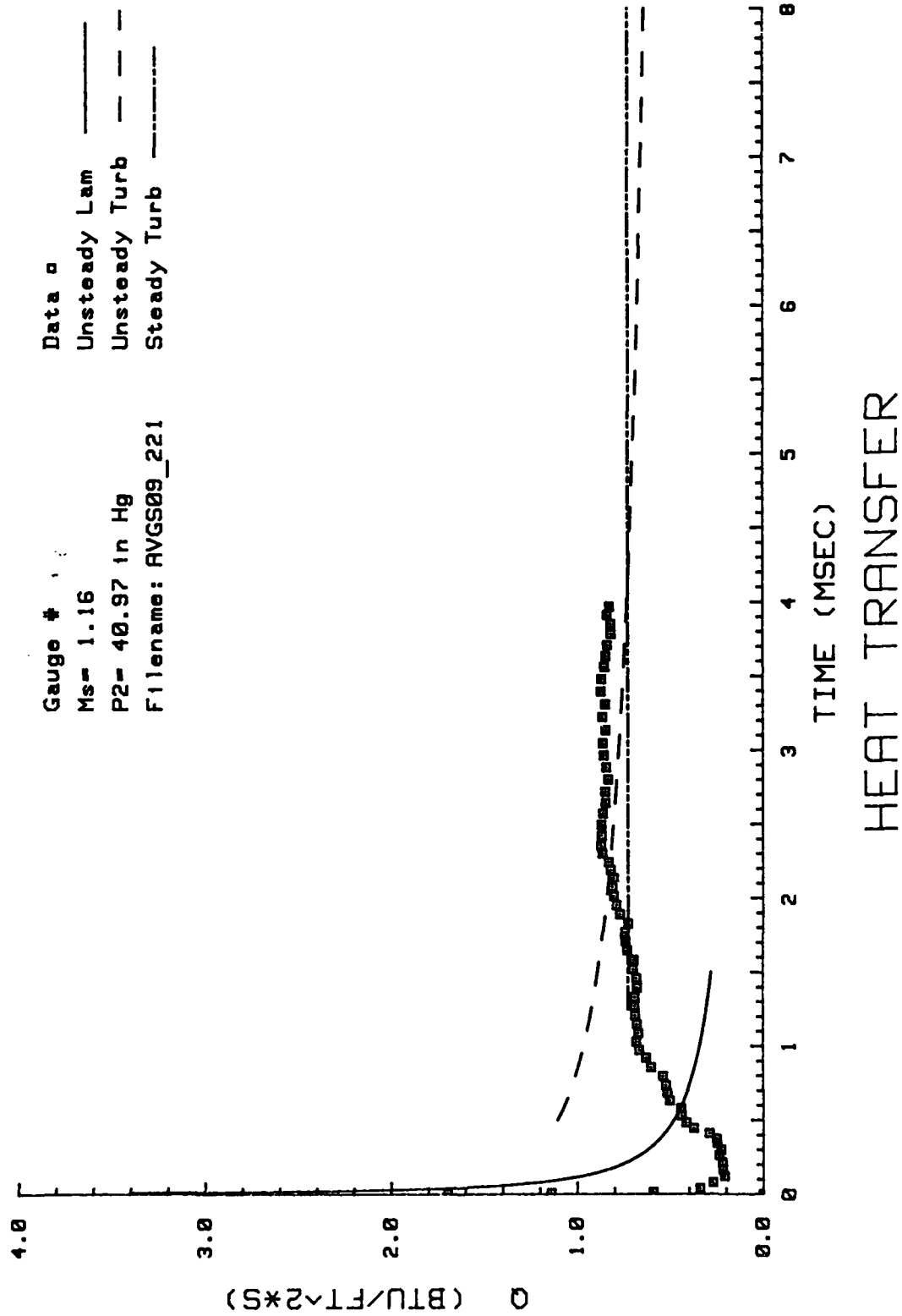Figure 178. Heat Transfer: Data Set X Gage #12
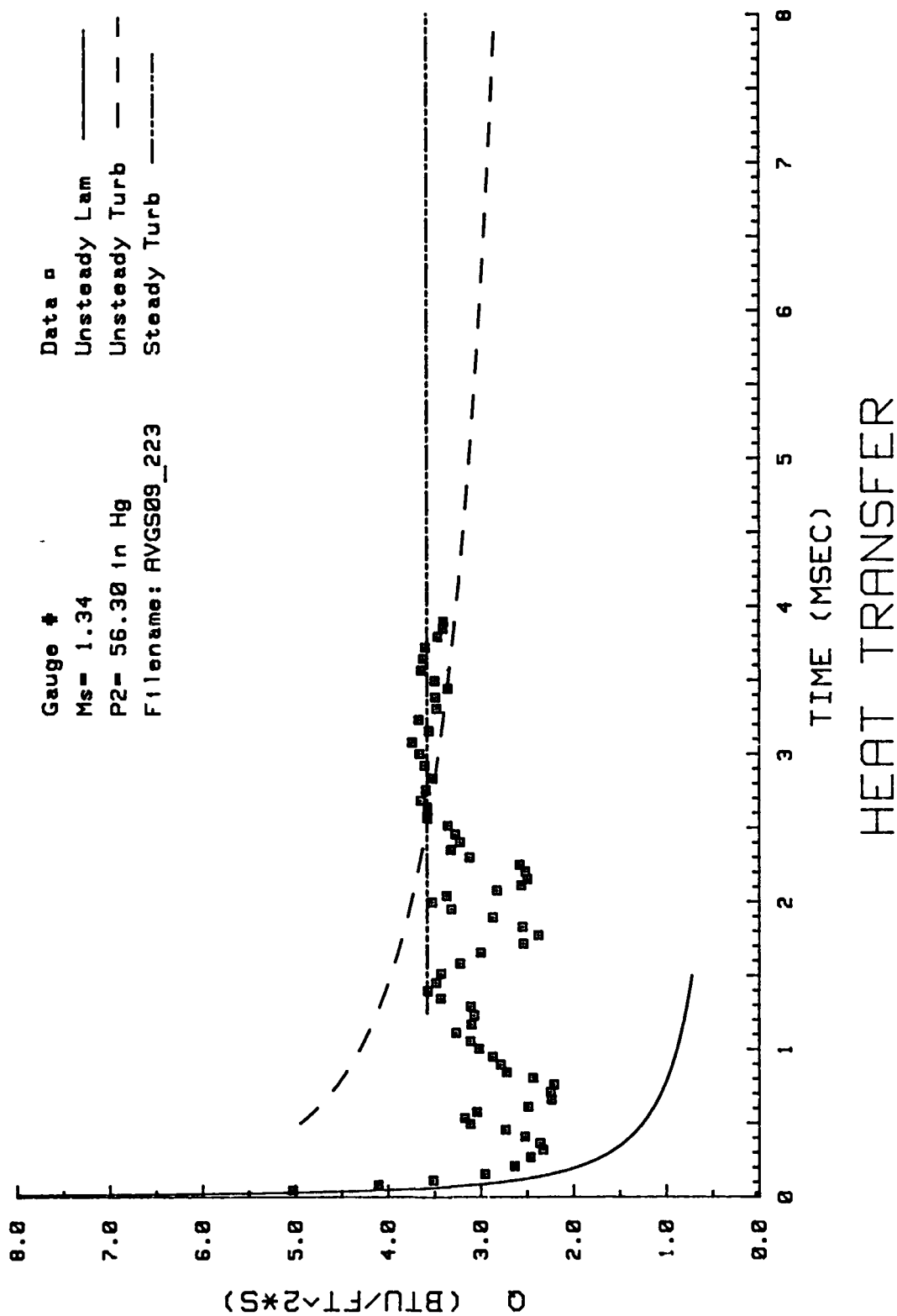
Figure 179. Heat Transfer: Data Set X Gage #9
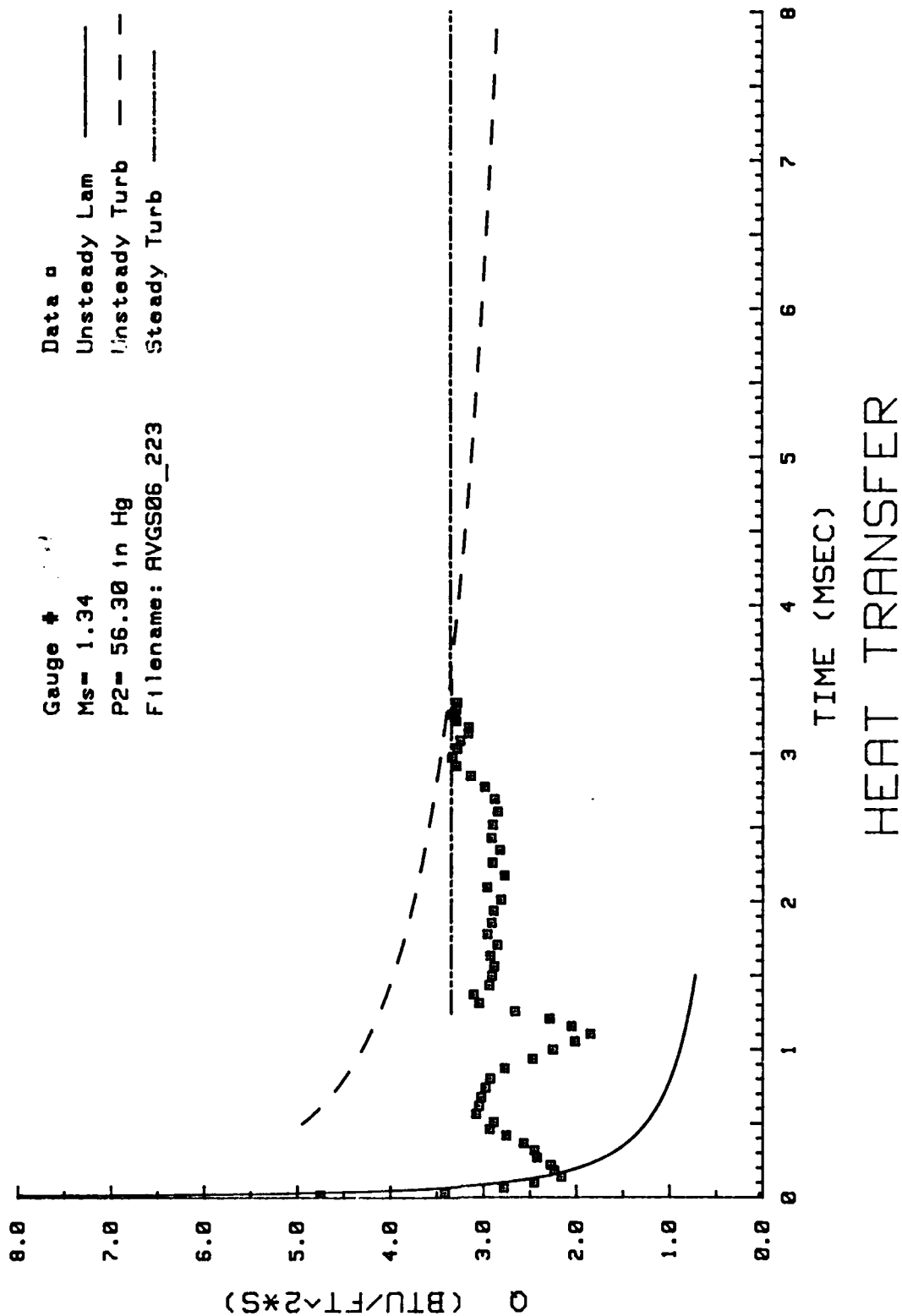
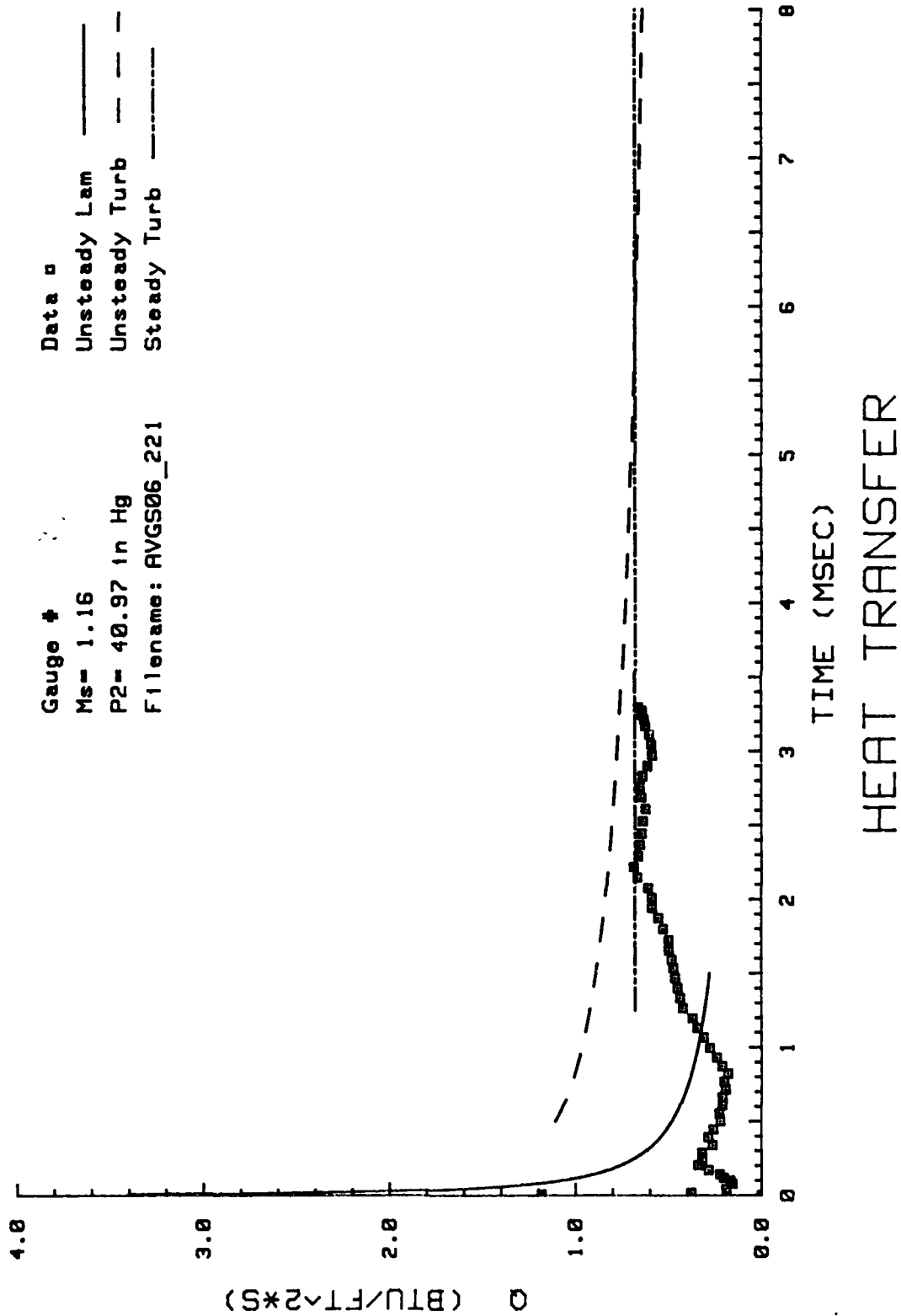Figure 180. Heat Transfer: Data Set X Gage #6
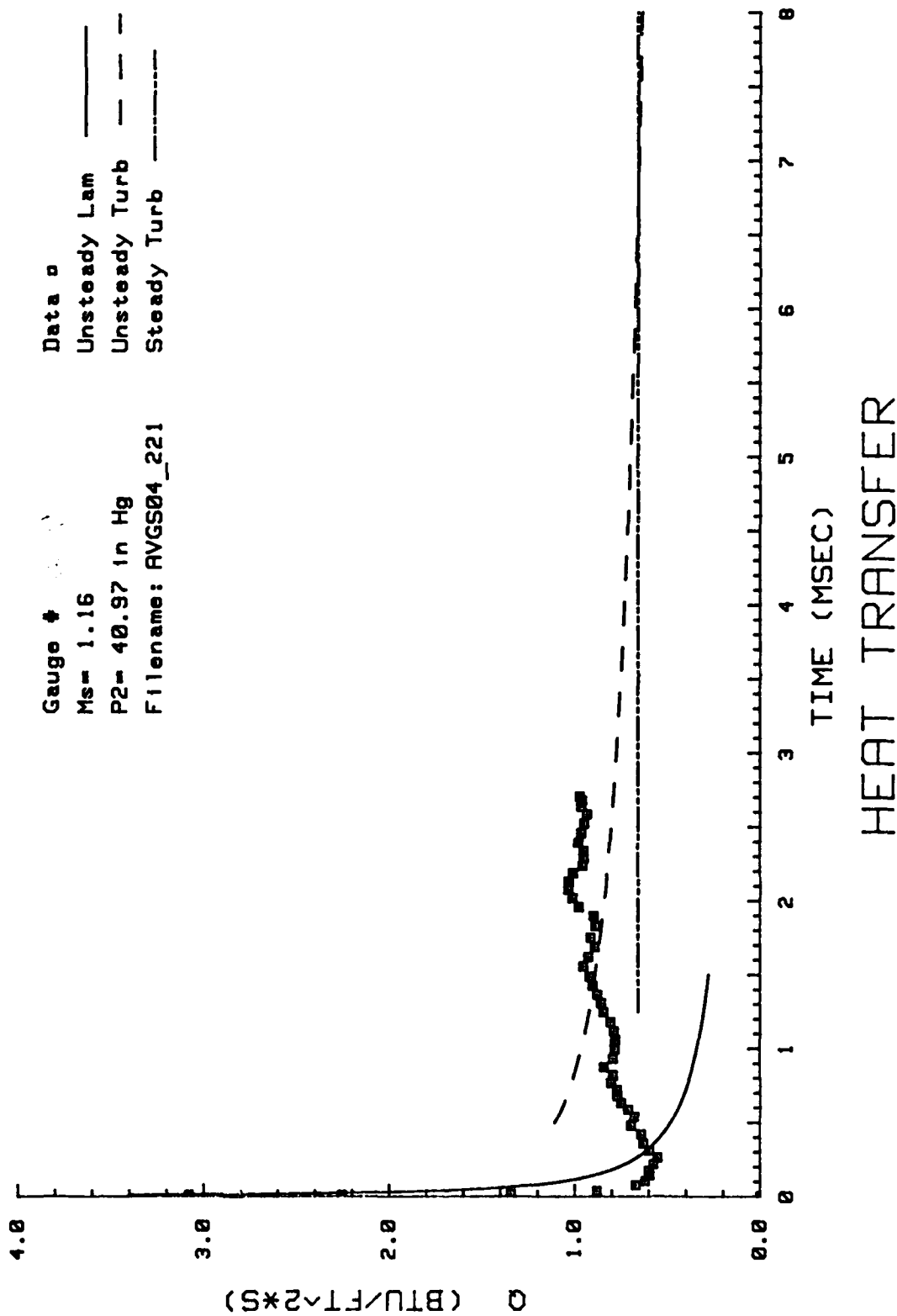
Figure 181. Heat Transfer: Data Set X Gage #4

Figure 182. Heat Transfer: Data Set X Gage #1
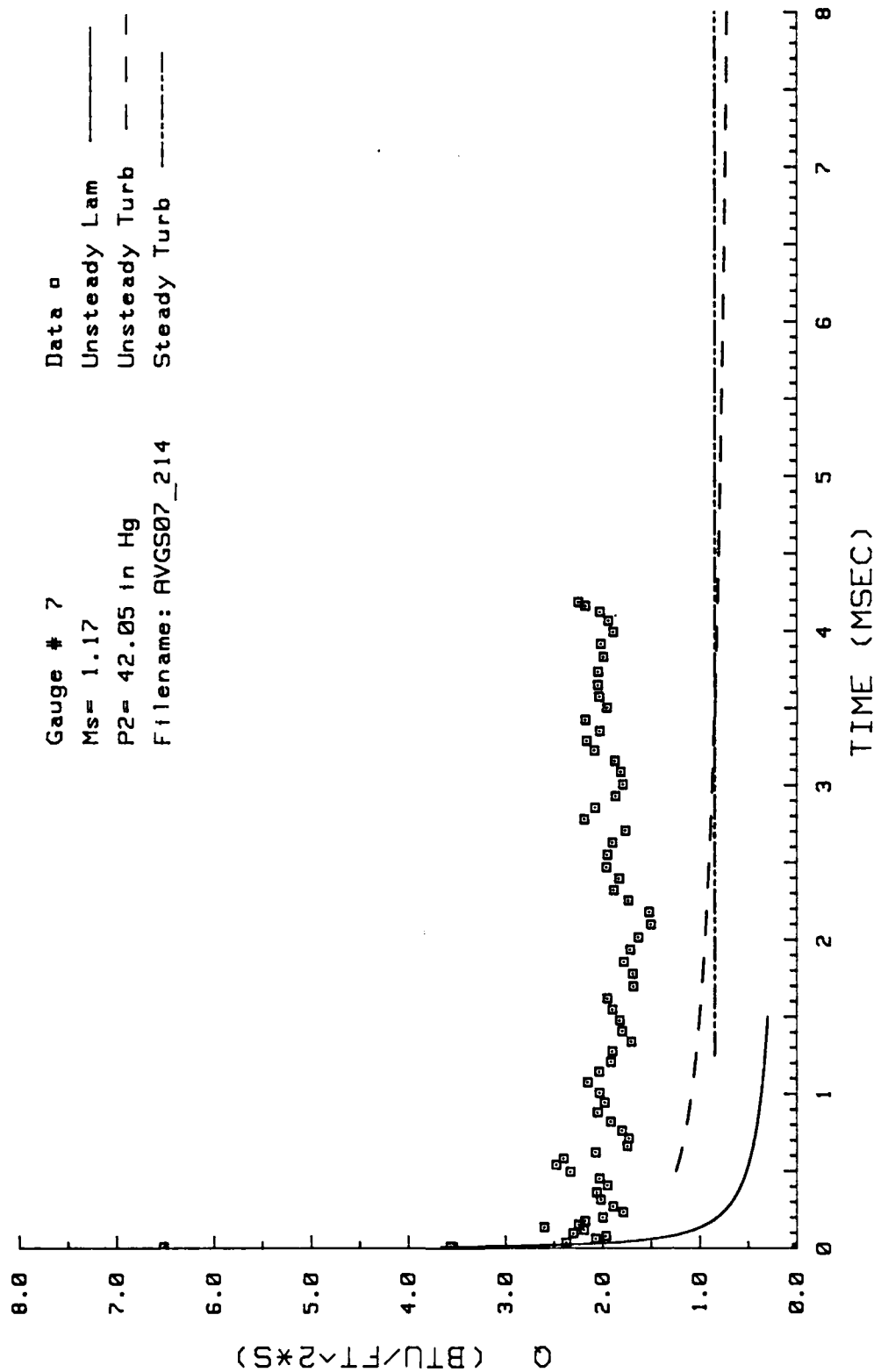
Figure 183. Heat Transfer Curves for $M_S=1.17$
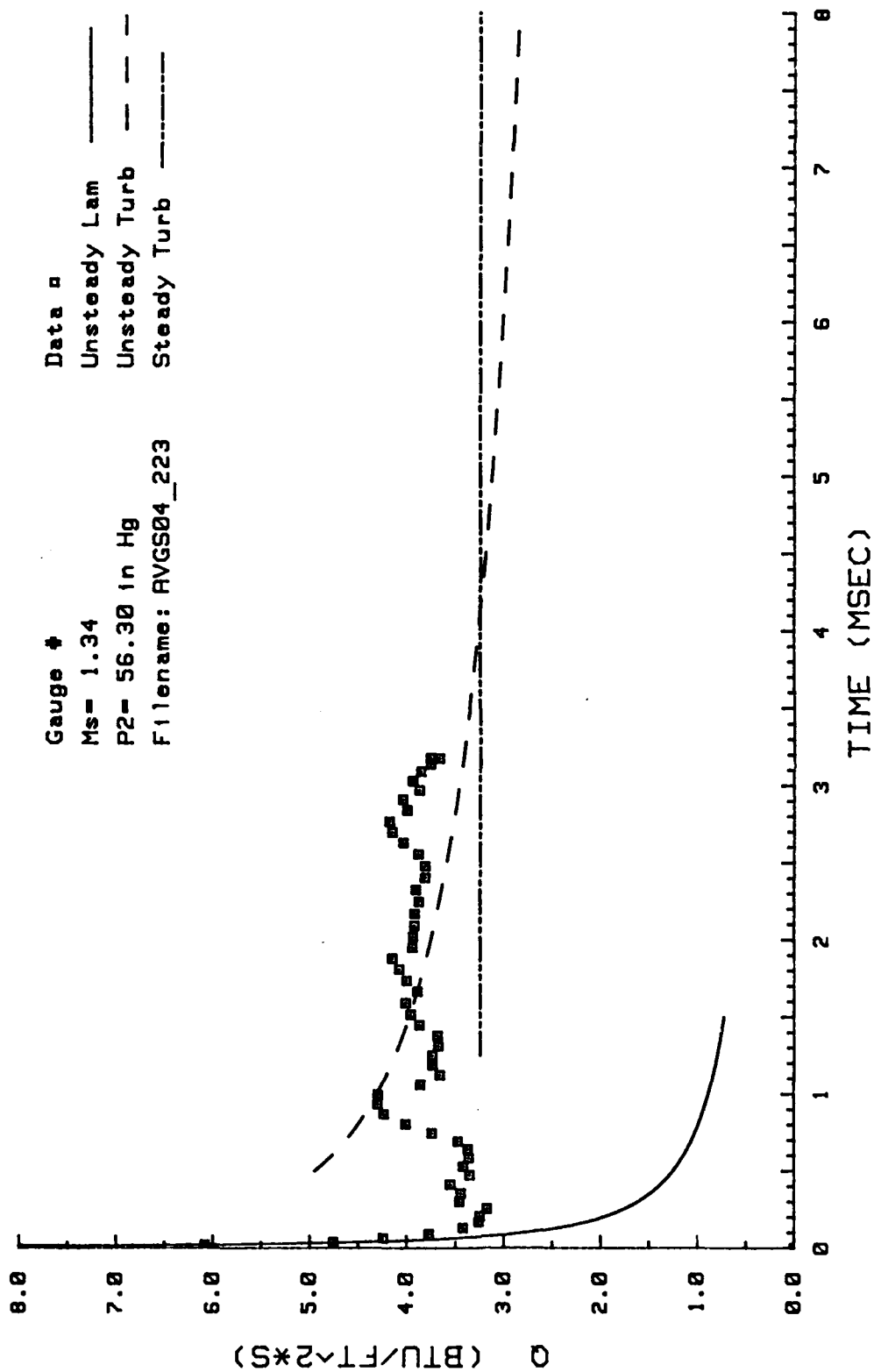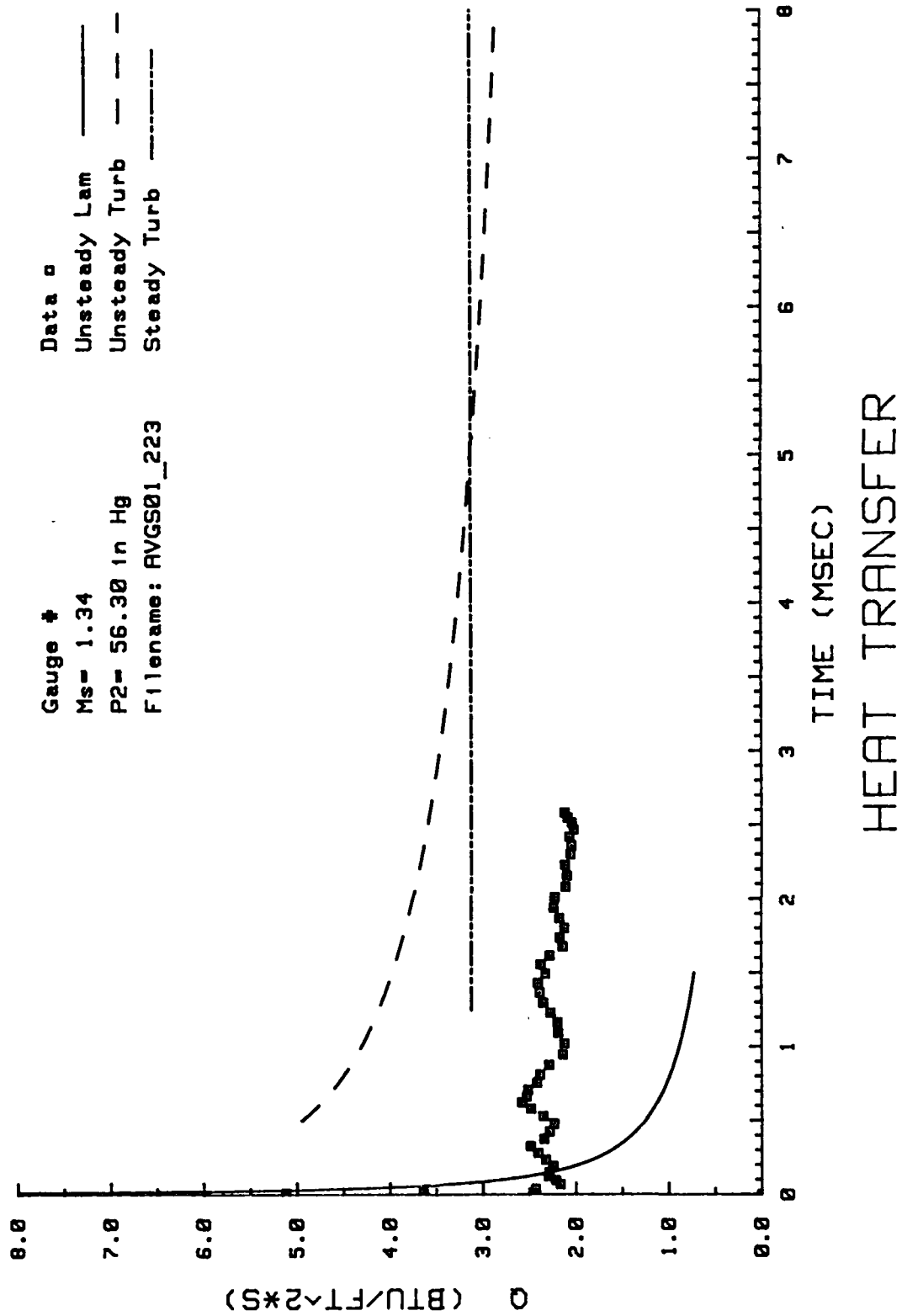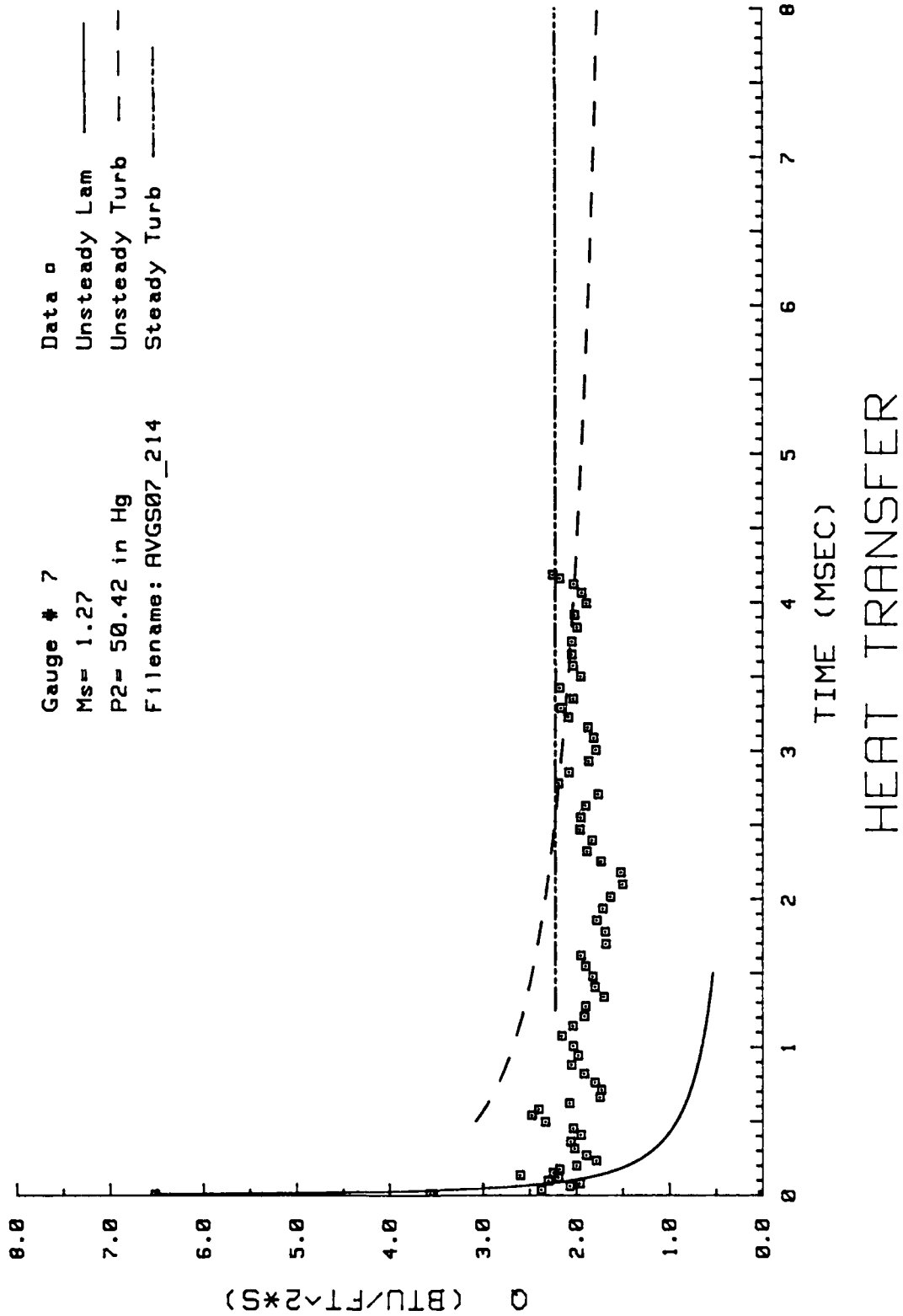
Figure 184. Heat Transfer Curves for $M_s = 1.27$

The data points shown are approximate mean turbulent heat transfer magnitudes obtained from the data sets for selected Mach numbers
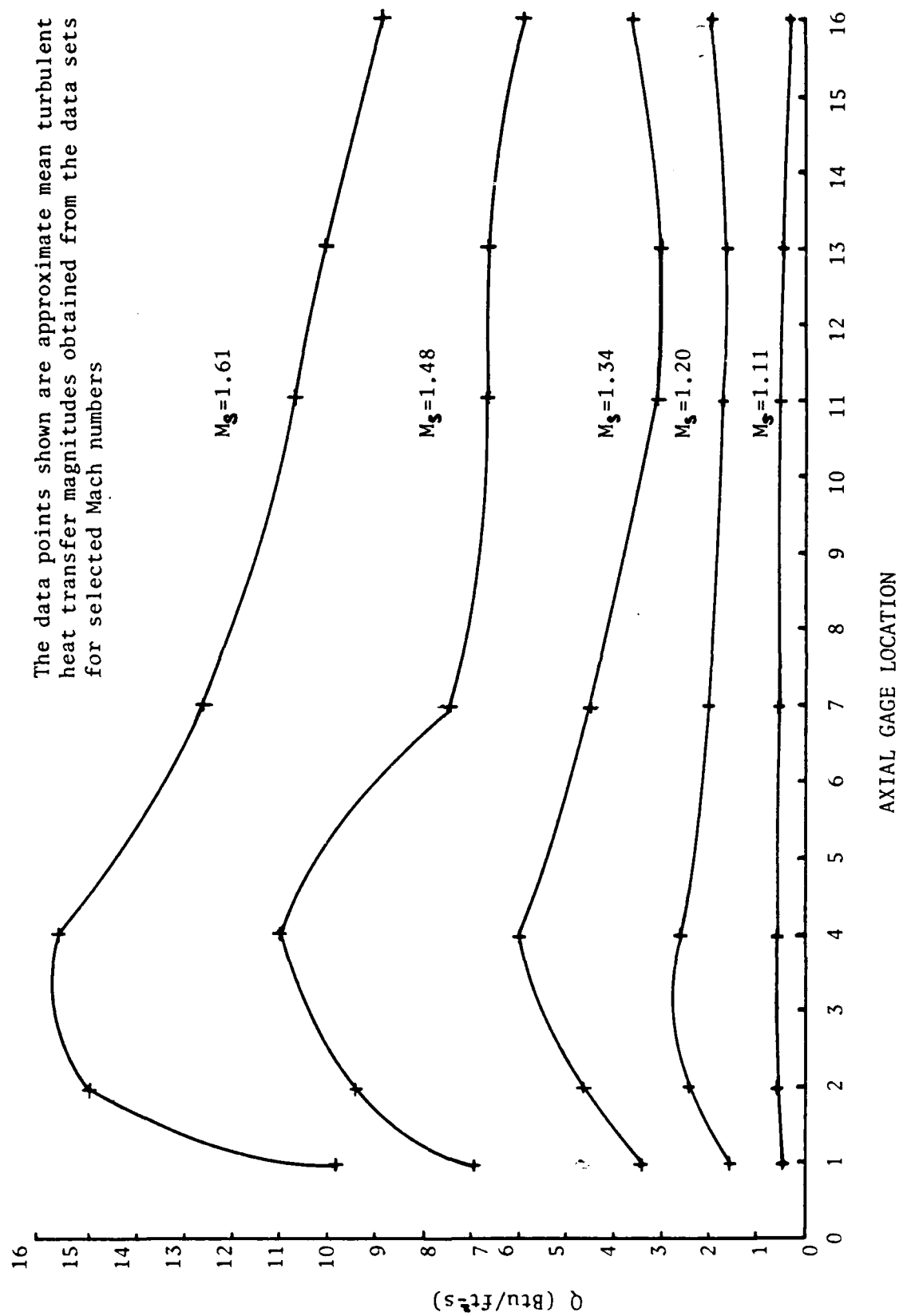
Figure 185. Heat Transfer Rates versus Axial Gage Location (Sharp Leading Edge)

234

Bibliography

Abbott, D.E., J.D. Walker, H.T. Liu. "Recent Developments in Shock Tube Research," Proceedings of the 9th International Shock Tube Symposium. Stanford University, 1973.

Blasius, H. "Grenzschichten in Flussigkeiten mit kleiner Reibung," Z. Math Phys, 56: 1-37 (1908). English trans. in NACA TM 1256.

Bogdan, Leonard and Joseph E. Garberoglio. Transient Heat Transfer Measurement with Thin-Film Resistance Thermometers-Fabrication and Application Technology. Technical Report AFAPL-TR-67-72. Cornell Aeronautical Laboratory Inc., June 1967.

Bogdan, Leonard. "Thermal and Electrical Properties of Thin-Film Resistance Gages Used for Heat Transfer Measurement," AIAA Journal (September 1963).

Brostmeyer, J.D. and H.T. Magamatsu. "Flat Plate Heat Transfer for Laminar Transition and Turbulent Boundary Layers Using a Shock Tube," AIAA Papers 19th Thermophysics Conference, AIAA-84-1726 (1984).

Chapman, Alan J. and William F. Walker. Introductory Gas Dynamics. Holt, Rinehart, and Winston Inc., 1971.

Cook, W.J. and E.J. Felderman. "Reduction of Data from Thin Film Heat Transfer Gages: A Concise Numerical Technique" AIAA Journal (March 1966).

Davies, W.R. and L. Berstein. "Heat Transfer and Transition to Turbulence in the Shock-Induced Boundary Layer on a Semi-infinite Flat Plate," J. Fluid Mech., Vol 36, Part 1 (1969).

Dillon, R.E. and H.T. Nagamatsu. "Heat Transfer and Transition Mechanism on a Shock Tube Wall," AIAA Journal, Vol 22, No. 11 (November 1984).

Dunn, Michael G. Measurement of Heat Flux and Pressure in a Turbine Stage. Technical Report AFWAL-TR-81-2055. Calspan Advanced Technology Center, July 1981.

Fillingim, P.K. Flat Plate and Turbine Vane Cascade Heat Transfer Investigation Using a Shock Tube. MS thesis, AFIT/GAE/AA/85D-7. School of Engineering, Air Force Institute of Technology (AU), Wright-Patterson AFB OH, December 1985.

Felderman, E.J. "Heat Transfer and Shear Stress in the Shock-Induced Unsteady Boundary Layer on a Flat Plate," AIAA Journal, Vol 6, No. 3 (1968).

Gaydon, A.G. and I.R. Hurle. <u>The Shock Tube in High-Temperature Chemical Physics.</u> New York: Reinhold Publishing Corporation, 1963.

Glass, I.I. "Shock Tubes, Part I: Theory and Performance of Simple Shock Tubes," <u>Utia Review No. 12.</u> Toronto, Canada: Institute of Aerophysics, University of Toronto, 1958.

Gochenaur, John E. <u>Investigation of Heat Transfer to a Turbine Blade Cascade Using a Shock Tube.</u> Master thesis, GAE-84D. School of Engineering, Air Force Institute of Technology (AU), Wright-Patterson AFB OH, December, 1984.

Kays, W.M. and M.E. Crawford. <u>Convective Heat and Mass Transfer.</u> New York: Mcgraw-Hill Book Company, 1980.

Kendall, David N. and Edward H. Schulte. <u>Semi-Conductor Surface Thermocouples and Heat-Flux Sensors,</u> Engineering Laboratories, McDonnell Company: April 1968.

Lam, S.H. and L. Crocco. "Shock Induced Unsteady Laminar Compressible Boundary Layer on a Semi-Infinite Flat Plate," <u>Princeton Report No. 428</u>, 1958.

MacMullin, Capt R. <u>Effects of Free-Stream Turbulence from a Circular Wall Jet on Flat Plate Heat Transfer and Boundary Layer Flow.</u> Master thesis, GA-86D. School of Engineering, Air Force Institute of Technology (AU), Wright-Patterson AFB OH, December 1986.

Mirels, H. "Boundary Layer Behind Shock or Thin Expansion Wave Moving into Stationary Fluid," <u>NACA TN 3712</u> (1956).

Mirels, H. "Laminar Boundary Layer Behind Shock Advancing into Stationary Fluid," <u>NACA 3401</u> (1955).

Schlichting, Hermann. <u>Boundary Layer Theory</u> (Seventh Edition). New York: Mcgraw-Hill Book Company, 1979.

Shapiro, Ascher H. <u>The Dynamics and Thermodynamics of Compressible Fluid Flow, Vol 2.</u> Florida: Kreiger Publishing Company, 1985.

Smith, Capt B.J. <u>Investigation of Heat Transfer to a Sharp Edged Flat Plate Using a Shock Tube.</u> MS thesis, AFIT/GAE/ENY/86D-16. School of Engineering, Air Force Institute of Technology (AU), Wright-Patterson AFB OH, December, 1986.

Stewartson, K. "On the Impulsive Motion of a Flat Plate in a Viscous Fluid," <u>Quart. J. Mech. Appl. Math., Vol 4:</u> 182 (1951).

VITA

Captain Joseph T. Novak was born on 7 August 1954 in Franklin, New Jersey, the son of George and Shirley Novak. He graduated from Franklin High School in 1972 and attended Montclair State College, from which he received the degree of Bachelor of Science in physics and mathematics in January 1978. After attending Air Force Officer Training School, he received his commission in July 1980. He then attended the Air Force Institute of Technology (AFIT) until March 1982, at which time he received the degree of Bachelor of Science in Aeronautical Engineering. From April 1982 until May 1986 he was assigned to the 6595th Aerospace Test Group, Vandenberg AFB, California, where he served as launch controller for military payloads launched aboard Titan space boosters. After attending school at night, he received the degree of Master of Science in Systems Management from the University of Southern California in September 1985. He entered the Master of Science degree program at AFIT in June 1986.

Permanent address: 458 Rutherford Avenue

Franklin, New Jersey 07416

AD-A189 538

REPORT DOCUMENTATION PAGE

Form Approved
OMB No. 0704-0188

1a. REPORT SECURITY CLASSIFICATION UNCLASSIFIED	1b. RESTRICTIVE MARKINGS

2a. SECURITY CLASSIFICATION AUTHORITY	3. DISTRIBUTION/AVAILABILITY OF REPORT
2b. DECLASSIFICATION/DOWNGRADING SCHEDULE	Approved for public release; distribution unlimited

4. PERFORMING ORGANIZATION REPORT NUMBER(S) AFIT/GA/AA/87D-5	5. MONITORING ORGANIZATION REPORT NUMBER(S)

6a. NAME OF PERFORMING ORGANIZATION School of Engineering	6b. OFFICE SYMBOL (If applicable) AFIT/ENA	7a. NAME OF MONITORING ORGANIZATION

6c. ADDRESS (City, State, and ZIP Code) Air Force Institute of Technology Wright-Patterson AFB OH 45433-6583	7b. ADDRESS (City, State, and ZIP Code)

8a. NAME OF FUNDING/SPONSORING ORGANIZATION AF Aeropropulsion Lab	8b. OFFICE SYMBOL (If applicable) AFWAL/POTC	9. PROCUREMENT INSTRUMENT IDENTIFICATION NUMBER

8c. ADDRESS (City, State, and ZIP Code) Wright-Patterson AFB OH 45433	10. SOURCE OF FUNDING NUMBERS			
	PROGRAM ELEMENT NO.	PROJECT NO.	TASK NO	WORK UNIT ACCESSION NO.

11. TITLE (Include Security Classification)
INVESTIGATION OF HEAT TRANSFER TO A FLAT PLATE IN A SHOCK TUBE (Unclassified)

12. PERSONAL AUTHOR(S)
Joseph T. Novak, M.S., Capt, USAF

13a. TYPE OF REPORT MS Thesis	13b. TIME COVERED FROM _____ TO _____	14. DATE OF REPORT (Year, Month, Day) 1987 December	15. PAGE COUNT 237

16. SUPPLEMENTARY NOTATION

17. COSATI CODES			18. SUBJECT TERMS (Continue on reverse if necessary and identify by block number)
FIELD	GROUP	SUB-GROUP	Flat Plate, Shock Tube, Heat Transfer, Thermal Boundary Layer
20	04		Transient Boundary Layer, Transition

19. ABSTRACT (Continue on reverse if necessary and identify by block number)

Title: INVESTIGATION OF HEAT TRANSFER TO A FLAT PLATE IN A SHOCK TUBE

Thesis Chairman: Dr. William C. Elrod

20. DISTRIBUTION/AVAILABILITY OF ABSTRACT ☐ UNCLASSIFIED/UNLIMITED ☒ SAME AS RPT ☐ DTIC USERS	21. ABSTRACT SECURITY CLASSIFICATION UNCLASSIFIED
22a. NAME OF RESPONSIBLE INDIVIDUAL Dr. William C. Elrod	22b. TELEPHONE (Include Area Code) (513) 255-3517 / 22c. OFFICE SYMBOL AFIT/ENY

DD Form 1473, JUN 86   Previous editions are obsolete.

ABSTRACT

The heat transfer mechanisms taking place in the flow induced behind a shock wave travelling across a flat plate were investigated for flat plates with sharp and rounded leading edges. The boundary layer behind the shock is described by a transient boundary layer followed by a steady-state boundary layer as the effects of the leading edge are transmitted downstream. The use of a multichannel high speed transient data recorder allowed thin film heat transfer gages at up to eight axial locations along the length of the flat plate to be simultaneously sampled. Heat transfer rate histories for each axial location were time correlated to the same flow conditions. The results indicate the existence of a threshold free stream velocity (relative to the plate) above which yields transition times, for all locations along the plate, which are confined to some narrow interval. The leading edge disturbance appears to have no influence on transition. For Mach numbers below 1.22, the sharp leading edge flat plate experienced heat transfer rates in excess of theory, but the rounded leading edge flat plate exhibited data which matched or was less than what theory predicted for each Mach number tested. The sharp leading edge flat plate data showed a consistent correlation between heat transfer magnitude and axial location on the plate; with limited data, the rounded plate showed no such correlation.

END

DATE
3-88
DTIC